DIELECTRIC PROPERTIES OF SOME ALUMINOSILICATES

A thesis submitted
for the degree of
Doctor of Philosophy
in the
University of London

by

E. A. Saxon-Napier.

Department of Chemistry,
Imperial College,
London, S. W. 7.

January, 1960.

Abstract.

An account has been given of dielectric measurements by the a.c. method of hydrothermally synthesised powdered aluminosilicates. In order to cover a frequency range between 100 c/s and 10 mc/s in these measurements, an Inductively Coupled Ratio Arm Bridge has been built and a Hartshorn-Ward apparatus adapted for powder measurements at temperatures between -183 and 250°C.

The aluminosilicates include species with occluded molecules which were expected to have unusual dielectric properties, species with decreasing openness of anionic framework structure to study the influence of the size of the intracrystalline cavities, and a series of ion-exchanged analcites to determine the influence of cation size on the dielectric properties.

The dielectric properties of compounds with occluded molecules are governed by d.c. conductivity and consequent interfacial polarisation effects. This may be due to occluded water or to structure defects associated with permanently occluded molecules. All these materials show high dielectric loss.

In a series of analcites the sodium mineral has a cation relaxation peak in the measurement range. This peak moves to lower frequencies with increase in cation size so that there is only an indication of it in the potassium mineral. The non-sintered rubidium and caesium species show dielectric loss ascribed to terminal OH groups. When these are driven off by heating, the resulting species are very good insulators. The potassium and the sintered rubidium and caesium analcites have identical permittivities at high frequencies, which proves the close equivalence of structure.

The activation energies obtained from the results for anhydrous basic sodalite, leucite, the domain mixture of rubidium analcite and ordinary pollucite vary with frequency and temperature. This is attributed to a distribution of relaxation times which is also found with sodium analcite and may be caused by a varying environment of the relaxing species.

Acknowledgements.

It is with a sense of deep gratitude that I wish to acknowledge the constant help and encouragement extended to me during the course of this work by Professor R. M. Barrer. I am also very grateful to Dr. I. S. Kerr who did the electron microscopy, to Miss E. M. Steel for her patience while typing this thesis, to the other members of Professor Barrer's research group for many fruitful discussions and to the staff of the Chemistry Department of Imperial College for their practical assistance.

My thanks are due to the Ministry of Supply who awarded the bursary which made this research possible and in particular to Mr. C. G. Garton of the British Electrical and Allied Industries Research Association for many useful discussions.

INDEX.

Page No.

Abstract.

1. Introduction. 1.

2. Silicates and Aluminosilicates. 6

2.1. Structural Principles and Classification. 6
2.1.1. The Structure of Silicates. 6
2.1.2. Aluminosilicates. 7

2.2. Zeolites. 10
2.2.1. Structure and Classification. 10
2.2.2. The Cations in Zeolites. 12
2.2.3. Water in Zeolites. 13

2.3. The Analcite Group of Minerals. 16
2.3.1. Analcite. 16
2.3.2. Leucite. 20
2.3.3. Pollucite. 21
2.3.4. Synthetic Analcites. 22
2.3.5. Analcite Minerals as a Group. 23

2.4. Sodalite and Basic Sodalite. 25

2.5. The Silver Nitrate Occlusion Compound of the Zeolite Sodium A, $AgA(AgNO_3)$. 27

3. Dielectrics and Dielectric Theory. 31

3.1. Dielectrics and Their Properties. 31

3.2. The Theory of Electric Polarisation. 35
3.2.1. The Static Dielectric Constant. 35
3.2.2. Polar Dielectrics at Low Frequencies. 38
3.2.3. Non-polar Dielectrics in a Static or Low-frequency a.c. field. 42
3.2.4. Equations developed by Statistical Mechanics. 44
3.2.5. The Complex Dielectric Constant. 45
3.2.6. The Refractive Index. 51
3.2.7. Dielectric Loss and Relaxation Time. 56
3.2.8. Distribution of Relaxation Times. 66
3.2.9. Polarisation of Solids. 73
3.2.10. The Dielectric Constant of Mixtures and Powders. 84

3.3. Dielectric Measurements on Some Aluminosilicates. 88

Page No.

4. Experimental Section. 95

4.1. Aluminosilicates. 95
4.1.1. General and Syntheses. 95
4.1.2. Identification of Materials. 97

4.2. Dielectric Measurements. 100
4.2.1. Apparatus in General. 100
4.2.2. The Inductively Coupled Ratio Arm Bridge. 102
4.2.3. The Hartshorn Ward Dielectric Test Set. 107
4.2.4. The Q-meter. 112
4.2.5. Thermostats. 112
4.2.6. Dielectric Cells, Cell Holders and Connections. 113
4.2.7. Use of the Böttcher Powder Formula. 118
4.2.8. Reproducibility and Errors. 121

5. Basic Sodalite. 125

5.1. Description of Sample. 128

5.2. Hydrated Basic Sodalite, Results and Discussion. 128

5.3. Anhydrous Basic Sodalite, Results and Discussion. 147

6. The Silver Nitrate Occlusion Compound of the Zeolite Silver A, $AgA(AgNO_3)$. 156

6.1. Description of Sample. 156

6.2. Slightly Hydrated $AgA(AgNO_3)$. 158

6.3. Anhydrous $AgA(AgNO_3)$. 161

7. Sodium Analcite. 172

7.1. Description of Sample. 172

7.2. Hydrated Sodium Analcite. 174

7.3. Anhydrous Sodium Analcite. 175

8. Leucite. 191

8.1. Description of Sample. 191

8.2. Leucite (Exchange Sample). 193

8.3. Sintered Leucite. 207

Page No.

9. Rubidium Analcite. 210
9.1. Description of Sample. 210
9.2. Rubidium Analcite, Domain Mixture. 213
9.3. Rubidium Analcite B. 220

10. Pollucite. 227
10.1. Description of Sample. 227
10.2. Ordinary Pollucite. 229
10.3. Sintered Pollucite. 239

11. Comparative Discussion of Results. 243

References. 254

1. INTRODUCTION.

The aluminosilicates of the mica group have for many years been used as insulators and dielectrics. Massey[1] points out that like asbestos, mica is used essentially for its heat resistance, which combined with its low dielectric loss[2,3], is an important factor in the construction of electrical apparatus which heats up on continued operation. Since mica is a natural material, careful selection is necessary to ensure the correct grade being used, and difficulties are experienced due to its loss of water of constitution, for instance under the conditions which obtain during its use as an electrode support in radio valves. Impurities may play an important part and cause additional dielectric loss. The continued use of mica, in spite of these shortcomings, emphasizes the lack of heat-resistant dielectrics and insulators. It is thus somewhat surprising that no systematic dielectric work has so far been undertaken in the field of aluminosilicates, and in particular of those synthetic species which do not act as water sorbents. The advantage of using non-hydrated materials is self-explanatory. Synthesis should in general produce materials which are of higher purity, and should thus have a lower dielectric loss than the corresponding natural minerals. Also the composition of synthetic species is reproducible.

It is the object of this work to investigate the electrical properties of some of the crystalline aluminosilicates synthesised in these laboratories by hydrothermal methods from hydrous gels of compositions

$$(M^{++},M_2^{+})O.Al_2O_3.nSiO_2 + aq.$$

where $1 < n < 12$, M^{++} is Ca^{++}, Ba^{++} and Pb^{++}, and M^{+} is Tl^{+}, Li^{+}, Na^{+}, K^{+}, Rb^{+} and Cs^{+}[4].

The aim is

(a) to find useful dielectric materials, and

(b) to attempt the correlation of structures and dielectric properties.

To this end the minerals chosen for investigation were all of known structure.

The study of hydrothermal mineral formation in the aluminosilicate field made in this laboratory, has been considerable. Barrer and White[5] investigated the lithium aluminosilicates, Barrer and White[6] and Barrer and Bultitude[7] the sodium aluminosilicates. The potassium aluminosilicates were explored by Barrer and Baynham[8]. These crystallisation fields provide a wide range of mineral species, some with and others without natural counterparts. Pure natural rubidium aluminosilicates are unknown, but Barrer and McCallum[9] synthesised a variety of these minerals and some caesium minerals, one of which is identical with the natural caesium mineral pollucite.

This work is still continuing, and the progress until about 1956 has been summarised by Barrer[4].

The sorption, ion-exchange and molecular sieve properties and reactions of some of these minerals and particularly of the zeolites are of great interest and have been examined by the above workers and by others[10,11,12,13,14,15,16,17].

The work in these laboratories showed that certain mineral groups of three-dimensional framework structure, as for instance felspars or analcites, have well established common structural frameworks, with rather minor differences between the frameworks of members of given type[4]. Thus the analcite framework retains its identity with only minor variations for the ions: Li, Na, K, Rb, Cs, Tl, NH_4, Ag. In the alkali metal analcite series, on account of the progressive increase in the size of the cation, the cations

become progressively more localized in the framework. Differences in dielectric properties, which in solids depend mainly on structure, must in this series be a function of the cation and its mobility. In order to find this dependence, the alkali metal analcites were studied in this work. Pollucite and one of each of the rubidium and potassium members of this group have high thermal stability and are anhydrous, and might therefore provide useful dielectric materials.

Another method of systematic study of dielectric properties is to choose a series of aluminosilicates with decreasing openness of the anionic framework structure, such as the zeolites sodium-A, sodium chabazite, sodium basic sodalite and sodium analcite, in which the size of the intracrystalline cavities decreases progressively. Dielectric measurements on sodium basic sodalite and sodium analcite were undertaken to show the effect of these variations. The zeolites are all water sorbents and cannot be of use as dielectrics or insulators. However measurements were made in both the hydrated and anhydrous states to determine the influence of the sorbed water on the dielectric properties.

Filling the cavities in open aluminosilicate structures with molecular or ionic compounds other than water, produces a number of stable species. The $AgNO_3$ filled derivative of the Ag exchange form of the zeolite sodium-A, is an example. From its structure this compound might be expected to show anti-ferroelectric behaviour[16,18]. The dielectric properties of this mineral were studied in the anhydrous and in a slightly hydrated state.

The large field of aluminosilicate structures puts other variables, which may lend themselves to systematic electrical studies, at the experimenter's disposal. Thus

monovalent cations may be replaced by divalent ones and it is possible to obtain other isomorphous replacements of the type $Si^{4+} \rightleftharpoons Na^{+}Al^{3+}$; $Al^{3+} \rightleftharpoons Ge^{3+}$; $Si^{4+} \rightleftharpoons Ge^{4+}$. No dielectric study has however been undertaken in these directions.

In order to give reliable information and to be of theoretical value, dielectric measurements should be made over the largest possible frequency range and at a number of temperatures. This is a recurring theme in modern literature on dielectrics and dielectric relaxation. No satisfactory general theory of dielectric relaxation has yet been developed to deal with measurements at a constant frequency but varying temperature, although many authors have developed semi-empirical equations to deal with such measurements. Nevertheless many of the dielectric measurements reported in the literature have been made at constant frequency and sometimes even only at one temperature. Those of the aluminosilicates which are the subject of this work, and of related minerals, are typical of this.

A number of authors have measured the d.c. resistivity of hydrated natural zeolites including analcite and chabazite by a d.c. method[19,20]. Beattie measured the d.c. resistivity of the anhydrous ion-exchange forms of synthetic analcite and chabazite by an a.c. method and from his results calculated diffusion coefficients[21,22,23].

The dielectric constants of analcite, chabazite, leucite and a number of other aluminosilicates in various conditions of hydration, sometimes not clearly defined, were measured by a number of authors[24,25,26,27,28]. Wetzlar[29] measured the dielectric constant of zeolites including chabazite and obtained relaxation times from his results. Glemser[30] studied the combination of water in zeolites by electrical methods. Finally Keymeulen and Dekeyser[31]

determined the dielectric loss of natural kaolinites over a large temperature and frequency range.

All these results, some of them contradictory, will be critically examined in a later section.

The crystallites obtained in the synthesis of aluminosilicates are usually too small to allow dielectric measurements on single crystals. The difficulties arising from this and the fact that natural crystals are normally not of the required purity to give results independent of the impurities, are probably the reason why so far no systematic dielectric work has been done on aluminosilicates.

A number of the species examined in this research, such as sodium analcite, are not sufficiently stable to heat to be hot-pressed. Thus in order to permit comparison of the members of the series under standardised conditions, measurements were made on the powdered samples, in dielectric cells sealed into glass holders. The 'real' dielectric properties are then calculated from these results and the degree of filling of the cells. Dielectric constants and dielectric losses were studied between 200 c/s and 20 mc/s. The low frequency measurements were made on a bridge constructed in these laboratories, while a Hartshorn-Ward dielectric test set and a Q-meter were used for the higher frequency range. No measurements of d.c. conductivity or dielectric strength were made.

Before describing the experimental apparatus, methods and results of this research, some topics of interest in the work will be considered.

2. SILICATES AND ALUMINOSILICATES.

This research is part of a larger programme, designed to examine the dielectric properties of aluminosilicates systematically. The minerals which are the subject of this work are only a small part of the vast aluminosilicate field. In order to show their position in this field, a general survey of silicate, aluminosilicate and zeolite structures and properties is given in the first part of this section. This survey is not comprehensive, since in any case the structures of silicates and aluminosilicates are well known from textbooks[32,33].

The structures of the minerals electrically examined are based on those of robust 'framework zeolites', although only two of the minerals, namely sodium analcite and sodium basic sodalite, can actually be classed as zeolites. A detailed account of their structures and properties is given in the second part of this section.

2.1. Structural Principles and Classification.

2.1.1. The Structure of Silicates.

Silicate structure is based on the SiO_4^{4-} group, in which four oxygen anions are coordinated with one silicon cation forming a stable structural unit in which the silicon is situated at the centre of a regular tetrahedron of oxygens. The oxygen ions may be shared between two tetrahedra and classification of silicates is based on the number of oxygens in a given tetrahedron which are so shared. This classification is mainly due to Bragg. Five groups are possible:

(i) The orthosilicates in which no oxygen ions are shared.

(ii) The sorosilicates. These structures contain

groups of a limited number of SiO_4 tetrahedra, each with one oxygen ion shared. The simplest case is that of two tetrahedra sharing one oxygen, i.e. $Si_2O_7^{6-}$; other combinations include those of three and six tetrahedra to form rings of composition $Si_3O_9^{6-}$ and $Si_6O_{18}^{12-}$ respectively.

(iii) The ionosilicates. In these minerals, by sharing two oxygen ions, tetrahedra form single chains which may be represented by $n(SiO_3)^{2-}$. Also included in this class are structures in which tetrahedra sharing alternately two and three oxygens have combined to form double chains, i.e. $n(Si_4O_{11})^{6-}$.

(iv) The phyllosilicates. From tetrahedra sharing three oxygen ions a two dimensional sheet or layer structure can be built up which may be represented by $n(Si_2O_5)^{2-}$. This results in a hexagonal network.

Since the Si - O frameworks of these four classes are negatively charged, cations must be present in these structures, to confer electrical neutrality on the systems. It is the electrostatic attraction between these cations and the silicate frameworks which hold the minerals together.

(v) The tectosilicates. These consist of a three-dimensional network, in which each tetrahedron by sharing four oxygen ions is linked to four other tetrahedra, i.e. $(SiO_2)_n$. These structures have no residual negative charge and do not require the presence of cations for electric neutrality.

2.1.2. Aluminosilicates.

Isomorphous replacement of some SiO_4^{4-} by AlO_4^{5-} tetrahedra in the frameworks of groups (iv) and (v) above, results in the group of minerals known as the aluminosilicates. The dimensions of the AlO_4 and SiO_4 tetrahedra are almost identical and thus the replacement can be made with the minimum of distortion. This replacement is subject to a

limitation discussed by Lowenstein[34], which is based on Pauling's third rule of valence[35]. Thus, in aluminosilicates with Al in four-fold coordination, there will be for stability reasons, no Al - O - Al bridges. This results in a maximum Al/Si ratio of unity in which AlO_4 and SiO_4 tetrahedra occupy alternate positions.

The framework resulting from the replacement of SiO_4 tetrahedra by AlO_4 tetrahedra in the tectosilicates has negative charges which are balanced by cations in the interstices. The framework remains rigid, but in certain aluminosilicates in which these interstices are interconnected by a network of channels intersecting the lattice, the cations can migrate through the mineral. This type of structure allows cation exchange.

Because of the many spatial arrangements of linked tetrahedra in a three-dimensional structure, a considerable variety of tectosilicate structures is possible. Examples are the felspars, zeolites and the sodalite-hauyne group. Felspars are built up of rings of four tetrahedra linked to form chains, the chains being linked to form three-dimensional frameworks.

Zeolites and the sodalite-hauyne group of felspathoids have very open frameworks with channels running throughout the structure containing, in the zeolites, cations and water, and in the sodalite type, halogens or acid radicles such as $CO_3^=$ and $SO_4^=$ as well as cations. The structure of members of the sodalite family is shown in Fig. 1. The unit shown is a truncated octahedron made up of four and six membered rings.

Mica minerals have been mentioned in the introduction and it is appropriate to mention their structure. They are derived from the phyllosilicates which have hexagonal networks. In the micas there are alternate

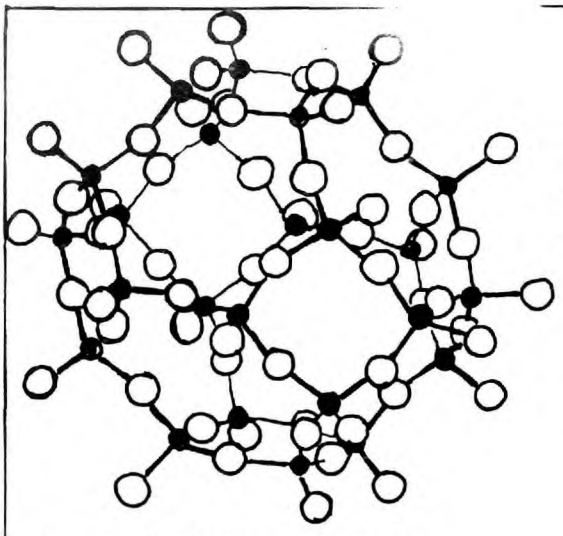


Fig. 1. SODALITE CAGE.

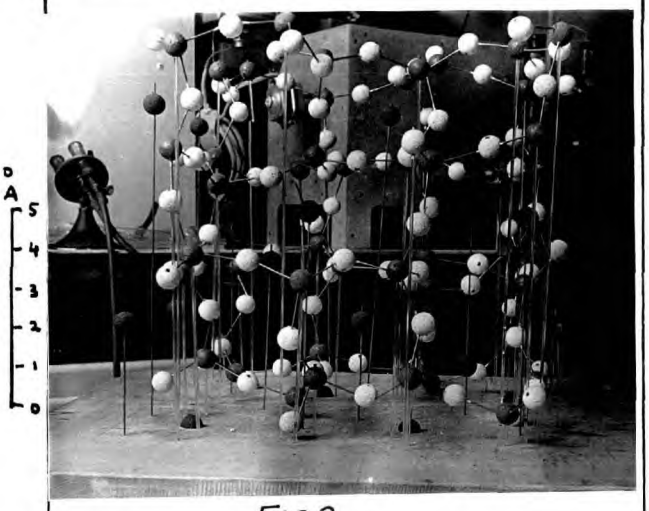
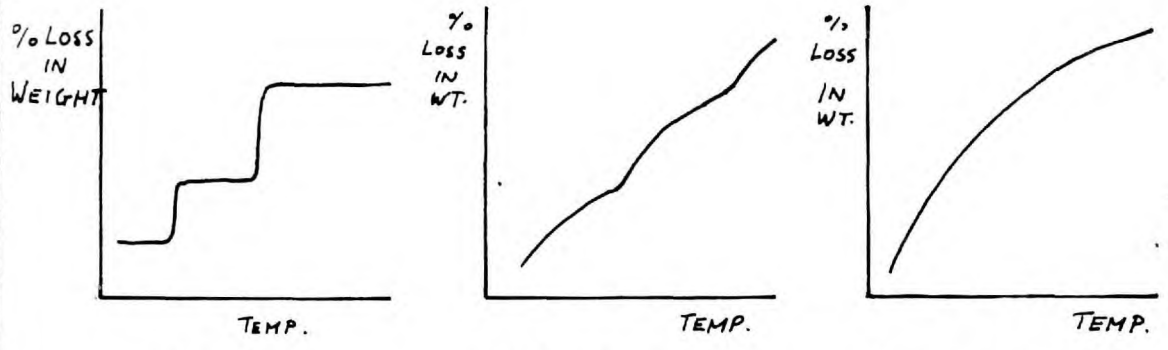


FIG. 3.



(a). STEPPED. (b). DISCONTINUOUS. (c). CONTINUOUS.

FIG. 2. DEHYDRATION CURVES OF ZEOLITES.

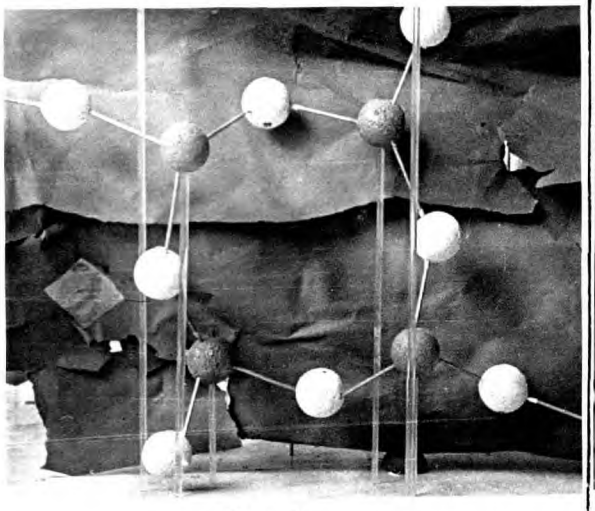


FIG. 4.

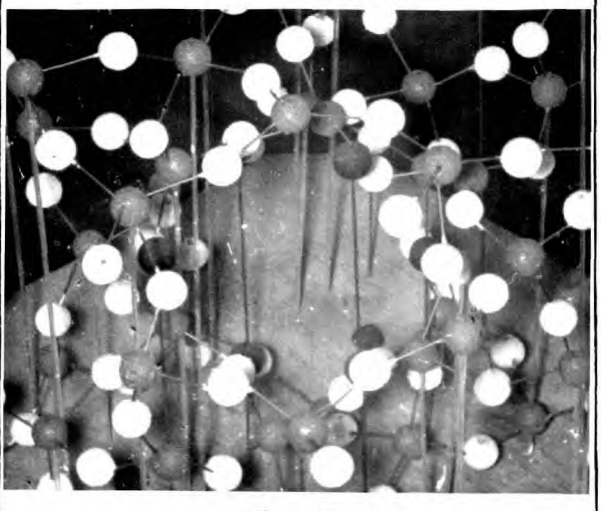


FIG. 5.

layers of this type which are joined by aluminium in octahedral coordination, the free tetrahedron corners being simultaneously corners in the octahedral layers. One of every four of the silicon ions is replaced by aluminium. To maintain neutrality cations of large coordination number are introduced between the sheets. Muscovite ($KH_2Al_3(SiO_4)_3$) is an example of this structure.

Each bond in an aluminosilicate exhibits some degree of covalency. Pauling has determined this relative covalency in such bonds as:

$Si^{4+} - O^{2-}$: 50 per cent; $Al^{3+} - O^{2-}$: 40 per cent.

2.2. Zeolites.

2.2.1. Structure and Classification.

Zeolites are hydrated aluminosilicates of framework structure and have the general formula

$$(R^{++},R_2^{+})O.Al_2O_3.nSiO_2.xH_2O$$

where 'n' and 'x' are variables. The ratio of base to alumina is 1:1, and the ratio O:(Al+Si) = 2:1. They may be considered in three main groups depending on whether the linking of tetrahedra is strong in one, two or three directions[36].

(i) The fibrous zeolites are characterised by chains of linked tetrahedra, within which the bonding is strong. Separate chains are linked only at infrequent intervals by sharing oxygen atoms which belong to only one tetrahedron in a chain, e.g. linking is strong in one direction only. Natrolite is an example of this group; it is structurally tetragonal but optically of a lower symmetry, i.e. orthorhombic. This phenomenon is often also found in the 'framework zeolites', analcite being an example.

(ii) The lamellar zeolites such as heulandite are more rigid in two dimensions than in the third, the bonding in successive planes is strong but the bonding between planes is much weaker.

(iii) The framework zeolites such as analcite and chabazite possess a rigid three-dimensional framework of rings of linked tetrahedra, linking being strong in all three directions. The rings may be composed of four, six or more linked tetrahedra.

It must be emphasized that all three groups belong to the tectosilicates, with all oxygen ions shared between two tetrahedra. All the structures comprise frameworks of $(Al,Si)O_4$ tetrahedra enclosing a network of channels. The channels intersect as in chabazite or have some interconnection as in analcite. Even in the fibrous zeolites where the channels are mainly parallel to the c-axis[37] there are still believed to be some interconnections[38]. The cations and water molecules lie in the channels and cavities in the structure. The channels give to zeolites their base exchange and sorption properties.

One major variation may occur in some structures, e.g. chabazite. Barrer and Baynham[8] synthesised a series of chabazites of varying alumina:silica ratio. This variation altered the cation content of the channels and caused slight differences in X-ray diffraction patterns and other properties. Winchell[39] forecasts isomorphous replacements $NaSi \rightleftharpoons CaAl$ in natural zeolites and showed their existence from a study of chemical analyses. The majority of naturally occurring zeolites do in fact vary in composition in this manner and may be considered as isomorphous series.

2.2.2. The Cations in Zeolites.

Taylor has shown that the cations in analcite and some of the fibrous zeolites occupy definite lattice sites. Their position in analcite, pollucite, ion-exchanged analcites and sodium chabazite have been discussed by Taylor[37], Naray-Szabo[40] and Beattie[41,42]. The co-ordination number of sodium ions is usually six and that of the calcium ion seven or eight. The water in the channels is closely associated with the cations.

Cation exchange may be brought about by fusion of the zeolite with a low melting salt, or by exposure to a solution or to vapour of a salt of the required cation. The exchange reaction takes place with true ionic equilibrium and may be completed by continual renewal of the reacting medium. The diameter of the interstitial channels which allow this process, limits the dimensions of the exchangeable cations.

Other factors also influence the ease of cation exchange. Most zeolites contain fewer cations than cation sites of equivalent energy. The cations are therefore probably in a continuous state of movement from site to site, and this must greatly increase the ease of diffusion. For instance in analcite sixteen cations migrate between the twenty-four equivalent positions[43], in order to maintain cubic symmetry. The excess of available sites and the consequent cation movement are also probably the reason why univalent cations may replace divalent ones in some zeolites without appreciable change of structure[44], e.g. Ba edingtonite $\rightleftharpoons$ K edingtonite.

The influence of the zeolitic water in the cation exchange process has never been clearly understood. The more highly hydrated a zeolite, the greater is the ease of cation exchange. This may, however, be due to the fact

that amount of hydration and openness of structure go hand in hand.

Recent investigations have been made of ion-exchange kinetics, ion sieve effects, limited solid solubility relationships, changes in unit cell constants and sorptive properties of zeolites on ion exchange. Much of this work is on analcite and will be considered under a separate heading. However the large change which occurs in the unit cell dimensions of ion-exchanged fibrous zeolites, e.g. edingtonite[36] must be mentioned. Unit cell changes on ion exchange are also apparent in analcite, chabazite and ultramarine[45,46], a felspathoid with a framework structure similar to that of zeolites.

2.2.3. Water in Zeolites.

On isobaric dehydration the zeolites give curves of three different types: (Fig. 2 a - c).

(a) The stepped curve which is characteristic of hydrate formation.

(b) Curves with distinct discontinuities or breaks.

(c) Continuous curves.

Theories which have been put forward to explain zeolitic dehydration vary between two extremes. According to one view the water occupies definite sites in the structure as in hydrates, and according to another the water molecules move about quite freely in the lattice. Probably zeolitic water is neither bound like true water of crystallisation nor is it physically adsorbed water. Some or all the water molecules take up preferred interstitial positions in the lattice, but are not rigidly fixed there as a necessary part of the structure. Thus within limits the water may be driven out reversibly, without radically altering the zeolitic framework.

Comparison of the dehydration phenomena of the zeolite groups reveals certain similarities in each group:

(a) Amongst the fibrous zeolites, work by Hey[36] and by Weiser and Milligan[47] on natrolite, scolecite, mesolite and edingtonite shows stepped dehydration curves of type 'a', with some of the water molecules more volatile than others. In some of these minerals, breakdown occurred and in others lattice shrinkage, on dehydration. For thomsonite, Weiser and Milligan reported a smooth dehydration curve and only slight lattice collapse, while Hey reported a transition to metathomsonite.

(b) The lamellar zeolites give dehydration curves of type 'b' with marked inflections. The dehydration isobar of heulandite was studied by many authors[47,48,49,50,51,58] and showed inflections; it is accompanied by contraction of the b parameter and is irreversible after prolonged heating at 350°C. The inflections occur at well defined molecular ratios of the water content to the zeolite residue and have been explained as due to certain preferred structural arrangements of the water within the unaltered crystal lattice. Stilbite showed an irreversible break, but the latter part of the dehydration curve was reversible.

Most of the investigators agree that dehydration to zero water content is irreversible[47,51,52], the last water molecules being necessary to maintain the stability of the weakly bonded sheets.

(c) The robust framework zeolites give smooth dehydration curves. In the case of faujasite[52], gmelinite[53] and chabazite[47] these are reversible, while analcite dehydration was reported not to be completely reversible until after the first dehydration[47]. Little lattice collapse or change of X-ray pattern was found for

analcite up to 400°C, and no lattice shrinkage and only slight differences in X-ray intensities for chabazite.

The smooth continuous dehydration isobars of these zeolites and their reversibility can in part be explained by their structure, in which the water is probably closely associated with the cations. This would put the water molecules into more or less equivalent surroundings. The anion, which is strongly bonded in all three directions, extends throughout the crystal and allows the removal of water under suitable temperature and pressure conditions without appreciable reorganization of the lattice.

Hartwig[54] and Lengyel[55] considered the water molecules not to be in fixed positions in analcite and chabazite respectively. However Taylor demonstrated that the water molecules in analcite occupy definite sites. Sites for the water molecules have also been specified in natrolite, thomsonite, scolecite and edingtonite, there being more than one type of site in all but the first.

Electrical conductivity measurements gave contradictory results: Weigel[19] attributed the conductivity to the water molecules rather than the cations in stilbite, chabazite, analcite, heulandite, scolecite and natrolite, while Rabinowitch and Wood[20] believed the cations to be the current carriers in chabazite. Glemser[30], considering dielectric constant measurements by Fairbanks[25], suggested that in natrolite and analcite water is in fixed positions, while in heulandite, chabazite and stilbite part of the water is mobile.

Differential thermal analysis curves have shown differences in the dehydration of zeolites, natrolite giving sharp peaks and analcite and chabazite flat curves. Useful information on the strength of water binding may be given by this technique[56,57].

The amount of water present in a zeolite depends on temperature and pressure. A dehydrated zeolite will take up water again when it comes in contact with water or its vapour, and subject to the phenomena of irreversibility discussed above. In the absence of water such a dehydrated zeolite will, sorb other molecules of dimensions suitable to enter the channels. The amount sorbed depends on temperature, pressure and the interstitial volume.

2.3. The Analcite Group of Minerals.

2.3.1. Analcite.

Analcite is a framework zeolite bonded strongly in three directions. Jaeger[59], Hartwig[54,60] and Schiebold[61] gave the cubic unit cell dimensions as a = 13.68 to 13.71 Å with 16 molecules of composition $NaAlSi_2O_6.H_2O$ per unit cell; the last two authors pointed out that the true symmetry is not cubic. Hartwig showed that there is no marked change in lattice constant or intensities of powder X-rays on dehydration, indicating the water to be 'zeolitic', while Schiebold believes the 'non-zeolitic' water to be bound to symmetric crystal locations by weak bonds.

The generally accepted structure has been determined by Taylor[43] and is pseudo-cubic; it is illustrated in Fig. 3. The real symmetry may be tetragonal but in any case is no higher. The number of atoms per unit cell of edge a = 13.7 Å corresponds to $8(Na_2O.Al_2O_3.4SiO_2.2H_2O)$. It is a robust three-dimensional framework. There is no isomorphous silicon-aluminium replacement and the fixed ratio of $Al_2O_3:SiO_2$ = 1:4. The aluminosilicate network, built of 4, 6 and 8 membered tetrahedron rings (Figs. 4, 5 and 6) is traversed by open channels, composed of the six membered rings, and lying

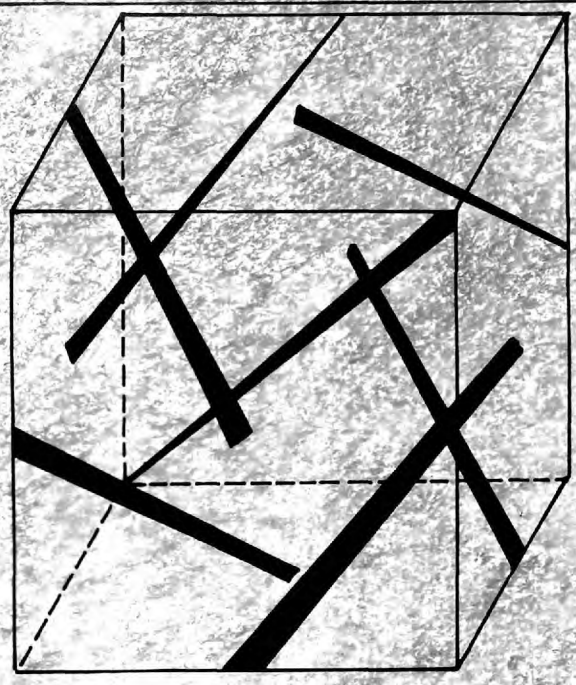


FIG. 7.
OPEN CHANNELS IN
ANALCITE.

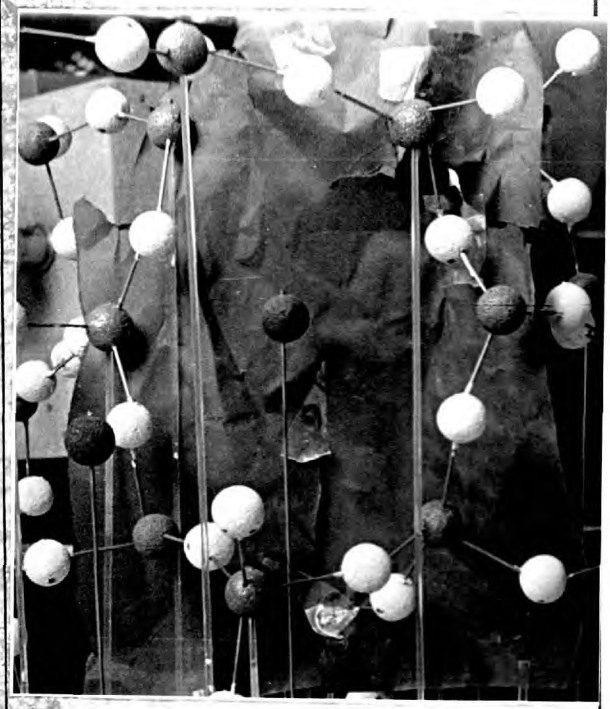


FIG. 6.

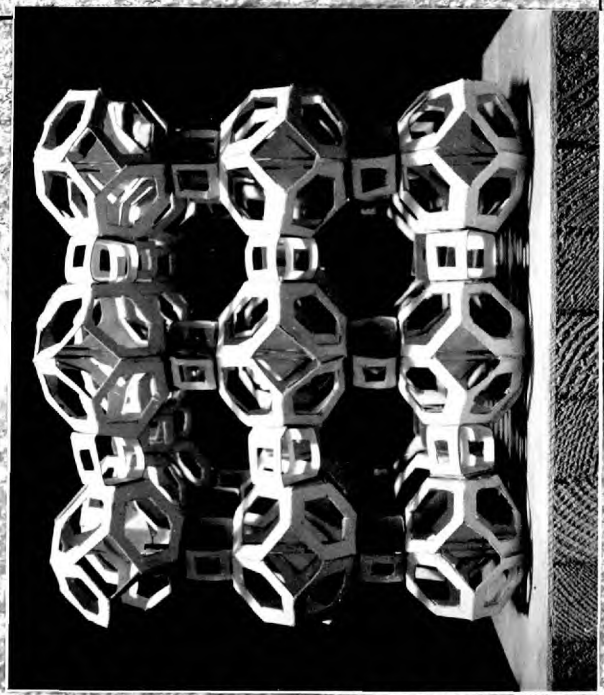


FIG. 9.

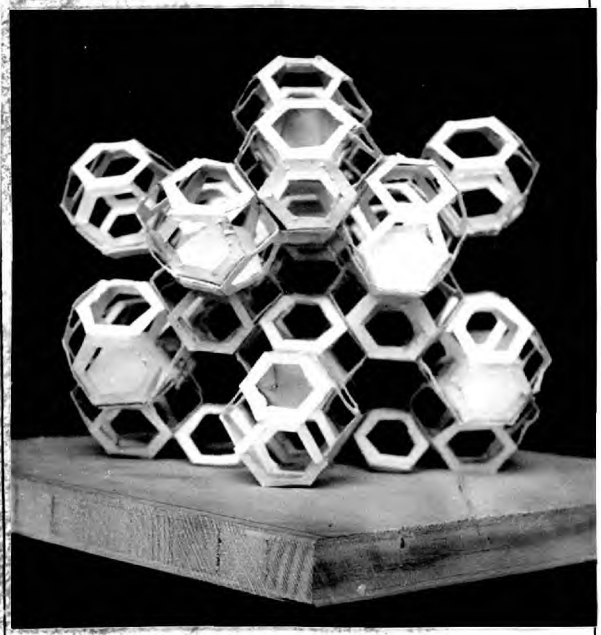


FIG. 8.

along the non-intersecting threefold axis (Fig. 5). These channels, the relative positions of which are shown in Fig. 7, are interconnected via the 8 membered rings. They allow the diffusion of certain cations and water through the structure (Fig. 3).

The 16 sodium ions are distributed at random between 24 equivalent positions which occur at the centres of the 8 membered rings (Fig. 6). The water molecules lie in the open channels (they have been omitted from the illustrations).

There has been some discussion about the cations in analcite. According to Taylor they occupy definite lattice sites. The placing of the 16 sodium ions in twenty-four fold positions means that eight sites must be unoccupied. The cation distribution must thus be a space average with some positions always vacant, or a time average, every site being occupied at some time. The latter is usually accepted which means that the cations must be mobile[62].

Pollucite has the same framework structure as analcite, with caesium ions replacing the sodium ions. Náray-Szabó[40] suggested that the sodium ions in analcite occupied the same sixteen fold positions as the caesium ions in pollucite. Taylor[75] however demonstrated that on dehydration of analcite, the X-ray diffraction intensity alterations observed, fit well with the positions he had postulated, while based on Náray-Szabó's positions some of the theoretical intensity changes are the opposite of those observed. The distribution of the aluminium ions in the lattice probably affects the crystallographically equivalent lattice sites energetically and these sites may therefore not all be energetically the same. Beattie[41] suggested that eight of the sodium ions per unit cell are in fixed positions of a lower energy state than the other eight, which are averaged over sixteen equivalent positions. He further

showed that the position of the ions in the ion-exchange forms of analcite depends on the ionic radii. The co-ordination number of the sodium ion in analcite is six, with four oxygens and two water molecules at a distance of 2.4 Å from the cation.

Kinetic ion exchange studies by Barrer and Hinds[11] showed that the diffusion of cations follows a $\sqrt{t}$ diffusion law, and diffusion coefficients and energies of activation were obtained. Only univalent cation exchanges could be brought about[10,46] and the Na-K exchange showed hysteresis which was attributed to the limited solid-solubility of the end members. Caesium cannot be introduced into the analcite lattice by ion exchange or removed from the caesium form, e.g. pollucite, which can be grown from gels by hydrothermal methods. These facts form the basis of a quantitative separation of sodium and potassium from caesium using silver analcite[74]. Barrer[10] defines an ideal exchanger as "an inert anionic framework into which cations of type A may be inserted, replacing an electrochemical equivalent of cations type B". Thus in analcite sodium ions can be directly exchanged for K, NH_4, Ag, Tl, and Rb, but not directly for Li, Cs, Mg, Ca or Ba. This can be explained in terms of constrictions in the channels which caesium ions cannot pass. Bivalent ions cannot be introduced because they cannot, for steric reasons, occupy the positions where neighbouring segments join, without causing local electrical disturbances. Rates of ion exchange diffusion have recently been studied quantitatively by Barrer and Falconer[13].

X-ray diffraction showed little lattice collapse or change in pattern on heating from 30 to 400°C[37,47,54,65,66] According to Gruner[63] the parameters of the unit cell of anhydrous and hydrated analcite are a = 13.54±0.05 Å and

13.63±0.05 Å respectively. Because of the small differences in X-ray patterns of the anhydrous and hydrated forms Hartwig[54] believed the water molecules were not in fixed positions, while Taylor showed that water removal leads to the observed differences only if both cations and water are in the positions he had suggested.

Weigel[19] attributed the electrical conductivity of analcite to the water molecules rather than the cations, and Glemser[30], from dielectric measurements, deduced the water positions to be fixed.

2.3.2. Leucite.

This mineral is a felspathoid. Wyart[67,68] reported a natural sample to be tetragonal with unit cell parameters a=12.95 Å and c=13.65 Å, containing 16 molecules $KAlSi_2O_6$ per unit cell. On temperature increase, a increases and c decreases, the mineral becoming cubic at 625°C with a=13.45 Å. The reversible inversion at 625° occurs with heat absorption. The structure of the mineral resembles that of analcite.

A synthetic sample[69] examined by Wyart was identical with the natural mineral and above 625° the O, Al and Si positions were the same as in analcite. Wyart describes the low temperature form as a framework of AlO_4 and SiO_4 tetrahedra with all corners shared, forming either Si_4O_{12} rings bonded together by Al ions or hexagonal $Al_2Si_4O_{18}$ rings bonded by their oxygens, with one such ring in each cube of a/2. Every potassium ion is surrounded by 12 oxygens at a distance of 3.5 Å.

Eitel[70] reports a congruent fusion point at 1686°C, and inversion accompanied by a 2% volume contraction at 603 and 620-625°C respectively for synthetic and natural leucite.

Náray-Szabó[71] considered the unit cell of a natural leucite to be that of a deformed pollucite containing 16 molecules $KAlSi_2O_6$ and of dimensions a=13.01 and c=13.82Å.

2.3.3. Pollucite.

Strunz[72] reported the formula of pollucite as $(Si_4Al_2O_{12})Cs_2.H_2O$, the structure as cubic with a=13.71 Å and a water loss of 2.58% at 500°C. Gossner and Reindl[79] found the same similarity as Strunz to analcite and leucite and gave the formula as $CsAlSi_2O_6$, containing a little unexplained water, and the unit cell parameter as 13.66 Å. Náray-Szabó[40] considered the unit cell to be pseudo-cubic, but really tetragonal, with a=c=13.74 Å and containing 16 molecules $CsAlSi_2O_6.xH_2O$. The framework consists of Si_4O_{12} rings connected through AlO_4 tetrahedra. The caesium ions are in the largest spaces surrounded by twelve oxygen ions at a distance of 3.50 Å.

Barrer and McCallum[73] showed that natural pollucite has the formula $(Na_xCs_{1-x})_2O,Al_2O_3.4SiO_2.2xH_2O$. The unit cell is of the same size as, and isostructural with, analcite. The cations must be similarly distributed to those in analcite. The water is associated with the sodium ions and not with the vacant sites. Thus pollucite containing only caesium should be anhydrous and this has in fact been found in the case of synthetic pollucite. This fact requires that $Na^+ + H_2O = Cs^+$. The anhydrous K, Rb and Tl analogues on the other hand have distorted anionic frameworks. Since the caesium ion is locked in the crystal, the distribution of the sixteen caesium ions is random in space but not in time, while the Na, Rb and Tl ions in the other forms of analcite are randomly distributed in space and time.

The size and immobility of the caesium ions in pollucite explains the difficulty of dehydration of natural pollucites (containing some sodium) since the water has to escape along channels occupied by the caesium ions.

2.3.4. Synthetic Analcites.

The whole series of alkali analcites have been synthesised in these laboratories by hydrothermal methods. Barrer and White[6] found the sodium mineral to be very dominant in its crystallisation field, up to 100% yields of spherulites, ikositetrahedra and cubes with hemihedral faces being obtained in up to 5 kg quantities. Crystals were isotropic and of unit cell cube edge 13.67 Å. On ignition at approximately 1150°C the mineral gave albite, the loss on ignition being 8.3%.

Barrer and Baynham[8] synthesised a hydrated potassium analcite $K_2O.Al_2O_3.4SiO_2.H_2O$ as spherulites showing no birefringence. Its refractive index depended on temperature. This is an expanded analcite type of a=13.79 Å, but on water loss at 450°C, 'a' changes to 13.70 Å. Leucite was also produced in this field, as spherulitic crystals showing moderate birefringence with mean refractive index n = 1.510 and unit cell dimensions, a=12.92 and c=13.70 Å. 100% yields, however, were not observed in direct hydrothermal syntheses. Such yields could only be obtained by ion exchange[10,11,12] from analcite by repeated 24-hour treatment with concentrated KCl solution at 200°C. Leucite thus produced contained 1.51% water.

Barrer and McCallum[9] synthesised two rubidium analcites (B and H) and pollucite amongst other minerals. The rubidium analcites were of composition $Rb_2O.Al_2O_3.4SiO_2$, both tetragonal, B with unit cell a=13.2 and c=13.6 and H with a=13.6 and c=13.3 Å. The mean refractive index

of species B was 1.52 and its melting point 1675±15°C. Species H was stable up to 1070°C, but above this transformed into B; its refractive index was 1.48. Synthesis usually produced a domain mixture of the two forms[17] which had an intermediate, variable refractive index and gave diffuse powder X-rays. Species B was obtained by heating the domain mixture above 1200°C for some time, while on heating below 1050°C species H was slowly produced. The latter conversion was sluggish and depended on the composition of the starting material This sluggishness suggests a reconstructive rather than the displacive type of transition exhibited by the leucite change from tetragonal to cubic at 625°C. The reconstruction process might be an order-disorder transformation of the Si and Al ions in the aluminosilicate framework. The refractive index and the unit cell dimensions indicate that species B is more compact than species H. Rubidium analcite was also produced by heating rubidium felspar above 900°C; ion exchange from sodium analcite was not complete and gave a domain mixture with 1.91% water.

Unlike the rubidium polymorphs the two potassium forms are not interconvertible, potassium analcite irreversibly changing to potassium felspar between 800and 1000°C, while leucite is stable to heat.

The pure caesium pollucite of formula $Cs_2O.Al_2O_3.4SiO_2$ was isotropic with a=13.7 Å, refractive index 1.523 and a melting point higher than 1700°C. The refractive index varied between 1.512 and 1.523 in different crystals, approaching the latter value on heating, but 'd' spacings were unaffected.

2.3.5. Analcite Minerals as a Group.

Table 1 is reproduced from Barrer,[4] and summarises the analcite group properties discussed in the preceding sections as a function of the interstitial cation.

Table 1.

Cation	Radius	Unit Cell	Hydrated	Ion exchange
Li^+	0.78	Cubic; a=13.5 Å	Yes	Yes
Na^+	0.98	Cubic; a=13.6$_6$	Yes	Yes
Ag^+	1.13	Cubic; a=13.7	Yes	Yes
K^+	1.33	(a) Cubic; a=13.7$_9$ (b) Tetrag; a=12.9$_2$; c=13.7$_0$	Yes No	Yes Yes
NH_4^+	1.43	Tetrag; a=13.1$_7$; c=13.6$_9$	No	Yes
Rb^+	1.48	(a) Tetrag; a=13.6$_4$; c=13.33 (b) Tetrag; a=13.2; c=13.6	No No	Yes Yes
Tl^+	1.49	Tetrag*;	No	Yes
Cs^+	1.63	Cubic; a=13.6$_6$	No	No

*This phase may also comprise two forms and so no unit cell is given.

The group shows a common structural framework, differences being small for the ions Li, Na, K, Rb, Cs, Tl, NH_4 and Ag. The stability of some of the synthetic members suggests, that this framework is characteristic of a stable group of minerals. Properties within the group correlate directly with ion size, going from a hydrated ion-exchanging zeolite to an anhydrous non-exchanger pollucite.

Thus the smallest ion analcites (Li, Na and Ag) are zeolites; the unit cell expands slightly with ionic size but remains cubic. Potassium forms either a cubic zeolite with further slight expansion of the unit cell, or leucite which is a very stable, anhydrous and slightly collapsed tetragonal structure. Analcites with larger ions are anhydrous and remain tetragonal until with the largest cation, caesium, the anhydrous but cubic mineral pollucite is formed, which has a unit cell identical to that of (sodium) analcite. While the K, NH_4, Rb and Tl varieties amongst the larger ions retain the ion-exchange properties of the sodalite type felspathoids, the Cs ion is too big to emerge from its cage. In fact leucite, rubidium analcite, pollucite and thallium analcite are usually classed as felspathoids.

2.4. Sodalite and Basic Sodalite.

The structure of the felspathoid sodalite has been determined by Barth[76], working with natural material. The edge of the cubic unit cell of composition $3(Na_2O.Al_2O_3.2SiO_2)2NaCl$ is 8.89 Å. The robust three-dimensional structure is based on a framework of linked four and six membered rings of SiO_4^{4-} (or AlO_4^{5-}) tetrahedra. Eight such six membered rings are grouped in a cage-like arrangement forming six four-membered rings. The channels through the six membered rings, lying along the four triad

axes, intersect at the cage centres. The chlorine ions are situated in the middle of the cages and the cations are positioned in the channels near the centres of the six membered rings, so that each chlorine ion is at the centre of the tetrahedron formed by four sodium ions. Thus apart from the sodium ions which neutralise the framework, there are intercalated NaCl molecules in the cages. This framework stands considerable heat treatment. Sodalite has been prepared as spherulites of up to 200μ diameter.

In the basic salt the NaCl molecules are replaced by NaOH and water[6]. The cubic unit celledges vary between 8.77 and 8.90 Å. X-ray powder photographs are similar to those of natural sodalite, yet regular shifts in spacings occur. A mineral of this composition has not been observed in nature. It is isotropic, with R.I. 1.488 to 1.495, the latter value for the most collapsed specimens. Barrer and White prepared samples from gels of composition $Na_2O.Al_2O_3.2SiO_2$ between 350 and 420°C, in the absence of NaCl but with approximately 300% molar excess NaOH present. It has also been grown from analcite by treatment with aqueous NaOH at 400-450°C[12] and by direct synthesis on the water bath[77].

Basic compounds of unit cell dimensions intermediate between expanded sodalite and collapsed nosean (which has the same fundamental structure but intercalated Na_2SO_4 molecules and unit cell dimensions of 9.3 to 9.6 Å) have been prepared. It is likely that a continuous range of compounds is possible, the formation of such a range being dependent on the amount of NaOH in (i.e. the pH of) the reaction mixture. A change of pH may progressively modify the proportions of sodium hydroxide and of water which are intercalated and this change in composition of the intercalated material may be accompanied by progressive modifications of the alumino-

silicate framework[6]. Fig. 7 is the diagram of a single cage of basic sodalite, the large circles represent oxygen atoms, and the black dots silicon and aluminium atoms.

Fig. 8 is the photograph of a model of basic sodalite; the corners of the cages each represent the site of an Al or Si atom; O atoms are near but not on the mid-points of edges.

Basic sodalite is an ion-exchanger and the Ag, Li and K forms have been obtained by Barrer and Falconer[13] who also studied the ion-exchange diffusion and equilibria.

Barrer and White proved the presence of the intercalated NaOH molecules by treatment of anhydrous basic sodalite with dry HCl gas, which was sorbed strongly and irreversibly above 100°C in amounts ranging from 40 to 100% of the full stoichiometric NaOH content required by the formula $3(Na_2O.Al_2O_3.2SiO_2).2NaOH$. Sodium chloride and a considerable amount of water appeared in the crystals after this sorption.

2.5. The Silver Nitrate Occlusion Compound of the Zeolite Sodium A, $AgA(AgNO_3)$.

The preparation and structure of this compound have been described by Barrer and Meier[16,78,80]. The occlusion compound is a derivative of the cubic zeolite 'sodiumA'. The structure and properties of this zeolite were determined independently by Barrer and Meier and Breck and co-workers[81,82], whose conclusions are in agreement. Meier established the formula as $Na_2O,Al_2O_3,2SiO_2,0.14NaAlO_2,4.77H_2O$. The lattice constants of the hydrated and anhydrous materials are 12.27 and 12.25 Å respectively. The density of 2.01 gm/cm^3 showed the unit cell to consist of 5.9 of the

above formula units and it therefore contains 12 Si, 12 Al, 48 O and 12 Na ions, one molecule $NaAlO_2$ and water.

The structure of the framework is illustrated in Fig. 9. The $(Al,Si)O_4$ tetrahedra form four, six and eight membered rings. The free diameter of the eight membered rings is 4.2 ± 0.2 Å, that of the six membered 2.5 ± 0.2 Å and the main channels formed have a diameter of 4.2 Å. There are three types of cages; the largest, which can hold an inscribed sphere of 11.4 Å diameter, linked by eight membered rings, form the main channels in the direction of the crystal axes. The free diameter of the apertures connecting these cages is 4.2 Å. The smaller cages are of the sodalite type (Fig. 1) and contain a permanently occluded molecule of $NaAlO_2$. The smallest cage which is entirely made up of four membered rings is too small to contain cations. Since each unit cell contains one large and one sodalite cage, there is one $NaAlO_2$ molecule per unit cell. The hydrated material contains twenty-eight water molecules per large cage.

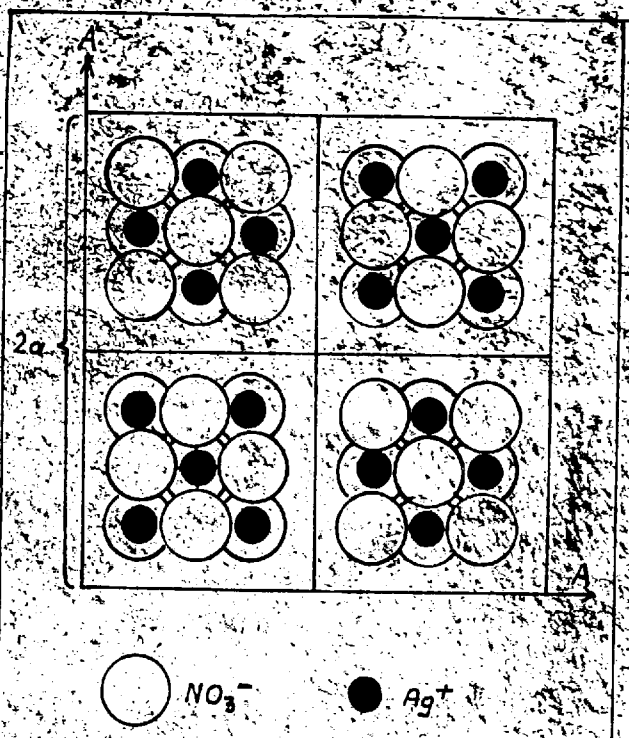
Breck found that eight of the monovalent cations are at the centres of the six membered rings and the remaining four are assumed to be statistically distributed in twelve positions within the eight membered rings.

As is to be expected this zeolite exhibits a wide variety of sorption and ion-exchange properties.

By heating sodium A with excess of low melting alkali nitrates above their melting point, the water molecules can be replaced by alkali nitrate, with formation of the occlusion compound. At the same time the cations of the zeolite are replaced by the cations of the alkali nitrate. $AgA(AgNO_3)$ so prepared contains 9 $AgNO_3$ molecules per large cage. X-ray powder photographs of the compound show superstructure lines which indicate an ordered arrangement of

the occluded $AgNO_3$ molecules. The new unit cell is now tetragonal, its lattice constant having doubled in two directions, i.e. if a is the cell constant of AgA, then A = 2a and C = a for the occlusion compound. The only sterically possible arrangement of $AgNO_3$ molecules which would show this superstructure is a parallel arrangement of the $AgNO_3$ molecules, with neighbouring molecules in opposite senses (Fig. 10). Thus the aggregates of neighbouring cages are polarised in opposite senses and Meier suggested that this structure might be antiferroelectric.

Meier found it impossible to prepare inclusion compounds which are completely filled but at the same time completely free of adherent $AgNO_3$, since small amounts of the guest molecule are easily extracted on washing. In fact his average sample contained 9.15 $AgNO_3$ molecules per unit cell. It is thus clear that there is almost certain to be either a defect in the occluded structure or extraneous $AgNO_3$. AgA had a unit cell constant of $a = 12.28$ Å and this expanded by 0.9% in the occlusion compound.



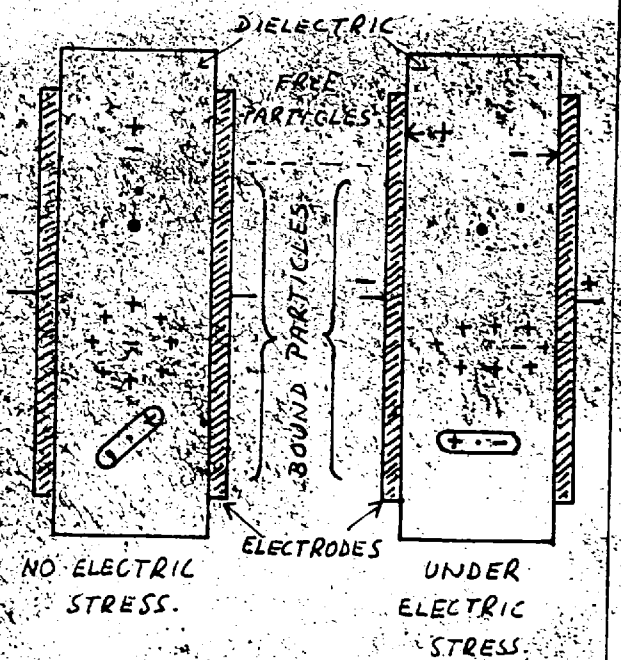
Ag^+ and NO_3^- ions in the large cages of $AgA(AgNO_3)$.

FIG. 10.



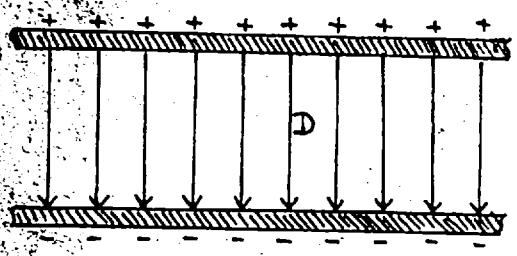
TYPICAL DISPERSION CURVE.

FIG. 13.



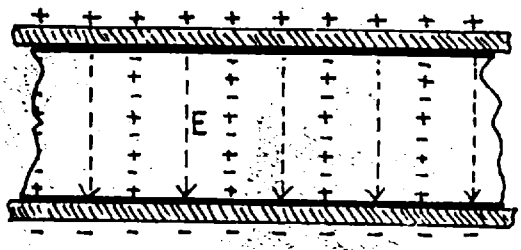
CHARGED PARTICLES IN A DIELECTRIC.

FIG. 11.



NO DIELECTRIC

FIG. 12.a.



WITH DIELECTRIC

FIG. 12.b.

3. DIELECTRICS AND DIELECTRIC THEORY.

3.1. Dielectrics and their Properties.

Most dielectrics or insulators are complex compounds often of variable constitution. Their chemical stability is less than that of conductors and electrical breakdown is nearly always due to insulation failure. Their importance is based on the fact that the life of electrical apparatus is governed by that of the insulation.

All electrical properties must ultimately be defined in terms of the motion of particles carrying a charge of electricity, the unit positive and negative charges being carried by protons and electrons respectively.

Dielectrics have four fundamental properties: conductivity, permittivity, dielectric loss and electric strength[1].

(a) Conductivity. Conductivity is measured by the electric current caused by the flow of charged particles, which are free to move under the influence of an e.m.f. (Fig. 11). In metals these particles are the electrons, but other materials may contain different carrier particles which are either free to move or can be freed by small electric stresses. The ideal dielectric containing no carriers is never achieved. The conductivity of metals decreases with rise in temperature and is independent of voltage, while in dielectrics a rise in temperature increases conductivity and a rise in voltage may also do so, in both cases by favouring molecular dissociation.

(b) Permittivity. In addition to free charged particles, dielectrics contain bound charges which can be elastically displaced by an e.m.f. thus an electron orbit may be distorted, a negative ion may deform but not pierce a surrounding shell of positive ions or a polar molecule may

be aligned (relaxation) but not displaced (Fig. 11). This displacement of bound particles during deformation or relaxation constitutes a flow of electric charge. The arrangement of two electrodes separated by a dielectric, which is called a condenser, is frequently used to store d.c. electricity or transmit energy from an a.c. source. The amount of electricity stored or transmitted is proportional to the electric displacement of the bound particles. The permittivity or dielectric constant of a material is the number expressing the magnitude of this displacement. Whether a material of high or low permittivity is desirable depends on its application.

(c) Dielectric loss. The movement of charged particles in a dielectric is opposed by internal, sometimes viscous forces, and heat is therefore developed. This heat energy cannot be recovered electrically and is called the dielectric loss. Its magnitude is expressed by the power factor, which is the ratio of the current associated with the energy absorbed as heat to the total current supplied to a condenser used for transmitting energy. The power factor varies with temperature and frequency of the a.c. e.m.f. It is obvious that good dielectrics should have low power factors.

(d) Electric strength. Permittivity, conductivity and dielectric loss are properties of a dielectric when the voltage applied is below a certain limiting value. For higher voltages a new set of mechanisms becomes operative, the material suddenly produces a large number of carrier particles and ceases to be a dielectric. The e.m.f. measured at the limiting value is the breakdown voltage and the voltage gradient the electric strength. In gases and liquids breakdown may be caused by ionisation through collision and in liquids and solids by impurities which may ionise. Local weak spots may also be the cause in solids.

The a.c. voltages employed in this work are always very low and electric breakdown has no bearing on the results. The d.c. conductivity has been measured by other authors and its contribution to the dielectric losses is either negligible or can be accounted for in our species, over the frequency ranges employed. Thus only permittivity and dielectric loss, which it was hoped would give the most valuable information, are further considered. Since the work concerns solids, the theory and properties of dielectric gases and liquids are only dealt with in detail when this affects solid theory.

In commercial insulation it is important that the dielectric loss and permittivity peaks which are found in liquids and solids are outside the working range. However these temperature dependent peaks give useful information about the molecular processes thought to be their cause. For instance in liquids the temperature at which the peak occurs may depend on dipole orientation and inner viscosity. They show no dipole component to dielectric constant or loss at very low temperatures because the dipoles are immobilised. As viscosity of the liquid decreases with rise in temperature the permittivity increases to a maximum value as the dipoles respond to the field; after which thermal agitation hinders dipole orientation causing permittivity to decrease. Similarly the dielectric loss of the liquid increases as displacement amplitude increases with temperature. When the maximum displacement has taken place the dielectric loss decreases, since the viscous friction continues to lessen with temperature. At a much higher temperature the loss will again rise when dipole orientation is opposed by thermal agitation. The frequency dependence of the maxima is explained by the fact that displacement against a viscous force is proportional to the time of application of the voltage in one direction.

The electrical behaviour of a substance is a function of its electronic structure. The more firmly an atom holds its electrons (and this depends on the nucleus-electron distance, the number of electrons in the shell and the shielding effect of lower shells) the better will be its insulating properties. Thus the elements in the top right hand triangle of the periodic table should be the best dielectrics.

Electrovalent compounds which may split into ions in presence of moisture, or polar molecules, give rise to comparatively high dielectric loss and permittivity. Coordinate links contribute to dielectric loss and permittivity because they are electrically assymetrical. Covalent links give rise to non-polar compounds and do not increase permittivity or dielectric loss.

As a first approximation the electrical properties of a single molecule are a function of those of the constituent atoms. Thus molecules containing atoms with easily distorted electron orbits will have polar moments due to deformation, unless in molecule building new forces control the loosely bound electron. Polar groups, unless symmetrically positioned in a molecule, cause polar moments. Generally molecular complexity in solids favours dielectric properties by limiting orientation and ionic mobility.

Good dielectrics must be free from polar liquids which give polar properties and ionise electrolytes. Thus absorption of and permeability to water vapour must be low and electrolytes should be eliminated even as impurities. Heterogeneity from which all composite dielectrics suffer is also a cause of dielectric loss and thus non-polar impurities of a different permittivity must be avoided. In some cases this heterogeneity may however be used to obtain large permittivities (barrier layer dielectrics).

Amongst solid dielectrics the inorganic type have a number of inherent advantages. Resins are difficult to produce without polar inclusions or have low softening points; in varnishes solvent elimination produces great problems, rubber ages and wood, textiles, paper and other organics are all limited in their heat resistance. The mineral type of inorganic dielectric seems to have great scope, provided it can be produced pure, both to replace less pure natural materials and for use in composite ceramic type dielectrics. At the moment the search is going on for good dielectrics incorporating some other unusual property, such as the absence of a temperature coefficient of expansion. Such a dielectric would be useful for ceramics.

The theory of dielectrics and electric polarisation in general is summarised in books by Böttcher[83] and Fröhlich[84], which have been used as the basis of the following discussion.

3.2. The Theory of Electric Polarisation.

3.2.1. The Static Dielectric Constant.

The dielectric constant of a substance in an a.c. field depends on frequency and on parameters which define the state of the material, such as temperature. It is independent of the strength of the electric field over a wide range, which is the range considered here. Below a certain critical frequency which depends on temperature and the structure of the dielectric, the dielectric constant is also independent of frequency and equals the static dielectric constant ϵ_s.

When a dielectric is brought into a field, displacement and separation of charges occurs within the dielectric, i.e. polarisation, and the resulting field strength $\bar{E}$ inside the dielectric is given by

$$\bar{D} = \epsilon_s \bar{E} \qquad (1)$$

where $\bar{D}$ = the dielectric displacement and $\bar{E}$ = the field intensity or field strength. The bars indicate vector quantities.

The physical picture of this process can be given in reference to Figs. 12a and b. An ideal parallel plate condenser with surface charge density σ is considered. In vacuum the electric field strength between the plates is given by

$$D = 4\pi\sigma \qquad \text{(Fig. 12a)} \qquad (2)$$

Thus D is defined in terms of the true charges and is independent of the medium between the plates; i.e. in vacuum:

$$D = E = \text{field strength between the plates } (= 4\cdot\pi\sigma) \qquad (3)$$

$$\text{The voltage between the plates} = V = |E|\, d \qquad (4)$$

where d = the distance between the plates.

On introduction of a dielectric the voltage decreases and the ratio of its former value to the present one is denoted by the static dielectric constant ϵ_s. Since (4) still holds, the electric field strength also decreases by a factor ϵ_s to

$$E = 4\pi\sigma/\epsilon_s \qquad (5)$$

This drop in field strength is equivalent to reducing the surface charge density by $P = \sigma\frac{(\epsilon_s - 1)}{\epsilon_s}$ (6)

Thus the influence of the field is to charge the surfaces of the dielectric with a charge density, P, in a sense opposite to that of the condenser plates. P, the polarisation arises from the displacement of charges within the dielectric

and equals the total charge passing through any unit area parallel to the plates within the dielectric. These surface charges cannot be removed from the dielectric but compensate charges of opposite sign on the condenser plates. Thus there is a field $4\pi P$ in opposite sense to the field D within the dielectric (Fig. 12b). The resulting field within the dielectric is E, i.e.

$$D = E + 4\pi P \tag{7}$$

and from (3), (4) and (5)

$$D = \epsilon_s E \tag{1a}$$

The dielectric constant of a material is usually defined in terms of capacitance, since this is the quantity measured except at very high and very low frequencies. A conductor charged with a quantity of electricity q at potential V has a capacitance C given by

$$C = q/V \tag{8}$$

The dielectric constant of a medium is then defined by

$$\epsilon = C/C_o \tag{9}$$

where C refers to the medium and C_o to vacuum between the condenser plates. It must now be shown that ϵ in equation (9) equals ϵ_s.

According to equation (8), $C_o = q/V_o$ and $C = q/V$, where $V < V_o$. Therefore using equation (9), $\epsilon = C/C_o = (q/V)(V_o/q) = V_o/V$; but since $V = |E|\,d$, $\epsilon = (E_o d)/(Ed) = E_o/E = \epsilon_s$ because $E_o = D$ by definition.

Equations (2) to (9) were derived for the ideal case of homogeneous field quantities (D,E,P) perpendicular to the parallel condenser plates. The equations are however quite general and correct as long as the field quantities are in the same direction. This is usually expressed by using vector quantities. Böttcher for instance

defines $\overline{P}$, the electric polarisation as the induced dipole moment per unit volume of the dielectric, then

$$\overline{D} = \overline{E} + 4\pi \overline{P} \qquad (7a)$$

and using equation (1):

$$\overline{P} = \frac{\varepsilon - 1}{4\pi} \overline{E} = \chi \overline{E} \qquad (10)$$

where χ is the dielectric susceptibility.

3.2.2. Polar Dielectrics at Low Frequencies.

ΔV, the average moment of a volume element ΔV, caused by a uniform a.c. field, is due to four effects.

(a) Permanent dipole orientation, which is connected with the rotational energy of a molecule, and is designated by a dipole moment μ.

(b) The axis of highest polarisability of an anisotropic particle is aligned with the field. This may be neglected at moderate field strength.

(c) Electronic polarisation: the electrons are shifted relative to the positive charges. This is associated with electronic transitions.

(d) Atomic polarisation: atoms or atom groups are displaced relative to each other and therefore atomic polarisation is associated with molecular vibrations.

(a) and (b) are the rotation or orientation effects which are counteracted by thermal movement and are therefore temperature dependent. (c) and (d) are the translation or deformation effects which are only slightly temperature dependent because they are intra-molecular.

The translation effects are usually expressed in terms of the average polarisability, α, of a particle. The anisotropy of polarisability is neglected here, because

of the polycrystallinity of most dielectrics, and α therefore becomes the mean polarisability. α, which has the dimensions of a volume is defined with the aid of the induced dipole moment, m, which is the difference of the dipole moment of a polarisable body before and after application of a uniform field E_o in vacuo, by

$$\bar{m} = \alpha \bar{E}_o \qquad (11)$$

since m is generally proportional to E_o.

The purpose of dielectric theory is to relate the molecular quantities (dipole moment, polarisability and radius) to measurable quantities (ϵ, refractive index, density). In this, polarisation is the link.

$$\bar{P} = \bar{P}_\alpha + \bar{P}_\mu \qquad (12)$$

where P_α is due to translation effects and P_μ to dipole orientation. These two quantities can be expressed in terms of the molecular quantities α and μ, and the field acting on the particle. Böttcher set up a general fundamental equation:

$$\frac{\epsilon - 1}{4\pi} \bar{E} = \sum_k N_k \left[\alpha_k (\bar{E}_i)_k + \frac{\mu_k^2}{3kT} (\bar{E}_r)_k \right] \qquad (13)$$

where the subscript k refers to the kth kind of particle, N = number of particles per cm^3, E_i = internal field = average field strength acting on the particle and E_r = directing field. The problem resolves itself into the calculation of these fields from dielectric models. The difficulty of this increases the more condensed the dielectric phase, and in the case of solids the theory is still in its infancy. The difference between the two fields is due to the reaction field, R^*, of the dipole. A dipole polarises the particles around it and the field produced at the dipole due to this polarisation of the surroundings is the reaction field. As long as this polarisation follows the dipole without

measurable lag, the reaction field does not contribute to dipole orientation and therefore

$$E_i = E_r + R^{\infty} \qquad (14a)$$

However, this may be only true for electronic polarisation. In other cases the difference, $E_i - E_r$, may be somewhat less than R^{∞}. In all older theories E_r and E_i are taken as equal, which Onsager[85] showed to be incorrect, except for gases at low pressures. Lorentz[86] considering the surroundings of the dipole as a continuum, derived a formula for E_i which is an average over the whole dielectric. It can however be shown that E_i has a different value in different parts of the dielectric. This can be taken into account in calculations by statistical mechanics, which however at present lead to unsurmountable difficulties even in the case of polar liquids.

Substitution of the Lorentz field

$$\bar{E}_i = \frac{\epsilon + 2}{3} \bar{E} \qquad (14)$$

in equation (13) and the assumption $E_r = E_i$ leads to the famous Debye equation[87]:

$$\frac{\epsilon - 1}{\epsilon + 2} = \frac{4}{3}\pi \sum_k N_k \left(\alpha_k + \frac{\mu_k^2}{3kT}\right) \qquad (15)$$

which describes the behaviour of polar gases in static and low frequency a.c. fields. This equation holds fairly well for gases at normal and lower pressures since then $\epsilon \approx 1$ and the Lorentz field is a good approximation. It also holds well for gas mixtures of greater density if the concentration of permanent dipoles is low. The equation can be used for the determination of μ and α of gases, but when used for measurements on dilute solutions of a dipolar compound in a non-polar solvent it becomes somewhat inaccurate.

Onsager[85] obtained the equation:

$$\mu^2 = \frac{9\ kT}{4\pi N} \frac{(\epsilon - n^2)(2\epsilon + n^2)}{\epsilon(n^2 + 2)^2} \qquad (16)$$

by substituting theoretical values of E_r and E_i in equation (13), using the Lorenz-Lorentz equation (see later) to give a value for the polarisability and assuming the molecules fill up the entire volume. This takes long range dipole interactions into account. The equation can be used for the calculation of μ from measurements on pure dipole liquids.

Recently Buckingham[88] has derived a general expression for ϵ_s by classical statistical mechanics, which includes the effect of short range directional forces. When these forces are zero the equation reduces to Onsager's. Application of the Buckingham equation to experimental results of some liquids, including water has given satisfactory results.

The Debye equation for a pure compound can be expressed as

$$[P] = \frac{4}{3}\pi N_a \left(\alpha + \frac{\mu^2}{3kT}\right) \qquad (15a)$$

where N_a is the Avogadro number and $[P]$ is a scalar with the dimensions of a volume and called the molar polarisation, defined by

$$[P] = \frac{\epsilon - 1}{\epsilon + 2} \frac{M}{d} \qquad (15b)$$

where d = density and M = molecular weight. In the case of a mixture, M becomes the average molecular weight given by

$$M = \sum_k x_k M_k. \qquad (15c)$$

where x_k are the molar fractions of the components of molecular weight M_k.

In case of a mixture equation (15) can be written:

$$[P] = \frac{4}{3}\pi N_a \sum x_k \left(\alpha_k + \frac{\mu_k^2}{3kT}\right) \qquad (15d)$$

since $N_k = x_k \frac{d}{M} N_a$, where M = average molecular weight,

$$\text{or } [P] = \sum_k x_k [P]_k \qquad (15e)$$

where $[P]_k$ is the molar polarisation of component k. According to these equations the molar polarisation of a compound at a given temperature is independent of the pressure, and that of a mixture equals the sum of the molar polarisations of the components. Also each component contribution can be divided into molar orientation, atomic and electronic polarisations. This idealised constancy of the molar polarisation however only holds as long as the Debye equation agrees with experiment.

3.2.3. Non-polar Dielectrics in a Static or Low-frequency a.c. Field.

For a non-polar compound the Debye equation simplifies to the Clausius-Mosotti equation[89,90]

$$\frac{\epsilon - 1}{\epsilon + 2} = \frac{4\pi}{3} \sum_k N_k \alpha_k \qquad (17)$$

Here the deviation caused by use of the Lorentz internal field is less than in the Debye case, since there is no large variation of E_i caused by the reaction field. The Clausius-Mosotti equation is thus a good approximation for non-polar dielectrics and holds well for gases at moderate pressures and for the less polarisable molecules even at high pressures. The molar polarisation for only one kind of particle becomes:

$$[P] = \frac{4}{3}\pi N_a \alpha \qquad (18)$$

From equation (17) for a single component, it can be seen that as long as α is independent of the pressure, ϵ increases much faster than linearly with the density d. For a density d_c corresponding to N_c given by $\frac{4}{3}\pi N_c \alpha = 1$, ϵ would be infinite, and negative for $d > d_c$. To fulfil this condition, $\frac{4}{3}\pi\alpha$ must be larger than the volume of a particle, since there are interstices between the particles. α is at most r^3 (r = radius of particle), in the case of a conducting sphere and thus the critical value is never reached in the case of gases and liquids. This value may however be reached by solids where the crystal lattice makes a contribution to the polarisability.

For a mixture, the Clausius-Mosotti equation is expressed as

$$\frac{\epsilon - 1}{\epsilon + 2} = \sum_k Q_k \frac{\epsilon_k - 1}{\epsilon_k + 2} \qquad (19)$$

where Q_k = volume fraction of component k. Mixtures of non-polar liquids deviate somewhat from this formula.

Deviations of the Clausius-Mosotti equation, noticed for gases at high pressures and for liquids, may be based on the pressure and temperature dependence of α but certainly on the use of the Lorentz internal field. Using an improved internal field formula the corrected Clausius-Mosotti equation, which agrees with experiment even at high pressures except for molecules with large $\frac{\alpha}{a^3}$, is obtained:

$$\frac{(\epsilon - 1)(2\epsilon + 1)}{12\pi\epsilon} = \sum_k N_k \alpha_k^{\#} \qquad (20)$$

with $\alpha_k^{\#} = \frac{\alpha_k}{1 - f_k \alpha_k}$ and $f_k = \frac{1}{a_k^3} \frac{2\epsilon - 2}{2\epsilon + 1}$

where a_k = radius of particle k.

Equation (20) allows determination of polarisabilities, which for small molecules (CO_2, CCl_4, etc.) are found to be of the order of 3 to 10 $\mathring{A}^3$. Many ions have polarisabilities between 0.3 and 3 $\mathring{A}^3$; very small ions, particularly those with large positive charge (Li^+, Be^{++}, Al^{+++}) have polarisabilities less than 0.1 $\mathring{A}^3$. Large molecules may have polarisabilities of 100 to 1000 $\mathring{A}^3$ and higher.

3.2.4. Equations developed by Statistical Mechanics.

In the theories summarised so far, the environment of the particle was treated as a continuum as by Bell[91]. The statistical mechanics approach accounts for fluctuations in the particle arrangements and is therefore preferable. The statistical theory of liquids has not yet been developed far enough to be applied to this problem. Kirkwood's[92] theory for instance can so far only be used for gases and then leads to the same result as the non-statistical method (Böttcher, p. 227).

Fröhlich[93] derived his general equation for any substance by using statistical mechanics and the 'Lorentz cavity field'. His treatment is a generalised Kirkwood method for dipolar liquids and the resulting dielectric constant depends on the structure of the material:

$$\epsilon_s - 1 = \frac{4\pi N_o}{3} \times \frac{2\epsilon_s}{2\epsilon_s + 1} \times \frac{\overrightarrow{mm^*}}{kT} \qquad (21)$$

where $N_o = N/V$ = number of unit cells per unit volume, m^* = the average dipole moment of a large spherical region volume V inside the specimen, polarised by one of the dipoles of moment m, and $\overrightarrow{mm^*}$ = average value of this product over all possible configurations, weighting them according to the probability of finding the dipole in such a configuration. Since the dielectric constant of crystals depends on the structure, no further general development can be given.

However, the equation can be extended by treating the electronic contribution on a macroscopic basis and it then becomes:

$$\epsilon_s = n^2 = \frac{3\epsilon_s}{2\epsilon_s + n^2} \times \frac{4\pi N_o}{3} \times \frac{\overline{mm^x}}{kT} \qquad (22)$$

where n = optical refractive index.

The general equations (21) and (22) represent ϵ_s in terms of the quantities $\overline{mm^x}$ which refer to the properties of the material in the absence of the field. Their calculation requires knowledge of the structure of the substance and of the particle interactions involved. This is generally done by use of approximations which then define the validity of the result. For liquids and gases equation (21) reduces to the Onsager, Clausius-Mosotti and Kirkwood equations.

Powles has extended the Fröhlich equation to anisotropic materials(94).

3.2.5. The Complex Dielectric Constant.

The dielectric theory considered so far has been concerned with conditions under which the polarisation does not lag behind the oscillation of the a.c. field. In this case ther is no phase difference between $\overline{D}$ and $\overline{E}$ and no energy is dissipated. At higher frequencies, which depend on the temperature and the type of material, the polarisation lags behind the a.c. field and there is a noticeable phase difference between $\overline{D}$ and $\overline{E}$ and thus also between $\overline{P}$ and $\overline{E}$. Then the relations 1 and 9 no longer apply and energy is absorbed by the dielectric from the electromagnetic field. This phenomenon is called dielectric loss.

An a.c. voltage applied to the condenser plates leads to a periodic a.c. field:

$$\bar{E} = \bar{E}_0 \cos\omega t \qquad (23)$$

where $\bar{E}_0$ = amplitude, ω = angular frequency and t = time. When $\bar{D}$ is in phase with $\bar{E}$

$$\bar{D} = \bar{D}_0 \cos\omega t \qquad (24)$$

The energy dissipated in the dielectric per cm^3 is given by:

$$W = \frac{\omega}{2\pi} \int_0^{2\pi/\omega} \bar{i}\,\bar{E}\,dt \qquad (25)$$

where $i = \partial\sigma/\partial t$ = electric current density; since $D = 4\pi\sigma$,

$$\bar{i} = \frac{1}{4\pi}\frac{\partial \bar{D}}{\partial t} = -\frac{\omega}{4\pi}\bar{D}_0 \sin\omega t \qquad (26)$$

Thus $\bar{i}$ and $\bar{E}$ are $\pi/2$ out of phase. Substituting (26) in (25):

$$W = -\frac{\omega^2}{8\pi^2}\bar{D}_0\,\bar{E}_0 \int_0^{2\pi/\omega} \sin\omega t \cos\omega t\,dt = 0$$

i.e. no energy is dissipated in the dielectric.
When there is a phase difference between $\bar{D}$ and $\bar{E}$, then for $\bar{E} = \bar{E}_0 \cos\omega t$, $\bar{D}$ is given by

$$\bar{D} = \bar{D}_0 \cos(\omega t - \delta) = D_0 \cos\omega t \cos\delta + D_0 \sin\omega t \sin\delta \qquad (27)$$

Substituting (27) in (26) gives

$$\bar{i} = -\frac{1}{4\pi}\bar{D}_0 \sin\omega t \cos\delta + \frac{\omega}{4\pi}\bar{D}_0 \cos\omega t \sin\delta \qquad (28)$$

The first part of (28) is $\pi/2$ out of phase with $\bar{E}$ and therefore does not lead to energy loss. The second part is in phase with $\bar{E}$ and using this part:

$$W = \frac{\omega^2}{8\pi^2} \bar{D}_o \bar{E}_o \sin\delta \int_0^{2\pi/\omega} \cos^2\omega t \, dt \qquad (29)$$

Therefore the dissipated energy per cm^3 of the dielectric per second = $W = \frac{\omega}{8\pi} \bar{D}_o \bar{E}_o \sin\delta$; (30)

$\sin\delta$ is called the power factor.

When there is a phase difference between $\bar{D}$ and $\bar{E}$, the relationship between the scalars D and E is usefully described by complex quantities. Then

$$\hat{E} = E_o e^{j\omega t} = (\cos\omega t + j \sin\omega t)E, \qquad (31)$$

The field intensity E is the real part of $\hat{E}$ and therefore D is the real part of (see equation 27)

$$\hat{D} = D_o e^{j(\omega t - \delta)} \qquad (32)$$

As long as the loss angle δ is independent of E (still depending on frequency, temperature, chemical composition and structure of the material however), the ratio between $\hat{D}$ and $\hat{E}$ is given by a complex dielectric constant $\hat{\epsilon}$:

$$\hat{D} = \hat{\epsilon} \hat{E} \qquad (33)$$

From (31, (32) and (33):

$$\hat{\epsilon} = \frac{\hat{D}}{\hat{E}} = \frac{D_o}{E_o} e^{-j\delta} = |\epsilon| e^{-j\delta} = \frac{D_o}{E_o}(\cos\delta - j \sin\delta) = |\epsilon| (\cos\delta - j \sin\delta) \qquad (34)$$

where $|\epsilon|$ is the modulus of $\hat{\epsilon}$. The complex quantities $\hat{D}$ and $\hat{E}$ have been defined in such a way that when $\delta = 0$, $\hat{\epsilon} = \epsilon$. $\hat{\epsilon}$ can be split into real and imaginary parts by introducing the real quantities ϵ' and ϵ'':

$$\hat{\epsilon} = \epsilon' - j\epsilon'' \qquad (35)$$

From (34) it follows that

$$\epsilon' = \frac{D_o}{E_o} \cos\delta = |\epsilon| \cos\delta \qquad (36)$$

and

$$\epsilon'' = \frac{D_o}{E_o} \sin\delta = |\epsilon| \sin\delta \qquad (37)$$

Dividing (37) by (36)

$$\frac{\epsilon''}{\epsilon'} = \tan\delta \qquad (38)$$

Tan δ at a certain frequency is often used to indicate the dielectric loss; it is called the dissipation factor and for small δ approximates to the power factor.

Combination of (30) and (37) gives:

$$W = \frac{\omega E_o^2}{8\pi} \epsilon'' = \frac{\omega E_o^2}{8\pi} |\epsilon| \sin\delta \qquad (39)$$

This equation shows that the dissipated energy per cm^3 per second is proportional to ϵ'' and thus to $\sin\delta$. ϵ'' is called the loss factor.

Mansel Davies[95] showed that

$$\epsilon = \epsilon' - 2j\sigma/f \qquad (40)$$

where σ = conductivity in e.s.u. and $\omega = 2\pi f$ = frequency in cycles per second, and therefore

$$\epsilon'' = 2\sigma/f = 1.80 \times 10^{12} K_f/f \qquad (41)$$

where K_f = the specific conductance at a frequency f in $ohm^{-1}\ cm^{-1}$.

It has already been mentioned that the phase difference between $\bar{D}$ and $\bar{E}$ is due to the polarisation lagging behind the field. Three different mechanisms may cause this lag:

(A) Electric conductivity giving a component of $\bar{I}$ in phase with $\bar{E}$ (see equation 41).

(B) Relaxation effects which occur at frequencies at which the orientation of the permanent dipoles cannot follow the field without measurable lag. Below this frequency limit, which depends on the chemical composition and structure of the material and the temperature, the field changes slowly enough to allow the dipoles to reach their equilibrium distribution before the field changes. In the case of water the frequency limit is 2×10^{9} sec^{-1}, but for larger polar molecules the limit is in the region of 10^{6} to 10^{7} sec^{-1}.

(C) Resonance effects caused by rotations and vibrations of atoms, ions or electrons are noticed in the infra-red, visible and ultra-violet regions near the characteristic absorption frequencies. Resonance effects are also caused by rotatory oscillations of dipoles (Fröhlich, p.98) with frequencies in the far-infra-red. Quantum mechanical description and the classical model of the harmonic oscillator lead to the same result for resonance effects.

It is important to get a clear physical picture of effects B and C. Whereas in C every charge is displaced elastically, it is wrong to assume that every dipole is turned from one equilibrium position to another. Actually the field first leads to contributions of type C and secondly slightly alters the probabilities of a rotational jump of a dipole.

Fröhlich[84] calculates the fraction of dipoles turned by a field, by considering a particle of charge e with two equilibrium positions separated by a distance b. In absence of an external field the particle has the same energy in the two positions. If in equilibrium with its surroundings, it will oscillate about one of the positions with an energy of the order of kT and will only occasionally, through fluctuations, acquire enough energy to jump over the

potential wall into the other position. Thus the probabilities of the particle being in either position will be equal. Introduction of a field alters the potential energy of the particle in the two positions and therefore also the probabilities. The particle is now more likely to be in one of the positions. The fraction of the dipoles turned by a field of reasonable strength is given by $\frac{1}{2}(p_B - p_A)$, where $(p_A - p_B)$ is the difference between the probabilities. Fröhlich states that the difference of the interaction energies of the particle in the two equilibrium positions with the external field is usually much smaller than kT. In this case, putting e = electronic charge, and b the distance between neighbouring atoms in a molecule as 10^{-8} cm at room temperature, the fraction of dipoles turned by the field of reasonable strength can be shown to be small, e.g. 10^{-4} in a field of 300 volts/cm and about 2% in a field of 100,000 volts/cm.

It remains to show how ϵ' and ϵ'' can be determined from the experimentally determined equivalent shunt resistance R_p and capacitance C_p, in terms of which the properties of every real condenser can be expressed[96]. This can be done by considering the phase lag in terms of the voltage applied and the current subsequently flowing.
$I = \omega C_o . V . \cos(\omega t + \pi/2)$ is the current flowing when an a.c. potential $V.\cos\omega t$ is applied to a vacuum condenser of capacitance C_o. The phase of this current is 90° in advance of the voltage. If the voltage is taken to be the real part of $Ve^{j\omega t}$, then the current is the real part of $j\omega C_o V e^{j\omega t}$ and the impedance = voltage/current if the circuit element is $1/j\omega C_o$. On introduction of a loss free dielectric, the element remains a pure capacitance which has now increased to C_p, the impedance becoming $1/j\omega C_p$ and the definition of ϵ follows as the ratio C_p/C_o.

When the dielectric is not loss free the current will lead the voltage by less than 90° and the component of the current in phase with the applied voltage causes the energy dissipation as heat. The circuit element can now be represented by C_p and R_p, giving an impedance $1/(j\omega C_p + 1/R_p)$. Both C_p and R_p are frequency dependent. Alternatively the impedance may be written in the form $1/(j\omega C_o \hat{\epsilon})$ when $\hat{\epsilon} = \epsilon' - j\epsilon''$. Equating the two equations for the impedance we find:

$$\epsilon' = \frac{C_p}{C_o} \qquad (42)$$

and

$$\epsilon'' = \frac{1}{\omega R_p C_o} \qquad (43)$$

therefore $\epsilon'' = \frac{\epsilon'}{\omega R_p C_p}$, i.e. $\tan\delta = \frac{\epsilon''}{\epsilon'} = \frac{1}{\omega R_p C_p}$ (44)

The measurement of C_p and R_p is convenient over the frequency range of 60 to 10^8 c/s.

3.2.6. The Refractive Index.

Maxwell in his theory of electromagnetic waves proved that

$$\epsilon = n^2 \qquad (45)$$

where n is the refractive index of a medium. This applies if there are no moving charges present in the medium, or if the movements of such charges are slow compared with the frequency independent velocity of the electromagnetic waves. Experiment showed that below a certain critical frequency ϵ is independent of frequency and equal to ϵ_s and n obeyed equation (45). The critical frequency depends on the chemical composition of the dielectric and the temperature. For instance in water n and ϵ are independent of frequency

and $n^2 = \epsilon$ below 2.10^9 sec^{-1}, while in non-polar materials $\epsilon_s = n^2$ of the cm-waves since loss due to resonance effects is mainly in the infra-red region.

In the frequency region where $\hat{\epsilon}$ must be used, n also depends on frequency and a complex refractive index is defined

$$\hat{\epsilon} = \hat{n}^2 \qquad (46)$$

which splits into real and imaginary parts:

$$\hat{n} = n' - jn'' \qquad (47)$$

n' is found to be the real refractive index/n, whereas n'' is related to the degree of damping of the wave. n'' can be expressed in terms of the absorption index $k = n''/n$, or by the absorption coefficient a, defined by Lambert's absorption law:

$$I/I_o = e^{-ax} \qquad (48)$$

where I_o = initial intensity of radiation and I = intensity after travelling distance x in the medium.

It can then be shown that $\epsilon' = n^2(1 - k^2)$ (49)

and $$\epsilon'' = 2n^2k \qquad (50)$$

The importance of the refractive index lies in the fact that its determination allows calculation of the atomic and electronic contributions to the polarisation, i.e. the contributions due to resonance effects. The dielectric loss due to these effects usually begins in the infra-red region and thus measurement of n or ϵ in the cm wave region gives the value of the total polarisability. Equation (17) can then be replaced by the Lorenz-Lorentz equation[97,98]

$$\frac{n^2 - 1}{n^2 + 2} = \frac{4}{3}\pi \sum_k N_k a_k \qquad (51)$$

and equation (20) by:

$$\frac{(\mathfrak{N}^2 - 1)(2n^2 + 1)}{12\pi n^2} = \sum_k \frac{N_k a_k}{1 - f_k a_k} \qquad (52)$$

with

$$f_k = \frac{1}{a_k^2} \frac{2n^2 - 2}{2n^2 + 1}$$

These two equations can be used to determine the total polarisability of polar compounds in a frequency region in which the dipoles cannot follow the field to a measurable extent and which is devoid of atomic resonance absorption. Usually these two absorption regions overlap and there is no region in which ϵ is independent of frequency and equals n^2. Equation (51) can then still be used and the total polarisability be obtained by extrapolation. This subject will now be considered.

In the region where the dielectric absorbs energy from the electromagnetic field, n depends on frequency, and the phenomenon is called dispersion. In the visible region this is of two types:

(a) Normal dispersion when n increases with increasing frequency;

(b) Anomalous dispersion when n decreases with increasing frequency. This always occurs near the characteristic frequency of maximum absorption and is stronger than normal dispersion.

Fig. 13 gives a typical dispersion curve.

The results obtained by the classical dispersion theory are similar to those from quantum mechanics, and give a good qualitative and sometimes quantitative description of the dispersion curves. The theory is based on the model of an elastically bound electron (harmonic oscillator) with

a characteristic frequency ν_o. Anomalous dispersion results from damped vibrations and equations have been set up for this case and for undamped vibrations. For such a resonance phenomenon without damping

$$\frac{n^2 - 1}{n^2 + 2} = \frac{N\epsilon_o^2}{3\pi m} \sum_k \frac{f_k}{\nu_{ok}^2 - \nu^2} \qquad (53)$$

in the case of gases at higher pressures, liquids and solids, when m = mass of electron and f_k = oscillator strength.

The total polarisability of a molecule may be split into two parts, α_e due to electronic and α_a due to atomic polarisability, i.e.

$$\alpha_{total} = \alpha_e + \alpha_a \qquad (54)$$

The two names are bad, since a displacement of atoms is always accompanied by an electron displacement which also appears in the infra-red region. It might therefore be better to name the polarisabilities by the region in which their absorptions appear.

The total polarisability of a non-polar compound is determined by measurement of the constant dielectric constant at low frequencies. With polar compounds this is only possible if there exists a region between the dipole and atomic polarisation absorption regions in which ϵ is independent of frequency. The two remaining problems namely calculation of α_{total} in the dipolar case when there is no such constant region, and the splitting of α_{total} into the atomic and electronic contributions can be solved by measuring the refractive index at different frequencies and extrapolating to infinite wavelength using a dispersion formula such as equation (53).

In this manner the total polarisability can be obtained by using frequencies below the lowest atomic

polarisation absorption when the influence of the absorption on n is not negligible, but when dipole absorption is negligible. n_{∞}^2 obtained by extrapolation is then the fictitious value the static dielectric constant would have if there were no permanent dipoles. α is obtained by substitution of n_{∞} in equation (51).

In the region of λ = 5000 to 8000 Å, the influence of the atomic absorption is negligible and that of the electronic absorption with frequencies in the violet and ultra-violet small. The extrapolation of n measured in the visible region to infinite wavelength then gives n_{∞}^{*} which is related to the electronic polarisability α_e by the Lorenz-Lorentz equation. Böttcher compares theoretically extrapolated refractive indexes with experimental values at various frequencies for some organic compounds and finds the third decimal place obtained reliable. It is interesting to note that the largest difference $n_D - n_{\infty}$ quoted (n_D = n sodium λ) is 1½% and usually this is much lower. Thus ϵ obtained from measurements at sodium light should at the most deviate 1 to 3% from values obtained by using n_{∞}^{*}.

The above methods allow an accurate enough estimate of the electronic polarisation from measurements in the visible spectrum. The atomic polarisation can then be found by the difference $\epsilon_s - n^2$ in the case of non-polar compounds and similarly when there is a constant ϵ region between the atomic and dipolar absorption regions in the polar case. The latter is rare and an accurate estimate of the atomic polarisation is then difficult. Only when the atomic polarisability is quite independent of temperature can α_{total} of polar gases be determined by use of the Debye equation, when this equation applies. The use of the Debye equation for a polar compound in dilute solution in a non-polar solvent and extrapolation to infinite dilution is also incorrect.

Actual measurement of n in the long wave infra-red is difficult and the extrapolation is inaccurate. Böttcher[99] suggests a comparison of the dipolar compound with a non-polar one of related structure and assumption of the same α_a/α_e ratio.

Since density and refractive index of a substance depend on temperature and pressure, attempts have been made to find a constant function independent of these parameters, the specific and molar refraction. Böttcher has shown that such an attempt is bound to fail. Nevertheless equations have been set up and used. The molar refraction is supposed to be additive in the case of mixtures, but Guggenheim[100] considers this to be only a rough approximation, proved neither by theory nor experiment. Thus the refractive index of a mixture should be measured whenever possible. The molar refraction of a compound is supposed to be additively built up from those of its constituent atoms, but this too appears to be an approximation, and the molar refraction must as a rule be considered to be a constitutive rather than an additive quantity.

3.2.7 Dielectric Loss and Relaxation Time.

The effect of the phase difference between $\overline{D}$ and $\overline{E}$ in the optical frequency range was shown in the last chapter. We now deal with high frequencies lower than the optical region, in which dielectric loss occurs. Loss in these regions is due to the relaxation effect of the permanent dipoles and can be described by a dielectric characterised by a relaxation time. This chapter deals mainly with liquids, but the same arguments apply to solids.

P_s, the polarisation at zero frequency, can be split into two parts, $(P_s)_{dip}$ due to permanent dipoles and P_∞ due to the polarisability, i.e.

$$P_s = P_\infty + (P_s)_{dip} \qquad (55)$$

$P_s = \frac{\epsilon_s - 1}{4\pi} E$ (equation 10) and $P_\infty = \frac{\epsilon_\infty - 1}{4\pi} E$ where $\epsilon_\infty = n_\infty^2$ and n_∞ refers to the total polarisability.

The time required for the permanent dipoles to reach an equilibrium distribution after application of the external static field depends on temperature, chemical composition and structure of the dielectric. It is of the order of 10^{-6} to 10^{-13} seconds and may be more in the case of solids. During this time $(P_s)_{dip}$ is built up and P increases from P_∞ to P_s, since the time required to establish P_∞ can be neglected relative to that required to build up $(P_s)_{dip}$. After time t during this interval

$$P_t = P_\infty + P_{dip} \qquad (56)$$

where P_{dip} is the part of $(P_s)_{dip}$ built up at time t. It is now assumed that the increase $d(P_{dip})/dt$ is proportional to the difference between the final value $(P_s)_{dip}$ and the actual value P_{dip}, i.e.

$$\frac{d(P_{dip})}{dt} = \frac{1}{\tau}\left\{(P_s)_{dip} - P_{dip}\right\} \qquad (57)$$

τ which has the dimension of time is a measure of the time lag, the relaxation time. At $t = 0$, $(P_{dip})_{t=0} = 0$ and therefore integration of (57) gives:

$$P_{dip} = (P_s)_{dip}\,(1 - e^{-t/\tau}) \qquad (58)$$

From decay of the polarisation, on the field being taken away, it is seen that τ is the time in which the polarisation decreases to $1/e^{th}$ part of its original value.

Two further assumptions are now made:

(1) the behaviour of the dielectric can be described by only one relaxation time, and

(2) equation (57) is also valid for an a.c. field. Then $(P_s)_{dip}$ is a function of t, being the value $(P)_{dip}$ would reach in a static field E_t, where E_t is the magnitude of the a.c. field at time t. Thus

$$(\hat{P}_s)_{dip} = \frac{\epsilon_s - 1}{4\pi} \hat{E}_t - \frac{\epsilon_\infty - 1}{4\pi} \hat{E}_t \qquad (59)$$

where $\hat{E}_t = E_o e^{jwt}$.

Equations (57) and (59) give

$$\frac{d\hat{P}_{dip}}{dt} = \frac{1}{\tau}\left[\frac{\epsilon_s - \epsilon_\infty}{4\pi} E_o e^{jw\tau} - \hat{P}_{dip}\right] \qquad (60)$$

The solution of which is

$$\hat{P}_{dip} = Ce^{-t/\tau} + \frac{1}{4\pi} \times \frac{\epsilon_s - \epsilon_\infty}{1 + jw\tau} E_o e^{jw\tau} \qquad (61)$$

$Ce^{-t/\tau}$ decreases to an infinitely small value after a short time and may be neglected.

Analogous to equation (55) we get

$$\hat{P} = \hat{P}_\infty + \hat{P}_{dip} = \left[\frac{\epsilon_\infty - 1}{4\pi} + \frac{1}{4\pi} \frac{\epsilon_s - \epsilon_\infty}{1 + jw\tau}\right] E_o e^{jw\tau} \qquad (62)$$

Thus P is a sine function of the time with the same frequency as the applied field and is retarded in phase with respect to E.

From equations (31) and (62)

$$\hat{D} = \hat{E} + 4\pi\hat{P} = \left[\epsilon_\infty + \frac{\epsilon_s - \epsilon_\infty}{1 + jw\tau}\right] E_o e^{jw\tau} \qquad (63)$$

and comparison with equation (33) shows that the complex permittivity is:

$$\hat{\epsilon} = \epsilon_\infty + \frac{\epsilon_s - \epsilon_\infty}{1 + jw\tau} = \epsilon_\infty + \frac{\epsilon_s - \epsilon_\infty}{1 + w^2\tau^2}(1 - jw\tau) \qquad (64)$$

Therefore

$$\epsilon' = \epsilon_\infty + \frac{\epsilon_s - \epsilon_\infty}{1 + w^2\tau^2} \tag{65}$$

and

$$\epsilon'' = (\epsilon_s - \epsilon_\infty) \frac{w\tau}{1 + w^2\tau^2} \tag{66}$$

These equations can also be written as:

$$\frac{\epsilon' - \epsilon_\infty}{\epsilon_s - \epsilon_\infty} = \frac{1}{1 + w^2\tau^2} \tag{65a}$$

$$\frac{\epsilon''}{\epsilon_s - \epsilon_\infty} = \frac{w\tau}{1 + w^2\tau^2} \tag{66a}$$

Plots of the left hand sides of equations (65a) and (66a) against $\log(w\tau)$ give the symmetrical curves of Figs. 14 and 15. The maximum of the absorption curve 15 is at $\log(w\tau) = 0$, i.e. $w\tau = 1$. Therefore the angular frequency at maximum absorption is given by:

$$w_m = \frac{1}{\tau} \tag{67}$$

Introducing $w\tau = 1$ into equations (65) and (66) gives the corresponsing maximum values ϵ'_m and ϵ''_m:

$$\epsilon'_m = \frac{\epsilon_s + \epsilon_\infty}{2} \tag{68}$$

and

$$\epsilon''_m = \frac{\epsilon_s - \epsilon_\infty}{2} \tag{69}$$

The cyclic frequency $f = w_m/2\pi$ which corresponds to the angular frequency w_m is called the 'critical frequency'. The corresponding wavelength λ_c, given by $\lambda_c = 2\pi c/w_m = 2\pi c\tau$, where c = velocity of light in vacuo, is the critical wavelength.

FIG. 14.

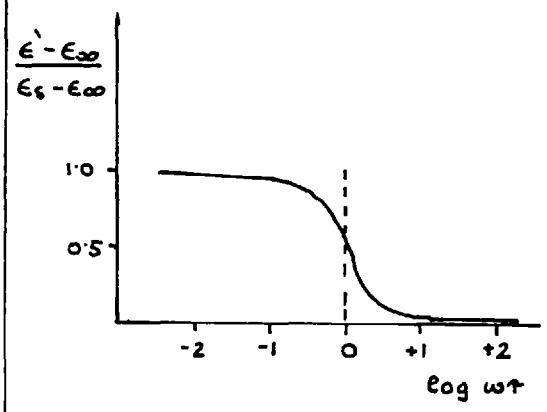
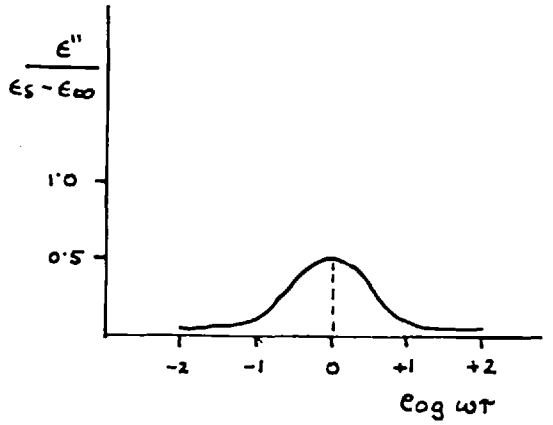
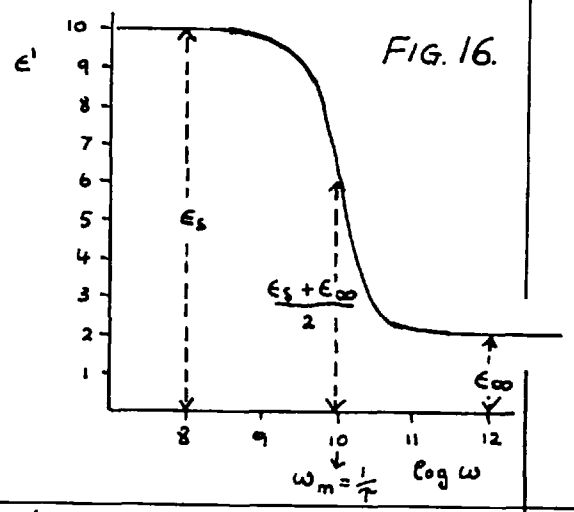


FIG. 15.



DISPERSION CURVE.

FIG. 16.



ABSORPTION CURVE.

FIG. 17.

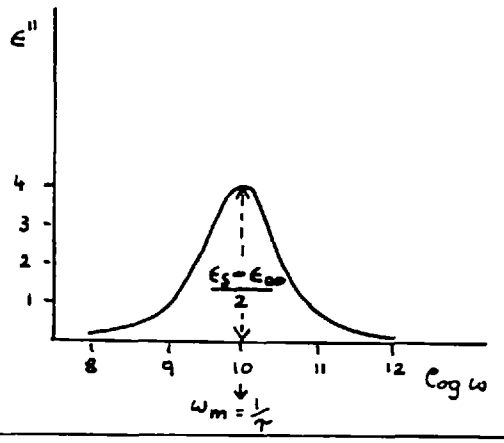


FIG. 18.

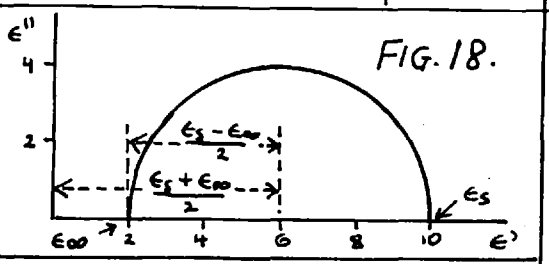


FIG. 19.

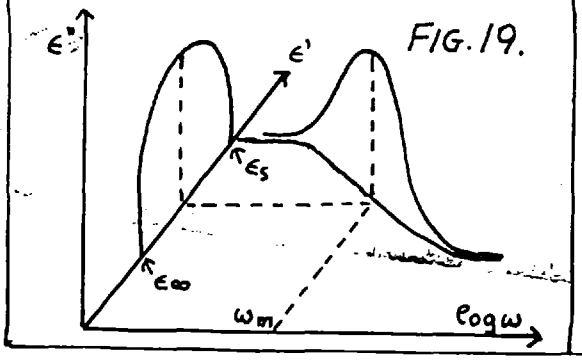
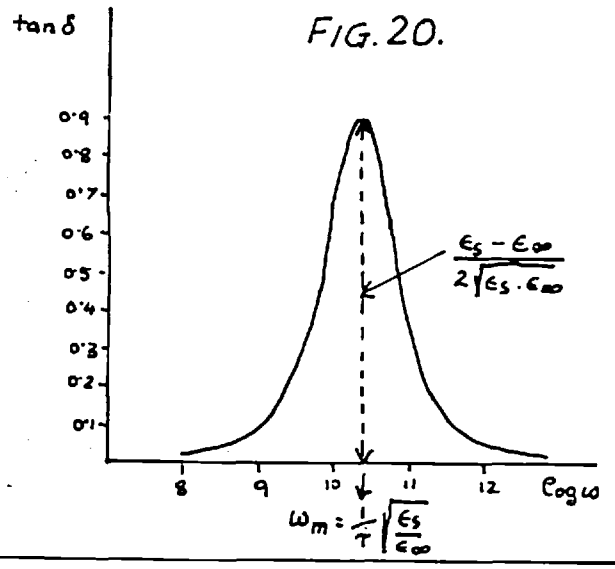


FIG. 20.



Equation (66) forecasts that ϵ'' approaches zero for small and high values of $w\tau$. Physically that means that at frequencies when $w\tau \ll 1$, i.e. well below the absorption maximum, equilibrium will be attained in a time which is short compared with the field alternation. Therefore the maximum permittivity is obtained and little energy is absorbed. At a frequency corresponding to $w\tau = 1$, the field reverses in a time comparable with τ, the polarisation has no time to build up to a maximum and the energy absorbed per cycle is a maximum. At frequencies when $w\tau \gg 1$ no significant dipole orientation can occur and therefore ϵ contains no contribution due to this polarisation.

The curves of ϵ' vs log w and ϵ'' vs log w (or log f) derived from equations (65) and (66) (Figs. 16 and 17) are also symmetrical. These curves for a dielectric with one relaxation time are called Debye curves, although Debye's contribution was actually the intrinsic relaxation time, to be mentioned later. The dispersion range moves to a lower frequency on lowering the temperature; ϵ_s and ϵ_∞ are also somewhat temperature dependent[101].

A strong decrease of ϵ' with decreasing temperature indicates dipole relaxation since when w is in the central part of the loss frequency region, ϵ' decreases strongly with decreasing temperature. This is because τ and therefore $w\tau$ increases with decreasing temperature. In the absence of dielectric loss ϵ of a polar liquid increases with decreasing temperature according to the term $\mu^2/3kT$ in the molar polarisation.

When ϵ_s, ϵ_∞ and w_m can be determined, the experimental curves can be compared with the theoretical ones calculated from equations (65) and (66). Cole and Cole have developed a method which does not require the knowledge of these parameters to compare results. They construct an

Argand diagram plotting ϵ'' against ϵ' for a number of frequencies in the dispersion region. From equations (65) and (66) we obtain:

$$\left(\epsilon' - \frac{\epsilon_s + \epsilon_\infty}{2}\right)^2 + (\epsilon'')^2 = \left(\frac{\epsilon_s - \epsilon_\infty}{2}\right)^2 \qquad (70)$$

Thus the Argand diagram describes a semicircle with radius $(\epsilon_s - \epsilon_\infty)/2$, its centre on the abscissa being at $(\epsilon_s + \epsilon_\infty)/2$ from the origin (Fig. 18). The intersections with the origin are at $\epsilon' = \epsilon_\infty$ and $\epsilon' = \epsilon_s$ respectively. The relation between Figs. 16, 17 and 18 is shown in Fig. 19. The Cole-Cole plot does not depend on the frequency range of the dispersion or the relaxation time when equations (65) and (66) are valid but is completely defined by ϵ_s and ϵ_∞. Cole[101] has suggested a treatment of experimental results which does not require a knowledge of ϵ_s and ϵ_∞. Multiplication of equation (64) by $(1 + jw\tau)$ and separation of real and imaginary parts gives:

$$\epsilon' = \epsilon_s - \tau(w\epsilon'') \qquad (71)$$

$$\epsilon' = \epsilon_\infty + \left(\frac{1}{\tau_o}\right)\left(\frac{\epsilon''}{w}\right) \qquad (72)$$

These are linear in ϵ', $w\epsilon''$ and ϵ''/w and thus ϵ_o, ϵ_∞ and τ can be obtained from the slopes and intercepts of their graphs. Alternatively a plot of C_p against G_p (parallel conductance) gives a straight line of slope $(-\tau)$ because C_p and G_p are proportional to ϵ' and $w\epsilon''$ for a dielectric with a single relaxation time. Systematic frequency independent measurement errors do not cause errors in this method, which is therefore better than the trial and error fitting of the original equations.

Experimental results are usually expressed in terms of $\tan\delta$. From equations (65) and (66)

$$\tan\delta = \frac{(\epsilon_s - \epsilon_\infty)\, w\tau}{\epsilon_s + \epsilon_\infty w^2\tau^2} \tag{73}$$

The maximum of $\tan\delta$ is obtained at a frequency

$$w_{m'} = \frac{1}{\tau}\sqrt{\frac{\epsilon_s}{\epsilon_\infty}} \tag{74}$$

and its value is given by:

$$(\tan\delta)_{max} = \frac{\epsilon_s - \epsilon_\infty}{2\sqrt{\epsilon_s \epsilon_\infty}} \tag{75}$$

The maximum values of $\epsilon'_{m'}$ and $\epsilon''_{m'}$ at $w_{m'}$ are:

$$\epsilon'_{m'} = \frac{2\epsilon_s \epsilon_\infty}{\epsilon_s + \epsilon_\infty} \tag{76}$$

and

$$\epsilon''_{m'} = \frac{\epsilon_s - \epsilon_\infty}{\epsilon_s + \epsilon_\infty}\sqrt{\epsilon_s \epsilon_\infty} \tag{77}$$

$w_{m'}$, $\epsilon'_{m'}$ and $\epsilon''_{m'}$ are different from w_m, ϵ'_m and ϵ''_m. The $\tan\delta$, log w curve is plotted in Fig. 20.

In the case of dielectric loss, a complex molar polarisation is defined by

$$[\hat{P}] = \frac{M}{d}\,\frac{\hat{\epsilon} - 1}{\hat{\epsilon} + 2} \tag{78}$$

A relaxation time τ^* of the molar polarisation for a.c. fields can be defined analogously to the definition of τ. τ^* is the intrinsic relaxation time of the individual dipole molecules in the medium and is related to τ the characteristic relaxation time of the medium by

$$\tau = \tau^* \frac{\epsilon_s + 2}{\epsilon_\infty + 2} \tag{79}$$

τ^* is only useful when the molar polarisation can be expressed in molecular quantities such as polarisability and permanent dipole moment, as for instance when the Debye

(eq. 15) or Onsager (eq. 16) equations are valid for a pure compound at sufficiently low frequencies. In these cases the complex molar polarisation is obtained from the static molar polarisation by replacing the term $\mu^2/(3kT)$ in the latter by $(\mu^2/3kT)(1/(1 + jw\tau^*))$.

Debye[103] connected the intrinsic relaxation time with the viscosity of a medium which hinders the rotary Brownian motion of the particle. He uses a spherical model with radius a and dipole μ at the centre, hindered by a continuous environment with viscosity η. He excludes saturation by supposing that $\mu E \ll kT$. The resulting equation is:

$$\tau^* = \frac{4\pi\eta a^3}{kT} \qquad (80)$$

Thus the relaxation time of the dipole molecule depends on its surroundings. Experiments with dilute solutions of dipole molecules in a non-polar solvent support this view, but show that (80) is only a rough approximation as would be expected from the simplified model used. Both η and T cause τ^* to decrease with increasing temperature. This is because the relative influence of the molecular interaction energy decreases with respect to that of the thermal energy as temperature increases. τ^* and η/T have a similar temperature dependence which is exponential, for instance, for liquids,

$$\tau^* = \frac{A}{T} e^{B/kT} \qquad (81)$$

where A and B are constants which are different in the equation for η/T.

This exponential temperature dependence has led to the consideration of dielectric relaxation as a chemical rate process[104,105,106,107]. It indicates that at some stage in the relaxation process a particle needs a certain amount

of energy in excess of the average thermal energy to overcome a potential barrier. The particle acquires this energy by thermal fluctuations and this causes the strong temperature dependence of the relaxation time. The same applies to the macroscopic viscosity coefficient η, and both temperature dependences are similar to that of a chemical rate process in which the particle has to acquire a certain activation free energy. Eyring obtained the expression:

$$\tau^{*} = \frac{h}{kT} e^{\Delta F_e^{*}/RT} \qquad (82)$$

and a similar one for the viscosity coefficient, which however has a different activation energy, since translational energy is also involved. In equation (82), ΔF_e^{*} is the free energy of activation for dipole relaxation, k is Boltzmann's constant and h Planck's constant. The different activation energies for τ^{*} and η show why equation (80) is only approximate. ΔF^{*} at room temperature, calculated from the slopes of experimental curves of $\log \tau^{*}$ vs 1/T for condensed phases turns out to be of the order of 10 RT and higher. Thus the dipoles change their direction by jumps. The conversion of electrical energy to heat which accompanies dielectric relaxation is similar to the change of chemical energy into heat in a chemical reaction. According to Debye's theory this electrical energy loss was due to inner friction.

The distribution of relaxation times can be understood by this theory. At a given moment thermal fluctuations cause differences in the neighbourhood of some of the molecules and thus the free energies of activation, which the molecules require to overcome the potential barrier, vary and there is a distribution of these energies. Such a distribution is symmetrical about the mean value, which, since the relaxation rates depend exponentially on the free energy,

accounts for the symmetrical curves of ϵ' and ϵ'' vs log w. Thus the dipoles have a number of positions of relatively minimum potential energy, separated by potential barriers. When the rotational energy allows a sufficiently frequent jumping of the barriers, the contribution of the dipoles to the polarisation in the applied field may be the same as in the case of free orientation.

Powles[108] has improved Debye's viscosity theory, by proposing a new value for the internal field. This leads to:

$$\tau = \tau^{*} \, 3\epsilon_s/(2\epsilon_s + \epsilon_\infty) \qquad (83)$$

and results in better values of a than calculated from equation (80). Powles' value of the internal field gives Cole-Cole plots in agreement with experiment for cases with two and more relaxation times.

At the end of this section it must be emphasised that conformation of the observed frequency dependence to equation (64) is not confirmation of a particular model, since an equation of the same form arises for models of diverse systems, for example, two phase suspensions, paramagnetic relaxation and other effects.

3.2.8. Distribution of Relaxation Times.

The experimental results for liquids and solids usually do not agree with the forecasts of equations (65) and (66). Generally the dispersion curves (Fig. 16) are flatter and extend over a wider frequency range, while the absorption (Fig. 17) and $\tan\delta$ vs log w curves (Fig. 20) are broader and have a lower maximum value. The Cole-Cole curve (Fig. 18) is mostly still a circular arc, but its centre now lies below the abscissa[102].

The deviaitions in liquids and solids arise because the model used to derive equations (65) and (66) is too

simple to describe such condensed phases. Here the conditions of each molecule are variable; the magnitude of the interaction forces, the directing force and the thermal influence vary with position and time. Thus at any moment each dipole has its own intrinsic relaxation time. Furthermore in long chain polar molecules, e.g. polymers, there are many possibilities of internal bending, twisting and rotation, each with a corresponding relaxation time. Measurements represent an average over spatial conditions, which will generally result in a spread of relaxation times around the most probable value.

For a spread of relaxation times, the complex permittivity equation (64) must be extended to

$$\hat{\epsilon} = \epsilon_\infty + (\epsilon_s - \epsilon_\infty) \int_0^\infty \frac{G(\tau)}{1 + jw\tau} \, d\tau \qquad (84)$$

$G(\tau)$ is the distribution function of the relaxation times. From the definition that $G(\tau)d\tau$ is the fraction of the molecules at a given instant with relaxation times between τ and $(\tau + d\tau)$ it follows that

$$\int_0^\infty G(\tau)d\tau = 1 \qquad (85)$$

Introduction of a distribution of relaxation times transforms equations (65) and (66) to:

$$\epsilon' = \epsilon_\infty + (\epsilon_s - \epsilon_\infty) \int_0^\infty \frac{G(\tau)d\tau}{1 + w^2\tau^2} \qquad (86)$$

and

$$\epsilon'' = (\epsilon_s - \epsilon_\infty) \int_0^\infty \frac{w\tau G(\tau)d\tau}{1 + w^2\tau^2} \qquad (87)$$

respectively.

The formal theory of a distribution of relaxation times was given by Von Schweidler[109]. Wagner[110]

obtained a value for the distribution function $G(\tau)$, by assuming that an infinite number of independent causes disturb an original relaxation time τ_o. This leads to a Gaussian probability function:

$$G(\tau)d\tau = \frac{b}{\sqrt{\pi}} e^{-b^2y^2} dy \qquad (88)$$

where b is a constant and $y = \log_n(\tau/\tau_o)$. Yager[111] used a similar function. Both deviate from the curves forecast by equations (65) and (66) as found experimentally.

Work on the distribution of relaxation times is mainly associated with the names of Fuoss and Kirkwood and Cole and Cole. The work is empirical, and although there is no satisfactory general theory for the ϵ' and ϵ'' dependence on frequency and for $G(\tau)$, the theoretical work of the above authors, which is to some extent based on experimental results, usually gives good agreement with the particular experimental results used, and has been successfully invoked by many authors.

Fuoss and Kirkwood worked with long chain polymers[112]. They showed that $G(\tau)$ can be derived when ϵ'' is given as a function of w[113]. They suggested an empirical relation, now often used, which fitted their results well:

$$\epsilon'' = \epsilon''_m \operatorname{sech} \left[\beta \log_n(w/w_m)\right] \qquad (89)$$

where β is a parameter between 0 and 1 and w_m corresponds to the maximum ϵ_m'' of ϵ''.

The relationship $\epsilon'' = \epsilon_m'' \operatorname{sech} \left[\log_n(w/w_m)\right]$ (90) can be derived from equations (66), (67) and (69) for one relaxation time. Introduction of β flattens the curves given by equation (90), the lower the value of β the wider being the distribution of relaxation times.

MacDonald[114] extended the Fuoss-Kirkwood treatment to a more general case by not using the modified Onsager relationship[85], but solving the Kronig-Kramers integral relations between the conjugate quantities ϵ' and ϵ''. He obtained analytical expressions for ϵ', which only for particular values of β' permit evaluation of the integral involved, and with the aid of the analytical expressions, tables of graphs for interpolation of ϵ' against $\log_n(w/w_m)$ and β' can be constructed.

Cole and Cole[102] empirically explained the deviation found in the circular arc plot for liquids and solids. The experimental results indicated that equation (64) must be modified to

$$\hat{\epsilon} - \epsilon_\infty = \frac{\epsilon_s - \epsilon_\infty}{1 + (j\omega\tau_0)^{1-h}} \qquad (91)$$

where τ_0 and h are constants. This leads to the equation of a circle:

$$\left[\epsilon' - \frac{\epsilon_s + \epsilon_\infty}{2}\right]^2 + \left[\epsilon'' + \frac{\epsilon_s - \epsilon_\infty}{2}\cot\frac{n\pi}{2}\right]^2 = \left[\frac{\epsilon_s - \epsilon_\infty}{2}\operatorname{cosec}\frac{n\pi}{2}\right]^2 \qquad (92)$$

with centre at $\left(\frac{\epsilon_s + \epsilon_\infty}{2}, -\frac{\epsilon_s - \epsilon_\infty}{2}\cot\frac{n\pi}{2}\right)$ and radius $\frac{\epsilon_s - \epsilon_\infty}{2}\operatorname{cosec}\frac{n\pi}{2}$ where $h = 1 - n$. The circle is shown in Fig. 21. The angle between the abscissa, and the line joining the centre of the circle to the left hand intersection point of the arc with the abscissa is $h\pi/2$, and determines the value of h. $h = 0$ when there is only one relaxation time, otherwise is between 0 and 1, the larger h the larger is the extent of the distribution of relaxation times. The equation for ϵ'' following from equation (91) shows ϵ'' is a maximum when the angular frequency equals $1/\tau_0$.

FIG. 22a.

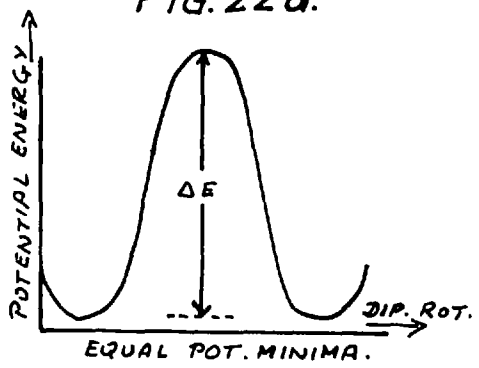
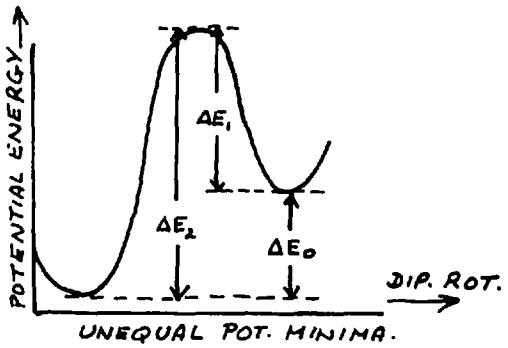


FIG 22b.



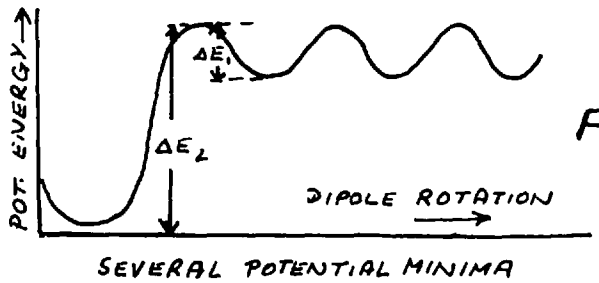
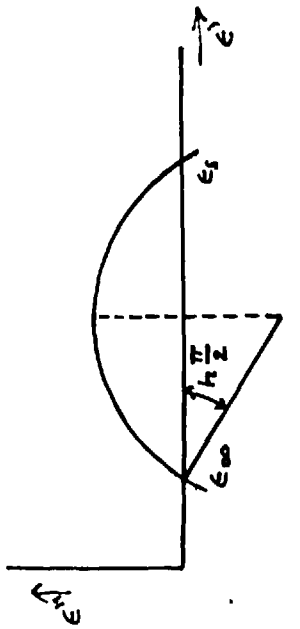
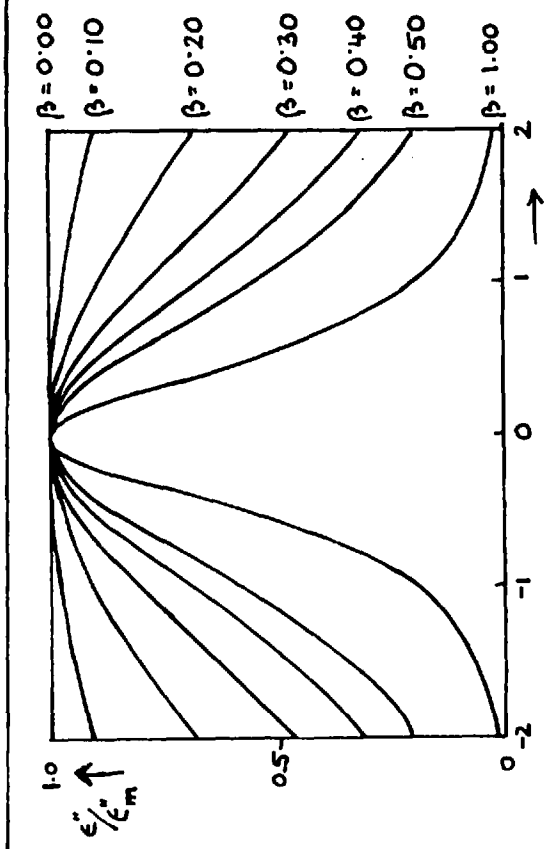


FIG 22c.

POTENTIAL ENERGY DIAGRAMS FOR ROTATING DIPOLES.



GEOMETRICAL INTERPRETATION OF 'h' FROM THE COLE-COLE FORMULA.
FIG. 21.



CURVES OF β OF THE FUOSS-KIRKWOOD RELATION.
FIG. 23.

In the case of only one relaxation time $\tau_o = \tau$ (where $w_m = 1/\tau$). In the case of distribution of relaxation times τ_o is the average around which the relaxation times are spread. Thus the maximum taken from an experimental ϵ'', log w curve in the case of a distribution of relaxation times, by putting $\tau = 1/w_m$ equals τ_o calculated from the Cole-Cole diagram. When h has been determined by measuring the angle indicated, τ_o can be calculated. A point on the ϵ'', ϵ' curve at some frequency w_1 is chosen. The distances u_1 and v_1 from this point to the ϵ_∞ and ϵ_s intersection points of the curve with the abscissa respectively are then related by

$$\frac{v_1}{u_1} = (w_1\tau_o)^{1-h} \qquad (93)$$

Stark[116] showed that a Cole-Cole circular arc plot is still obtained when frequency and temperature are interchanged and equation (91) is obeyed both for a single and for a distribution of relaxation times.

It can be shown mathematically[83] that the Cole-Cole and Fuoss-Kirkwood relationships are in agreement, a constant value of β leading to a constant value of n. Using equations (89) and an equation $\int_o^\infty \epsilon'' \, dw/w = \pi/2(\epsilon_s - \epsilon_\infty)$ (which was obtained from equation (66) to give the total area under the ϵ'', log w curve and holds for a distribution of relaxation times), the maximum of the Cole-Cole plot is derived as

$$\epsilon''_m = \beta\frac{\epsilon_s - \epsilon_\infty}{2} \qquad (94)$$

Comparing this with equation (69) we see that in the case of a distribution of relaxation times, the centre of the semi-circle is depressed, β being the measure of this depression.

Although the Cole-Cole relation often applies well it has not been explained theoretically. Recently Cole and Davidson[115] suggested a new empirical ϵ'', ϵ' relation in the case of glycerol, but it is doubtful whether this has any advantage over equation (91)[83]. Cole and co-workers[101] have also attempted to explain the asymmetric dispersion obtained with glycols by a function

$$\hat{\epsilon} = \epsilon_\infty + (\epsilon_s - \epsilon_\infty)/(1 + jw\tau_0)^\beta \qquad (95)$$

where β is empirical, $0 < \beta < 1$, however this is not entirely satisfactory and might perhaps be explained by two different processes taking place.

Departure from the circular arc plot may be due to cases with more than one absorption region or with an asymmetric distribution of relaxation times.

Sometimes ϵ'' does not approach zero outside the main absorption range, but remains at a small finite value almost independent of frequency. Garton[117] suggested this was due to a very wide distribution of relaxation times due to the temporary formation of additional equilibrium positions of the molecules caused by thermal fluctuations. Frohlich[84] showed that the assumption of such small potential energy wells does in fact lead to the experimentally observed results.

In conclusion it must be emphasised that in order to give a satisfactory test for a dispersion equation, measurements must be made over a large frequency range (at least two decades) and the temperature dependence of ϵ_s and ϵ_∞ must be established over a wide range, this temperature dependence being the disadvantage when using the Cole-Cole plot[101].

3.2.9. Polarisation of Solids.

The development of a quantitative theory of electric polarisation of solids is not very advanced. The difficulties encountered are based on the condensed and fixed nature of solids, and the fact that a theory of the internal field in solids is still lacking. The Lorentz formula of the internal field applies to point particles in a cubic lattice, but in a real crystal the idealisation of point-shaped particles cannot be maintained, since the distances between the particles are small. Also most crystals are not cubic and since the particles are fixed, the structure of the crystal should not be neglected as was done by Lorentz in the case of liquids and gases. Kirkwood's theory[92] of polar liquids, which takes into account the structure of the immediate neighbourhood of the particle and considers only the remaining dielectric as a continuum, might be extended to the case of solids.

To a certain extent every solid has its own dielectric behaviour which depends on its chemical structure, type of lattice and degree of molecular freedom. Unlike liquids and gases, a solid may for instance be polarised without an external field (seignette or ferroelectrics). This in itself argues against the possibility of a general theory for solids but suggests that development of a theory may be possible, for series of closely related structures.

The dielectric behaviour of a solid made up of non-polar molecules is similar to that of the corresponding non-polar liquid, since there is no qualitative difference in the atomic and electronic polarisations in the two cases. Due to density differences in the two states such a material shows a slight increase of polarisation, i.e. permittivity at the freezing point. In ionic crystals however[118] the atomic polarisation is much larger than is usual. This is due to a large contribution caused by the displacement of the

positive ions with respect to the negative ones.

Measurement of the atatic dielectric constant of polar compounds as a function of temperature gives important information about molecular freedom[119]. In some cases the possibility of dipole orientation disappears on solidification and the dipoles become fixed in the lattice[120,121]. In these cases ϵ_s increases slightly on cooling the liquid, but falls considerably at the freezing point. In hydrogen chloride and sulphide[122,123] the dipole axes become fixed at a solid transition point well below the freezing point, the crystal symmetry being higher above than below this transition point. This is therefore an order-disorder transition, positive $\partial\epsilon/\partial T$ coinciding with increasing, and negative $\partial\epsilon/\partial T$ with decreasing order. Free orientation of dipoles may sometimes occur at very low temperatures (e.g. 32°K in the case of AsH_3) and even in large molecules[124,125]. Spherical form of the molecules and a lattice of high symmetry, mostly cubic, are conducive to free orientation. In such a lattice the energy of the molecule depends less on its orientation than in a low symmetry lattice. In the case of hydrogen bromide[122] the dielectric constant rises rapidly to a very high value at the lower transition point and then decreases less sharply than in the former cases. This is explained by assuming the occurence of spontaneous polarisation, i.e. in the absence of the field the state of lowest energy is that, with the dipoles in the same direction. Then a relatively weak field will support the mutual parallel orientation of the dipoles, probably in the direction of the applied field, leading to a large polarisation and dielectric constant. This phenomenon is called seignette or ferroelectricity. This is a large subject and will not be discussed here.

In a sufficiently high frequency field a polar solid with freely orientating dipoles will show relaxation effects. Qualitatively these are similar to the effects in liquids, but quantitatively the relaxation starts at much lower frequencies, since the relaxation times are much larger than in liquids. Since the relaxation occurs at low frequencies ϵ_s can often not be measured directly, but can sometimes be determined by extrapolating the dispersion curve to zero frequency. Most solids show a wide distribution of relaxation times, the Cole-Cole plots are circular arcs and there is only one absorption region.

The simplest model for dipole relaxation in solids is that of a dipole having two possible positions of equal energy (Fig. 22a), different in direction and separated by an energy barrier ΔE, or the jump of an ion from one position to another of equal energy, in so doing altering its position relative to another ion or charge of opposite sign, which gives a similar result. Unequal potential minima and more than two minima are also possible (Figs. 22b and c)[126].

The relaxation time for dielectric absorption in a system with two positions of equal energy[84] is given by

$$\tau = \frac{D_o}{(2f_o D_1)} \exp \frac{\Delta E}{RT} \qquad (96)$$

f_o is the vibration frequency of the dipole or ion and therefore $f_o \exp(-\Delta E/RT)$ the probability of the ion or dipole escaping from the potential trough in unit time, assuming uniform density of states and $\Delta E \gg RT$. The factor D_1/D_o accounts for the non-uniform density of states, being the relative density of states just above the top of the energy barrier and in a region RT within the bottom of the trough. The measured relaxation times differ from the above ionic or molecular value by a factor which depends on the magnitude of

the absorption and is given by

$$\frac{\tau_{\text{macroscopic}}}{\tau_{\text{molecular}}} = \frac{1 + (\epsilon'_s - \epsilon'_\infty)}{(2\epsilon'_s + \epsilon'_\infty)} + \frac{(\epsilon'_s - \epsilon'_\infty)^2}{3\epsilon'_\infty \epsilon'_s} \quad (97)$$

for $\epsilon'_s/\epsilon'_\infty = 5/4$ the factor is 1.09 and for $\epsilon'_s/\epsilon'_\infty = 3/2$, 1.18.

When $\tau_{\text{molec.}} = \tau_{\text{macro.}}$

$$f_{max} = \frac{1}{2\pi\tau} = \left(\frac{f_o}{\pi}\right)\left(\frac{D_1}{D_o}\right) \exp\left(-\frac{\Delta E}{RT}\right) \quad (98)$$

Therefore plots of $\log_n f_{max}$ against $1/T$ give the value of ΔE. The ratio D_1/D_o can be considered as an entropy term; we then replace it by $\exp(\Delta S/R)$, where ΔS is an entropy of activation, and then

$$f_{max} = \left(\frac{f_o}{\pi}\right) \exp -\left\{\frac{(\Delta E - T\Delta S)}{RT}\right\} = \frac{f_o}{\pi} \exp\left\{-\frac{\Delta F}{RT}\right\} \quad (99)$$

where ΔF = the Helmholtz free energy of activation. It has already been mentioned (page 65) that some authors apply the absolute reaction rate theory to the dielectric absorption process and f_o is replaced by kT/h. This is perhaps far-fetched, since it is only based on the similarity of the temperature coefficients of τ and the specific reaction rate.

Dryden and Meakins used a value of 10^{12} for the vibration frequencies of ions (correct for alkali halides and of the right order for molecules in molecular crystals which may have slightly lower vibration frequencies) and using equation (99), calculated f_{max} in the absorption curve at 20°C for different values of the free energy of activation (Table 2).

Table 2.

F, k.cal. mole^{-1}	F eV	f_{max} c.s.	F, k.cal. mole^{-1}	F eV	f_{max} c.s.
18	0.78	10^{-1}	8	0.36	10^{6}
17	0.72	1	6.5	0.29	10^{7}
15	0.66	10	5.4	0.23	10^{8}
14	0.60	10^{2}	4.2	0.18	10^{9}
13	0.54	10^{3}	2.8	0.12	10^{10}
11	0.48	10^{4}	1.4	0.06	10^{11}
9.5	0.42	10^{5}			

In the case of unequal energy positions (Fig. 22b):

$$\tau = \left(\frac{1}{2f_o}\right)\left(\frac{D_o}{D_1}\right)\left\{\exp\left(-\frac{\Delta E_1}{RT}\right) + \exp\left(-\frac{\Delta E_2}{RT}\right)\right\}^{-1} \qquad (100)$$

where ΔE_1 refers to the smaller barrier. This does not have to be much smaller than ΔE_2 before τ reduces to

$$\tau = \left(\frac{1}{2f_o}\right)\left(\frac{D_o}{D_1}\right) \exp\left(\frac{\Delta E_1}{RT}\right) \qquad (101)$$

Thus experimentally the f_{max} against 1/T variation gives the value of the smaller barrier.

Hoffmann and Pfeiffer[127] have extended the treatment to a larger number of equilibrium positions (Fig. 22c) with different, i.e. asymmetric, energy barriers and minimum levels. This leads experimentally and theoretically to broadened asymmetric peaks and not to discrete absorption regions.

The magnitude of the absorption can be approximated to by using equation (22), replacing n^2 by ε'_∞ . Its variation with temperature depends on the value of ΔF_o (Fig. 22b). When this is zero the magnitude will vary with

$1/T$, when $\Delta F_o \gg RT$ it varies in proportion to $(1/T)\exp(-\Delta E_o/RT)$. If ΔE_o, which is the energy difference between the equilibrium positions, is large enough, the magnitude of the absorption may be too low to be detected.

In the case of a very wide distribution of relaxation times the Cole-Cole plots are rather inaccurate and the empirical Fuoss-Kirkwood relation (89) is preferable. It can be written:

$$\frac{\epsilon''}{\epsilon''_m} = \operatorname{sech}\left(\beta \log_n \frac{w}{w_m}\right) \qquad (102)$$

Plots of ϵ''/ϵ''_m against $\log(w/w_m)$ give a series of curves for different β values (Fig. 23) to which experimental results can be fitted to determine β. For β of 0.50 to 1.00, which is the narrow distribution of relaxation times, the curves are too close and Cole-Cole plots are preferable.

For many insulating materials the distribution of relaxation times is very wide and in the radio-frequencies $\tan\delta$ is almost independent of frequency (see also page 72). Gevers[2,3,128] obtained an empirical relation between this constant $\tan\delta$ and $\partial\epsilon/\partial T$:

$$\frac{1}{\epsilon'}\frac{\partial\epsilon'}{\partial T} = 0.06 \tan\delta \qquad (103)$$

$$\text{therefore } \frac{\partial\epsilon'}{\partial T} = 0.06\,\epsilon'' \qquad (104)$$

The theoretical explanation of equation (104) was given in the case of a very flat distribution of relaxation times[128,129].

In solids the dielectric loss is often due to ions, particularly when present as impurities. Generally these ions move across a potential barrier between positions of minimum potential energy. This mechanism occurs when ions are missing in an ionic lattice, especially when these ions are adjacent positive and negative ones. Such open places

may be due to the presence of an impurity of higher valency. Ionic relaxation of this type nearly always leads to a distribution of relaxation times, since there are local differences in potential energy. It is equivalent to a local conductivity increase, which can be considered as a type of heterogeneity.

According to Gemant[130], the ionic mobility in dielectrics under a.c. stress makes a finite contribution to the permittivity and loss factor. It is controlled by viscosity, elasticity and solid friction and its contribution to the loss factor is several orders higher than the d.c. contribution. This contribution is of the same order as for dipole relaxation, whereas the d.c. conductivity of these ions is not large enough to explain the a.c. losses.

Suchow and Pond[131] measured the conductivity of pressed samples of Ag_2HgI_4 at 1 kc.s. Over the linear part of the curve, interfacial polarisation effects were negligible and ionic conductivity could be calculated from:

$$\sigma = \sigma_o \, e^{-(Q/RT)} \qquad (105)$$

where σ = specific conductivity at T° absolute, Q = activation energy and σ_o = a constant. Since electronic conductivity follows the same law, Q and σ_o are weighted averages when both ionic and electronic conductivity are present. Ketelaar's results from d.c. measurements on the same system were 33% lower.

Dryden and Meakins[126] explained the increase of the low frequency dielectric loss with decreasing frequency, which is finally characterised by a region where ϵ'' is proportional to 1/f as due to d.c. conductivity. This occurs in many materials (see also equation (41)). Dryden and Meakins also point out that interfacial polarisation could occur at the electrodes.

In a heterogeneous material, an interfacial polarisation arises from the accumulation of charges at the interfaces of the phases which differ in permittivity and conductance[132,133]. This polarisation depends on the geometric forms of the phases and the difference between their conductances and permittivities. The classical work in this field was done by Wagner[132,134]. He showed that for a system of spherical particles of conductivity K_2 sparsely distributed throughout a material of low dielectric loss, the loss angle of the matrix is given by:

$$\tan\delta = \frac{\epsilon''}{\epsilon'} = \frac{KwT}{1 + K + w^2T^2} \qquad (106)$$

where

$$K = \frac{9q\epsilon_1'}{2\epsilon_1' + \epsilon_2'} \qquad (107a)$$

and

$$T = \frac{2\epsilon_1' + \epsilon_2'}{4\pi K_2} \qquad (107b)$$

ϵ_1' and ϵ_2' are the dielectric constants of the continuous and disperse media respectively, T is the time constant, w the angular frequency and q the quantity of dispersed material expressed as a fraction by volume. ϵ' is the dielectric constant and ϵ'' the loss factor of the matrix. In the later paper Wagner extended this to larger concentrations of phase 2. Equations (106) and (107) give a frequency dependence similar to (65) and (66). However the loss forecast by equations (106) and (107) occurs at frequencies which are much lower than those of the anomalous dispersion of normal liquids. The coexistence of two such different phases may lead to sharp peaks in the apparent value of the dielectric constant in the vicinity of the freezing point.

Hirsch[135] analyses the Wagner model, considering a polycrystalline semi-conducting body as consisting of conducting grains separated by high resistance boundary

regions. In an a.c. field any two surfaces facing each other on adjacent grains form a capacitor with the region of high resistance as dielectric. The specimen can be represented by a series-parallel array of resistors and capacitors. Generally the equivalent parallel capacitance C_p and conductance G_p of the array are frequency dependent, i.e. show dispersion. If one associates a single time constant with all grains and another with all boundaries, the model becomes equivalent to the two-layer dielectrics of Maxwell and Wagner and leads to similar results. This mechanism has been applied to polycrystalline films and sintered bodies of a variety of semiconductors (references 137 to 144 and many others). Billig and Plenner in particular, present the model for this case, pointing out its equivalence with the model of an inhomogeneous dielectric. The model is shown in Fig. 24 and the equivalent circuit in Fig. 25, where subscripts 'g' refer to grains and 'b' to barriers. R_b is much greater than R_g due to the air gap which reduces the grain contact area. At high frequencies the capacitance and resistance measured are due to the grains and at low frequencies due to the barriers. Bedause the boundaries are much thinner than the grains, C_b is much larger than C_g. Thus an abnormally high permittivity is obtained when the large capacitance value measured at low frequencies is referred to the total thickness of the sample. The measured permittivity and loss angle vary with frequency in a similar way as in the case of Debye dispersion. The expressions resulting for this circuit are:

$$R_p = R_b \frac{1 + w^2 R_g^2 C_b^2}{1 + w^2 R_g R_b C_b^2} \qquad (108)$$

$$C_p = C_b \frac{1 + w^2 R_g^2 C_g C_b}{1 + w^2 R_g^2 C_b^2} \qquad (109)$$

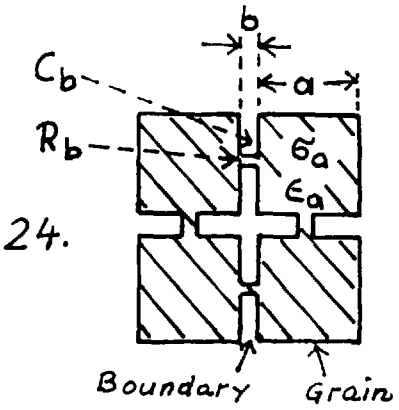
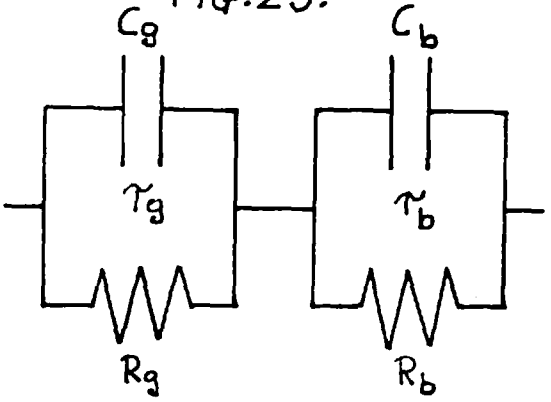


FIG. 24.

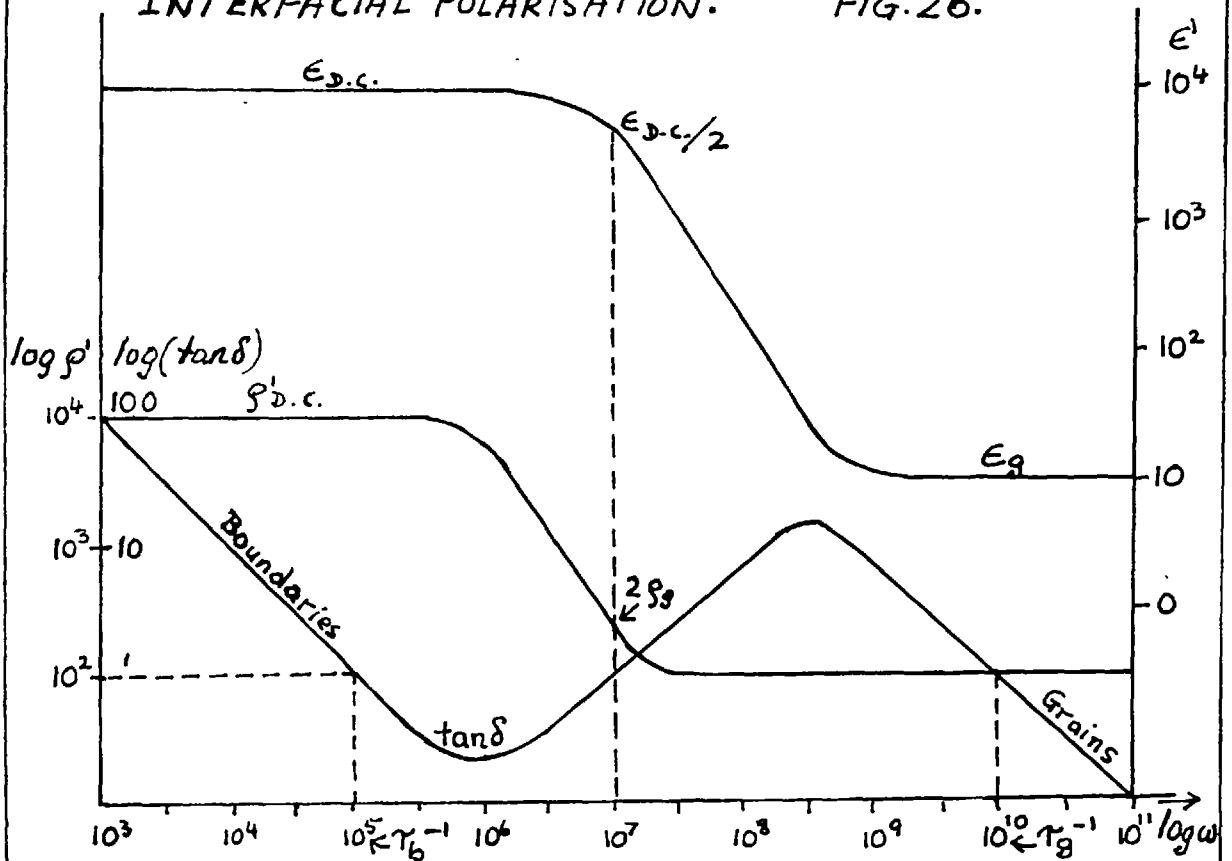
INTERFACIAL POLARISATION MODEL (MAXWELL-WAGNER).

FIG. 25.



EQUIVALENT CIRCUIT MAXWELL-WAGNER MODEL.

INTERFACIAL POLARISATION. FIG. 26.



Parameters for model in Plot:-

	grains	boundaries
ϵ'	10	10
ρ (Ohm cm)	10^2	10^7
Thickness, t cm	10^{-2}	10^{-5}
R Ω	1	$\ll 10^2$
C p.F.	10^2	$\ll 10^5$

	grains	boundaries
time constant τ(sec)	10^{-10}	$\ll 10^{-5}$

	High Freq.	Low Freq.
apparent ε	10	10^4
apparent resistivity	10^2	10^4

$$\tan\delta = \frac{1}{R_p C_p w} = \frac{1}{R_b C_b w} \times \frac{1 + w^2 R_g R_b C_b^2}{1 + w^2 R_g^2 C_g C_b} \qquad (110)$$

since $R_b \gg R_g$ and $C_b \gg C_g$.

Owing to the power loss component $(wCR_b)^{-1}$ due to the d.c. conductivity, the value of $\tan\delta$ first drops as the frequency is increased, goes through a minimum

$$\tan\delta_{min} = 2(R_g/R_b)^{\frac{1}{2}} \quad \text{at} \quad w_{min} = 1/C_b(R_b R_g)^{\frac{1}{2}} \qquad (111)$$

and then passes through a maximum value:

$$\tan\delta_{max} = \tfrac{1}{2}(C_b/C_g)^{\frac{1}{2}} \quad \text{at} \quad w_{max} = 1/R_g(C_g C_b)^{\frac{1}{2}} \qquad (112)$$

The a.c. component of $\tan\delta$, i.e.

$$\frac{1}{wR_p C_p} - \frac{1}{wR_b C_p} = \frac{wR_g C_b}{1 + w^2 R_g^2 C_g C_b} \qquad (113)$$

is of the standard Debye form.

Fig. 26 shows the plots obtained for such a polycrystalline semiconductor, where ρ' is the specific resistivity.

Thus both an inhomogeneous semiconductor and a dielectric may give rise to a set of Debye equations. This again emphasises that dielectric measurements do not decide the mechanism causing the dielectric dispersion. However the magnitudes involved may point to the inhomogeneous semiconductor model as the most likely explanation of a particularly high dielectric constant. Certainly the true electrical parameters of the grains are measured at high frequencies.

Hirsch pointed out that R_b arises from the actual grain contact while C_b is the capacitance of the air gap.

For the circuit to be correct the boundary time constants must be equal to, or be distributed over a narrow range around, the most likely value τ_b. According to Hirsch, C_b and R_b in the 'air-gap' model are not directly related to material constants and therefore this condition might not hold. He shows that it might however apply in a well sintered slab in which the boundaries are not gaps between the grains which restrict current flow, but non-conducting regions. Hirsch's equations for this case will not be considered, since Billig and Plenner's view must be nearer the truth with powder samples containing air gaps, although there may be a larger distribution of relaxation times than originally considered by these authors. However considering Hirsch's objection it must be pointed out that Plenner had actually considered such a distribution of 'barrier heights'[137]

Morgan[145] pointed out that for dipole relaxation the changes of τ with temperature are largely due to viscosity changes and the value of ϵ''_{max} increases with decreasing temperature. In the case of Maxwell-Wagner polarisation the value of τ depends on ϵ' and the conditions of the dielectric components, one of which has a greater conductance, and ϵ''_{max} decreases with decreasing temperature.

Finally, MacDonald[146] has explained single relaxation time Debye dispersions as due to free charges which cause a space charge, and O'Konski[147] considered Debye type relaxation in dilute suspensions as due to charge carrier mobility at the surface of the particles, a distribution of particle sizes giving a distribution of relaxation times.

3.2.10. The Dielectric Constant of Mixtures and Powders.

Badzioch and Cornford[148] and Reynolds and Hough[149] have summarised the formulae relating the measured permittivity of a mixture to that of its constituents. Rayleigh[150] and

Breit[151] set up equations for regular arrangements of the dispersed particles.

The formulae by Lorentz[98], Wagner[132], equations (106) and (107), and Sillars[133] mentioned in different connections earlier, all come under this heading, and so do equations by Ollendorf[152] and Niesel[153] which will not be considered further. Polder and van Santen[154], Reynolds and Hough, and Higuchi[157] proposed general formulae which require approximations of structural factors before use and reduce to some of the other equations.

Wiener[155] proposed an improvement on Rayleigh's formula which included all arrangements of rods and grains embedded in a medium:

$$\frac{\epsilon - 1}{\epsilon + u} = d\,\frac{\epsilon_o - 1}{\epsilon_o - u} \qquad (114)$$

where ϵ is the measured dielectric constant, ϵ_o is the dielectric constant of the particles, d is the fraction of the volume occupied by the microcrystals and u is a form number, which is a function of the particle shape and of the permittivity of the medium. Measurements on barium titanate were well represented by this formula for $d \neq 0$ to 0.30 and 0.70 to 1.00. However, u varied with d and particle size.

Brüggeman[156] elaborated Wiener's method for regularly arranged aggregates of definite shape and derived a formula for an arbitrary dielectric:

$$\frac{\epsilon_o - \epsilon}{\epsilon_o - 1} = (1 - \delta)\sqrt[3]{\epsilon} \qquad (115)$$

This, too, is not exact.

Böttcher[158] considering spherical particles with continuous environment, theoretically derived a special form of Wiener's equation, which applies to an irregular distri-

bution of particles. A number of authors showed this equation to be practically very useful, particularly for measurements on ionic crystal powders such as sodium chloride.

Lichtenecker and Rother[159] derived a formula for a mixture of prisms and polyhedra, which has been used by a number of authors:

$$\log \epsilon_m = \Sigma_i V_i \log \epsilon_i \qquad (116)$$

where ϵ_m = mean ϵ and V_i is the volume fraction of component i.

Polder and van Santen showed that for low values of the permittivity, the influence of particle shape is only of minor importance and Böttcher's equation is then a good approximation even for non-spherical particles, while with large permittivity values, Böttcher's equation applies only to spherical particles.

Poley[160] criticizes the existing formulae, particularly those of Wiener, Brüggeman, Lichtenecker-Rother and Böttcher for considering the particle surroundings as a continuum. He shows that in the overlapping region the same results are not obtained for a mixture A and B, in the cases where A and B respectively are the disperse phase. He bases his objections on the non-interchangeability of the particles due to the shape effect, and the particle-particle interactions at high concentrations.

It is difficult to see how the first of these objections can really apply to an equation such as Böttcher's, which is based on the irregular dispersion of a powder in a continuous phase, when the equation is used not for a mixture of two solids, but for a powder dispersion in a continuous phase such as air, vacuum or a liquid. Poley's test does then surely not apply and this may explain why, when Böttcher's equation has been used in some cases, errors were found to be

comparatively small, when the results were compared with those from single crystals. Poley's second objection is the old problem of the calculation of the correct internal field in solids. The good results obtained with Böttcher's equation suggest either that the second effect is smaller than expected, or that the two effects cancel each other which seems unlikely if Poley's first objection does not apply.

Reynolds and Hough's general equations for randomly arranged mixtures of isotropic particles and for particles dispersed in a continuous phase, suffer from the difficulty of arriving at the correct 'field factor'. By calculating the field factor and using the respective authors' assumptions and approximations, Reynolds and Hough show that all the published formulae except that of Lichtenecker-Rother are special cases of their own formula. They assume that the theoretical assumptions made by Lichtenecker and Rother are incorrect. They conclude that the earlier equations (Lorentz, Wagner, Ollendorf and Sillars) ignored particle interactions and only apply to low concentrations of the disperse phase, while Brüggeman, Böttcher, Polder-van Santen and Niesel made allowance for this interaction.

Böttcher's equation which has given good results for alkali halides, which like aluminosilicates (see results later) show large atomic polarisations, will be discussed in detail.

According to electrostatics, E_s, the electric field in a particle of dielectric constant ϵ_o, in a continuous dielectric of permittivity ϵ equals:

$$E_s = \frac{3\epsilon}{2\epsilon + \epsilon_o} E \qquad (117)$$

when E = field strength in the dielectric. The polarisation of the dielectric is restricted to the powder particles and per cm^3 of the dielectric is given by:

$$P = \frac{\epsilon - 1}{4\pi} E = d \frac{\epsilon_o - 1}{4\pi} E_s \qquad (118)$$

From equations (117) and (118)

$$\frac{\epsilon - 1}{3\epsilon} = d \frac{\epsilon_o - 1}{\epsilon_o + 2\epsilon} \qquad (119)$$

which was first derived by Böttcher who averaged the internal field over all the points of a dielectric, obtaining the Lorentz expression $\overline{E_i}_{(average)} = \frac{\epsilon + 2}{3} \overline{E}$. Therefore

$$\epsilon_o = \frac{3\epsilon d + 2\epsilon(\epsilon - 1)}{3\epsilon d - (\epsilon - 1)} \qquad (120)$$

It has already been mentioned that for low permittivities the shape of the particles is of minor importance, but for high permittivities equations (119) and (120) are only correct in the case of spherical particles.

The derivation of equation (117) assumed the dimensions of the particles to be neglibibly small compared with those of the condenser. Van Vessem and Bijvoet[161] showed that this condition is fulfilled for a grain size of 0.005 cm and a condenser of 500 cm^3. Sodium chloride permittivity values so obtained are constant and approximately 0.7% low between d = 0.485 and 0.561, whereas values obtained by Brüggeman's equation are not constant and are on an average 2.3% low. Measurements[162] showed the superiority of Böttcher's equation to those of Rayleigh and Brüggeman. Böttcher's and Brüggeman's equations have been extended to suspensions, emulsions and colloidal solutions of near spherical particles.

3.3. Dielectric Measurements on Some Aluminosilicates.

Table 3 summarises most of the results.

Table 3.

Substance	Author and Paper	Conditions stated	ϵ	ΔH k-cal mole (for ionic migration)	Specific resistance d.c.
(Na) Analcite	Int.Crit. Tables Liebisch + Rubens (24)	10^{12} c/s	6.7		
	Weigel (19)	d/c			5.63-6.33 x 10^{9} Ω-cm^{-1}
	Fairbanks (25)	$\lambda = \infty$; 31°C, hydrated.	13±1		
	Rosenholtz + Smith (26)	60 c/s, 220V, 20°C, powder dried at 110°C to get rid of surface moisture.	6.44		
	Takubo (27, 28)	λ = 101.43 cms, 25°C, natural mineral	5.88 5.87		
	Beattie (21)	50-500 c/s 2-50 V/cm synthetic anhydrous.	500°K	12.5 to 13	
	Beattie (23)	(anhydrous) (hydrated) synthetic	,	13 16	
Leucite	Rosenholtz + Smith (26)	60 c/s, 220V, 20°C, powder dried at 110°C to get rid of surface moisture.	6.78		
	Takubo (27, 28)	Natural mineral, λ = 101.43 cms, 25°C Also measured temperature dependence	7.08 7.13 7.18		
	Beattie (21)	K analcite, synthetic, 50-500 c/s, 2-50 V/cm, 500°F, anhydrous		17	

Substance	Author and Paper	Conditions stated	ϵ	ΔH k-cal mole (for ionic migration)	Specific resistance d.c.
Rb Analcite	Beattie (21)	Rb-analcite probably domain mixture as above for same author		18	
Pollucite	Beattie (21)	Cs-analcite. As above for same author		24	
Li Analcite	Beattie (21)	As above for same author.		17	
Ag Analcite	Beattie (21)	As above for same author.		14	
Tl Analcite	Beattie (21)	As above for same author.		15	
Sodalite	Rosenholtz + Smith (26)	As above for same authors.	6.81		
Chabazite=	Rosenholtz + Smith (26)	As above for same authors	8.70		
	Weigel (19)	d.c., 21.3°C			2.17-3.05 x 10^8 Ω-cm^{-1}
	Fairbanks (25)	As above for same author.	19 ± 1		
	Rabinowitch + Wood (20)	Single crystal, anhydrous, 100-500 V d.c.			1.8-3.7 x 10^8 Ω-cm^{-1}
	Wetzlar (29)	20°C, long waves hydrated, 14-500 km (200 c/s. to 2 kc/s).		τ=-5 2.5 x 10^{-6}sec.	
Albite	Rosenholtz + Smith (26)	As above for same authors.	6.02		
	Takubo (27, 28)	As above for same author.	5.45 -5.64		

Substance	Author and Paper	Conditions stated	ϵ	ΔH k-cal mole (for ionic migration)	Specific resistance d.c.
Gmelinite	Fairbanks (25)	As above for same author.	>36		
Heulandite	Weigel (19)	d.c., 15.7°C			$3.86-7.86 \times 10^{10}$ Ω -cm^{-1}
Kaolinite	Keymeulen + Dekeyser (31)	Natural hydrated, outgassed 24 hrs. at 200°C. 20 to 300°C		0.69 -0.83 eV	
Lepidolite	Rosenholtz + Smith (26)	As above for same authors.	7.36		
Natrolite	Weigel (19)	As above for same author			$1.52-1.65 \times 10^{12}$ Ω -cm^{-1}
	Fairbanks (25)	As above for same author	11 ± 1		
Spodumene	Rosenholtz + Smith (26)	As above for same authors	8.40		
Stilbite	Weigel (19)	d.c.			2.5×10^{8} Ω cm^{-1}
	Fairbanks (25)		22 ± 1		
		After heating at 100°C for 3 hours	36		

Rosenholtz and Smith and Takubo used a measurement technique based on the equivalence of the crystal permittivity with that of a known liquid mixture. The former authors state

a reproducibility of 5-10% and indicate the state of hydration but Takubo does not. Fairbanks states an accuracy of ± 1, but gives no experimental details. Fairbank's permittivity results, where comparison is possible, are invariably higher than those of the other authors, whose results are in fair agreement. The information available does not allow us to explain the differences either in terms of the frequency of the measurements or the state of hydration of the materials. The d.c. measurements of Weigel and of Rabinowitch and Wood have been discussed in an earlier section.

Beattie bases his work on the assumption that the conductivity is cationic. The conductivities of his compressed plugs of anhydrous materials[21] were 'normally' independent of frequency and voltage in the range 50-500 c/s and 2-50 V/cm. The activation energies were calculated from the straight line plots of $\log \sigma$ vs $\frac{1}{T}$, by Arrhenius' equation. Eyring's rate process theory identifies these activation energies with the heat of activation, ΔH, for ionic migration, ΔH representing the height of the potential barrier and the work necessary to form a defect in the structure. ΔH shows a large increase from Na to K, a slight increase from K to Rb and another sharp increase from Rb to Cs. Beattie suggests this is due to structure differences. In his second paper[22] Beattie concludes that in mixed cation analcites, conductivity is governed by the slower ion except at low concentrations of the latter. In his last paper[23] he measures conductivity of Na-analcite as a function of temperature and water content. At water contents up to 25% of theoretical ΔH = 13 k.cals and Beattie suggests that the main process is Na ion migration as in anhydrous Na-analcite, while at higher water contents (ΔH = 16 k.cals) the rate controlling process involves the energy barrier

for migration of the water molecules. ΔH calculated from self-diffusion experiments by Beattie agrees well with the high water content value. However Rees[163] measured the diffusion coefficient of sodium analcite by a radioactive tracer method, finding a ΔH value lower even than 13 k.cal.

Beattie is correct in assuming that a frequency independent conductivity at low frequencies may be equal to the d.c. conductivity of the sample (see page 80), however it may also be due to an interfacial polarisation effect (Fig. 26). Beattie used compressed powders, which must be porous, i.e. heterogeneous, and the presence of water would then tend to favour Maxwell-Wagner loss. This suggests that Beattie's low frequency measurements of the hydrated material are representative of the state of aggregation of the sample rather than its material. Unfortunately, Beattie does not mention the variation of the capacitance of his plugs with frequency, and in absence of this the matter cannot be decided.

In addition to the above authors a number of workers found relaxation peaks in dielectric measurements on aluminosilicates.

Vodop'yanov found a $\tan\delta$ maximum for mica (composition not stated) in the acoustical frequency range, and two maxima each for gypsum and talcum, the higher frequency one being less distinct. The $\tan\delta$ maxima are attributed to the orientation of the crystalline water, and activation energies which vary with temperature, due to changes in water content, are calculated by

$$U = k(T_1 T_2/(T_1 - T_2)) (\log_n f_1 - \log_n f_2) \qquad (121)$$

where f_1 and f_2 are the $\tan\delta_{max}$ frequencies at temperatures T_1 and T_2. For gypsum measurements at 293 and 243°K give $U = 0.59$ and 1.62×10^{-13} erg for the two maxima.

Muir[165] studied the dielectric loss of water adsorbed on kaolinite, halloysite, metahalloysite and talc powders between 2.5 kc/s and 25 mc/s. He attributes peaks of constant magnitude the frequency position of which varies with change in water content (halloysite and metahalloysite) to a complete water layer adsorbed on OH groups, and other peaks which change in magnitude but remain at the same frequency (talc) to a first layer of water adsorbed upon a surface of oxygen atoms. The first type of peak shows a distribution of relaxation times. Muir expects one maximum for each adsorbed water layer. Kaolinite shows both type of peak.

Between 100 c/s and 100 kc/s Keymeulen and Dekeyser also found tanδ peaks in powdered kaolinites at various stages of hydration. The activation energies were calculated from

$$2\pi\nu_{max}\tau_o = \exp(-U/kT) \qquad (122)$$

where U = height of potential barrier, τ_o = time of natural lattice vibration, and T = ° absolute, by plotting log ν_{max} against 1/T.

Anhydrous samples gave no maxima. The authors attributed these results to structure defects due to divalent impurities and not to heterogeneity.

In conclusion it might be noted that the peaks of type one observed by Muir and Keymeulen and Dekeyser, both suggest interfacial polarisation effects; insufficient information is available to comment on the peaks found by Vodop'yanov.

4. EXPERIMENTAL SECTION.

4.1. Aluminosilicates.

4.1.1. General and Syntheses.

The following aluminosilicates were electrically examined:

(a) Basic Sodalite, both hydrated and anhydrous.
(b) AgA($AgNO_3$), slightly hydrated and in the anhydrous state.
(c) Caesium Analcite.
(d) Sintered Caesium Analcite.
(e) Rubidium Analcite, domain mixture.
(f) Rubidium Analcite B, the sintered 'e'.
(g) Leucite.
(h) Sintered Leucite.
(i) Sodium Analcite, both hydrated and anhydrous.

Only the general methods of synthesis and identification will be given here, the details concerning the individual samples being more conveniently left for the 'results section'.

The minerals were prepared hydrothermally from gels, under conditions based on the work of those mentioned in section 2. 30 gm quantities were prepared, the conditions being chosen to give 100% yields of the pure materials. This required trial and error experiments in the cases of basic sodalite and rubidium and caesium analcite, and in the case of some of the sintered materials.

Basic sodalite was prepared by a low temperature synthesis on the water bath and AgA($AgNO_3$) from the zeolite sodium A by ion exchange followed by fusion at atmospheric pressure. The analcite series was synthesised at elevated temperatures in an electrically heated autoclave of litre capacity supplied by Chas. W. Cook and Sons Ltd., the temperature of this autoclave being controlled by a

platinum resistance thermometer, coupled with a furnace control. Leucite was prepared by ion exchange from sodium analcite, in sealed glass tubes rotated inside a conventional thermostatically controlled oven. The trial experiments were made in stainless steel autoclaves of about 20 ml capacity, sealed by copper washers between the stopper and the bomb. The sintered materials were obtained by heating the original species, contained in alumina crucibles suspended by platinum wire inside a concentric platinum wound furnace, at 1350$\pm$20°C for $2\frac{1}{2}$ days or longer. Temperatures were measured by a Pt - (Pt + 13% Rh) thermocouple.

After synthesis, the products and mother liquor were cooled as quickly as possible, the containers opened and the materials filtered off and washed free from mother liquor with hot water. The final products were dried in air or by washing with absolute alcohol and anhydrous ether.

The silica used in the preparations was supplied by Monsanto Chemicals Ltd., as a water clear stable dispersion (Syton 2-X) which contained 30% by weight of SiO_2 and had a specific gravity of 1.2.

A sodium aluminate, supplied under the trade name 'Alfloc' by I.C.I. Ltd., was used in the sodium mineral syntheses. It contained 87% $NaAlO_2$, 13% NaOH and a trace of iron which was filtered off as the hydroxide before synthesis. In all other cases the alumina was prepared from pure aluminium foil, which was cut into small pieces and washed with distilled water. This was amalgamated with 3% mercuric chloride solution, washed thoroughly and allowed to stand in ice-cooled, distilled water overnight. The precipitated alumina was filtered off, washed with water and alcohol and air dried; the moisture content was determined. The alumina had to be used soon after

preparation, since it aged rapidly to bayerite on standing in the cold.

The other alkali hydroxides were prepared from 'Analar' or 'Laboratory Reagent Quality' B.D.H. or pure Johnson and Matthey alkali sulphates, by reaction with the equivalent quantity of 'Analar' barium hydroxide and filtering off the barium sulphate produced.

In the case of sodium minerals, alkali to give the required base:alumina ratio and the necessary molar excess of alkali, was added to the ferric hydroxide free 'Alfloc' solution. While stirring a suitable quantity of 'Syton' was then added and stirring was continued for about ½ hour afterwards. During this time, the silica which had gelatinised in the presence of the cations, dispersed evenly throughout the mixture. The resulting gel was then put into the reaction vessel, which was brought to the required temperature as quickly as possible. The strength of the original solutions used was calculated to give the desired water content. Where 'Alfloc' could not be used, the alumina was added to the alkali solution in the reaction vessel, and after a few minutes stirring 'Syton' was added as before.

4.1.2. Identification of Materials.

Powder X-rays of all materials were taken. A 'Nonius' Guinier camera fitted with a quartz monochromator and a Debye-Scherrer 9 cm camera were used with CuKα radiation. In case of the 9 cm camera a nickel filter had to be used to cut off CuKβ radiation. The 9 cm camera was needed only for anhydrous samples which were then contained in sealed thin-walled glass tubes.

On the films from the 9 cm camera, the distance T between two equivalent powder lines was measured to 0.005 cm

and a correction factor applied to these readings to account for alterations in length during film processing, by comparing the known distance between the knife edges on the camera to the two shadows cast by the knife edges on the film. From the Bragg equation:

$$\lambda = 2d \sin\theta \qquad (123)$$

where d = the 'normal' distance between a set of equivalent planes, λ = the wave-length of the X-rays and θ = the angle between the incident beam and the reflecting plane, and the geometry of the camera it is found that

$$d = \frac{\lambda}{2 \cos T/4R} \qquad (124)$$

From this, d spacings were calculated using plots of d against T for the particular camera used.

On the Guinier camera the θ value of each diffraction line could be obtained by dividing the distance between the unreflected beam and the diffraction line by four. Allowance for change in length of film was again made, this time by comparing quartz lines obtained with the same exposure, with the correct d spacings for quartz as reproduced in the A.S.T.M. index of X-ray diffraction data[166]. The corrected θ values were then converted to d values by Bragg's equation (accuracy 1 in 1000).

In both cases the intensities of the lines were noted visually. Results of d spacings were then compared with the X-ray data supplied by the A.S.T.M. index and with photographs of known minerals, a library of which had been collected.

The crystal symmetry was in all cases known to be tetragonal or cubic. The h,k,l indices for each d value were found by fitting the logarithm of the d spacings to the lines on a Bjurstrom chart. The unit cell parameters a and

c were then calculated for each d line using the equations[167]:

$$d_{hkl} = \frac{a}{\sqrt{h^2 + k^2 + l^2}} \qquad (125)$$

for the cubic lattices, and

$$d_{hkl} = \frac{1}{\sqrt{\frac{h^2 + k^2}{a^2} + \frac{l^2}{c^2}}} \qquad (126)$$

for the tetragonal lattices. Consistency of the results showed that a correct fit had been obtained on the Bjurstrom chart.

The observed unit cell parameters, in conjunction with the known unit cell composition allowed calculation of densities of the minerals using:

$$\text{Density} = \frac{\text{Weight of Avogadro Number of Unit Cells}}{6.0247 \times 10^{-1} \times a^3} \qquad (127)$$

for the cubic crystals, and

$$\text{Density} = \frac{\text{Weight of Avogadro Number of Unit Cells}}{6.0247 \times 10^{-1} \times a^2 \times c}$$

for tetragonal crystals.

The refractive indexes of the crystals were determined by the Becke method. When the crystal is immersed in a liquid of different refractive index, then the bright Becke line moves from the edge of the crystal into the medium of lower refractive index on lowering the objective of the microscope. The refractive indexes were thus determined to 0.002, by using a series of liquids. This procedure proved rather difficult in the case of very small crystals. Sodium light was used in the experiments.

Electron micrographs of the crystals were obtained,

on a Phillips electron microscope by Dr. I. S. Kerr of Imperial College. These gave the following information:

1. crystal size;
2. crystal form;
3. absence of impurities or gel in amounts too small to be detected by powder X-rays or under the microscope.

Basic sodalite was analysed by the conventional method for silicates, to show the presence of the interstitial NaOH. A gravimetric water loss curve was obtained by suspending a weighed amount of the hydrated material, contained in an alumina crucible, from the pan of a balance into an electrically heated oven and taking to constant weight at a number of temperatures. Baffle plates shielded the balance pan from disturbing thermal effects. The empty crucible showed no weight change over the temperature range employed. Relative humidities were determined at the same time. The other materials did not require analysis, the analcites because they have a fixed alumina:silica ratio, i.e. are stoichiometric compounds, and AgA($AgNO_3$) because a full analysis on the parent compound by Meier[80] in conjunction with powder X-rays gave the required information. However moisture determinations were made in all cases, by heating in platinum crucibles over a Meker burner in case of the analcites, on the thermogravimetric balance for Na analcite and in an oven at 170°C in the case of AgA($AgNO_3$).

4.2. Dielectric Measurements.

4.2.1. Apparatus in General.

In order to obtain a maximum of information from a.c. measurements, it is desirable to cover as large a frequency and temperature range as possible. A survey of the literature revealed the best methods of measurement over the frequency ranges indicated[96,168,169]:

1. 60 c/s to 100 kc/s - a bridge method.
2. 100 kc/s to 200 mc/s - a resonance method.
3. Above 200 mc/s - a cavity or wave-guide method.

Methods 1 and 2 were used in this work, allowing frequencies up to 100 mc/s to be reached. Actually the lower frequency limit depended mainly on the dielectric loss of the sample and varied from 200 c/s to 5 kc/s. The upper frequency limit was in the region of 3 to 8 mc/s, since above this frequency induction effects, which were due to the use of an outside circuit on the Hartshorn-Ward dielectric test set, became very noticeable. The literature survey revealed that in the lower frequency range, the Schering type bridge is now being supplanted by a bridge with 'inductively coupled ratio arms'(168,170,171,172,173). This is a more versatile and quicker reading instrument. It can be designed to cover a large range of dielectric loss and capacitance, whereas the Schering bridge is mainly designed for low loss measurements. This type of bridge of our own design, which can be assembled comparatively cheaply, was built in this laboratory and used throughout this work. Its greatest advantage is that unwanted leakages and impedances, such as between the detector circuit and the bridge arms are reflected to the other side of the bridge by the tightly coupled coils when 1:1 coupling is achieved and therefore do not affect the bridge balance.

Above 50 kc/s a resonance method of measurement was adopted. A Hartshorn-Ward radio-frequency dielectric test set manufactured by Messrs. H. Tinsley and Co. Ltd., and a Marconi Q-meter type TF 329 G were lent to us by the Signals Research Station of the Ministry of Supply. The Q-meter which is a quick reading instrument requiring an external sample, has been used by a number of workers(165,174,175 and others). It is not considered to be very accurate. The Hartshorn-Ward apparatus which

normally requires compressed disc samples to be inserted in the main condenser, is much more cumbersome, but is an accurate instrument. Since dielectric measurements on aluminosilicate powders required an external cell sealed into an air-tight container for dehydration purposes, i.e. a comparatively large outside circuit, it was assumed that the Q-meter would prove more accurate and versatile in this instance. This assumption was incorrect. The Hartshorn-Ward apparatus could be adapted for fairly accurate measurements of widely varying tanδ values, whereas the Q-meter proved useless except in the intermediate tanδ range. Above 5 mc/s the use of the outside circuit on the Hartshorn-Ward apparatus caused large inductance effects and the Q-meter was used above this frequency in the case of anhydrous basic sodalite, where the tanδ range of the apparatus permitted measurements.

4.2.2. The Inductively Coupled Ratio Arm Bridge.

The design of the bridge is based on the Mullard bridge[173], but incorporates certain major modifications to suit our particular purposes. The essence of these modifications is that:

(i) We measure shunt capacitance and resistance instead of the series values measured by the Mullard bridge. This simplifies the balance equations and lowers the total resistance in circuit for any given resistance measured. Thus, the measurement of higher resistances is possible, than would have been with the series arrangement.

(ii) Our measurements are by substitution.

Mullard measured mainly capacitances above 1000 pF; our capacitances are generally much lower. This reduction in capacitance makes the earth capacitances of the bridge components more significant and a substitution method becomes essential for accuracy.

The circuit diagram of the inductively-coupled ratio arm bridge is given in Fig. 27. The design of the standard air condensers necessitated their movable plates being earthed. Thus the mid-point of the inductively-coupled ratio arms could not be earthed as is usual. The bridge has been built into one box with three earthed compartments containing (a) in the left one, C_1 and C_2; (b) in the middle one, the carbon resistor switches of R_1, and (c) in the right one, R_2, C_3 and the inductively coupled ratio arms.

R_1 consists of 4 ceramic 11 pole switches in series, one with ten 10K Ohm carbon resistors in series; the second with ten 100K Ohm, the third with ten 1 Meg Ohm and the fourth with two 5 Meg Ohm resistors.

The carbon resistors used were 1 Watt high stability types, 1%, which prior to use were measured to 0.12% on a direct current Wheatstone bridge made up of Sullivan resistance boxes. The a.c. impedance of the carbon resistors is substantially the same as the d.c. resistance up to 10 mc/s. To take account of the comparatively large negative temperature coefficient of the resistors all measurements are corrected to 25°C. The values of the resistors were checked periodically.

R_1 leads to a terminal for a coaxial cable, for connection of the 10 K Ohm resistor switch to a Sullivan 0.05% non-inductive resistance box with 1000, 100, 10 and 1 Ohm resistor switches. A box with 10 x 0.1Ω resistors could be added when required.

R_2 is the balancing switch. The values of the resistances in it do not enter into the balance equations. The switch contains the following 1% carbon resistors in series: 1000 Ohm, 10000 Ohm, 100000 Ohm, 1 Meg-Ohm and four 5 Meg-Ohms.

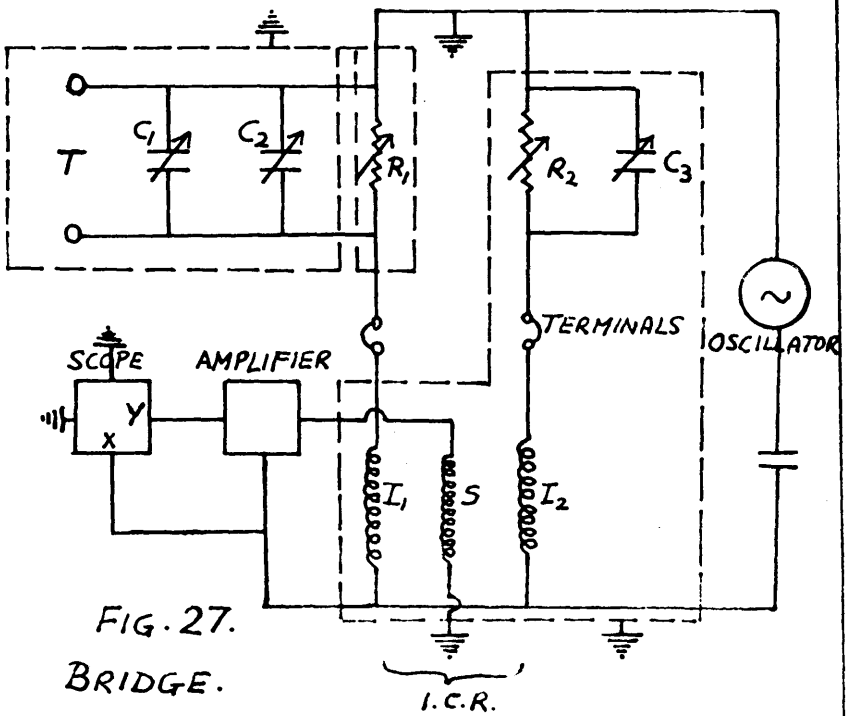


FIG. 27.

BRIDGE.

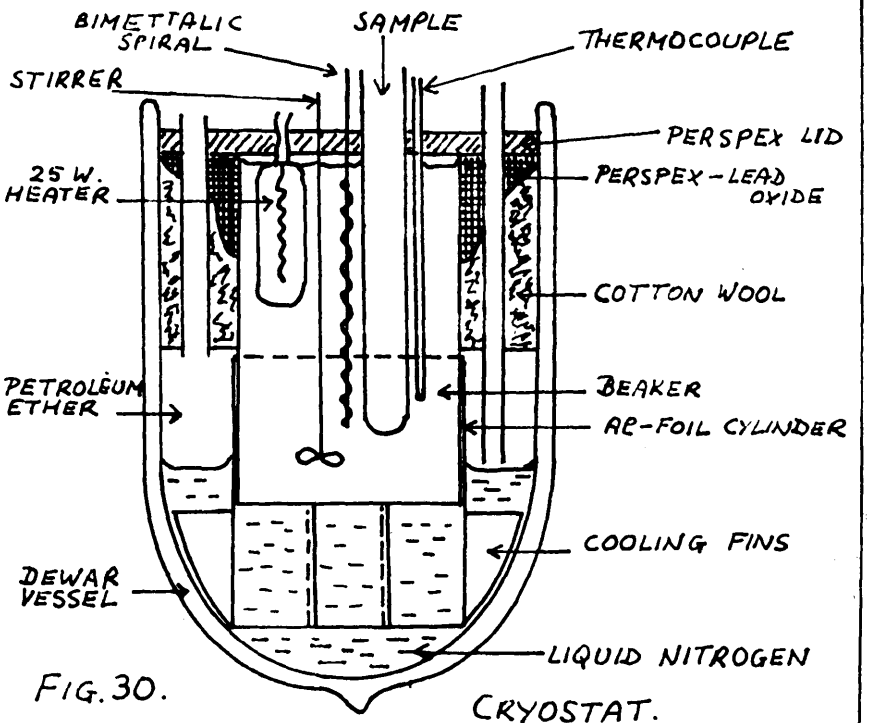


FIG. 30.

CRYOSTAT.

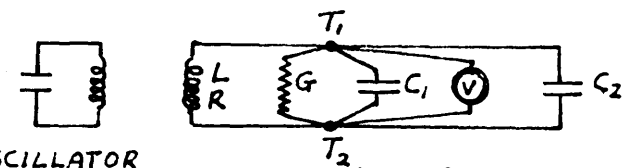


FIG. 28.

THE ESSENTIAL PARTS OF A RESONANCE CIRCUIT.

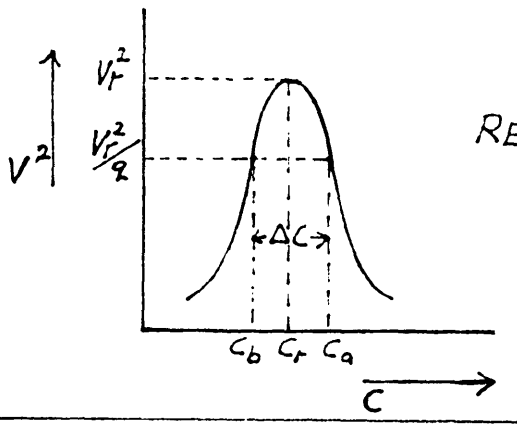


FIG. 29.

RESONANCE CURVE.

C_1 is a Sullivan variable air condenser of 0 -47 pF, accurate to 0.01 pF.

C_2 is a Sullivan variable air condenser of 0 - 305 pF, accurate 0.40 pF.

C_3 consists of a 500 pF wireless air condenser in parallel with a similar condenser of 3000 pF. Both have the moving plates earthed. Their values do not appear in the balance equations. Fixed condensers may be added if required.

The inductively coupled ratio arms (ICR in Fig. 27) were wound here in form of a toroid. They are a copy of the 1:1 ratio arms used by Mullard:

Core: Two 1155 A 2 ferroxcube rings held together with Araldite.

Windings: (From core outwards)

1 layer Empire tape.

Bifilar windings (I_1 and I_2) 2 x 256 turns in single layer, 36 swg enammelled single silk.

2 layers Empire tape.

Copper foil screen.

3 layers Empire tape.

Secondary (S): 696 turns, 36 swg enammelled single silk in two layers of 348 turns each, with 1 layer of Empire tape between the two layers.

2 layers of Empire tape.

Cu foil screen.

The oscillator is an Advance Audio Frequency Generator type H.1. In order to block off a constant d.c. potential of 8 volt at the output socket, a 0.1μ F condenser has been inserted in the output lead.

Separate amplification is used for the X and Y plates of the oscilloscope (Solarscope type CD 513),

the oscilloscope amplifiers being reinforced by a mains stabilised amplifier giving up to 50 x amplification at the X plate and up to 3000 x amplification at the Y plate.

The leads inside the bridge are all of rigid thick copper wire, while the outside leads are of coaxial cable with the sheathing earthed. All leads are as short as possible and are rigidly fixed.

Four terminals allow the inductively coupled ratio arms to be replaced by a radio push pull output transformer, which might be useful at the lower frequencies, or by 100:1 ratio arms. The connections to the dielectric cell are screwed into Belling-Lee terminals (T), which are in parallel with R_1, C_1 and C_2.

At balance the trace on the oscilloscope should be a horizontal straight line, made into an ellipse by resistance unbalance and tilted by capacitative unbalance.

The balancing procedure and equations are quite simple. Balancing procedure:

1. The bridge is balanced with the sample in circuit at T. Only the readings of C_1, C_2, R_1 and of the bridge temperature are of importance in the equations and are noted.

2. The bridge is rebalanced without the sample, altering only C_1, C_2 and R_1. C_1', C_2', R_1' and T' are again noted.

$\overline{R_1}$ and $\overline{R_1'}$ are corrected for temperature giving $\overline{\overline{R_1}}$ and $\overline{\overline{R_1'}}$. Then

$$R_p = \frac{\overline{\overline{R_1}} \cdot \overline{\overline{R_1'}}}{\overline{\overline{R_1}} - \overline{\overline{R_1'}}} \qquad (129)$$

and

$$C_p = C_1' - C_1 \qquad (130)$$

In order to get balance in both (1) and (2) above, R_1' must be smaller than R_p and C_1' must be larger than C_p.

A large number of measurements have been made to show that the bridge gives accurate results. Except at very high resistances (above about 100 Meg-Ohm), resistance measurements are to 1%. Capacitance measurements are accurate to 1% provided small capacitances are measured by C_1 only. At values of resistances above 100 Meg-Ohm the bridge still gave tanδ values reproducible to 0.0001 or $\pm$2% whichever is the higher, and probably better. It was found useful for sensitivity to keep the total resistance in circuit at 111.100Ω down to a frequency of 10 or 8 kc/s, the 1 Meg-Ohm resistors being only used at lower frequencies.

4.2.3. The Hartshorn Ward Dielectric Test Set.

This is a commercial instrument, and its detailed design will therefore not be reproduced. The apparatus is fully described by Hartshorn and Ward[176,177]. It consists of a large (N.P.L.) calibrated air condenser between which the specimen may be clamped, and a sensitive valve voltmeter with a square law scale, which measures in arbitrary units the voltage across the specimen. A micrometer condenser, also calibrated (N.P.L.), with a range of approximately 8 pF, serves to measure small changes of capacitance required to decrease the deflections of the volt-meter from the value at resonance to certain fractions of that value. A set of inductance coils, one of which is connected in parallel with the main condenser while a second is made part of the loosely coupled radio-frequency oscillator circuit, allow frequencies between 50 kc/s and 100 mc/s to be obtained by correct choice of the coils. Only these turning coils and the oscillator frequency have

to be changed to proceed from one part to another of the frequency scale. Electrostatic screens, which prevent capacitative coupling between oscillator and measuring circuit, are provided for use with the coils. The voltmeter deflection is read at a distance of 1 meter on a galvanometer scale and the micrometer condenser is adjusted with a wooden rod from the same distance. The apparatus is constructed to be very compact so as to reduce to a minimum residual inductances and resistances, due for example to the leads.

The apparatus is based on the method of capacitance variation in a tuned circuit, both permittivity and power factor being obtained as the ratio of capacitance readings; frequency is not involved. This is advantageous since capacitances are the only reliable standards at higher frequencies. The frequency of the oscillator remains constant and the condition of constant induced voltage in the measuring circuit is therefore more likely to be obtained than in the frequency-variation resonance method. All the components in the measuring circuit are in parallel and screening is therefore simple.

The essential elements of a resonance circuit are shown in Fig. 28. The sample is placed between the plates of C_1, V is the thermionic voltmeter, C_2 the microcondenser. This oscillating circuit is loosely (inductively) coupled to the oscillator of angular frequency w. The circuit is divided into two parts:

(i) the coil system, L, R and its capacitance, and
(ii) the external circuit, C_1, C_2 and V.

(i) and (ii) are screened separately, the screens being connected together at T_2, making the impedances of the two parts independent. As a result of the magnetic coupling between coil and oscillator, a potential difference V_∞

will exist between the terminals of the coil in absence of the external circuit. When the circuit is completed a current I will leave the coil system at T_1 and flow through the external circuit:

$$I = \frac{V_{\infty}}{R + jLw + \frac{1}{G + jCw}} \qquad (131)$$

R and L being the equivalent series resistance and inductance of the coil system at the angular frequency w, and G and C the equivalent shunt conductance and capacitance of the external circuit including electrodes, sample, condenser and voltmeter.

Since the impedances of the two circuits are independent of each other, the voltmeter indicates the potential difference between the terminals of the external circuit and this is given by:

$$V = \frac{V_{\infty}}{R + jLw} \cdot \frac{1}{G + \frac{R}{Z^2} + jw(C - \frac{L}{Z^2})} \qquad (132)$$

where $Z^2 = R^2 + L^2w^2$.

If C is varied the voltage will reach a maximum when

$$C = \frac{L}{Z^2} = C_r \qquad (133)$$

C_r is the total capacitance corresponding to voltage resonance. The ratio of the voltage V at any other capacitance C to the value V_r at resonance is given by:

$$\frac{V_r^2}{V^2} - 1 = q - 1 = \frac{w^2(C - \frac{L}{Z^2})^2}{(G + \frac{R}{Z^2})^2} \qquad (134)$$

Thus the capacitance C corresponding to any given value of $q = V_r^2/V^2$ is given by

$$C = \frac{L}{Z^2} \pm \frac{(G + \frac{R}{Z^2}) \sqrt{q - 1}}{w} \qquad (135)$$

R/Z^2 is the equivalent shunt conductance of the coil so that $G + R/Z^2$ is the total equivalent conductance G_t of the whole circuit. Thus the equation becomes

$$C = C_r \pm \frac{G_t \sqrt{q - 1}}{w} \qquad (136)$$

If C_a and C_b are the two values of C on either side of the peak of the resonance curve giving one value of V or of q, we have

$$C_r = \frac{1}{2}(C_a + C_b) \qquad (137)$$

and

$$G_t = \frac{w(C_a - C_b)}{2\sqrt{q - 1}} = \frac{w\Delta C}{2\sqrt{q - 1}} \qquad (138)$$

which means that the resonance curve Fig. 29 is strictly symmetrical. The total conductance can be determined in terms of the width ΔC of the resonance curve measured on the variable condenser at any ordinate q. In practice the voltmeter deflection is proportional to V^2 and q is therefore given directly as the ratio of the corresponding deflections.

To determine the properties of the sample, C_r, Θ_r, and ΔC at a certain value of q are obtained with the sample in position. The sample is removed and resonance is re-established, a series of observations, similar to the first being made (using the same value of q). Since equation (133) is independent of the conductance, which is the only factor which has been varied, the total capacitance in the two cases is the same and the value C_1 in the second case with the sample out of circuit equals C_s, the capacitance

of the sample. G_s of the sample is the difference of the conductances with the sample in and out, i.e.

$$G_s = \frac{w(\Delta C_i - \Delta C_o)}{2\sqrt{q-1}} \qquad (139)$$

and

$$\tan\delta = \frac{G_s}{C_s w} = \frac{\Delta C_i - \Delta C_o}{2C_s\sqrt{q-1}} \qquad (140)$$

Thus the quantities required for the measurement of power factor are independent of frequency. The apparatus is stated (N.P.L.) to measure $\tan\delta$ to 0.00005, if used in the way described.

As already mentioned an outside cell had to be used in this work. The leads to this cell were kept as short and simple as possible (they will be described later) and were screwed to the plates of the main condenser. The total capacitance of the sample is now given by $(C_1'' - C_1')$, the difference in the settings of the main condenser with sample cell out of and in circuit. Allowance was made for the capacitance of the leads and edge capacitance of the cell, and the condenser settings were corrected for temperature variation from that of calibration. The corrected value of C_s so obtained was then used in equation (140) for $\tan\delta$. Experience showed that $\tan\delta$ measurements were under those conditions $\pm$0.0001 to 0.0002 while the capacitance results were $\pm$1% but usually better. For larger values of $\tan\delta$ (above about 0.02), the incremental capacitance on the micrometer condenser was not large enough to measure the width of the resonance curve, it was however found that use of the main condenser for this purpose then gave results of accuracy comparable to the above. For this purpose the main condenser was also adjusted at 1 meter distance, by means of a slow movement device attached to the condenser and a 1 meter wooden rod.

4.2.4. The Q-meter.

The Q factor is given as the ratio of the energy stored to the energy dissipated in the circuit:

i.e. $$Q = \epsilon'/\epsilon'' = 1/\tan\delta \qquad (141)$$

The Q-meter is a well-known commercial instrument, which is based on voltage resonance, discussed in the last section. Its accuracy was found to be much worse than that of the two types of apparatus mentioned earlier. The $\tan\delta$ range obtainable is quite limited and the instrument was not generally used in this work. No further details will therefore be given.

4.2.5. Thermostats.

For measurements above room temperature the sample holder was immersed in a round, well-lagged air oven, the windings of which are enclosed by earthed metal sheets. Temperature control of the oven is by Sunvic bi-metallic strip coupled with a relay control which switches 20% of the resistance in and out of circuit when required. A fan circulates the air within the enclosure. Temperature control is to 0.2°C up to about 100°C and to 0.4°C at higher temperatures (up to 300°C). Temperature in this range is measured by mercury in glass thermometers.

At lower temperatures measurements were made at the temperatures of melting ice and liquid oxygen, and over a range of temperatures down to about -140°C, by using a cryostat built for the purpose (Fig. 30). In the latter the sample holder is immersed in petroleum ether, which is cooled by liquid nitrogen and can be heated by a small heating bulb. Temperature control is again by Sunvic control and relay, temperatures are measured by a standardised copper-constantan thermocouple.

4.2.6. Dielectric Cells, Cell Holders and Connections.

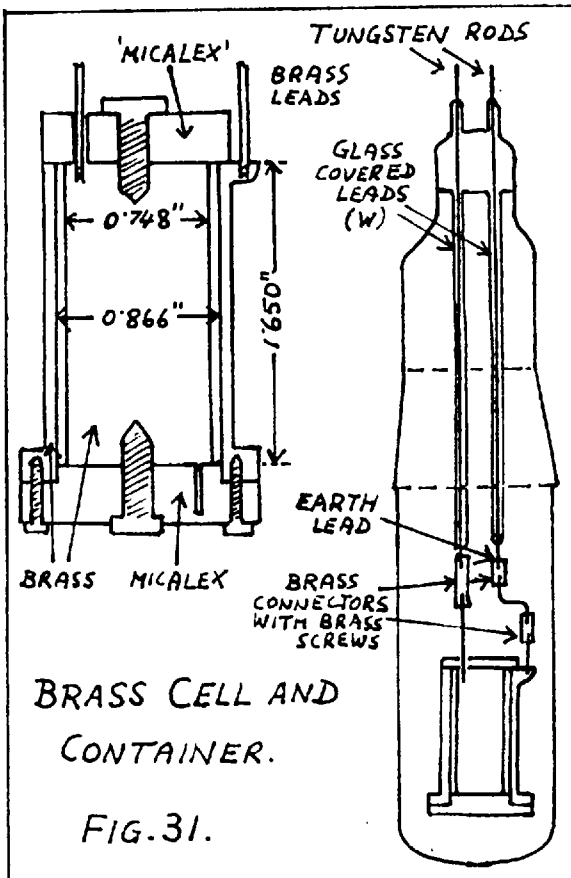
The cell containing the sample is held in a glass container, with two glass-metal (tungsten) sealed contacts. In the case of the high loss materials (basic sodalite and AgA($AgNO_3$), connection between this container and the apparatus is made by a ceramic switch in a perspex 'cage', which is clamped to the top of the oven lid. Contact between the outside leads of the cell holder and the stout leads from the switch are made by means of screw connectors. Both plates of the cell can be switched in and out of circuit, or the earthed side of the cell can be left in circuit all the time. The latter arrangement was found to give good results and was used. The position of the cell, cell holder and switch relative to each other and to the measuring apparatus are always reproducible, although changing their positions caused no measurable effects. In the case of low loss samples, the dielectric loss caused by the use of a ceramic switch is too high. Since it was also found that these switches become unreliable after frequent use, a new very satisfactory type of connection was employed with all other samples. This consists of a stout copper wire connection rigidly held in a large bore copper tube by two insulating spacers. The copper tube serves as an earth connection and is always in circuit. The 'hot' side of the cell is connected to the stout copper wire by a copper clip, while a screw connector links the 'earth' side of the cell and the firm lead from the copper tube.

The cell and cell holder are the items in the arrangement which have caused most difficulties. All cells are of the concentric type, consisting essentially of an insulating disc to which a metal cylinder and concentric metal plate are fixed. Three types of cell were employed:

(i) Brass cells were used for measurements involving

hydrated basic sodalite and hydrated and anhydrous $AgA(AgNO_3)$, since dehydration under vacuum was not necessary. The insulating disc is of 'Micalex' into which the brass plates are screwed. The terminals are copper wire screwed into the top of the concentric plates and connected to the tungsten rods, which serve as the main leads, by brass screw connectors. The cell is held in a 'Quickfit' cone and socket closed at both ends and with the tungsten rods sealed through the top as terminals. The arrangement is shown in Fig. 31.

(ii) For anhydrous basic sodalite, which had to be dehydrated under vacuum, a cell made of 'nicosel' metal was used. The concentric metal plates are spaced by a glass bottom sealed to the 'nicosel'. Nicosel leads are spot-welded to the plates and connected by nickel or stainless steel screw connectors to the tungsten leads. The cell (Fig. 32) is now held in a sealed glass container with side tube, the tungsten leads being sealed in as before. This air-tight container is attached to a high vacuum (approx. 6×10^{-6} mm Hg) pumping system and is evacuated. The container and cell are then heated to the predetermined 'outgassing' temperature of the sample and are kept at this temperature until the sample is completely dehydrated. Dry nitrogen is then admitted to 1 cm pressure, to give thermal contact and the side tube of the cell is sealed off carefully, so as not to allow any gases to enter during sealing. This cell can be used for samples with comparatively large dielectric loss, such as anhydrous basic sodalite. However the resistance of the cell was too low for measurements on samples with low loss angles and furthermore decreased with every 'outgassing'. This decrease was due both to the insulation of the cell and to the deposition of metal and metal oxide from the cell and the leads on the insulation between the cell plates and the



BRASS CELL AND CONTAINER.

FIG. 31.

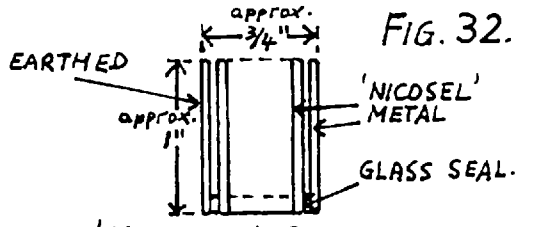
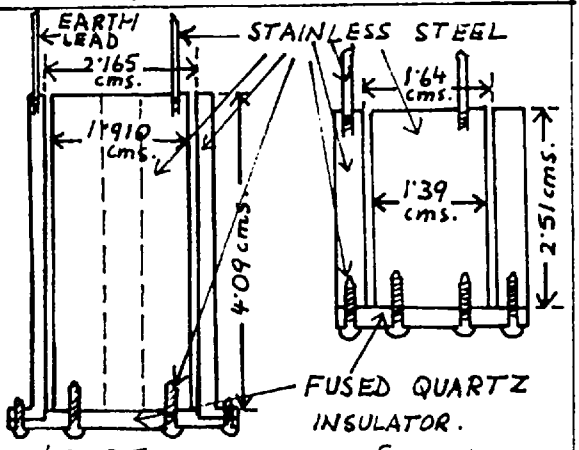


FIG. 32.

'NICOSEL' CELL.

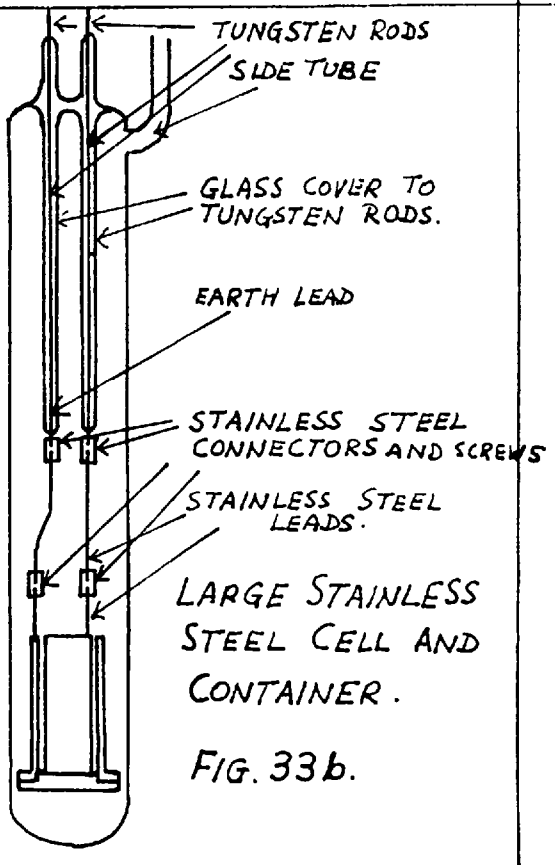


LARGE STAINLESS STEEL CELL.

FIG. 33a.

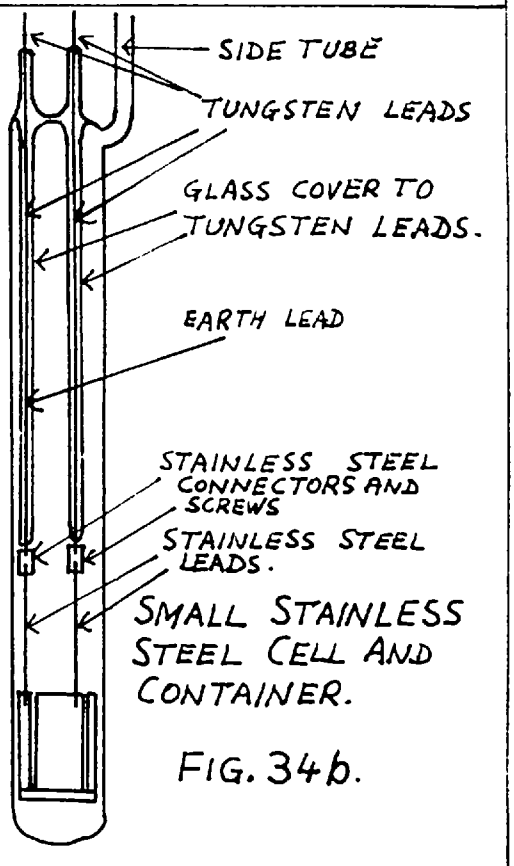
SMALL STAINLESS STEEL CELL.

FIG. 34a.



LARGE STAINLESS STEEL CELL AND CONTAINER.

FIG. 33b.



SMALL STAINLESS STEEL CELL AND CONTAINER.

FIG. 34b.

terminals at the glass-metal seals.

(iii) The third type of cell has tanδ values less than 0.0001 up to 50 kc/s, and slightly higher values at higher frequencies (e.g. 0.00016 at 313 kc/s and 0.00049 at 2.07 mc/s) This known constant and reproducible value was taken into account in all calculations. The cell, two types of which were made (Figs. 33 and 34) consists of concentric stainless steel plates, screwed into a fused quartz spacer. All screws and leads are of stainless steel except the tungsten rods, which are now covered with glass down to the stainless steel connectors. Thus no oxidation of tungsten takes place during sealing the cell holder, which is done in a nitrogen atmosphere. Cell holder and 'outgassing procedure' are similar to case (ii). In order to preserve the rather fragile quartz spacers, dehydration and measurement temperatures were kept as near room temperature as possible.

Cells of type (i) and (iii) can be taken to pieces for cleaning purposes, without changing their dielectric properties. The powders were compressed into the cells by hand compression with the help of plungers. The amount of material in the cell was determined in each case. The capacitance and shunt resistance of each empty cell were measured over the whole frequency and temperature range under the same conditions in which the cell was later used. The capacitance of the cells in pure, dry benzene and sometimes also in chloroform was measured. For such a cell at a given temperature:

$$C = \epsilon C_o + n \qquad (142)$$

where C = measured capacitance of the cell in pF,

C_o = real air capacitance of the cell,

ϵ = dielectric constant of substance filling the cell,

and n = a constant which takes into account lead and insulator capacitance effects of the cell. Measurements

with air and dry benzene thus give C_o and n. The values of Hartshorn and Oliver[178] for 'AnalaR' benzene, i.e. $\epsilon = 2.300$ at 15°C and $\partial\epsilon/\partial t = -0.0020_5$ were used. Since in practice C did not change appreciably with temperature or frequency, the volume and C_o of the cells were considered constant and the small changes in C were ascribed to n. The volume of the nicosel cell was determined by weighing with water and mercury, taking the meniscus of the liquids into account, the volumes of the other cells were calculated from the accurately known dimensions of the plates and insulators. The shunt resistances of the brass and nicosel cells, which changed with temperature and frequency were in each case much lower than those of the samples measured with these cells, and could thus be neglected. The shunt resistance of the stainless steel cells was temperature independent and its change with frequency was accurately determined. These shunt resistances are in parallel with the sample resistance and all resistance measurements were corrected for their effect. Except in the cases of the sintered rubidium and caesium analcites this correction was very small. Details of all the cells used are given in Table 4 and Fig. 35 is a diagram of the dielectric set-up using the later type connection.

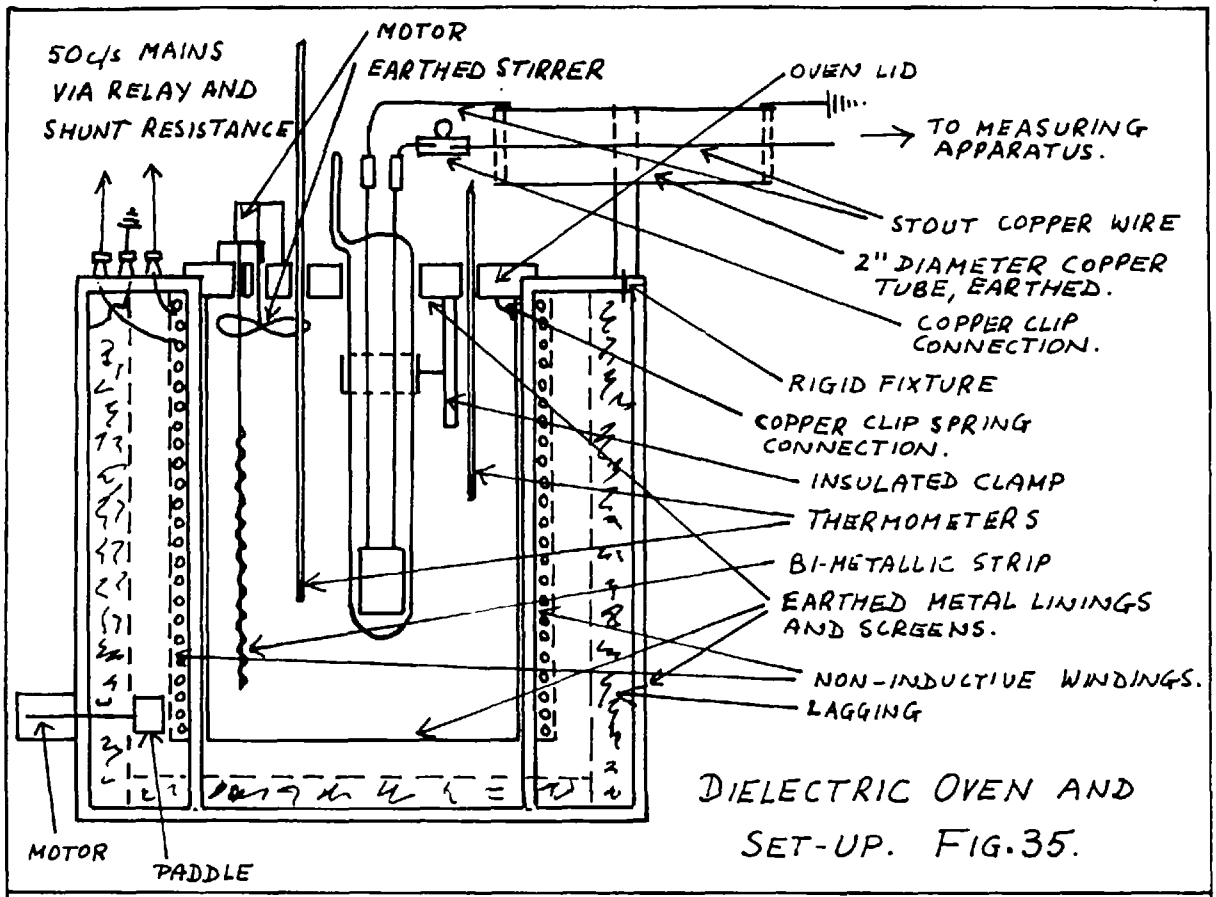
Table 4.

Details of Dielectric Cells.

Type of cell	Used for	C_o pF	Volume cm^3	Remarks
Brass, No.1	Hydrated Basic Sodalite	16.60	4.04	R_p much larger than that of sample.
Brass, No.2	AgA($AgNO_3$)	15.85	4.04	R_p much larger than that of sample.
Nicosel	Anhydrous Basic Sodalite	12.00	1.143	R_p much larger than that of sample.
Large Stainless Steel	Cs Analcite, Rb Analcite (domain mixture), Rb Analcite B, Leucite, Na Analcite hydrated and anhydrous.	19.60	3.34	R_p measured and taken into account.
Small Stainless Steel	NaCl, Sintered Cs Analcite, Cs Analcite, Sintered Leucite.	10.15	1.49	R_p measured and taken into account

4.2.7. Use of Böttcher's Powder Formula.

The density of the samples and the cell volume give 'd' in formula (119). An expanded form of this equation was used to determine the dielectric properties of the solid crystals from measurements made on powder samples.



DIELECTRIC OVEN AND SET-UP. FIG. 35.

The equation given by Böttcher is:

$$\frac{\epsilon - 1}{3\epsilon} = \frac{\epsilon_o - 1}{\epsilon_o + 2\epsilon} \times d \qquad (119)$$

where ϵ = measured dielectric constant = ϵ_{app},
ϵ_o = dielectric constant of compact crystal,
d = part of the total volume occupied by the microcrystals = packing fraction.

Replacing ϵ and ϵ_o by the complex quantities $(\epsilon' - j\epsilon'')$ and $(\epsilon'_o - j\epsilon''_o)$ respectively gives the following three equations:

$$\epsilon'_o = \frac{(3d-1)(3d-2)(\epsilon'^2+\epsilon''^2)+(3d-1)(2\epsilon'^3+2\epsilon'\epsilon''^2)+(3d-2)\epsilon'+2(\epsilon'^2-\epsilon''^2)}{(3d-1)^2(\epsilon'^2+\epsilon''^3)+(3d-1)2\epsilon' + 1} \qquad (143)$$

$$\epsilon''_o = \frac{(3d-1)(2\epsilon''^3+2\epsilon'^2\epsilon'') + \epsilon''(3d-2) + 4\epsilon'\epsilon''}{(3d-1)^2(\epsilon'^2+\epsilon''^2) + (3d-1)2\epsilon' + 1} \qquad (144)$$

$$\tan\delta_o = \frac{(3d-1)(2\epsilon''^3+2\epsilon'^2\epsilon'') + \epsilon''(3d-2) + 4\epsilon'\epsilon''}{(3d-1)(3d-2)(\epsilon'^2+\epsilon''^2)+(3d-1)(2\epsilon'^3+2\epsilon'\epsilon''^2)+(3d-2)\epsilon'+2(\epsilon'^2-\epsilon''^2} \qquad (145)$$

In these equations $\epsilon' = \epsilon'_{app}$ and $\epsilon'' = \epsilon''_{app}$ denote the measured or 'apparent' values. Quantities with the subscript '$_o$' denote the values for the massive crystalline substance. d has the same meaning as in equation (119) and is given by:

$$d = \frac{\text{Volume occupied by the substance}}{\text{Volume of cell}}$$

$$= \frac{\text{Amount (in gms) of substance filling the cell}}{\text{Amount (in gms) of substance theoretically required to fill the cell}} \qquad (146)$$

4.2.8. Reproducibility and Errors.

The measurements on hydrated samples are of qualitative value only. Studies of change of dielectric properties with water content require more elaborate equipment and to obtain such results was not the purpose of this research. In all other cases the samples were allowed to come to equilibrium at a certain temperature (this never required longer than three hours) and measurements over the whole frequency range were then made. The results at each temperature were checked at a number of selected frequencies, the sample being brought to another temperature for at least 1 day between determinations at the same temperature. Results (see later sections) indicated that this "repeatability" was usually better than 1%, or 0.0001 in the case of $\tan\delta$ values below 0.0100. The voltage of the bridge oscillator (2 to 22 Volts) had no effect on the results. The results thus obtained on the powder are the 'apparent results' (subscript '$_{app}$'). Experience showed that this consistency, which holds for all results obtained with one 'filling' of the cell, was maintained in the ϵ'_o and $\tan\delta_o$ values (the subscript '$_o$' refers to the 'real' crystal values obtained by equations (143) to (145)).

In cell blank determinations it was surprisingly found that there was no capacity difference between measurements of the cell filled with benzene and completely immersed in it. The C_o values thus obtained, forecast the capacitance of the cells filled with, or immersed in chloroform to 0.2%, and can therefore be assumed to be correct. This also means that the edge capacitance at the top of the cells is negligible, and we can therefore consider the meniscus error incurred in the cell blank determinations to be small. Further there should be little error on this account when the cell is filled with powder, provided the powder surface is even with the top of the cell plates.

The cell volume which is important in the use of equations (143) to (145) can be determined by weighing the cell filled with liquids, particularly mercury. This involves a doubtful meniscus correction and the mercury tends to amalgamate with the cell metal. The method was used for the nicosel cell after completion of the basic sodalite measurements, and this may have helped in rendering this cell useless for further measurements. Calculation of the volume from C_o and the gap between the plates, involves accurate knowledge of a very small quantity and assumes no irregularities in the gap. The latter depends on the insulation, which cannot be manufactured with the required accuracy. The cell plates were precision made, and their dimensions were accurately known. Volume calculations were thus generally made by using these dimensions.

It remains to estimate how true the real values obtained in these measurements are. Percentage errors due to an error in the volume of the cell, which is small (1 to 3 cm^3) and can therefore not be determined with great percentage accuracy, due to the packing of the powder, particularly at the top of the cell and due to the approximate nature of the powder equation, are the same for all values obtained with one 'filling' of the cell. Such errors will thus not affect the consistency (i.e. "repeatability") of the real results. The errors can however be estimated by measurements on materials of known dielectric properties and by comparison of results of the same material in two different cells. Different cells had to be used, since the standardised packing method, which was employed, gave fairly reproducible degrees of packing of a given powder in the same cell. In any case the procedure of using different cells determines the maximum possible error.

Using the small stainless steel cell and equation (143) gave $\epsilon'_o = 5.39$ independent of frequency at 21.6°C for 'AnalaR' sodium chloride. Van Vessem and Bijvoet[161] had similarly obtained a value of 5.58 at 17°C and single crystal measurements give 5.62. Our error is approximately 4%, which is reasonable considering that the sodium chloride was of large crystal size (2×10^{-2} to 9×10^{-2} mm) and van Vessem's condition (page 88) was not obeyed. This condition should be obeyed with the much smaller alumino-silicate crystals. Also volume and packing errors must be expected to be larger with the small, low cell than with the higher, large stainless steel cell which was used in most measurements.

Finally, the results on caesium analcite, obtained with the large stainless steel cell at 30°C (Run 93) and checked in Run 129A using the small stainless steel cell, are compared in Table 5.

Table 5.

Frequency	ϵ'_o Run 93 (Table XCV)	ϵ'_o Run 129A (Table CVII)	Approx. % difference.	$\tan\delta_o$ Run 93	$\tan\delta_o$ Run 129A	Approx. % difference.
5	7.28	7.04	3.3	0.0062	0.0057	8
10	"	"	"	0.0056	0.0050	11
16	"	6.98	4.1	0.0051	0.0046	10
20	"	"	"	"	"	"
40	"	"	"	0.0047	"	2

ϵ'_o values again agree to 4%. The larger difference in the $\tan\delta_o$ values is not surprising since the $\tan\delta_{app}$ values from which these 'real' results are derived are of the order of 0.0020 and the stated accuracy of $\pm$0.0001, e.g. 5%, thus

allows a difference of about 10% between two different determinations. In terms of tanδ, an almost insignificant error in the apparent results thus appears as a substantial error (if translated into direct measurements) in the real results.

5. BASIC SODALITE.

5.1. Description of Sample.

The sample (sample II) used for dielectric measurements was synthesised from a $Na_2O.Al_2O_3.2SiO_2$ gel, by heating this gel with 300% molar excess NaOH and a minimum amount of water (3.8 gms water for 1 gm anhydrous gel) for $3\frac{1}{2}$ days on a water bath at 95°C. The sample was washed with hot distilled water until the pH of the wash water reduced to approximately 9. At this stage further washing of a test sample produced no further pH reduction in progressive washings. The same effect had been shown with an earlier sample and it is probable that the further washing may here have caused the replacement of intercalated NaOH molecules by water. The test sample was therefore rejected and the bulk sample was air-dried.

The X-ray powder photograph (Guinier camera) shows the sample to be cubic with a = 8.96 Å. The 'd' spacings and intensities of the lines in the powder X-ray are given in Table I and are there compared with the values for a sample of natural normal sodalite and with the values given by Bultitude[77]. The powder X-ray reveals no impurities.

Under the microscope the sample is shown to consist of spherulites. Sieving through a 240 mesh B.S. sieve freed the sample from the small number of gel particles it had originally contained and reduced the average particle size. Electron migrographs on the sieved material confirm the absence of gel particles and show the particle size to be between 1 to 2.10^{-5} cms. Thus Van Vessem's condition (p. 88) is satisfied in brass cell No. 1 and approximated to in the nicosel cell.

The density found by centrifugation with benzene-methylene iodide mixtures is 2.195 gms/cm^3. This gives

Böttcher's packing fraction 'd' for hydrated basic sodalite in brass cell No. 1, as 0.371.

Chemical analysis showed the following composition: SiO_2 = 35.34%, Al_2O_3 = 29.93%, Na_2O = 18.11%, NaOH = 4.23% and H_2O = 12.39%. The NaOH result quoted, was arrived at by difference, since the experimental Na determination consistently gave a slightly lower result. On the basis of this analysis the ratio SiO_2/Al_2O_3 = 2.002 and the formula is $3(Na_2O,Al_2O_3,2SiO_2),7.04\ H_2O,1.08$ NaOH.

The equilibrium water content of the sample at each temperature was determined by thermogravimetric balance (p. 100). Results are reproduced in Table 6.

Table 6.

Thermogravimetric Determination

Basic Sodalite (Sample II) 240 mesh.

Temp. °C	% Water loss	Rel. humidity	Rel. hum. deviation from 53.3	Temp. °C	% Water loss	Rel. humidity	Rel. hum. deviation from 53.3
23	NIL	55.4	+2.1	208	8.85	56.9	+3.6
29.3	0.31	52.1	-1.2	220	9.68	50.3	-3.0
37	0.45	58.5	+5.2	234	10.34	49.7	-3.6
51	1.32	59.3	+6.0	249	10.86	58.4	+5.1
59	1.80	54.7	+1.4	258	10.97	60.5	+7.2
70	2.29	57.6	+4.3	270	11.14	57.8	+4.5
80	2.62	64.0	+10.7	284	11.32	58.4	+5.1
88.5	3.19	55.8	+2.5	293	11.63	52.6	-0.7
98.5	3.40	58.0	+4.7	324	11.91	53.0	-0.3
107	4.58	46.8	-6.5	349	12.01	52.8	-0.5
130.5	5.45	50.9	-2.4	388	12.22	49.7	-3.6
140	6.00	50.9	-2.4	428	12.29	40.4	-12.9
156	6.70	47.7	-5.6	464	12.36	46.5	-6.8
175	7.22	49.6	-3.7	492	12.39	46.0	-7.3
194	8.26	51.3	-2.0				

Relative Humidities by interpolation from the 'Handbook of Chemistry and Physics', 38th edition, 1956-57, Chemical Rubber Publishing Co. Average humidity = 53.3%.

Plotting the dehydration curve in terms of the 'percent water loss' at each temperature, there are only slight deviations from a straight line up to 240°C. Comparison of the sense of these deviations with the deviation of the relative humidity from its average value of 53.3% is instructive. In general, positive humidity deviations are accompanied by negative deviations from a straight line of the 'percent water loss', while negative humidity deviations correspond to small positive deviations of the 'percent water loss'. It can thus be assumed that at constant relative humidity the water loss curve up to 240°C would be a straight line. At higher temperatures the atmospheric humidity seems to be of no importance. The water loss curve of basic sodalite is shown in Fig. 36, the straight line up to 240°C having been obtained by using only the points at which the humidity curve crosses the abscissa of average relative humidity. The dehydration curve obtained is of the type given in Fig. 2c, which is characteristic of the robust framework zeolites. The total water loss of the sample at 500°C was 12.39%. The electrical measurements also suggest that the water content of basic sodalite varies noticeably with the relative humidity of the atmosphere. In general basic sodalite behaves like a zeolite.

Immediately after the thermogravimetric experiment, the X-ray powder photograph of some of the material sealed into a capillary tube was taken by a 9 cm camera (Table I). No crystalline change had taken place, but the unit cell had expanded to $a = 8.98$ Å. The result is only qualitative since the sample had obviously picked up a certain amount of water during the unavoidable cooling which took place while dismantling the thermogravimetric apparatus and during the filling of the capillary tube. An X-ray powder photograph taken by a 9 cm camera, of the anhydrous material dehydrated

in vacuum at 350°C also shows that no crystalline change had taken place on dehydration but the unit cell of the sample had expanded to a = 9.02 Å. (Table I). A similar expansion has been observed in the case of other zeolites by Bultitude[77].

The density of the anhydrous material, determined by calculation from the density of the hydrated sample and from its water content is 1.923 gms/cm³. Taking the unit cell expansion into account, this density reduces to 1.885 gms/cm³. This gives the packing fraction 'd' of the anhydrous basic sodalite in the "nicosel" cell as 0.377.

The refractive indices, determined with sodium light, are 1.501 and 1.430 for the hydrated and anhydrous samples respectively. Thus the electronic contributions to the dielectric constant ϵ_o' are 2.25 for hydrated basic sodalite and 2.04 for anhydrous.

5.2. Hydrated Basic Sodalite.

The resistance of the sample was so low that the width of the resonance curve had to be measured with the main condenser of the Hartshorn-Ward apparatus. Fixed condensers had to be inserted in the bridge to measure some of the very high capacitances. The oscillator voltage was 22 V. There was no difference between results at this voltage and others at 2 V. At 30° and 50°C no results could be obtained between 50 and 216 kc/s. Measurements were made at 30, 50, 80 and 114.7°C. The results are given in Tables II to IX and ϵ'_{app}, $\tan\delta_{app}$, ϵ''_{app}, $R_{p(app)}$, $\log(R_{p(app)})$, ϵ'_{app} and $\tan\delta_{app}$ respectively are plotted against log(frequency) in Figs. 37 to 43. Figs. 37 to 41 inclusive cover the whole of the experimental frequency range, while Figs. 42 and 43 are larger scale plots at the higher frequencies of ϵ'_{app} and $\tan\delta_{app}$.

The following are the percentage water losses at the temperatures of measurement (see Fig. 36):

30°C 0.33%; 50°C 1.26%; 80°C 2.62%; 114.7°C 4.86%.

Judging by these figures and the compact arrangement of the cell it seems unlikely that water equilibrium had been obtained at the higher temperatures in spite of long pre-heating periods. Only the 30° and possibly the 50°C results may approximate to equilibrium conditions, and in general the qualitative results are of main interest.

The ϵ'_{app} curves in Fig. 37 in each case sweep up to a very high and still increasing value with decreasing frequency and show no inflexion point. The 30° $\tan\delta_{app}$ curve (Fig. 38) has only one maximum, the 80° curve two, the higher frequency one already being indicated on the 50° curve. At 114.7° there appears an indication of a second maximum at the lowest frequencies of measurement. It can be assumed that the maximum in the 30° curve corresponds to the high frequency maxima at the other temperatures. The change with temperature of the frequency position of these maxima is then parallel to the change of ϵ'_{app} values with temperature over the same frequency range. The high frequency maximum in the $\tan\delta_{app}$ curves moves to a higher frequency with increase in temperature from 30 to 80°C and then drops to a lower frequency at 114.7°C; the values of ϵ'_{app} increase between 30 and 80° and then drop to a lower value at 114.7°C. This suggests that both effects are due to the same cause.

Since water equilibrium had obviously not been reached except at the lower temperatures, the drop in $\tan\delta_{app}$ values with increasing temperature cannot be quantitatively correlated with the corresponding water loss. However this as well as the large ϵ'_{app} values at low frequencies, the fact that while ϵ'_{app} increases from 30 to 80°C it shows a

large drop at 114.7°, and the relative magnitude of the shunt resistance curves can be explained qualitatively. The explanation is based on the Maxwell-Wagner model of an inhomogeneous semiconductor (pp. 80-84) as expanded by Billig and Plenner. The effect giving rise to such behaviour is commonly termed 'interfacial polarisation' or the 'barrier layer effect'. The very high and increasing values of the apparent permittivity at low frequencies, point to this as the only feasible mechanism to explain the results.

If, as an approximation, the particles are considered as close packed spheres between the plates, there will be many equivalent, parallel direct paths. One such path is considered, keeping in mind that the real picture must undoubtedly be complicated by:

(i) interaction between spheres in neighbouring paths;
(ii) the variation in size of the particles and barriers;
(iii) non-uniform packing of the spheres; and
(iv) some of the particles not being perfect spheres.

The electrical behaviour of the material suggests that whereas the inside of the spheres is conducting or semi-conducting by some provess to be specified, there is a barrier to conduction at the contact points between the spheres. If the conduction within the particles is due to the actual movement or drift of charge, we can imagine that at any given instant a surplus of charge of opposite sign will have accumulated at adjacent sides of contact making spheres, provided the process is such that the resistance to charge transport across the contact point of the two particles is large compared with the resistance to charge transport within the particles themselves. Between particles X and Y with barrier B this will produce the situation of Fig. 44, giving the equivalent circuit of Fig. 45, where C_x, C_y, R_x, R_y,

referring to the particles are small, while C_b and R_b referring to the barrier are large. The fall of potential for the whole path is indicated in Fig. 46, the equivalent circuit being just a series arrangement of Fig. 45 for every particle contact.

The total resistance and capacitance of such a chain of particles would be

$$\frac{1}{C} = \sum_{1}^{n} \frac{1}{C_n} \qquad (147) \qquad\qquad R = \sum_{1}^{n} R_n \qquad (148)$$

where C_n and R_n include both R_b and C_b and the corresponding quantities for the particles.

The particles contain in their interstices both H_2O and NaOH, i.e. Na^+ and OH^- ions. Thus two processes may be visualised:

1. Hydration giving Na^+ ions increased mobility,
2. The process $H_2\underline{O} + OH^- = \underline{O}H^- + H_2O$.

Either or probably both these processes may take place. It is easy to see that whereas this conduction process may take place unhindered throughout the particle width within the particle, the contact points (the nature of which on a molecular scale it seems difficult to define) provide narrow necks which will not allow the process to proceed unhindered. Furthermore there must be repulsion between particles of the same sign of charge trying to approach each other laterally, as at the necks.

The conduction process explains the increase of ε'_{app} with decreasing frequency. It can be imagined that at the highest frequencies, change of polarity is so rapid, that the conduction process does not have time to build up a space charge on both sides of the contact between particles and so does not give a barrier capacitance which is appreciable

compared with the capacitance of the anhydrous crystals themselves. This suggests constancy of ϵ'_{app} which is approximated to in Fig. 37 for the highest frequencies. It might be noted that even between 216 kc/s and 5.3 mc/s there is always a slight decrease in ϵ'_{app} with increasing frequency (Table 7 and Fig. 42). As the frequency decreases the process of space charge formation takes place to an increasing extent, giving the rise of ϵ'_{app} actually found. At the lowest frequencies the values of $R_{p(app)}$ in Fig. 40 would not be expected to vary very much with frequency (Fig. 26). In fact at 30 and 50°C almost straight lines of small slope are found up to 50 and 300 kc/s respectively. It will however later be shown that these constant values correspond to the high rather than the low frequency constant part of ρ' in Fig. 26. The decrease of $R_{p(app)}$ with increasing frequency, found at the high frequencies at 30 and 50°C is then shown to be due to the waning influence of d.c. conductivity, whereas the decrease in the 80 and 114.7°C curves suggests that with increasing temperature and dehydration the experimental $R_{p(app)}$ values fall, as expected, into the intermediate range of the ρ' curve in Fig. 26.

From Figs. 37 to 41 it appears that two opposed and simultaneous factors govern the effects produced by temperature increase:-

1. the mobility of the current carriers increases very rapidly and probably exponentially with temperature. This will tend to increase C_b and to decrease R_c, R_b and C_c;

2. water is lost. This loss causes a decrease in the ease of charge transport by the two mechanisms given on page 131. Thus C_c, R_c and R_b will increase and C_b decrease.

Evidently to produce the observed behaviour the changes of C_c are small compared with the changes of C_b.

Between 30 and 50°C water loss is small (see p. 129) and the increase in the mobility of current carriers due to temperature increase is the dominant factor (Figs. 37 and 40). Between 50 and 80°C water loss dominates the resistance changes (Fig. 40), but increase in the mobility of current carriers and water loss exercise rather similar opposing influences upon capacitance (Fig. 37). Between 80 and 114.7°C a large water loss determines the over-all effect upon both $R_{p(app)}$ and ϵ'_{app}. The equivalent circuit for this case where some water is still present is given in Fig. 47.

When no water is left, the Na^+ ions are held more firmly in the lattice and also no proton jumps between H_2O and OH^- are possible. Then C_c, R_c, C_b and R_b will become characteristic of the anhydrous crystals and if $C_c \ggg C_b$ and $R_c \ggg R_b$ the situation would approach that shown in Fig. 48.

The high frequency curves of ϵ'_{app} and $\tan\delta_{app}$ against frequency (Figs. 42 and 43, 63 kc/s to 5.3 mc/s) are easily explained if it is assumed that the influence of the water plays a smaller part here. ϵ'_{app} tends to a more and more constant value with frequency and temperature increase (Table 7 and Fig. 42). $\tan\delta$ at first increases with temperature (30 to 50°C), as would be expected if there were no water loss, and then decreases for higher temperatures pointing to the effect of water loss (Table 7 and Fig. 43).

Table 7.

Hydrated basic Sodalite.
(The variation of ϵ'_{app} and $\tan\delta_{app}$ over the linear part of the curves in Figs. 37 and 38).

Temperature °C	ϵ'_{app}		$\tan\delta_{app}$	
	216 kc/s	5.3 mc/s	216 kc/s	5.3 mc/s
30	6.95	3.48	2.24	0.53
50	7.27	3.69	2.50	0.58
80	6.95	3.40	1.54	0.44
114.7	5.64	2.96	0.55	0.28

A Cole-Cole plot is not obtainable for these results. This means that there is a wide distribution of boundary time constants, which is undoubtedly due to a combination of the factors mentioned on page 130, which complicate the simple model. The possibility of such a wide distribution of time constants in a polycrystalline material had been pointed out by Hirsch (p. 83). It must be concluded that the picture of a barrier layer semi-conductor given here is much over-simplified. Nevertheless some semi-quantitative conclusions can be drawn.

The frequency independent capacitances and resistances measured at the higher frequencies represent the values for the grains (p. 81), and therefore ϵ'_o and $\tan\delta_o$ values were calculated from the 'apparent' values at the flattest part of the curves (Figs. 37 and 38), namely at 5.3 mc/s, using equations (143) and (145). From consideration of Tables II to IX it can be seen that, particularly in the case of ϵ'_o, these results should give an approximation of the values for the massive crystalline substance. The results are given in Table 8,

Table 8.

Hydrated Basic Sodalite.

Temperature °C	ϵ'_{app}	ϵ'_o	$\tan\delta_{app}$	$\tan\delta_o$
30	3.48	12.62	0.53	1.21
50	3.69	13.62	0.58	1.37
80	3.40	12.79	0.44	0.95
114.7	2.96	10.56	0.28	0.22

In the lower frequency range of the 30 and 50°C curves of Fig. 39, $\log \epsilon''_{app}$ is proportional to log(1/f). Dryden and Meakins[126], Nesbitt and Pink[179] and Taylor[180] obtained analogous results on different systems. These workers showed that the low frequency dielectric loss is due to d.c. conductance in the region where $\log \epsilon''$ is porportional to log(1/f), the contribution due to a.c. loss being negligible under these conditions. The specific d.c. resistance can then be calculated from equation (41) which gives:

$$\log \epsilon'' + \log f = \text{constant} \qquad (149)$$

The theoretical dotted line in Fig. 39 and any curve parallel to it satisfies equation (149) and indicates a dielectric loss due to d.c. conductivity only. The 30 and 50°C $\log \epsilon''$ curves of hydrated basic sodalite obey this condition to about 50 kc/s, and the specific resistances calculated by equation (41) are shown in Table 9.

Table 9.

Frequency	Specific Resistance, Ω 30°C	50°C	E k.cal/ mole	Frequency	Specific Resistance 30°C	50°C	E k.cal/ mole
560 c/s	724000	541000	2.82	4.0 kc/s	701000	510000	3.09
620 "	723000	540000	2.84	5.0 "	698000	505000	3.15
700 "	721000	539000	2.84	6.3 "	696000	499000	3.24
800 "	720000	536000	2.86	8.0 "	693000	492000	3.32
890 "	719000	536000	2.85	10.0 "	693000	486000	3.46
1.0 kc/s	718000	534000	2.88	13.0 "	688000	478000	3.53
1.15 "	716000	532000	2.89	16.0 "	685000	473000	3.59
1.3 "	715000	531000	2.90	20.0 "	685000	467000	3.71
1.6 "	712000	527000	2.92	25.0 "	680000	463000	3.74
2.0 "	709000	524000	2.94	32.0 "	675000	457000	3.79
2.5 "	707000	520000	2.98	40.0 "	673000	453000	3.84
3.2 "	704000	515000	3.03	50.0 "	669000	451000	3.84

The results show a slight variation with frequency but approximately straight line plots of specific resistance against frequency are obtained between 560 c/s and 1.6 kc/s. These, when produced to zero frequency give the specific resistances as 7.3 x 10^5 ohm at 30°C and 5.5 x 10^5 ohm at 50°C.

Similarly the low frequency $R_{p(app)}$ results are insensitive to frequency and correspond to d.c. resistances[179] The straight line $R_{p(app)}$/frequency plots give the resistances at zero frequency as 3880 Ohm at 30°C and 2900 Ohm at 50°C. By using the approximately known cell dimensions (plate surface area = 27 cm^2, plate gap = 0.15 cm), the specific resistances were found to be 7.0 x 10^5 and 5.2 x 10^5 Ohm at 30 and 50°C respectively. These results are of the same order as the more accurate values obtained from equation (41).

Since it is assumed that the conduction is purely ionic (p. 130), that the 30 and 50°C results are equilibrium values (p. 129) and that the ionic conduction is not affected by the comparatively small water loss (p. 129) between the two temperatures, a free energy barrier against the ionic movement can be calculated from the specific resistances by using the Arrhenius equation:

$$\log(R_2/R_1) = (E/4.57)\,(1/T_2 - 1/T_1) \qquad (150)$$

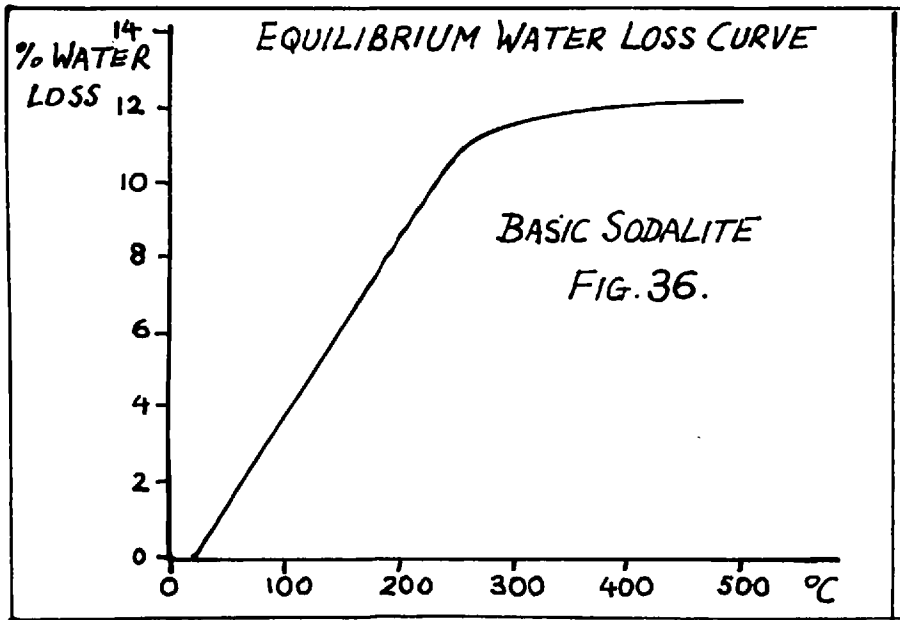
The results of this calculation at various frequencies are given in Table 9. Extrapolating the 'E' values to zero frequency, or calculation from the specific resistances at zero frequency, gives the activation free energy E = 2.77 k.cal/mole, while the more accurate value obtained directly from $R_{p(app)}$ at zero frequency is 2.83 k.cal/mole. Two types of energy barrier against ion movement are involved in the model on page 130, one within the grains between favoured ion positions and one between the grains which causes the interfacial polarisation.

Obviously the latter must be the larger. Consideration of Table 2 and the 30°C $\tan\delta_{app}$ curve (Fig. 38) indicates that the relaxation peak corresponds to an activation energy much larger than 2.8 k.cal/mole and is therefore associated with the grain-grain barriers. Thus 2.8 k.cal/mole is the activation energy characteristic of ion conductance within the grains. This is supported by consideration of Fig. 26, the Billig and Plenner model, which has two regions of constant specific resistance. Comparison of the low frequency experimental results at 30 and 50°C with Fig. 26 shows that the frequency region used in the calculation of activation energy corresponds to the higher frequency constant resistance region of Plenner's model, i.e. gives the grain $R_{D.C.}$. The activation energy of 2.8 k.cal/mole within the grains is too small to be due to sodium ions. It is therefore probably due to conduction by protons by the process:

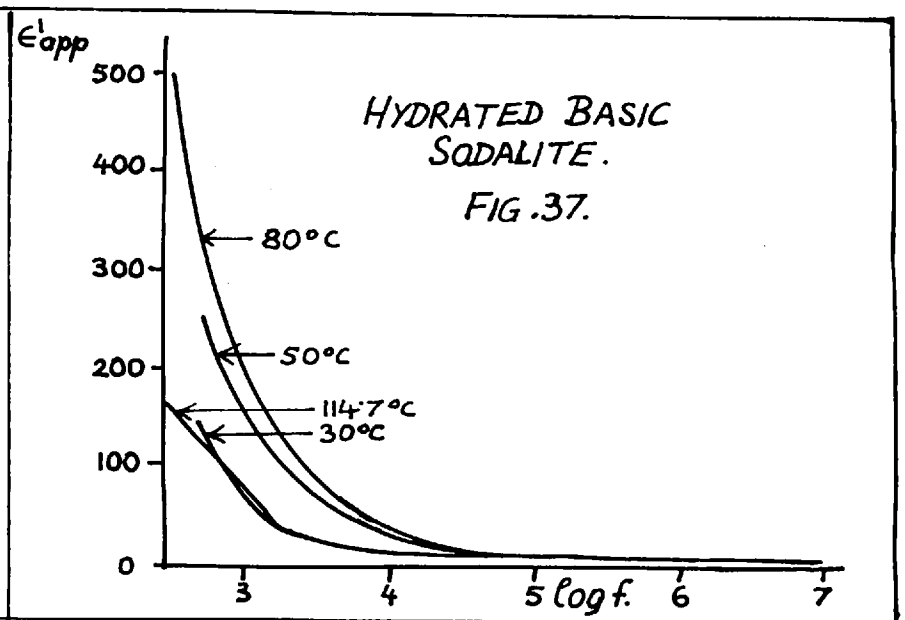
$$H_2\underline{O} + OH^- = \underline{O}H^- + H_2O$$

The specific d.c. resistances for the solid crystalline substance can be calculated by dividing the zero frequency 'apparent' specific resistances obtained above, by the Böttcher packing fraction. Then:
Specific resistance at 30°C = 1.96 meg-Ohm, and the specific resistance at 50°C = 1.48 meg-Ohm, both for the massive crystalline substance. The activation energy (see equation 150) is not affected by this calculation, but it must be kept in mind that it is only correct if the influence of the water loss between 30 and 50°C on this calculation is indeed negligible, as is anticipated.

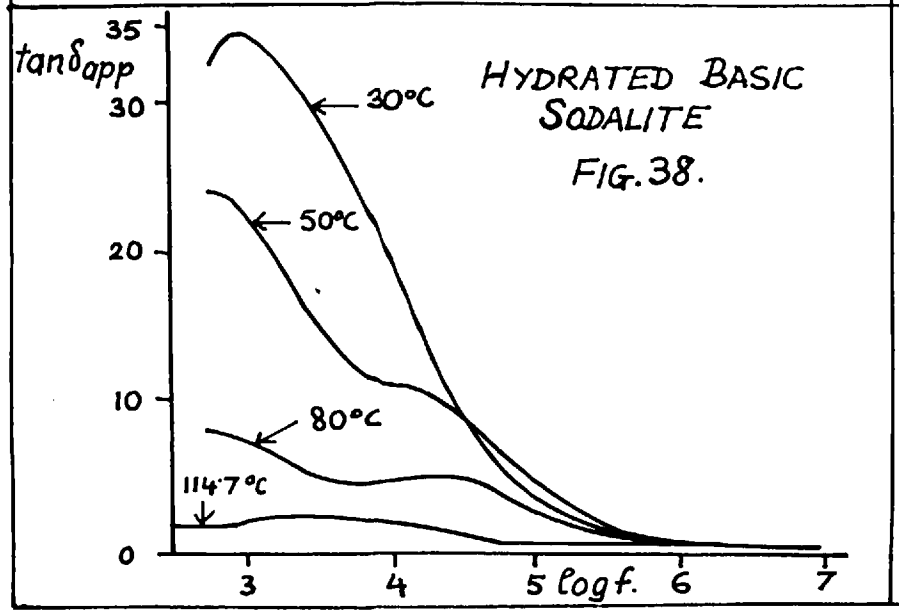
The results obtained point to the possibility of using the powder method of measurements as a means of determining d.c. resistance by an a.c. method. Similar successful attempts to make d.c. measurements on 'sandwich' slabs of materials have in fact been carried out by Lewis and Bickford[139].



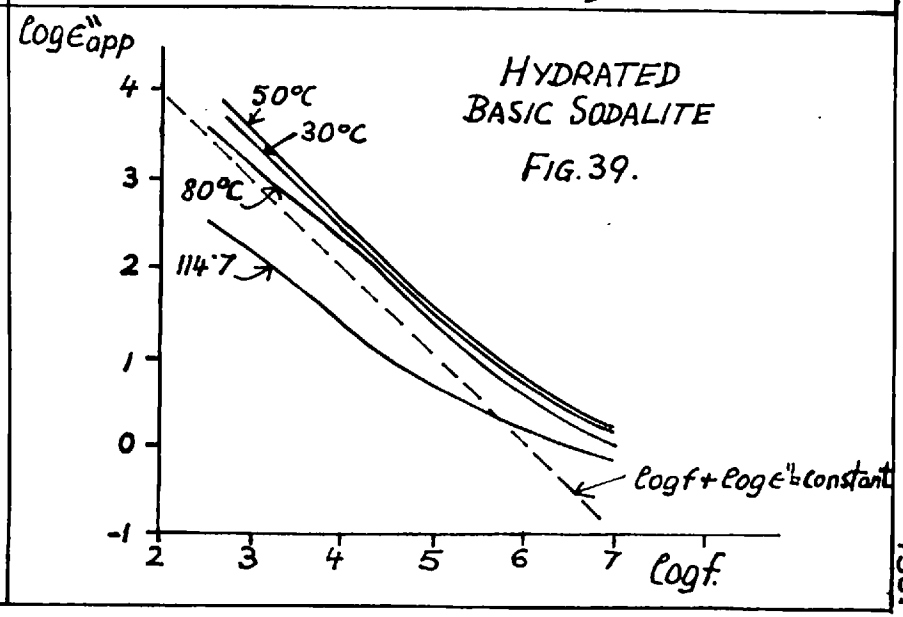
BASIC SODALITE
FIG. 36.



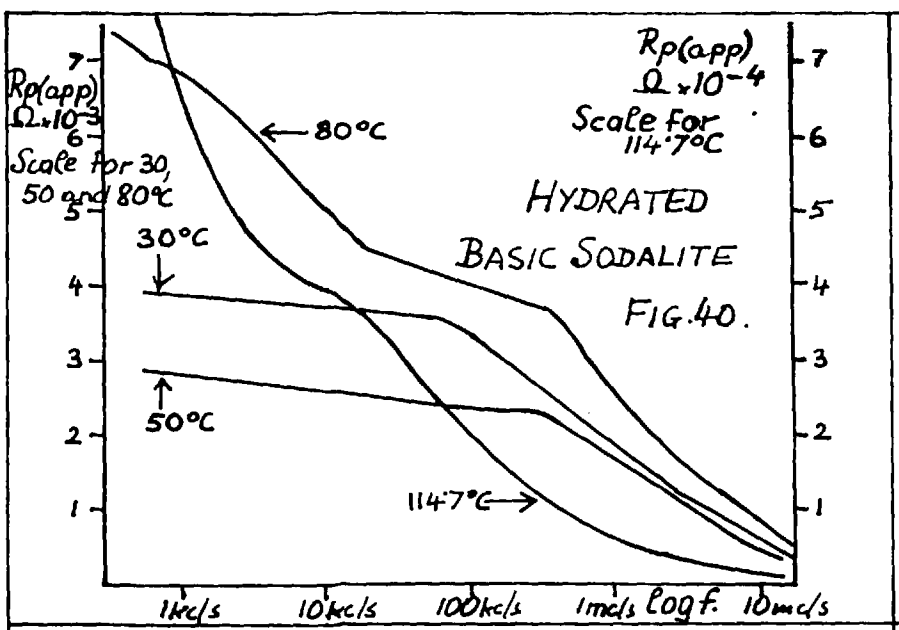
HYDRATED BASIC SODALITE.
FIG. 37.



HYDRATED BASIC SODALITE
FIG. 38.

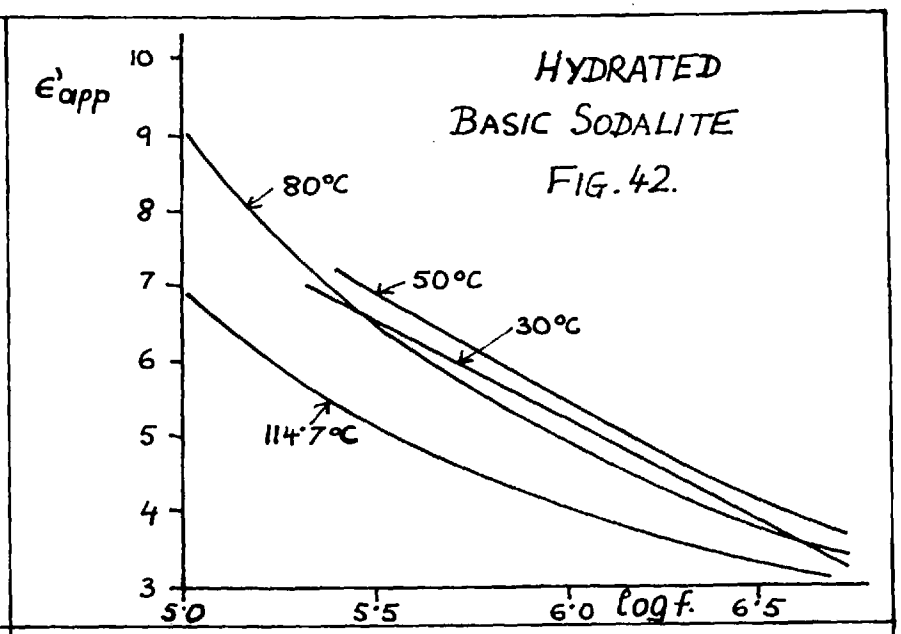


HYDRATED BASIC SODALITE
FIG. 39.



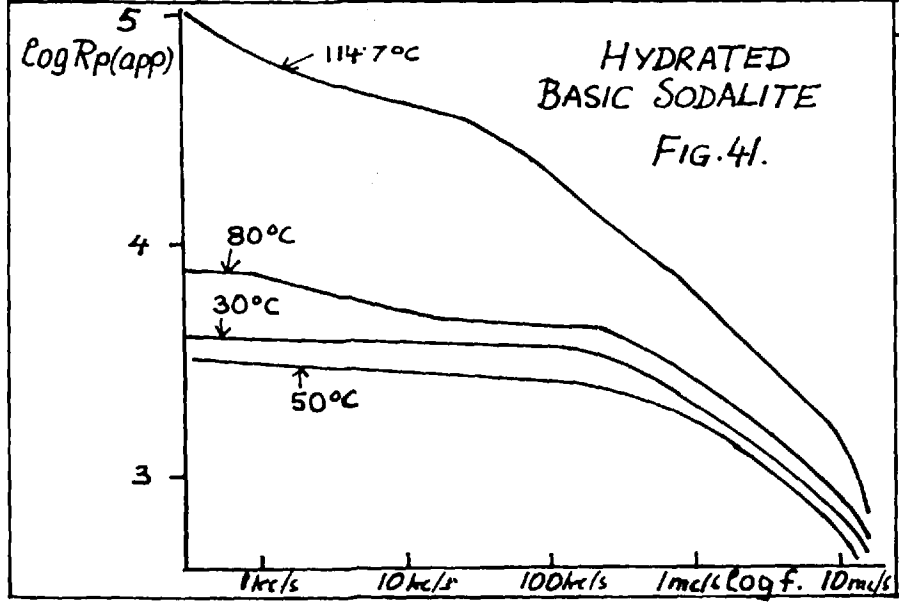
HYDRATED BASIC SODALITE

FIG. 40.



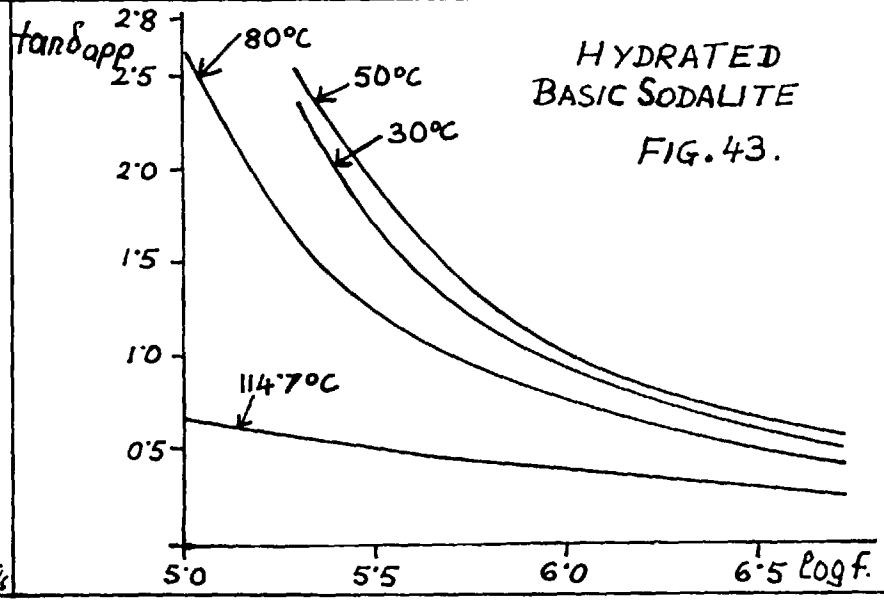
HYDRATED BASIC SODALITE

FIG. 42.



HYDRATED BASIC SODALITE

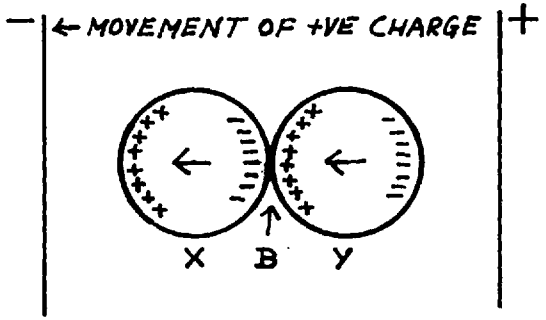
FIG. 41.



HYDRATED BASIC SODALITE

FIG. 43.

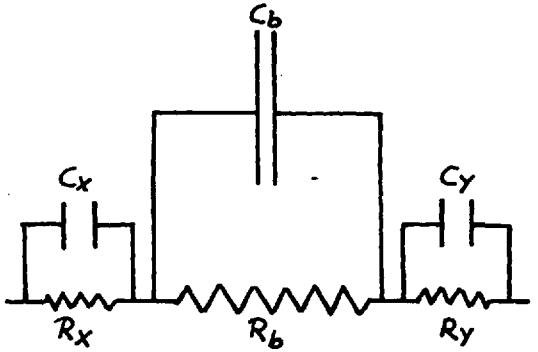
HYDRATED BASIC SODALITE.



POSITION AT ANY INSTANT

FIG. 44.

HYDRATED BASIC SODALITE.

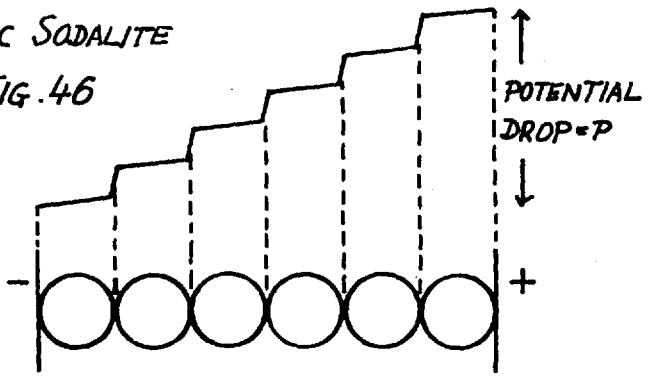


EQUIVALENT CIRCUIT OF FIG. 44.

FIG. 45.

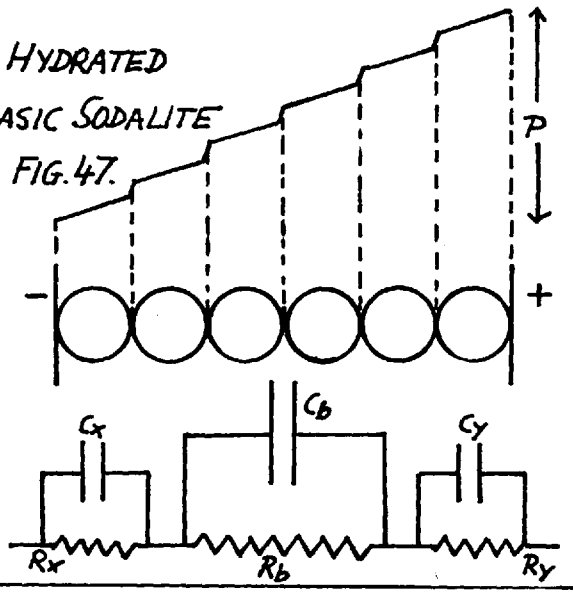
HYDRATED BASIC SODALITE

FIG. 46

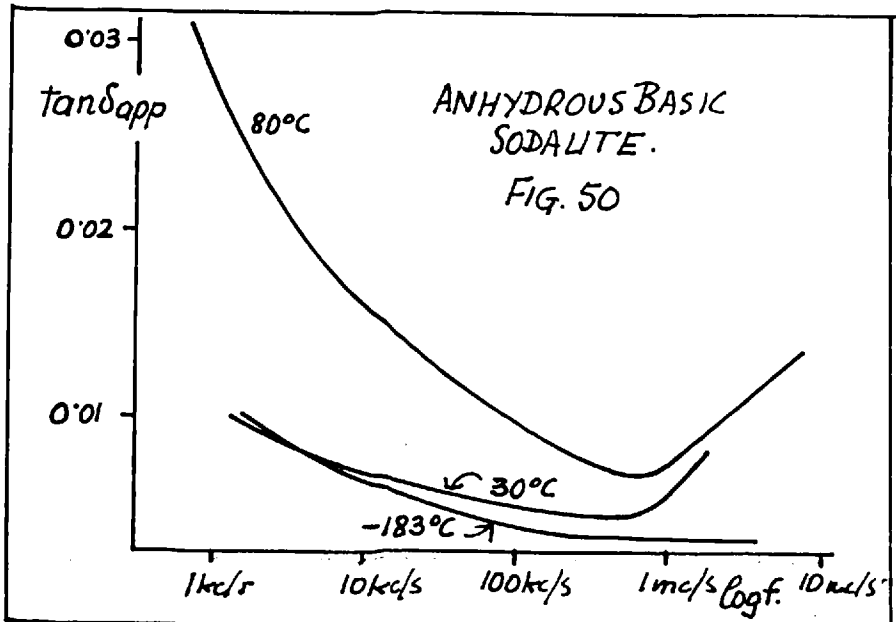


HYDRATED BASIC SODALITE

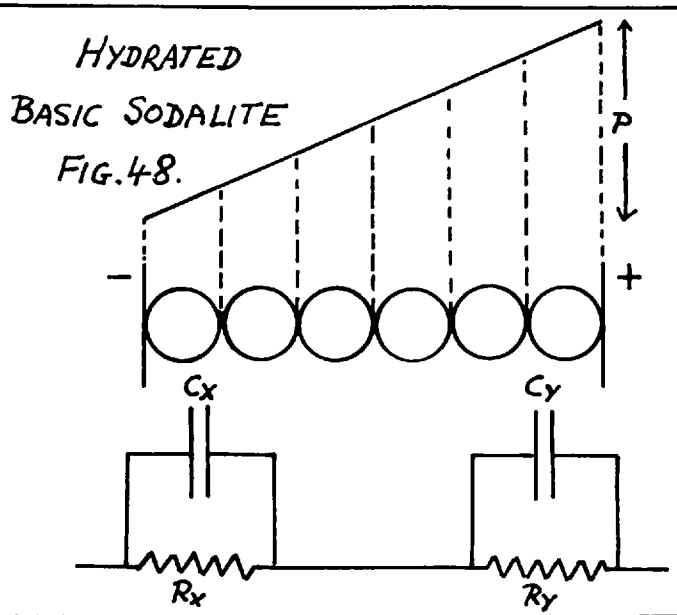
FIG. 47.



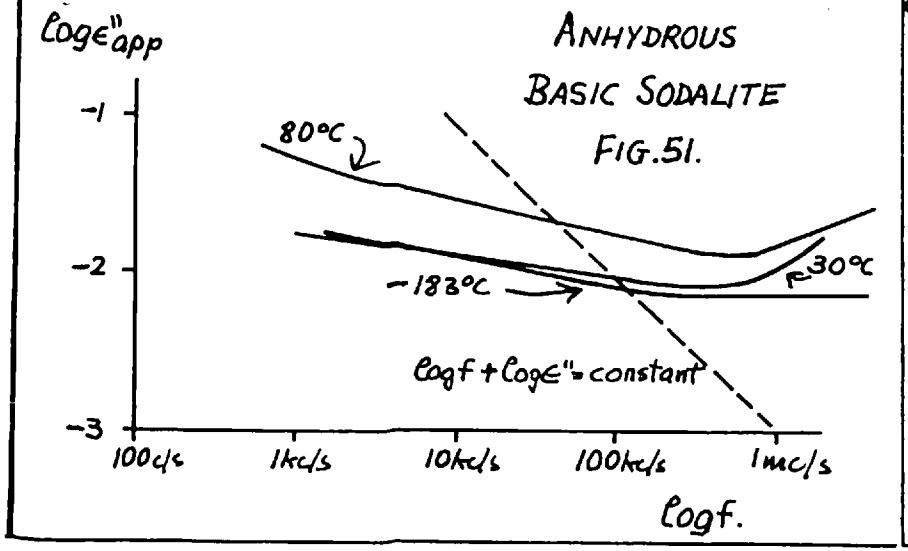
140.



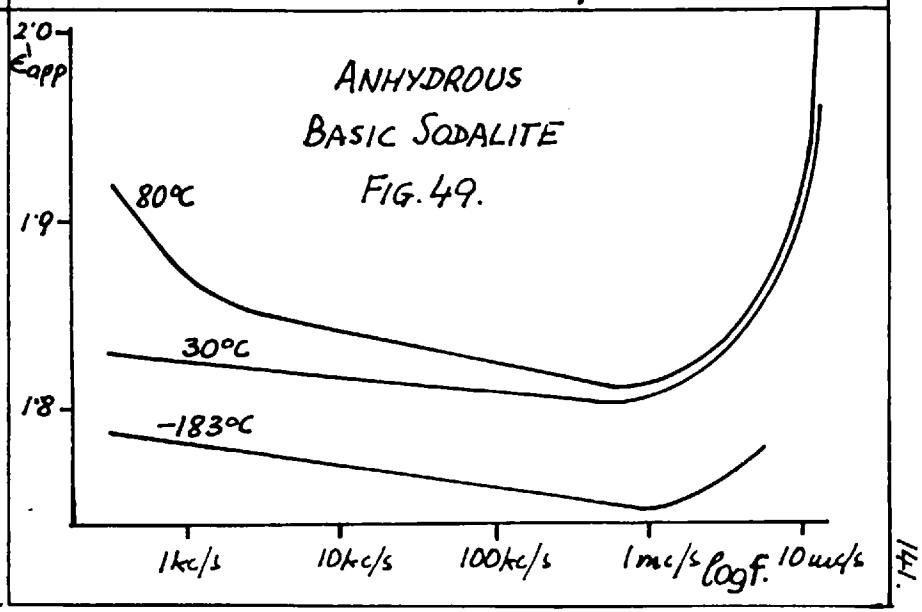
ANHYDROUS BASIC SODALITE.
FIG. 50



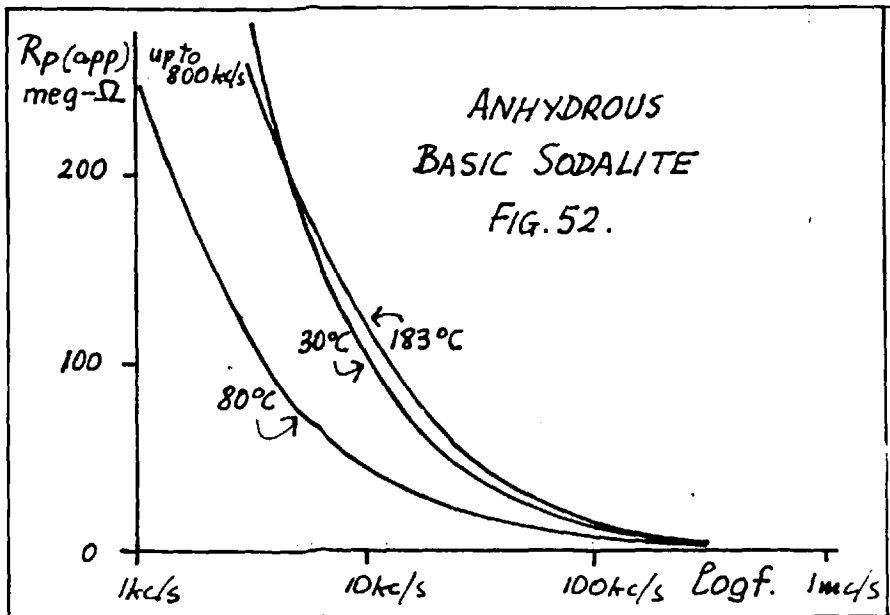
HYDRATED BASIC SODALITE
FIG. 48.



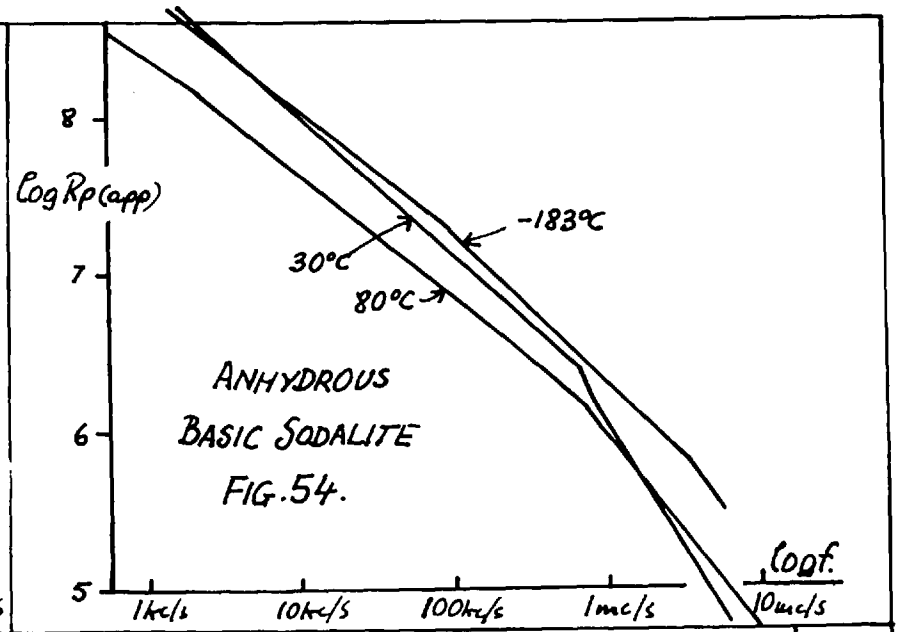
ANHYDROUS BASIC SODALITE
FIG. 51.

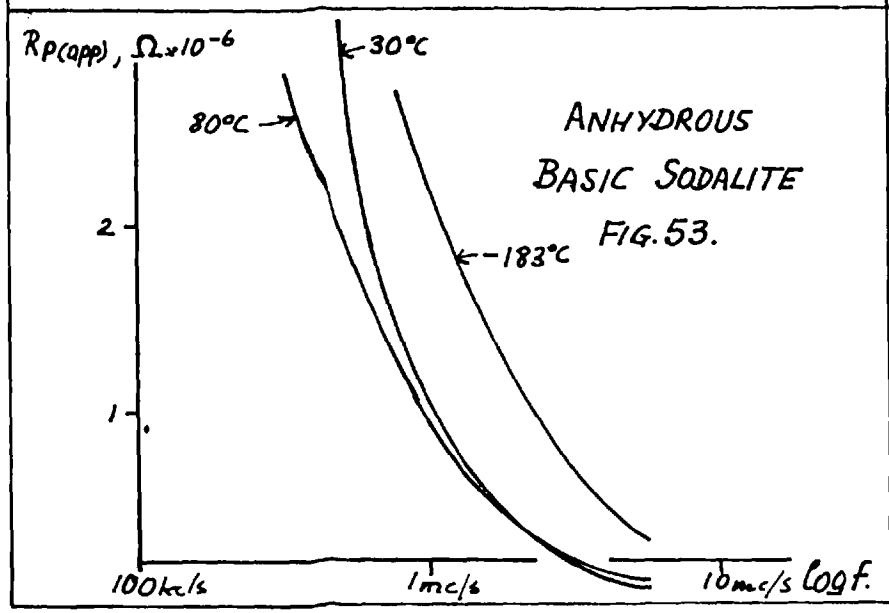


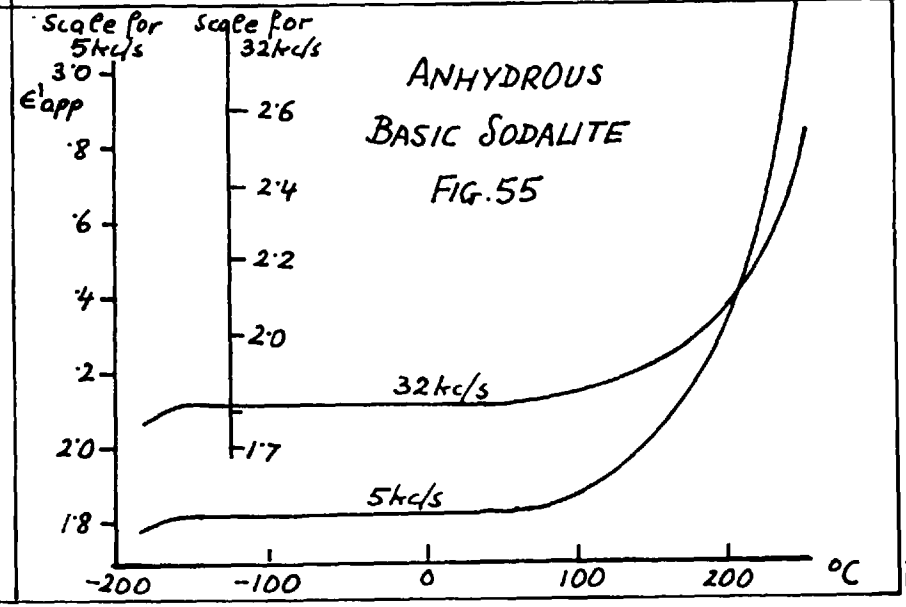
ANHYDROUS BASIC SODALITE
FIG. 49.

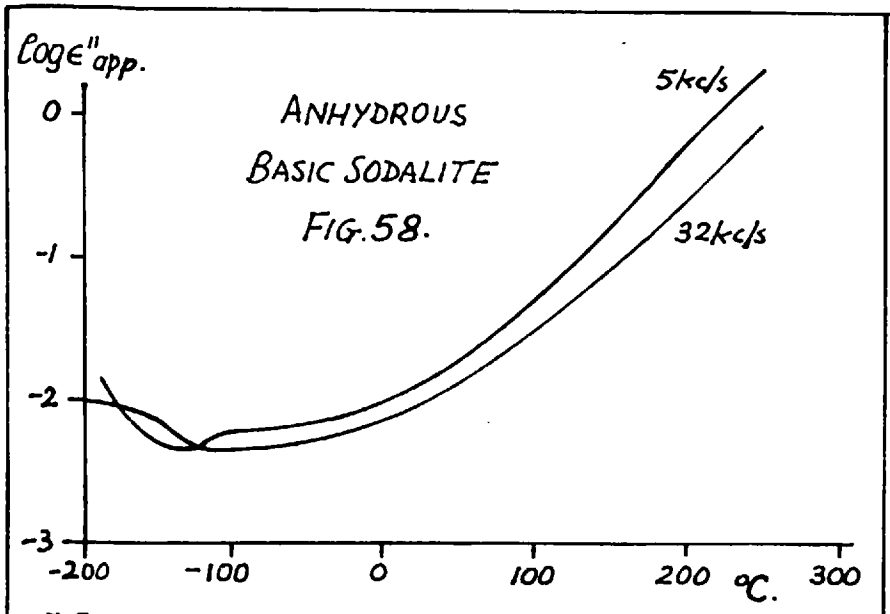


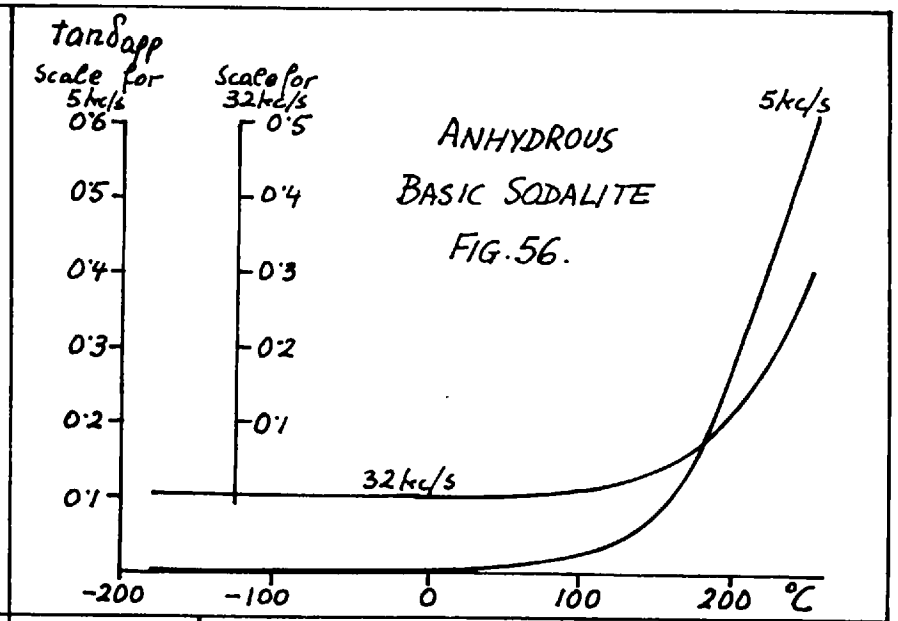
ANHYDROUS
BASIC SODALITE
FIG. 52.

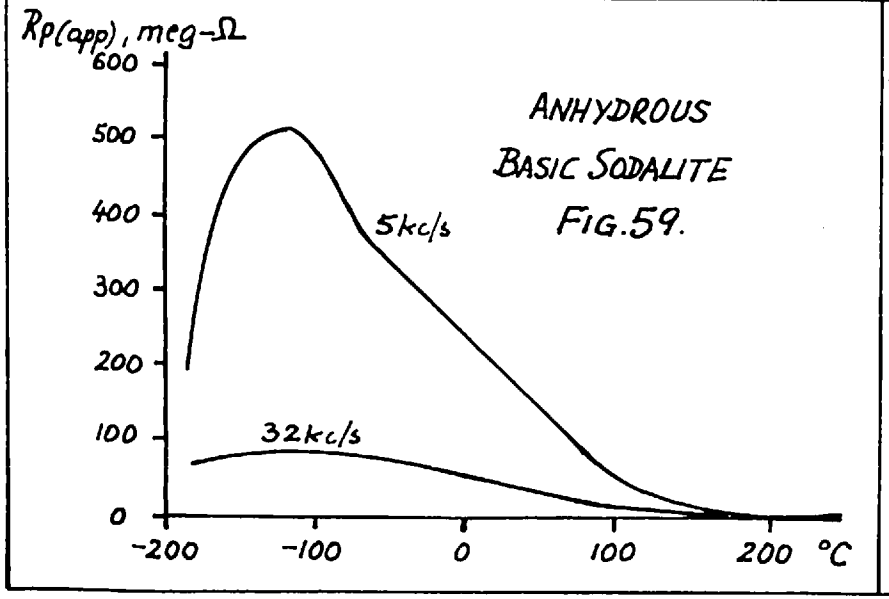


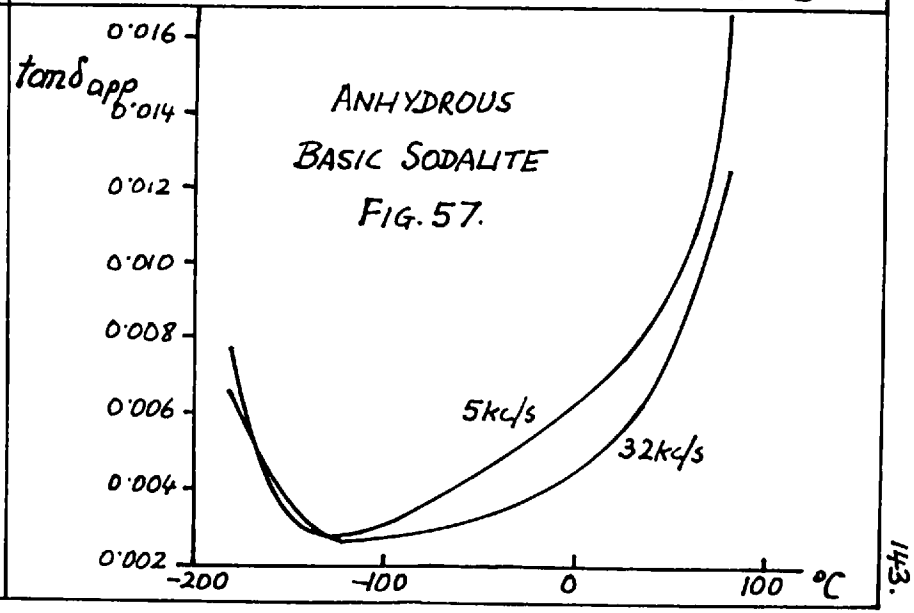


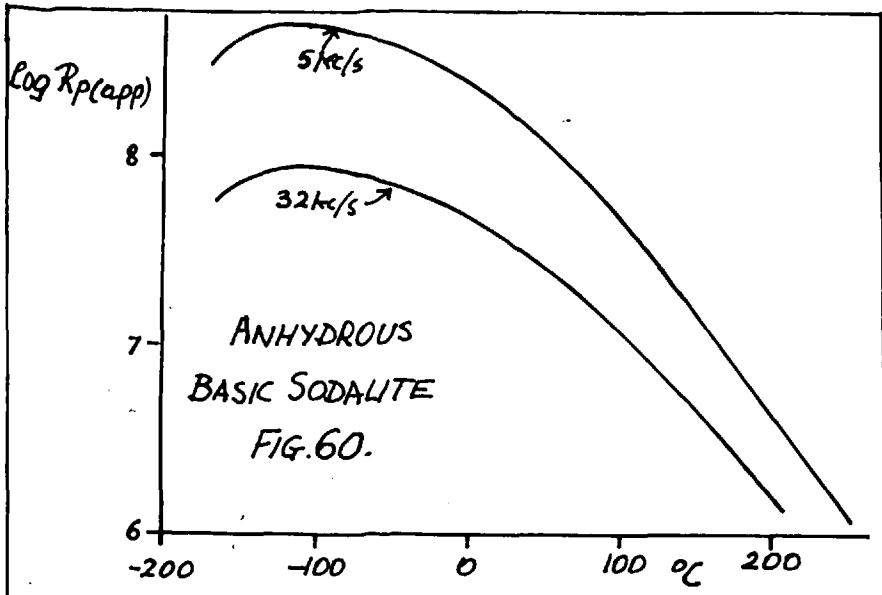


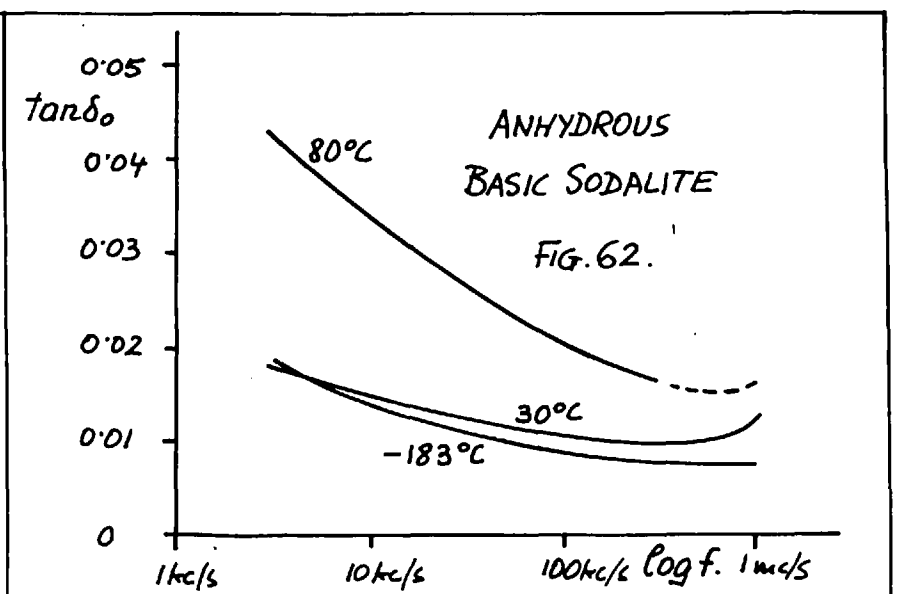

Log ε" app.
0
-1
-2
-3
-200
-100
0
100
200
300
°C.
5kc/s
32kc/s
ANHYDROUS
BASIC SODALITE
FIG. 58.

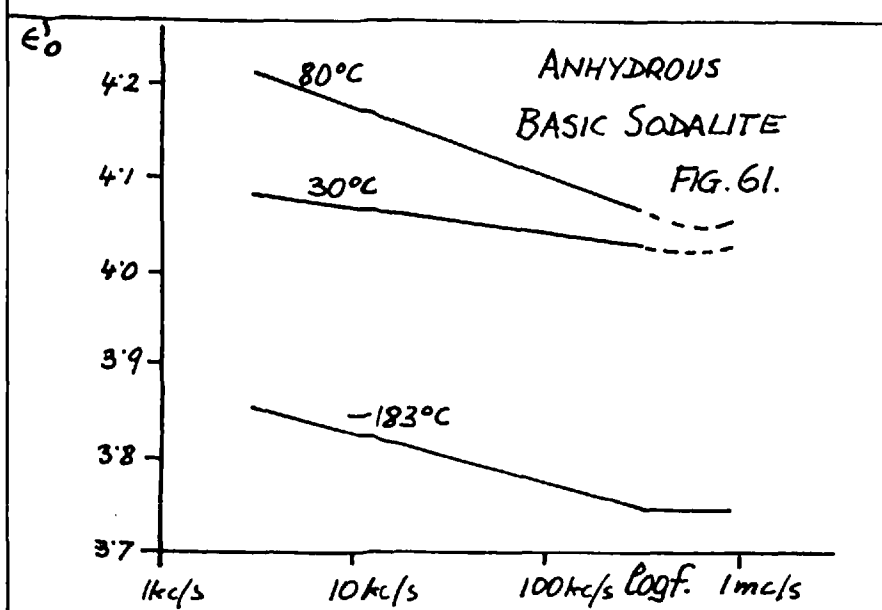

tan δ app
Scale for 5kc/s
Scale for 32kc/s
0·6
0·5
0·4
0·3
0·2
0·1
0·5
0·4
0·3
0·2
0·1
-200
-100
0
100
200
°C
5kc/s
32kc/s
ANHYDROUS
BASIC SODALITE
FIG. 56.

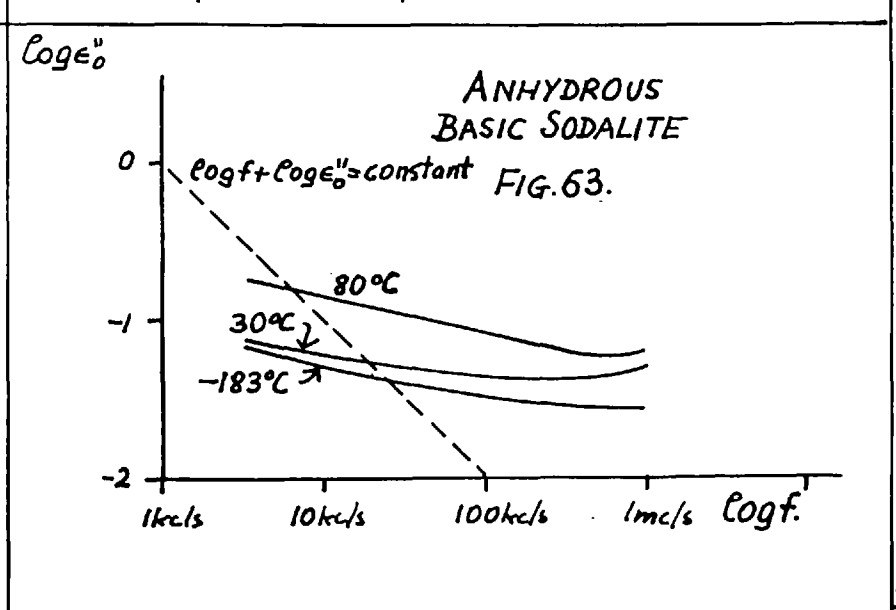

Rp(app), meg-Ω
600
500
400
300
200
100
0
-200
-100
0
100
200
°C
5kc/s
32kc/s
ANHYDROUS
BASIC SODALITE
FIG. 59.

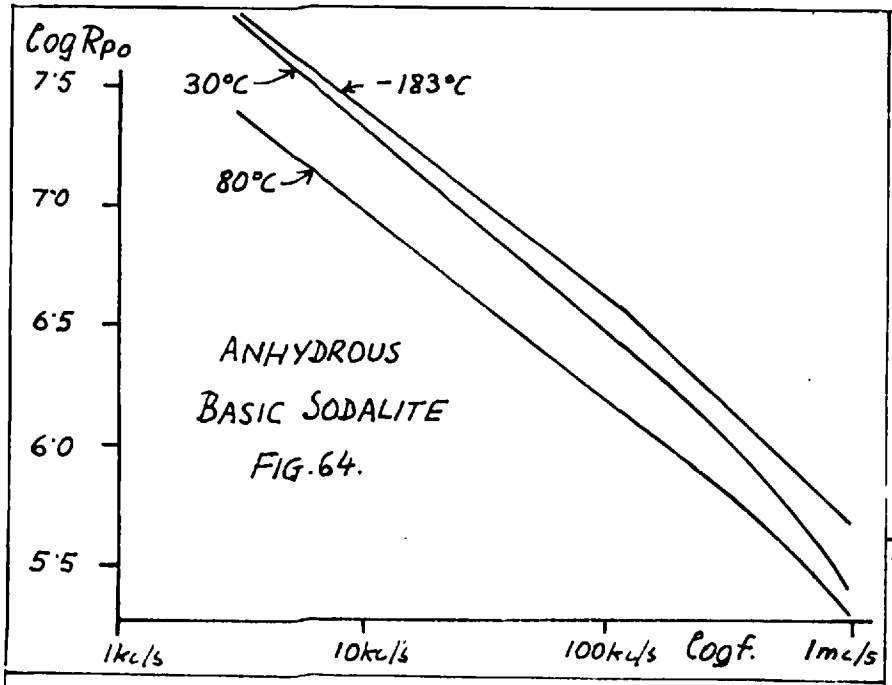

tan δ app
0·016
0·014
0·012
0·010
0·008
0·006
0·004
0·002
-200
-100
0
100
°C
5kc/s
32kc/s
ANHYDROUS
BASIC SODALITE
FIG. 57.

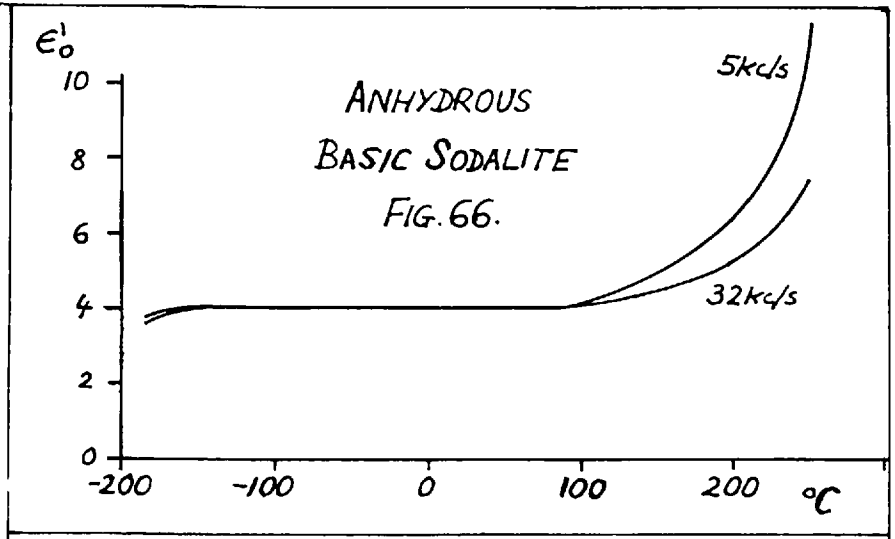

Log Rp(app)
8
7
6
5kc/s
32kc/s
-200
-100
0
100
°C
200
ANHYDROUS
BASIC SODALITE
FIG.60.

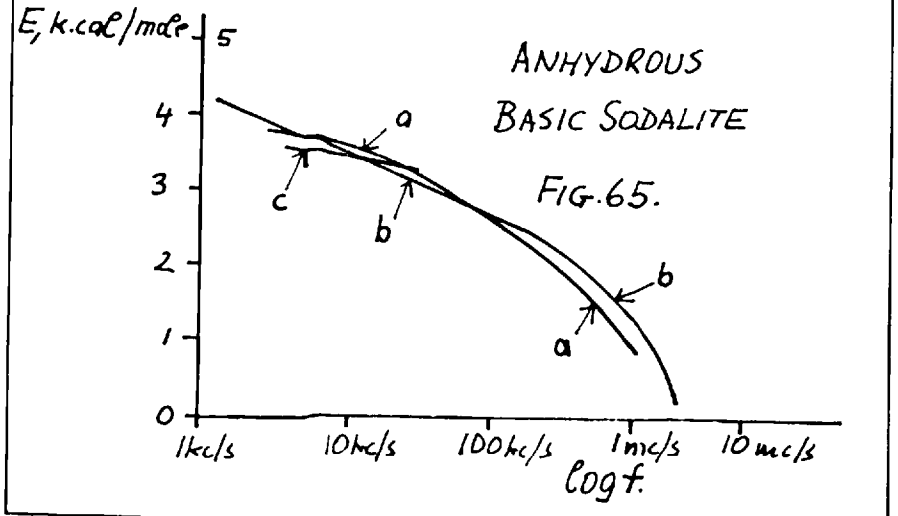

tanδo
0·05
0·04
0·03
0·02
0·01
0
80°C
30°C
-183°C
1kc/s
10kc/s
100kc/s
Log f.
1mc/s
ANHYDROUS
BASIC SODALITE
FIG.62.

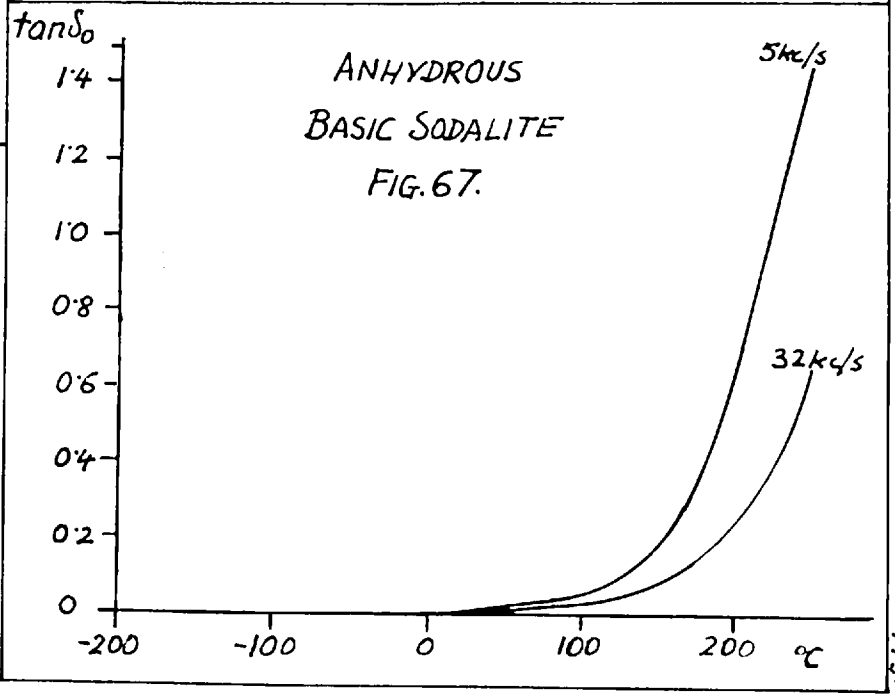

ε'o
4·2
4·1
4·0
3·9
3·8
3·7
80°C
30°C
-183°C
1kc/s
10kc/s
100kc/s
Logf.
1mc/s
ANHYDROUS
BASIC SODALITE
FIG.61.

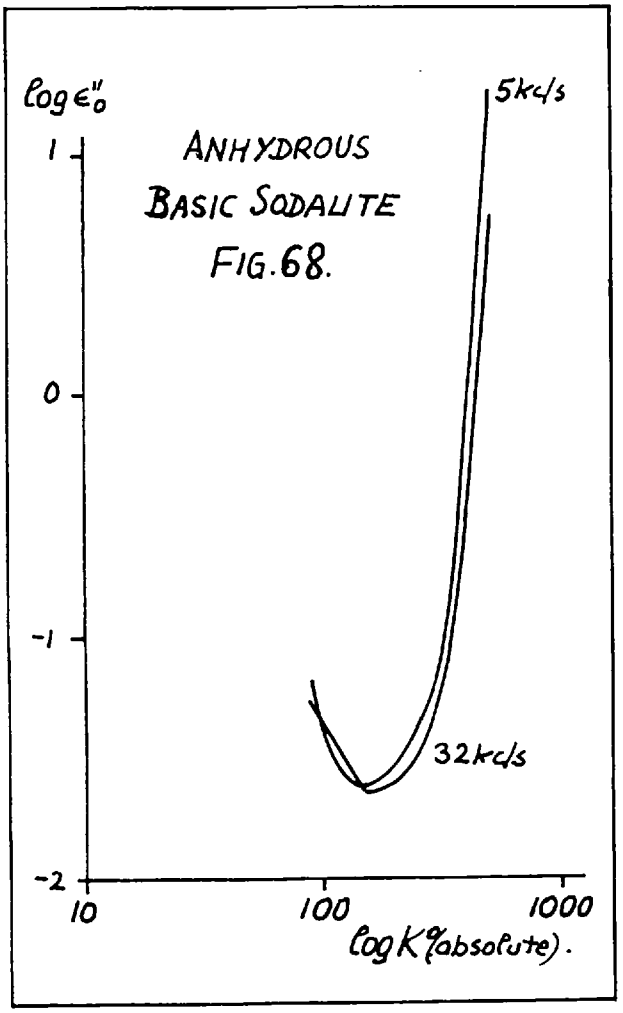

Logε"o
0
-1
-2
Logf+Logε"o=constant
80°C
30°C
-183°C
1kc/s
10kc/s
100kc/s
1mc/s
Logf.
ANHYDROUS
BASIC SODALITE
FIG.63.


Log Rpo
7·5
7·0
6·5
6·0
5·5
30°C
-183°C
80°C
ANHYDROUS
BASIC SODALITE
FIG. 64.
1kc/s
10kc/s
100kc/s
Log f.
1mc/s


ε'o
10
8
6
4
2
0
5kc/s
ANHYDROUS
BASIC SODALITE
FIG. 66.
32kc/s
-200
-100
0
100
200
°C


E, k.cal/mole
5
4
3
2
1
0
a
c
b
b
a
ANHYDROUS
BASIC SODALITE
FIG. 65.
1kc/s
10kc/s
100kc/s
1mc/s
10mc/s
Log f.


tanδo
1·4
1·2
1·0
0·8
0·6
0·4
0·2
0
5kc/s
ANHYDROUS
BASIC SODALITE
FIG. 67.
32kc/s
-200
-100
0
100
200
°C


Log ε''o
5kc/s
ANHYDROUS
BASIC SODALITE
FIG. 68.
1
0
-1
-2
32kc/s
10
100
1000
Log K°(absolute).

5.3. Anhydrous Basic Sodalite.

Measurements were made in the nicosel cell using the procedure described on page 114. The sample was vacuum dehydrated for two days at 350°C. To avoid possible pneumatolytic sintering of the compressed material due to water vapour, the initial temperature increase to 350°C was performed in small steps over two days, the temperature not being increased as long as water loss continued at the lower temperature. The final N_2 pressure in the cell holder was adjusted to 30 cm of Hg at 100°C.

The weight of the anhydrous basic sodalite in the cell was found by weighing the filled cell after equilibration over saturated ammonium chloride solution and determination of the water content of another sample similarly equilibrated. This method gave the same result as other procedures.

After completion of the measurements on anhydrous basic sodalite it was found that the empty cell resistance decreased with every outgassing (see page 116). This did not affect these measurements since even after their completion the cell resistance was still large enough to be negligible when in parallel with the much lower resistance of the sample. However the cell could not be used for further samples.

Measurements at -183, 30 and 80°C cover the whole available frequency range and are reproduced in Tables X to XXV. Figs. 49 to 54 are the plots of ϵ'_{app}, $\tan\delta_{app}$, $\log\epsilon''_{app}$, $R_{p(app)}$ up to 800 kc/s, $R_{p(app)}$ at the high frequencies and $\log(R_{p(app)})$ against log(frequency) respectively. Measurements covering the temperature range from -183 to 250°C were made at 5 and 32 kc/s (Tables XXVI and XXVII) and are plotted in Figs. 55 to 60 in terms of ϵ'_{app}, $\tan\delta_{app}$ on a small and larger scale,

$\log\varepsilon''_{app}$, $R_{p(app)}$ and $\log(R_{p(app)})$ against °C. All the curves in Figs. 49 to 54 were compounded from at least two separate runs, the sample having been brought to a different temperature for at least 12 hours between runs at the same temperature. Results repeated to $\pm$1%.

A different procedure was used in the temperature runs (Tables XXVI and XXVII). At 30, 80 and -183°C, the values obtained during the frequency runs were utilised; the sample was then taken to 0°C until results at this temperature were constant, the final constant value being used in Figs. 55 to 60. The sample was then progressively heated to 250°C, measurements at every temperature being taken until constant at this temperature. The procedure was repeated for a number of temperatures between 0 and -183°C. Below room temperature, a constant stream of air had to be passed across the exposed cell leads to avoid water condensation on the leads and the top of the cell holder.

Measurements made on the Hartshorn-Ward apparatus showed a sharp interference peak in the 3.5 to 5.5 mc/s region, which also appeared in cell blank measurements. Results so affected have been rejected. The high frequency determinations were repeated using a Q-meter; however the results obtained showed a much larger spread in values than the Hartshorn-Ward results, which they generally confirm. The Hartshorn-Ward values have thus been retained except in the region of the interference peak, while Q-meter values bridge the gap in this region and at the highest frequencies where no values could be obtained with the Hartshorn-Ward apparatus.

The increase of ε'_{app} and $\tan\delta_{app}$ at 30 and 80°C above 1 mc/s (Figs. 49 and 50) and the corresponding change of slope in the $\log(R_{p(app)})$ curves (Fig. 54) at 1 mc/s is

caused by the onset of induction effects which, due to the use of an outside circuit on the Hartshorn-Ward apparatus and the Q-meter, become appreciable at this frequency.

At -183°C, ϵ'_{app} is constant to within 2% over the whole frequency range, the same is true at 30°C up to 3.2 mc/s and at 80°C between 3 kc/s and 4.2 mc/s (Fig. 49). However the 80°C curve shown an increase at the low frequency end. Similarly the increase in the $\tan\delta_{app}$ values at the lower frequencies of Fig. 50 is small at -183° and 30°C compared with their increase at 80°C. The low frequency ϵ'_{app} and $\tan\delta_{app}$ increase at 80°C may be due to either onset of interfacial polarisation effects due to the interstitial anhydrous cations, or to a relaxation effect of these cations or those of the framework.

The slopes of the ϵ''_{app} curves of Fig. 51 show the insulating character of the anhydrous sample as compared with the hydrated sample of basic sodalite. Equations (143) and (145) were used to calculate ϵ'_o and $\tan\delta_o$, the real values for the massive crystalline substance, between 3 kc/s and 1 mc/s. The values are compared with the 'apparent' values in Table 10. Figs. 61 and 62 are the plots of the results and ϵ''_o is plotted in Fig. 63.

Between 30 and 80°C, the variation of $\log(R_{p(app)})$ with temperature is approximately linear at both 5 and 32 kc/s and therefore activation energies 'E' have been calculated between these temperatures by using the Arrhenius equation (eqn. 150). This has been done in two ways:-

(a) Values of R_{po} have been calculated from the corresponding $\tan\delta_o$ and ϵ'_o values (Figs. 61 and 62); these are plotted in Fig. 64. Activation energies calculated from the R_{po} values are given in Table 11 and are plotted as a function of frequency in Fig. 65a.

Table 10.

Anhydrous Basic Sodalite.

Density 1.885 gm/cm^3.

Packing fraction = d = 0.377.

		Frequency	ϵ'_{app}	ϵ'_o	$\tan\delta_{app}$	$\tan\delta_o$
A.	80°C	3 kc/s	1.850	4.21	0.0204	0.043
		10 kc/s	1.841	4.17	0.0159	0.034
		30 kc/s	1.834	4.14	0.0125	0.027
		100 kc/s	1.825	4.11	0.0098	0.021
		300 kc/s	1.818	4.06	0.0077	0.016
		1.0 mc/s	1.817	4.06	0.0077	0.016
B.	30°C	3 kc/s	1.822	4.08	0.0085	0.018
		10 kc/s	1.818	4.06	0.0070	0.015
		30 kc/s	1.813	4.04	0.0060	0.013
		100 kc/s	1.810	4.03	0.0052	0.011
		300 kc/s	1.807	4.01	0.0048	0.010
		1.0 mc/s	1.807	4.01	0.0059	0.013
C.	-183°C	3 kc/s	1.774	3.86	0.0085	0.018
		10 kc/s	1.768	3.83	0.0065	0.014
		30 kc/s	1.762	3.80	0.0051	0.011
		100 kc/s	1.756	3.77	0.0041	0.0088
		300 kc/s	1.750	3.75	0.0036	0.0077
		1.0 mc/s	1.750	3.75	0.0035	0.0075

Table 11.

Anhydrous Basic Sodalite.

Activation Energies calculated from R_{po}.

Frequency	Activation energy k.cal/mole
3 kc/s	3.83
10 kc/s	3.59
30 kc/s	3.21
100 kc/s	2.63
300 kc/s	2.05
1.0 mc/s	0.93

(b) Values of $\log(R_{p(app)})$ (Fig. 54) were used to calculate the activation energies directly. The results are given in Table 12 and are plotted in Fig. 65 b. There was a certain spread of results and Fig. 65b is up to 216 kc/s the best straight line resulting.

Table 12.

Anhydrous Basic Sodalite.

Activation Energies calculated from $R_{p(app)}$.

Frequency	Activation energy k.cal/mole	Frequency	Activation energy k.cal/mole
1.3 kc/s	4.45	20.0 kc/s	3.25
1.6 kc/s	4.16	25.0 kc/s	3.26
2.0 kc/s	4.14	32.0 kc/s	3.24
2.5 kc/s	4.21	40.0 kc/s	2.93
3.2 kc/s	3.90	50.0 kc/s	3.05
4.0 kc/s	3.67	151.0 kc/s	2.40
5.0 kc/s	3.68	216.0 kc/s	2.30
6.3 kc/s	3.50	313,0 kc/s	2.08
7.0 kc/s	3.32	1.1 mc/s	1.32
10.0 kc/s	3.56	1.77 mc/s	0.55
13.0 kc/s	3.51	2.07 mc/s	0.26
16.0 kc/s	3.30		

It is interesting to note that in Fig. 65b between 4 and 32 kc/s, E = 3.4 $\pm$ 0.3 k.cal/mole. Even in this range however there is a definite change of E with frequency. The best straight line over this range alone is indicated in Fig. 65c.

The values obtained by the two methods are in fairly good agreement. In both cases the activation energy is a function of frequency. Thus the process which has this activation energy must depend on frequency over the range of frequencies and temperatures of measurement.

The temperature runs provide little new theoretical information. The increase of $\tan\delta_{app}$, ϵ'_{app} and ϵ''_{app} with temperature (Figs. 55, 57 and 58) is parallel to the increase of these quantities at the low frequencies of the 80°C runs. The $\tan\delta_{app}$ and ϵ''_{app} minima and the $R_{p(app)}$ maximum at the low temperatures could only be explained as due to the onset of some relaxation effect, which at room temperature would give a peak at some very high frequency. If this were true we would however expect a fairly large temperature coefficient of ϵ'_o which is not found. The values of ϵ'_o, $\tan\delta_o$ and ϵ''_o are given in Table 13 and plotted in Figs. 66 to 68.

The significance of the activation energies and their large variation with frequency must now be explained. From graphs 51 and 63 and following the argument on page 135, it transpires that d.c. conductivity plays only a very minor part in the results. Furthermore the activation energies were obtained from parallel log R_p curves which show a large frequency variation and the changes with frequency of the ϵ'_{app} values at low frequencies are of a much smaller magnitude than in hydrated basic sodalite, i.e. interfacial polarisation is not indicated. In all these respects the anhydrous sample differs fundamentally from hydrated basic

Table 13.

Anhydrous Basic Sodalite, Temperature Runs.

5 kc/s				32 kc/s			
Temp. °C	ϵ'_o	$\tan\delta_o$	ϵ''_o	Temp. °C	ϵ'_o	$\tan\delta_o$	ϵ''_o
-183.0	3.88	0.0167	0.065	-183.0	3.84	0.0141	0.054
-147.2	4.10	0.0065	0.027	-14717	4.08	0.0089	0.036
-121.9	4.10	0.0059	0.024	-122.1	4.08	0.0055	0.022
-100.3	4.08	0.0076	0.031	-100.3	4.08	0.0057	0.023
-66.1	4.04	0.0084	0.034	-66.1	4.06	0.0065	0.026
30.0	4.12	0.0166	0.068	30.0	4.10	0.0124	0.051
80.0	4.15	0.0391	0.163	39.4	4.02	0.0145	0.058
130.2	4.70=	0.114	0.54	49.9	4.06	0.0171	0.069
171.0	5.67	0.311	1.76	59.0	4.08	0.0193	0.079
205.8	6.64	0.719	4.77	69.5	4.09	0.0227	0.093
250.0	11.58	1.47	17.0	80.0	4.12	0.0268	0.110
				130.2	4.44	0.0627	0.278
				171.0	4.82	0.139	0.670
				205.8	5.53	0.284	1.57
				250.0	7.55	0.665	4.95

sodalite, and this suggests that a different mechanism is responsible for the activation energies in the two cases. Since the d.c. conductivity is negligible in the anhydrous sample, the low frequency increase in the 80° ϵ'_{app} and $\tan\delta_{app}$ curves is probably due to the onset of a relaxation effect due to the sodium ions, both interstitial and framework. The fact that sodium analcite gives a relaxation peak in the frequency region of measurement (see later) seems to support this contention by analogy. This means that the sodium ions in anhydrous basic sodalite are not as mobile as in the hydrated sample, i.e. are fixed

to definite lattice sites from which they can only move by discrete jumps to similar positions. This view is in agreement with the determined structure (see page 25). In comparison, the cations in the hydrated material behave as if they were in a viscous solution. We would expect tanδ of the anhydrous sample to be zero outside the absorption frequency region. That this is not so can be explained by analogy with the suggestion made independently by Garton (page 72) and Gevers (page 78), of a very wide distribution of relaxation times due to the temporary formation of additional equilibrium positions of the cations caused by thermal fluctuations which occurs with some dielectrics. The energy of activation obtained then becomes a measure of the average small energy barrier involved. In the case of anhydrous basic sodalite the additional equilibrium positions (which may have barrier heights which vary from large to small) are due to the varying cation environment rather than to thermal fluctuations. As the frequency is raised and moves away from the absorption region the height and numbers of the additional energy barriers gradually decrease and thus the activation energy measured varies with frequency.

Since the ionic relaxation phenomenon in anhydrous basic sodalite appears at the lowest frequencies of measurement, the constant value of ϵ'_o obtained at the highest frequencies (Table 10 and Fig. 61) is the dielectric constant due to the polarisability of anhydrous basic sodalite. The electronic contribution ($\epsilon'_o = 2.04$) is known from refractive index measurements and the atomic contributions can thus be calculated. The results, which surprisingly vary with temperature between -183 and 30°C, are shown in Table 14.

Table 14.

Anhydrous Basic Sodalite. Dielectric Constants.

Temp. °C	ϵ'_o contributed by total polarisability.	ϵ'_o contributed by atomic polarisation.	ϵ'_o contributed by electronic polarisation.
80	4.06	2.02	2.04
30	4.01	1.97	2.04
-183	3.75	1.71	2.04

6. THE SILVER NITRATE OCCLUSION COMPOUND OF THE ZEOLITE SILVER 'A' $Ag_4A(AgNO_3)$.

6.1. Description of Sample.

The sample was synthesised from Silver A, the ion exchange compound of Sodium A. All operations were conducted in the dark, as far as possible. Silver A was prepared by stirring 20 gms of Sodium A, washed free from alkali, for one hour with excess silver nitrate solution. The washed and acetone dried Silver A was then ground with excess $AgNO_3$ and fused at 258°C for 24 hours. The product was reground and fusion repeated. The product of the second fusion was rapidly washed with distilled water to remove excess $AgNO_3$, was dried with acetone and stored in the dark.

The final sample contains no gel and the particle size of the spherulites which is 2μ is of the order required by Van Vessem (p. 88). X-ray powder photographs show the superstructure lines. The sample is tetragonal with $a = 24.6$ Å and $c = 12.3$ Å. After heating at 170°C there is less than 1% change in unit cell size. The 'd' spacings are reproduced in Table 15. The compound contains about 2% water; since on strong heating silver nitrate volatilises this cannot be determined exactly. The cages of the occlusion compound are theoretically completely filled and therefore this water must be surface water (but see page 29). The density of the compound calculated on the assumption that all 13 sodium atoms have been exchanged, is 3.94 gms/cm^3. Experimentally it was shown to be larger than 3.3 gms/cm^3.

The refractive index of the sample, determined with sodium light is 1.678 and thus the electronic contribution to the dielectric constant 2.82.

Table 15.

The $AgNO_3$ Occlusion Compound of Silver A - X-ray Data.

Prep. 16				Prep. 16 heated to 170°C			
d	Comparative strength	hkl	a Å	d	Comparative strength	hkl	a Å
12.13	v.v.w.	200		12.34	v.v.w.	200	
10.07	v.v.w.	111		10.01	v.v.w	111	
8.59	v.v.w.	201		8.70	v.v.w.	201	
7.09	w.	221		7.09	w.	221	
6.14	s.	002		6.16	s.	002	
5.47	w.	202		5.49	v.w.	202	
				4.85	v.v.w.		
4.50	v.w.	511		4.50	v.v.w.	511	
4.34	w.	402		4.34	w.	402	
4.08	s.	003		4.11	s.	003	
3.88	v.w.	203		3.91	v.v.w	203	
3.70	v.w.	223		3.72	v.w.	223	
3.64	v.v.w.	303					
3.54	v.v.w.	442		3.56	w.	442	
3.406	m.	403	24.56	3.422	w.	403	24.68
3.283	s.	622	24.57	3.295	s.	662	24.66
3.140	v.v.w.	503	24.52				
3.071	w.	004	24.57	3.079	v.v.w.	004	24.63
				3.036	v.v.w.	114	24.66
2.977	v.s.	204	24.55	2.991	s.	204	24.66
2.892	m.	224	24.54	2.906	m.	224	24.66
2.813	w-m.	623	24.52	2.828	w.	623	24.65
2.744	m.	404	24.54	2.758	m.	404	24.67
2.681	v.w.	424	24.57	2.690	w.	424	24.65
2.616	s.	504		2.629	v.s.	504	
2.506	w.	444	24.55	2.516	v.v.w.	444	24.65
2.456	w.	005	24.56	2.467	w.	005	24.67
2.404	w-m.	205	24.52	2.420	w.	205	24.68
2.362	w-m.	225	24.55	2.368	w.	225	24.61
				2.293	v.w.	405	24.70
2.234	v.w.	425		2.252	v.v.w.	425	24.67
2.169	s.	804	24.54	2.179	s.	804	24.65
2.105	v.w.			2.113	w.		
2.075	v.w.			2.086	w.		
2.045	v.w.			2.054	w.		
2.017	v.v.w.			2.026	v.v.w		
1.992	v.v.w.			1.999	v.w.		
1.952	v.w.			1.952	v.v.w.		
1.917	w.			1.926	w.		

contd.

Table 15 (contd.)

Prep. 16				Prep. 16 heated to 170°C			
d	Comparative strength	hkl	a o A	d	Comparative strength	hkl	a o A
1.893	v.v.w,			1.902	v.w.		
1.866	v.v.w.						
1.736	m.			1.744	w.		
1.703	v.v.w.			1.708	v.w.		
1.684	v.v.w.			1.693	v.w.		
1.572	w.			1.578	w.		
1.509	v.w.			1.511	w.		
1.463	v.w.			1.476	v.w.		
				1.436	v.v.w.		
1.413	w.			1.416	w.		
1.384	v.v.w.			1.390	v.w.		
1.342	v.v.w.			1.347	v.w.		
1.310	v.v.w.			1.314	v.w.		
∴a=24.55 ∴c=12.275	Average of the 14 shown results			∴a=24.65 ∴c=12.325	Average of the 16 shown results.		

Measurements were made on the slightly hydrated sample and on a sample dehydrated at 170°C for 7 days and then sealed into the cell holder. The compound cannot be heated to higher temperatures in vacuum without fear of breakdown of the superstructure. All measurements were made in the brass cell, the identical sample and filling being used for the hydrated and anhydrous measurements.

6.2. Slightly Hydrated AgA($AgNO_3$).

Although the sample was left at the temperatures of measurement for several days, complete constancy of electrical properties could not be obtained. This was probably due to the small but variable amount of water present. The results at 30° and 80°C are given in Tables XXVIII to XXXI and are plotted in Figures 69 to 73

in terms of ϵ'_{app}, $\log(\epsilon''_{app})$, $R_{p(app)}$, $\log(R_{p(app)})$ and $\tan\delta_{app}$ against log(frequency).

Figure 70 shows that the dielectric loss below 100 kc/s is mainly due to d.c. conductivity, although the influence of a.c. loss is seen in the fact that the curves are not as steep as the experimental curve derived from equation (149). In consequence the specific resistances calculated from the values of ϵ''_{app}, which are shown in Table 16, vary much more with frequency than in the case of hydrated basic sodalite. Similarly the $R_{p(app)}$ values vary considerably with frequency (Figs. 71 and 72). However the $\log(R_{p(app)})$ curves are parallel between 1.3 and 50 kc/s and allow calculation of activation energies which are given in Table 17. The results show only a very slight variation with frequency. If it is assumed, as in the case of hydrated basic sodalite (page 136), that the water loss between 30 and 80°C is of minor importance to the comparative results and that the conductance is purely ionic, then the results in Table 17 represent the free energy of activation required to overcome the energy barrier against the movement of both the interstitial and framework Ag^+ ions in the crystallites (see pages 136 and 137). In view of the difficulties of obtaining constant measurements and because of the small amount of water present, there must be some doubt about the accuracy of these activation energies. It is however interesting to note that Beattie obtained a value of 14 k.cal/mole for the activation energy associated with cation migration in silver analcite (Table 3) and 17 k.cal/mole in silver chabazite[21].

Due to the non-constancy of measurements the remaining results are only of qualitative value. They are discussed in conjunction with the reproducible results of the anhydrous material.

Table 16.

Hydrated AgA($AgNO_3$). Specific Resistances Calculated from ϵ''_{app}.

Frequency	Specific Resistance		Frequency	Specific Resistance	
	30°C meg-Ω	80°C Ω		30°C meg-Ω	80°C Ω
400 c/s	13.4	-	5.0 kc/s	7.55	292000
530 c/s	11.8	-	6.3 kc/s	7.25	284000
620 c/s	11.2	-	8.0 kc/s	6.97	274000
800 c/s	10.3	-	10.0 kc/s	6.64	266000
1.0 kc/s	9.78	-	13.0 kc/s	6.30	255000
1.3 kc/s	9.29	329000	16.0 kc/s	6.02	245000
1.6 kc/s	8.93	327000	20.0 kc/s	5.70	235000
2.0 kc/s	8.66	321000	25.0 kc/s	5.33	225000
2.5 kc/s	8.37	315000	32.0 kc/s	5.02	212000
3.2 kc/s	8.11	306000	40.0 kc/s	4.65	203000
4.0 kc/s	7.81	298000	50.0 kc/s	4.29	193000

Table 17.

Hydrated AgA($AgNO_3$).

Frequency	Activation Energy k.cal/mole	Frequency	Activation Energy k.cal/mole
1.3 kc/s	14.1	10.0 kc/s	13.7
1.6 kc/s	14.1	13.0	13.6
2.0 kc/s	14.0	16.0	13.6
2.5 kc/s	13.9	20.0	13.5
3.2 kc/s	13.9	25.0	13.5
4.0 kc/s	13.9	32.0	13.4
5.0 kc/s	13.8	40.0	13.3
6.3 kc/s	13.8	50.0	13.2
8.0 kc/s	13.7		

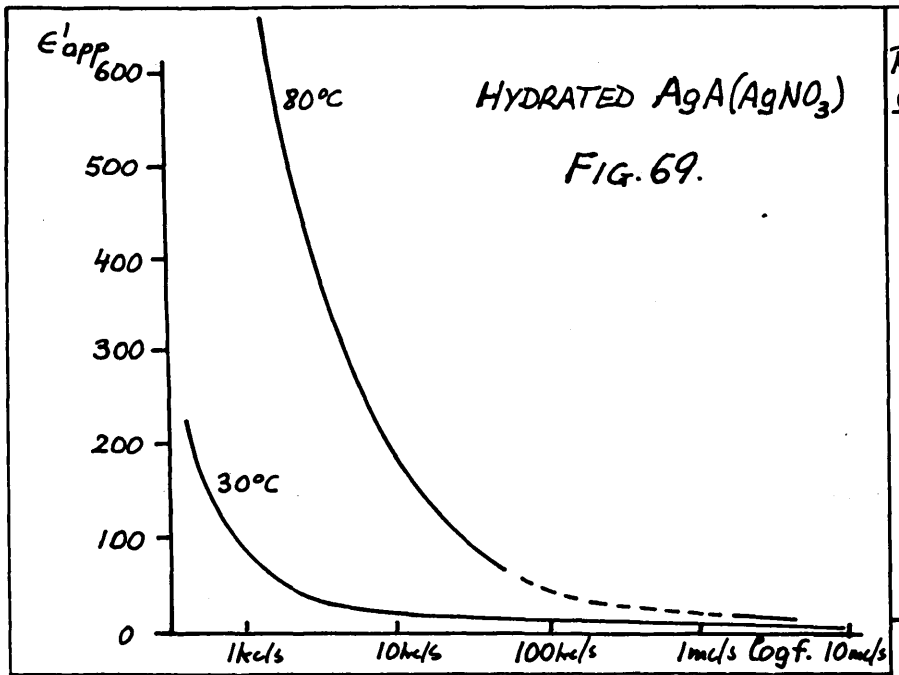
6.3. Anhydrous $AgA(AgNO_3)$.

Reproducible measurements, made at 0, 30 and 50°C are given in Appendix Tables XXXII to XL. Figures 74 to 79 which are the plots of ε'_{app}, $\tan\delta_{app}$, ε''_{app}, $\log(R_{p(app)})$ and $R_{p(app)}$ respect. against log(frequency) are each compounded from at least two determinations, the sample having been brought to a different temperature between determinations at the same temperature. Figures 80 to 83 represent the results in Appendix tables XLI and XLII, which were obtained at the constant frequencies of 5 and 32 kc/s butcover a larger temperature range.

The interfacial polarisation effect (barrier layer effect), which has already been encountered in hydrated Basic Sodalite, is operative in both hydrated and anhydrous $AgA(AgNO_3)$. This and the comparatively small change of ε'_{app} and $\tan\delta_{app}$ values on dehydration, compared with the correspondingly large changes in the case of hydrated basic sodalite (compare Figs, 74, 75, 69 and 73 with Figs. 49, 50 37 and 38) suggest that the interfacial polarisation effect in $AgA(AgNO_3)$ is due to only one process, which operates in both states. This process is the mobility of the non-hydrated Ag^+ ions. These ions cannot be hydrated in the completely filled occlusion compound, and hydration therefore has comparatively little effect on the electrical properties. The Ag^+ ions in the zeolite Silver A are located at a number of positions of lowest energy[82], but since there are more such positions of lowest energy than cations, there is a possibility of cationic movement. In the $AgNO_3$ occlusion compound of AgA, defects certain to be present in the arrangement of the occluded $AgNO_3$ molecules (see page 29) will thus allow the process:

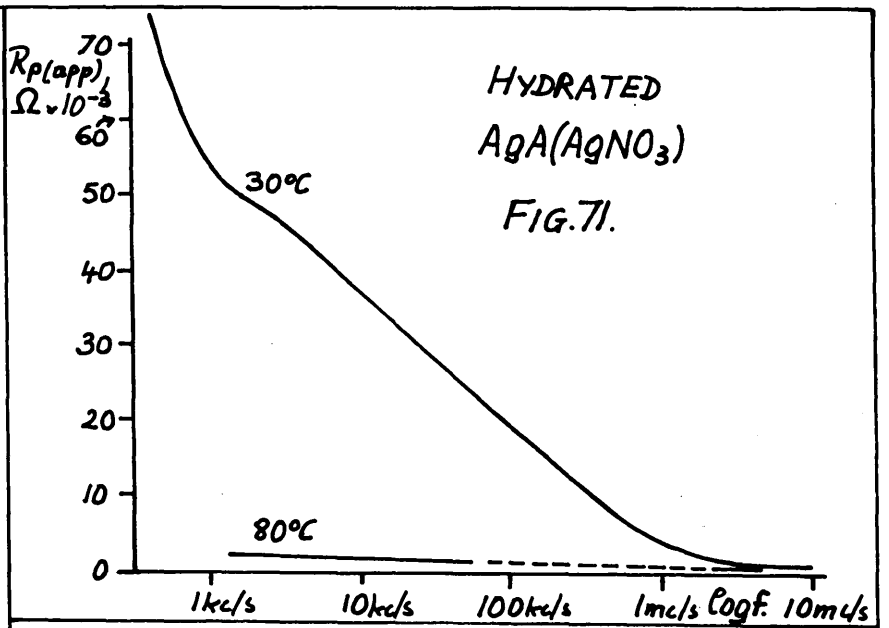
$$\underline{Ag}^+ + AgNO_3 = \underline{AgNO_3} + Ag^+ ,$$

between places of equal lowest energy in the framework.



HYDRATED $AgA(AgNO_3)$

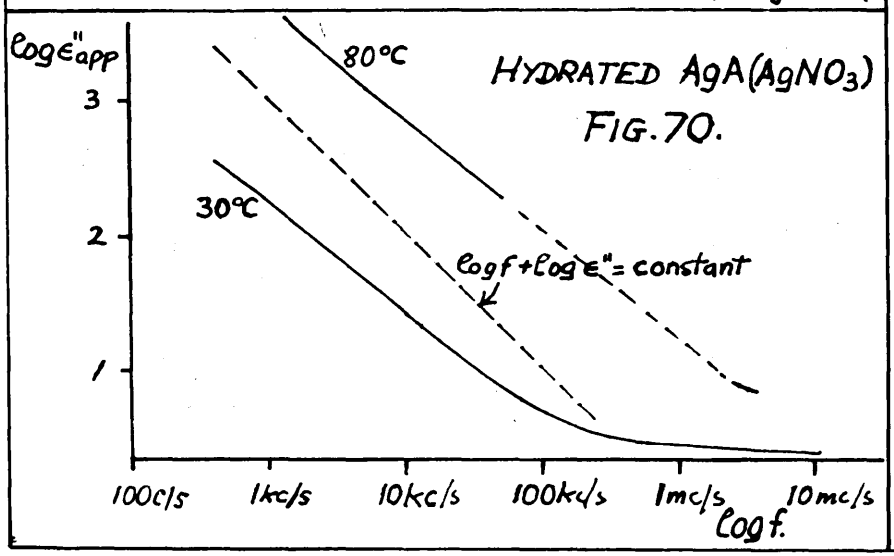
FIG. 69.



HYDRATED

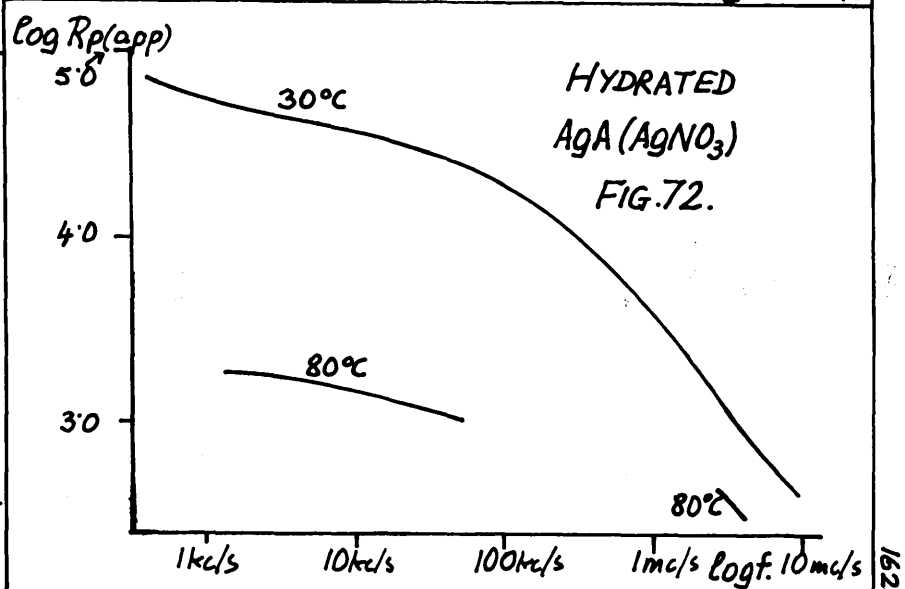
$AgA(AgNO_3)$

FIG. 71.



HYDRATED $AgA(AgNO_3)$

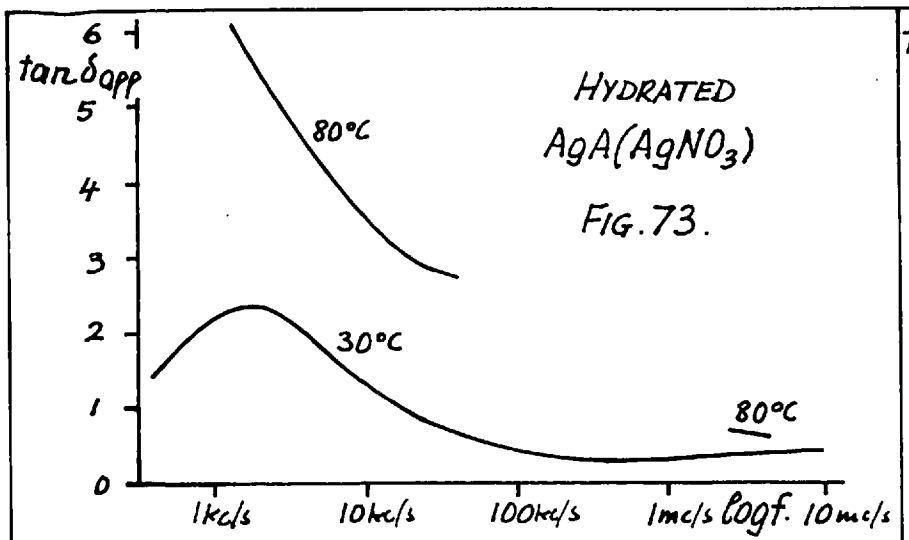
FIG. 70.



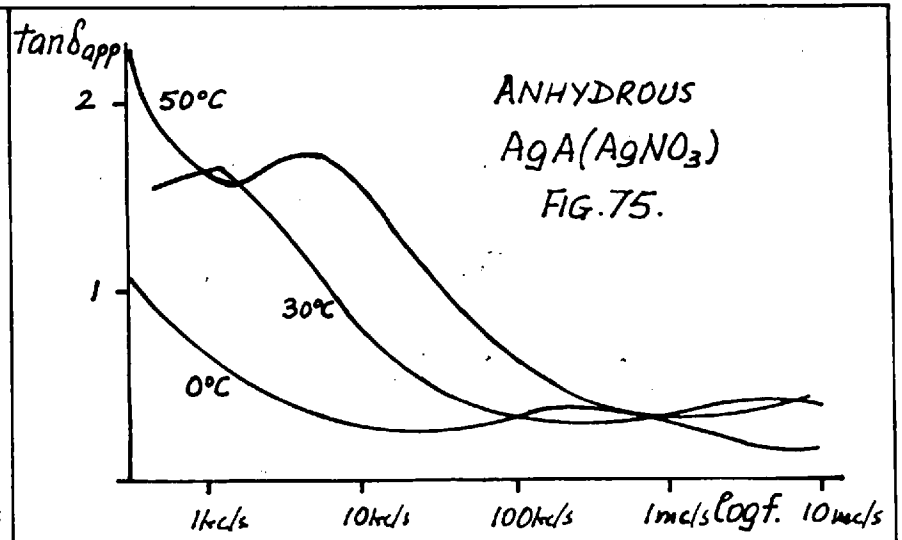
HYDRATED

$AgA(AgNO_3)$

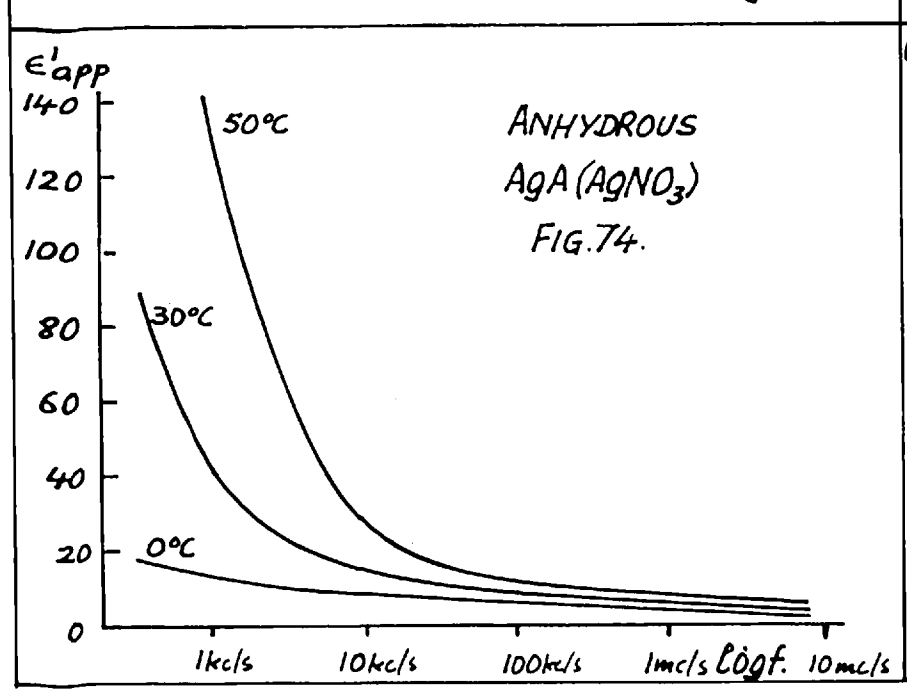
FIG. 72.



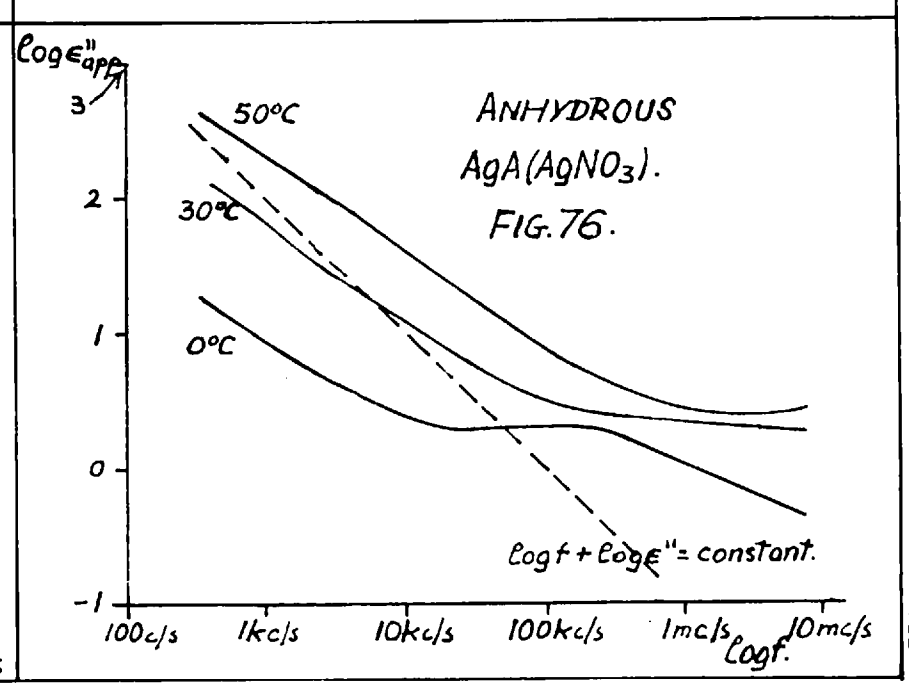
HYDRATED
$AgA(AgNO_3)$
FIG. 73.



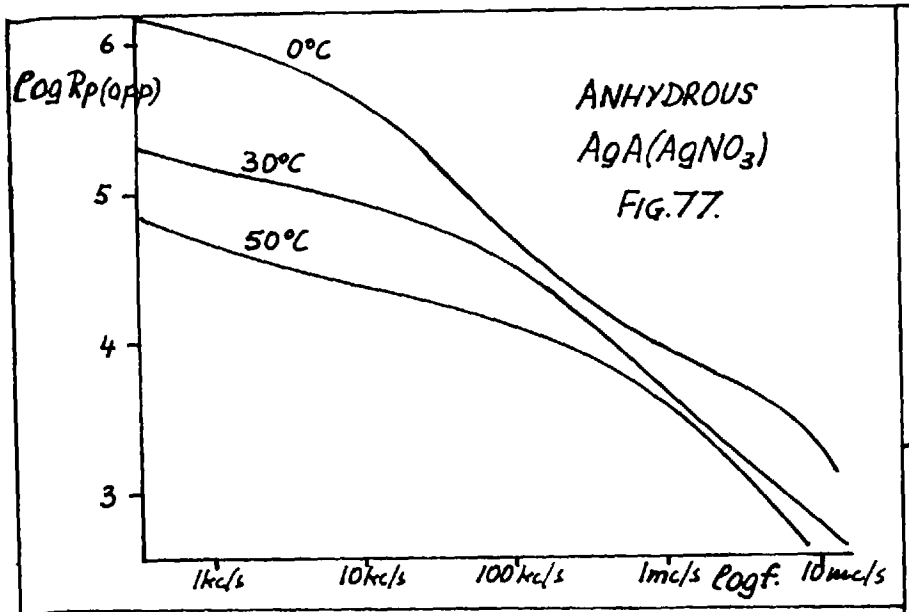
ANHYDROUS
$AgA(AgNO_3)$
FIG. 75.



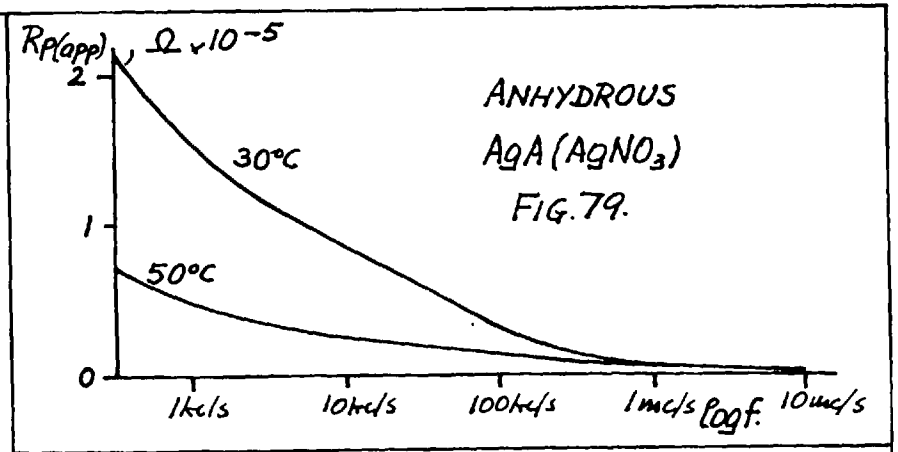
ANHYDROUS
$AgA(AgNO_3)$
FIG. 74.



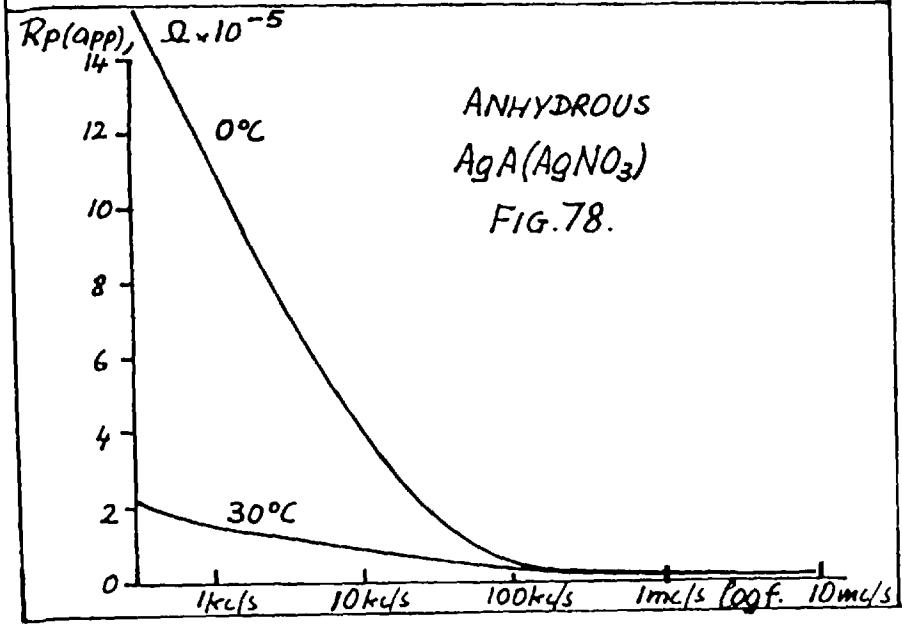
ANHYDROUS
$AgA(AgNO_3)$.
FIG. 76.



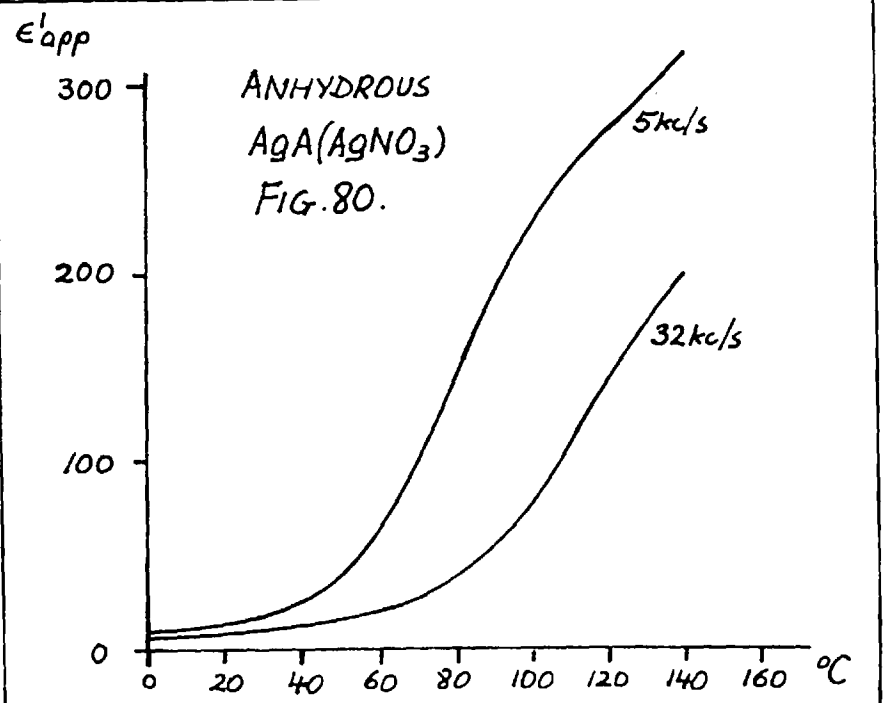
ANHYDROUS
$AgA(AgNO_3)$
FIG. 77.



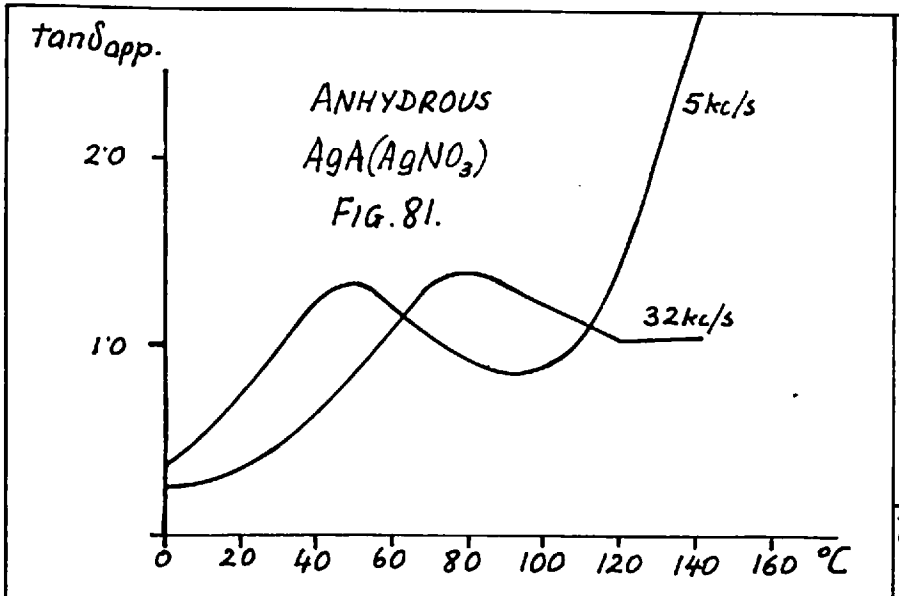
ANHYDROUS
$AgA(AgNO_3)$
FIG. 79.



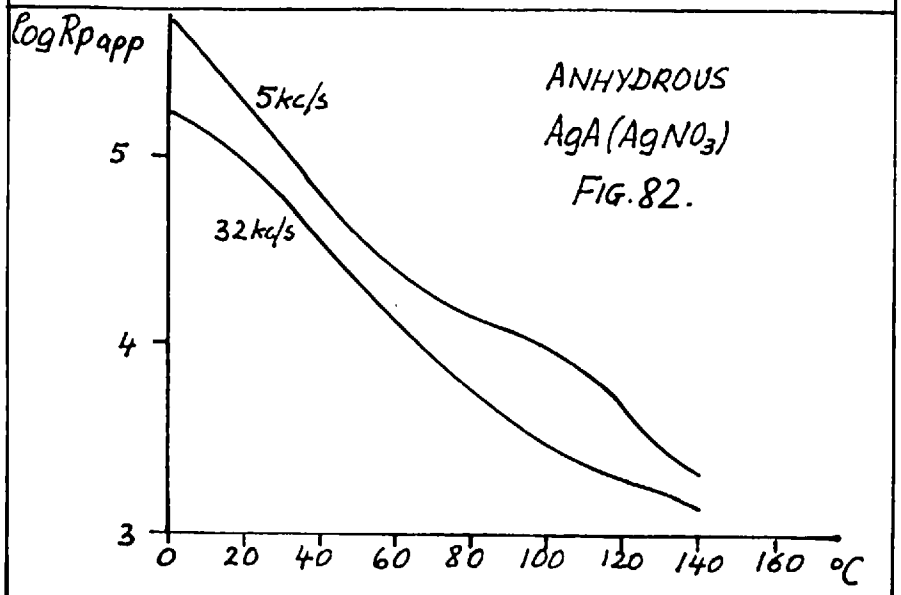
ANHYDROUS
$AgA(AgNO_3)$
FIG. 78.



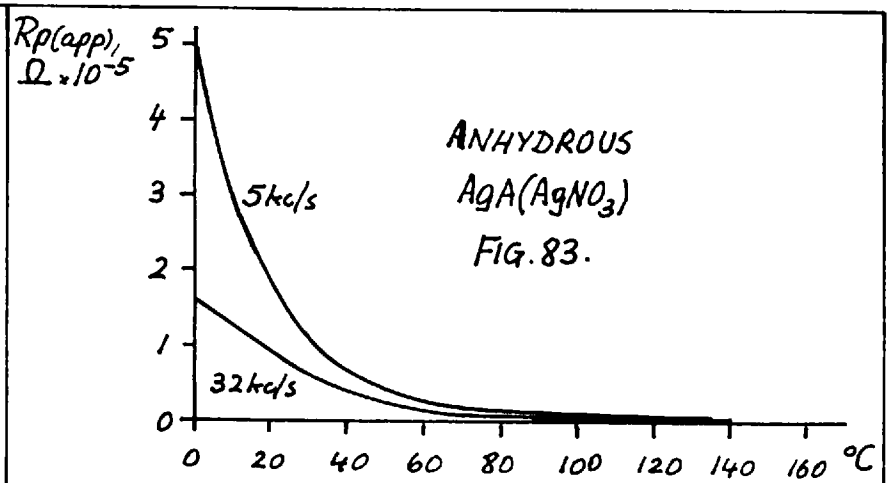
ANHYDROUS
$AgA(AgNO_3)$
FIG. 80.



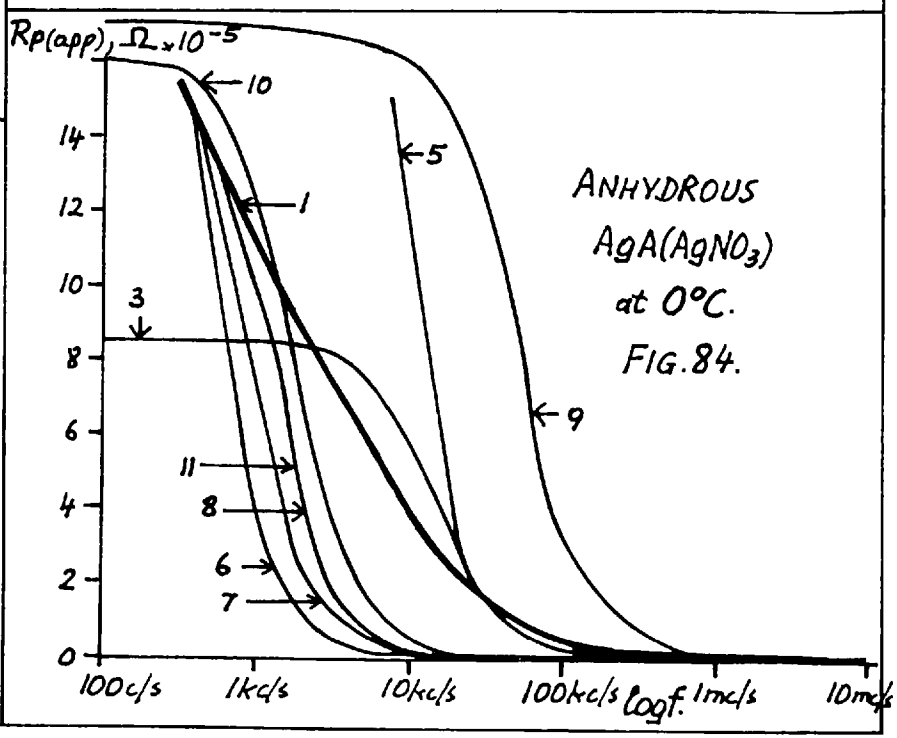
ANHYDROUS
$AgA(AgNO_3)$
FIG. 81.



ANHYDROUS
$AgA(AgNO_3)$
FIG. 82.



ANHYDROUS
$AgA(AgNO_3)$
FIG. 83.



ANHYDROUS
$AgA(AgNO_3)$
at 0°C.
FIG. 84.

(Ag^+ ions in the framework are probably indistinguishable from those in the $AgNO_3$ molecules). The effects produced by temperature increase can thus only be governed by the increase in the mobility of the current carriers. The barrier layer effect is active even at the highest frequencies of measurement.

All further remarks concern only the anhydrous compound.

The 50°C curves in particular are the typical dispersion curves for the Maxwell-Wagner model of a poly-crystalline semi-conductor[135], (Figs. 24 to 26 and 44 to 48). The principal maximum in the $\tan\delta_{app}$ curves shows a temperature coefficient of frequency, as does the secondary peak in the high frequency region (Fig. 75). Only the 0°C curve gives a region of constant ε'_{app} at the higher frequencies, namely between 3.22 and 7.6 mc/s; at 30°C the ε'_{app} value is the same at 5.3 and 7.6 mc/s, but there is no constancy at 50°C. The values are given in Table 18.

Table 18.

Temperature, °C	ε'_{app} at 3.22 mc/s	ε'_{app} at 7.6 mc/s
0	3.4	3.4
30	5.2	4.6
50	7.0	5.9

Since the results obtained for AgA($AgNO_3$) depend mainly on the state of aggregation of the crystallites, there is no point in applying the Böttcher formula (equations 143 and 145) which under these circumstances would not give the real grain properties. However it will be seen later that an approximate value for the activation energy of Ag^+ ion migration can be obtained. Since neither the maxima of

the absorption curves (Fig. 76) nor ε'_s or ε'_∞ were obtained in the measurements, the activation energy in respect of the Ag^+ ion movement between crystallites cannot be calculated directly. However consideration of the $\tan\delta$ maxima (Fig. 75), which theoretically appear at higher frequencies than the corresponding ε''_{maxima} (Figs. 15 and 17) and of Table 2 shows that these energy barriers must be in excess of 13 k.cal/mole.

In order to obtain the electrical properties of the grains and barriers separately, equations (151) and (152) connecting the measured quantities R_p and C_p with R_x and C_x of the grains and R_b and C_b of the barriers, were set up. This was done on the basis of Figs. 44 to 48 (Maxwell-Wagner model), assuming shortest path packing between the plates of the cell, absence of cross-linking paths between the particle rows so produced and that $C_b \gg C_x$ and $R_b \gg R_x$.

$$R_p = \frac{[nR_x+(n+1)R_b]^2 + w^2R_b^2R_x^2[nC_b+(n+1)C_x]^2}{nR_x+(n+1)R_b + w^2R_bR_x[nC_b^2R_b+(n+1)C_x^2R_x]} \qquad (151)$$

$$C_p = \frac{nC_xR_x^2+(n+1)C_bR_b^2 + w^2C_bC_xR_b^2R_x^2[nC_b+(n+1)C_x]}{[nR_x+(n+1)R_b]^2 + w^2R_b^2R_x^2[nC_b+(n+1)C_x]^2} \qquad (152)$$

Theoretically substitution of four experimental values in each of these equations should give four simultaneous equations which allow calculation of R_x, R_b, C_x and C_b. Once these quantities are found at each temperature, activation energies for Ag^+ ion movement within the grains and across the barriers can be calculated. In setting up equations (151) and (152), the contacts between the outermost particles of a series row and the cell wall are considered to be of the same nature as the particle contacts, and thus there are n particles and (n+1) barriers per row. If n is assumed to be large (n=750 for this sample), then effectively

n=(n+1) and the equations can be simplified. The simplified equation (151) has been used to try and reproduce the experimental R_p curves for the anhydrous sample at 0°C. By substituting three experimental values at different frequencies in the simplified equation (151) (which due to the above simplification is only in terms of R_x, R_b and C_b) equations connecting R_p and the w (w = angular frequency = $2\pi f$, where f = frequency in c/s) were set up. The resulting equations are found to be dependent on the points chosen for the original substitution and when plotted as curves 2 to 9 in Figure 84 do not reproduce the experimental curve 1. In some of these calculations values for R_p at zero frequency are assumed, since the experimental results do not reach the region of constant R_p at low frequencies, which is forecast by both the Maxwell-Wagner model and equation (151). The details of the curves shown are as follows:-

Table 19.

Curves on Figure 84.

Curve No.	Frequency of experimental R_p values used	R_p value assumed and its frequency
3	2.5 kc/s, 32 kc/s and 1.1 mc/s	None
5	32 kc/s and 1.1 mc/s	4.65 meg-Ohm at 0 c/s
6	400 c/s and 7.6 mc/s	3 meg-Ohm at 0 c/s
7	400 c/s and 7.6 mc/s	1.8 meg-Ohm at 0 c/s
8	400 c/s and 7.6 mc/s	1.65 meg-Ohm at 0 c/s
9	770 kc/s and 7.6 mc/s	1.65 meg-Ohm at 0 c/s

Curve 10 is obtained from the average of the results in '8' and '9'. This assumes these two types of resistances to be in parallel in the cell, i.e.

$$R_{10} = \frac{2R_8 \cdot R_9}{R_8 + R_9} \qquad (153)$$

Finally, curve 11 which coincides with curve 8 is plotted by using the same R_p values as in curve 8 and equation 154, which was set up assuming the two types of barriers R_c and R_d where $R_c=2R_d$ and $C_c=\frac{1}{2}C_d$.

$$R_p = \frac{n}{2} \frac{(2R_x+3R_d)^2+w^2R_d^2C_d^2\left[(4R_x+3R_d)^2-8R_x\right]+4w^4R_x^2R_d^4C_d^4}{(2R_x+3R_d)+w^2R_d^2C_d^2(1R_x+3R_d) + 2w^4R_xR_d^4C_d^4} \quad (154)$$

It is not surprising that these theoretical treatments are unsatisfactory. The equations for R_p and C_p forecast sigmoid curves, in agreement with the experimental and theoretical results of Lewis and Bickford[139], who show that when interfacial polarisation dominates a system, C_x and R_x should be equal to the experimental values at high frequencies, and C_b and R_b should be obtained at low frequencies. The measurements on anhydrous $AgA(AgNO_3)$ are in the intermediate range and do not reach low enough frequencies to give frequency independent R_p and C_p values. Furthermore there is obviously a large distribution of barrier heights whereas only two types of barrier at most have been considered in the above theoretical treatments. The mathematical treatment involving a distribution of barrier heights is lengthy and is not attempted since it would only give accurate values of the large R_b and C_b values which vary with sample packing, while the much lower grain resistance and capacitance which are the quantities of interest would only be obtained approximately.

The $\log\epsilon''_{app}$ curves of Fig. 76 are parallel at the lower frequencies and comparison with the theoretical curve forecast by equation (149) ($\log\epsilon'' + \log f$ = constant) shows that d.c. conductivity predominates although the a.c. influence is appreciable. Comparison of the relative positions of the ϵ'_{app}, $\tan\delta_{app}$ and $\log(R_{p(app)})$ curves (Figs. 74, 75 and 77) with the theoretical figure 26 indicates that these low frequency parallel ϵ''_{app} curves approximate to the high frequency part of Fig. 26, i.e. the grain resistance range.

However the change with frequency of the $\log(R_{p(app)})$ results again emphasises the a.c. influence on these results. Activation energies calculated over the range of the parallel $\log(R_{p(app)})$ curves are given in Table 20. These R_p values are influenced by a.c. conductivity and the activation energies calculated from them are therefore only approximate. It follows from above that the activation energies correspond to the movements within the grains of Ag^+ ions, of both the framework and the interstitial molecules.

Table 20.

Anhydrous AgA($AgNO_3$).

Frequency	Activation energies, k.cal/mole calculated between the temperatures of:			
	0-30°C	0-50°C	30-50°C	Average
320 c/s	--	10.8	-	10.8
400	10.8	10.9	11.0	10.9
500	-	10.8	-	10.8
620	11.1	10.9	10.7	10.9
800	10.9	10.8	10.7	10.8
1.0 kc/s	11.0	11.0	11.0	11.0
1.3	10.7	11.0	11.5	11.1
1.6	10.7	11.0	11.5	11.1
2.0	10.3	10.9	12.0	11.1
2.5	10.5	11.1	12.1	11.2
3.2	9.9	10.8	12.5	11.1
4.0	10.0	10.8	12.4	11.1
5.0	-	-	12.6	-
6.3	-	-	12.4	-
8.0	-	-	12.5	-
10.0	-	-	12.1	-
13.0	-	-	12.1	-
16.0	-	-	11.6	-
20.0	-	-	11.6	-
25.0	-	-	11.1	-
32.0	-	-	11.0	-
40.0	-	-	10.4	-
50.0	-	-	10.3	-
Average	10.6	10.9 (to 4 kc/s 11.5)	11.6	11.0

The average activation energy is therefore 11.2 k.cal/mole.

The interfacial polarisation effects encountered in basic sodalite and $AgA(AgNO_3)$ are fundamentally different. In $AgA(AgNO_3)$ the effect is intrinsic and is caused by a conductivity due either to structure defects or to the fact that there are more cation positions than cations in the molecule or to both. Thus hydration has little influence on the interfacial polarisation effect in $AgA(AgNO_3)$. In basic sodalite, interfacial polarisation depends entirely on hydration, i.e. on the water sorbed in the zeolite. One may however look upon hydrated basic sodalite as the water occlusion compound of the zeolite. Dryden and Meakins[126] explain that dielectric dispersion and loss in occlusion compounds is due to dipole orientation of the occluded polar molecules. However the magnitude of the ε'_{app} values at low frequencies of both hydrated basic sodalite and $AgA(AgNO_3)$ points in these instances to interfacial polarisation effects rather than to the explanation given by Dryden and Meakins.

The arrangement of intracrystalline $AgNO_3$ clusters in $AgA(AgNO_3)$ suggested possible anti-ferroelectric properties in this material [18], but these have not been found in the behaviour of the crystalline powder.

7. SODIUM ANALCITE.

7.1. Description of Samples.

The sample of sodium analcite (preparation 23) was prepared by hydrothermal synthesis in the large autoclave. The 1:1:4 gel, i.e. $Na_2O, Al_2O_3, 4SiO_2$, was heated for 2½ days at 210°C in the presence of a 50% molar excess of sodium hydroxide[12]. The cubic unit cell parameter 'a' of the product is 13.72 Å; the 'd' spacings are compared with those given by Barrer and Baynham[8] in Table 21.

Table 21.

Powder X-rays of Sodium Analcite.

Preparation 23				Sodium Analcite from Barrer and Baynham(8)	
'd' spacing	I intensity	hkl	'a'	'd'	I
5.60	s.	112	13.71	5.59	s.
4.84	w.	202	13.69	4.85	m.
3.66	v.w.	312	13.68	-	-
3.43	v.s.	400	13.70	3.43	v.v.s.
2.92	s.	323	13.71	2.93	s.
2.80	v.v.w.	224	13.72	-	-
2.69	w.-m.	413	13.72	2.69	m.
2.55	w.-m.	432	13.73	2.50	m.
2.43	w.	440	13.73	2.42	m.-w.
2.23	w.	325	13.73	2.22	m.
1.90	w.	406	13.72	1.90	m.
1.87	v.w.	217	13.73	1.86	m.
1.74	w.-m.	327	13.73	1.74	m.s.

The powder X-ray photograph and electron micrographs establish the absence of impurities and gel particles. The particle size of the spherulitic crystallites is 3.10^{-4} cm. Since the volume of the large stainless steel cell, which was used for all these measurements, is 3.34 cm^3, van Vessem's condition (page 88) is approached much more closely than in the sodium chloride measurements which served

to test the applicability of the Böttcher equation (page 123). Consideration of these sodium chloride results thus shows that results for sodium analcite obtained using the Böttcher equation are accurate.

The sample contains 8.49% water, which is of the correct order for this material (see page 22). The moisture content was determined at all temperatures by thermogravimetric balance. These results can however not be used to determine the water content of the hydrated sample at the temperatures of measurement, since the dielectric measurements were obtained with the cell in an anhydrous atmosphere. In order to evaporate surface water prior to dielectric work, the cell holder containing the hydrated sample was evacuated in the high vacuum system for 2 hours (2.10^{-4} mm Hg), until the Tessler coil showed that no further water was given off.

To obtain the anhydrous material the sample used for hydrated measurements was 'outgassed' in the high vacuum apparatus by heating for two days at 380°C. The correct dehydration temperature had been determined by Beattie, Barrer and Barrer and Ibbitson[21-23,66,65], The densities calculated from X-ray data, refractive indices determined by sodium light and the electronic contributions to the dielectric constant determined from these refractive indices are shown in Table 22.

Table 22.

Material	Density gms/cm^3	Refractive Index	ε' electronic	Packing Fraction
Hydrated Na analcite	2.272	1.477	2.18	-
Anhydrous Na analcite	2.079	1.446	2.09	0.411

7.2. Hydrated Sodium Analcite.

Measurements made at 30, 58 and 90°C in that order, gave repeatable results reproduced in Tables XLIII to XLV. The measurements at 58 and 30°C were repeated after the 90°C run and gave the results shown in Tables XLVI and XLVII, which are different from those originally obtained. All the results are plotted in Figures 85 to 88.

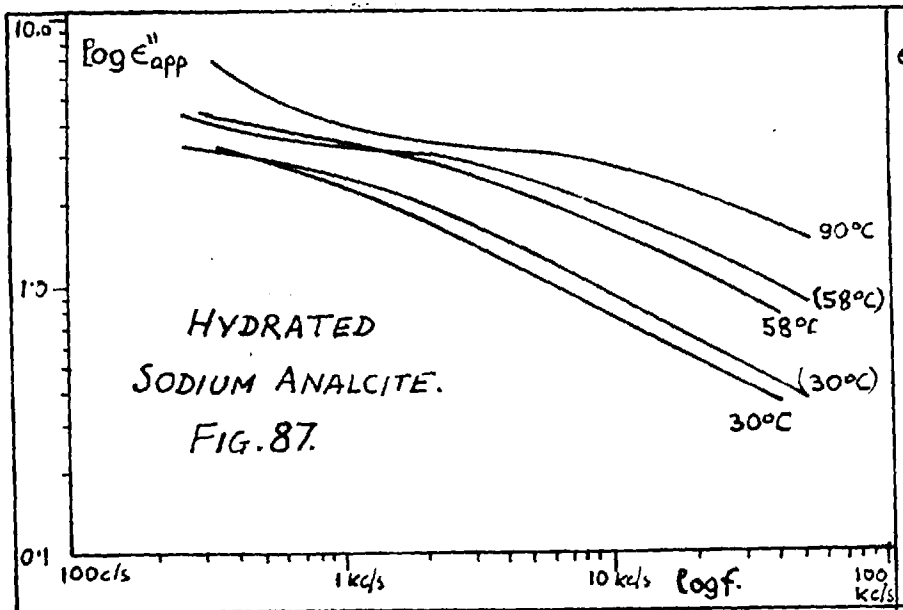
The order of the ϵ'_{app} values clearly shows that the tanδ peaks are due to a relaxation effect rather than to interfacial polarisation. The earlier discussions of sodium analcite structure and earlier work (page 12) make it clear that this relaxation effect is due to the cations neutralising the zeolite framework, which in this case are hydrated. The ϵ'_{app} and $\tan\delta_{app}$ curves are of the correct type (Figs. 16 and 20) for a relaxation effect, while, however, the ϵ''_{app} and 90° $\tan\delta_{app}$ curves at low frequencies indicate that some interfacial polarisation occurs at these lowest frequencies. In the repeat runs 149 and 150 (58 and 30°C) the $\tan\delta_{app}$ peaks move to a lower frequency than in the original runs, thus indicating larger activation energies. Activation energies referring to a relaxation effect should really be calculated from ϵ''_{app} peaks; the latter are only roughly indicated in Fig. 87, but lead to the same conclusion as the tanδ peaks. The results of the calculations of activation energy will be discussed with the results for anhydrous sodium analcite, but the above observations indicate that the cations were less hydrated in runs 149 and 150 than in runs 144 and 145. This is as expected from the experimental procedure, since the water removed at 90°C is unlikely to be returned to the zeolite on cooling under the experimental conditions used. Runs 149 and 150 thus represent a material in the same state of hydration as in run 148, while runs 144 and 145 do not. The repeat runs are therefore more reliable and the activation energies

calculated from them are not affected by water loss. The activation energies are therefore reliable, although the state of hydration of the zeolite for which they are calculated is not known.

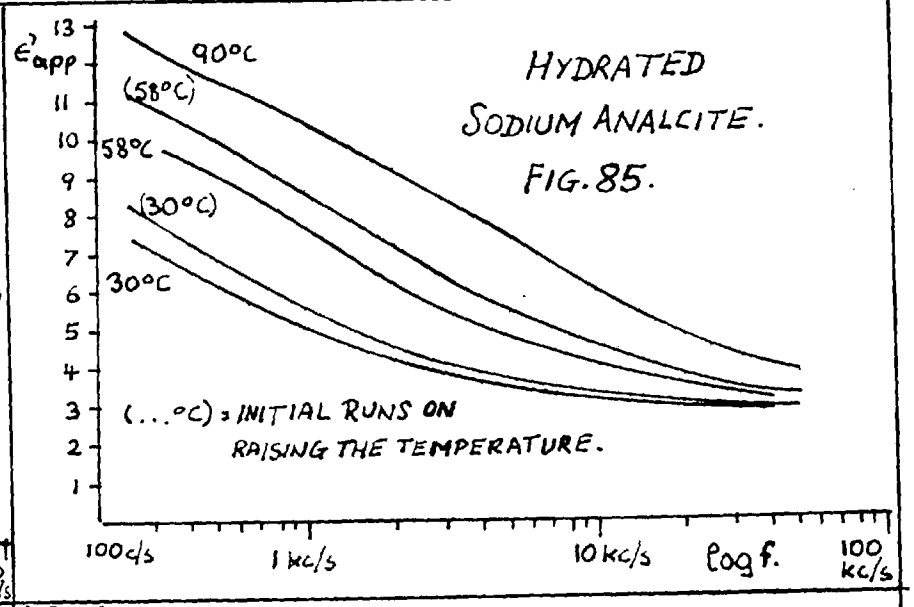
The log (ϵ''_{app}) curves confirm that the dielectric loss is due to an a.c. relaxation effect caused by some limited charge movement rather than by a d.c. conductivity from electrode to electrode. The 'real' results for the massive crystalline substance have not been calculated, because the state of hydration of the material is not known and the results would therefore be of no value. Furthermore, activation energies calculated from the 'apparent' results are the same as those calculated from the 'real' ones (see tables 11 and 12 in the case of basic sodalite), when calculations are made from Rp values or dielectric loss peaks (see anhydrous sodium analcite results where the real and apparent ϵ'' peak values give the same activation energies) and hence activation energy calculations do not require 'real' results.

7.3. Anhydrous Sodium Analcite.

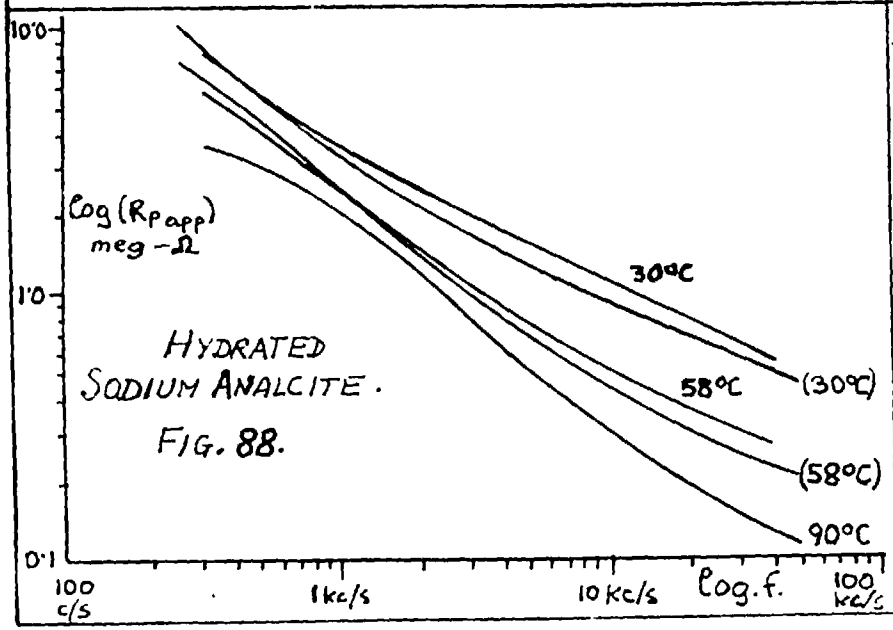
Results of measurements at 30, 45 and 60°C are given in Appendix tables XLVIII to LIII and plotted in Figs. 89 to 92 in terms of the apparent quantities. Runs 161 to 163 shown in tables LIV to LVI were obtained after completion of run 160 (table L) as repeatability checks. From page 107 it follows that the maximum difference between repeat results of ϵ'_{app} should be 2% and of $\tan\delta_{app}$ 4%. Except for one point the repeat results at 45 and 60°C are much closer than required by these limits. At 30°C the maximum ϵ'_{app} difference is 4% and the maximum $\tan\delta_{app}$ difference 7%. However this unexplained deviation is not serious since the $\tan\delta_{app}$ maxima appear at the same frequency in the two 30°C runs and activation energies and relaxation times are therefore not effected by the inaccuracy of the values.



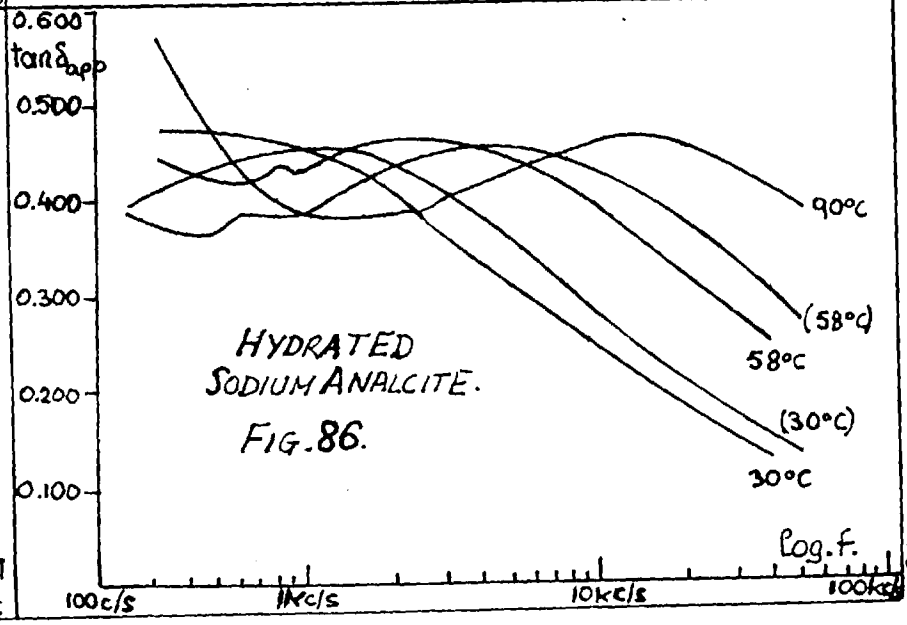
HYDRATED
SODIUM ANALCITE.
FIG. 87.



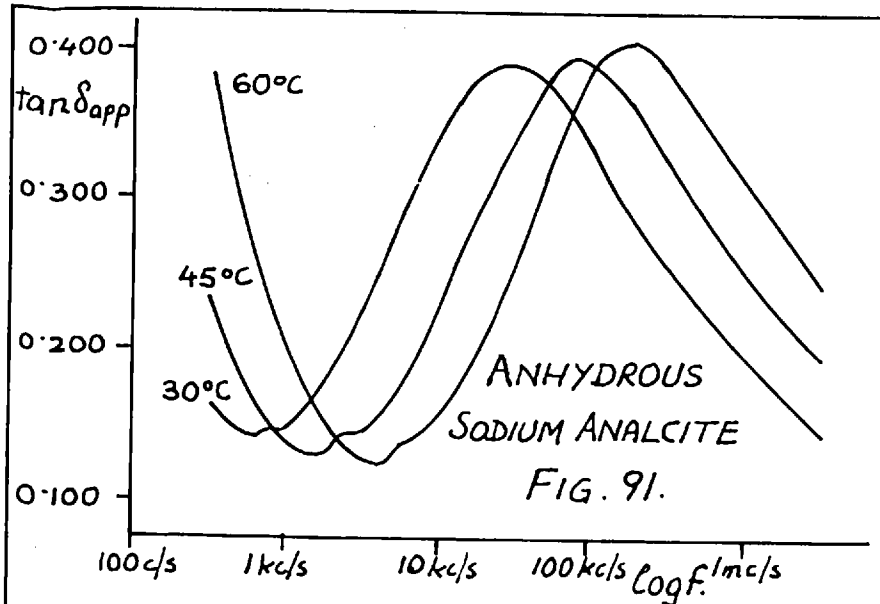
HYDRATED
SODIUM ANALCITE.
FIG. 85.



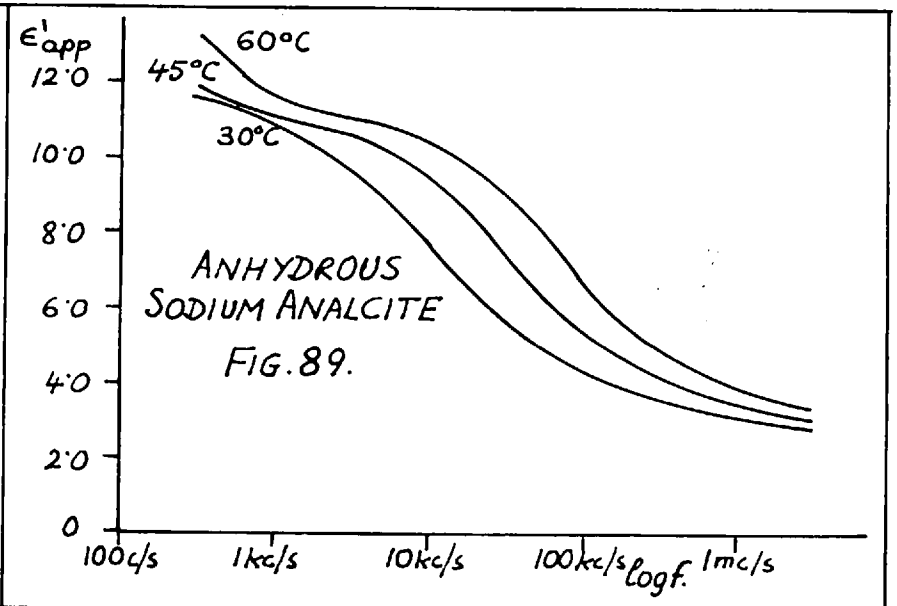
HYDRATED
SODIUM ANALCITE.
FIG. 88.



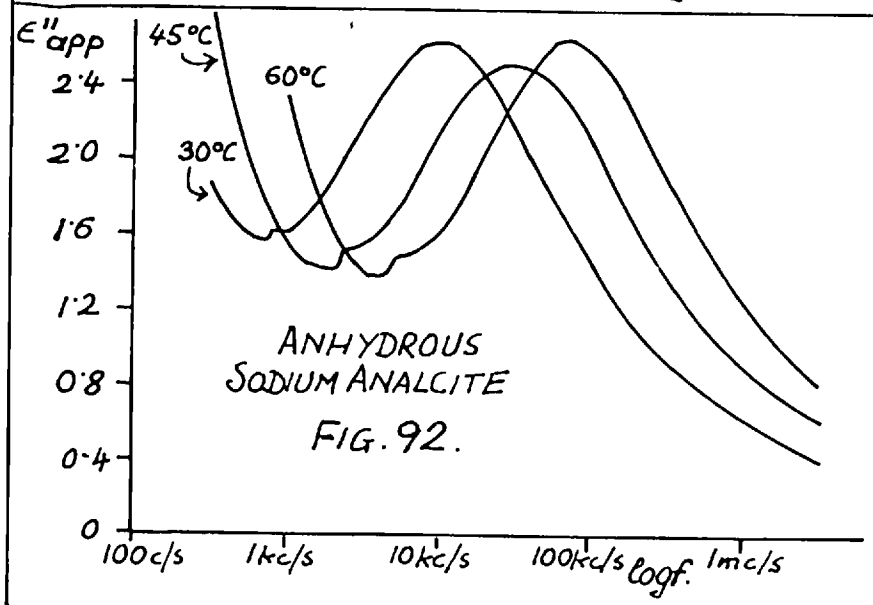
HYDRATED
SODIUM ANALCITE.
FIG. 86.



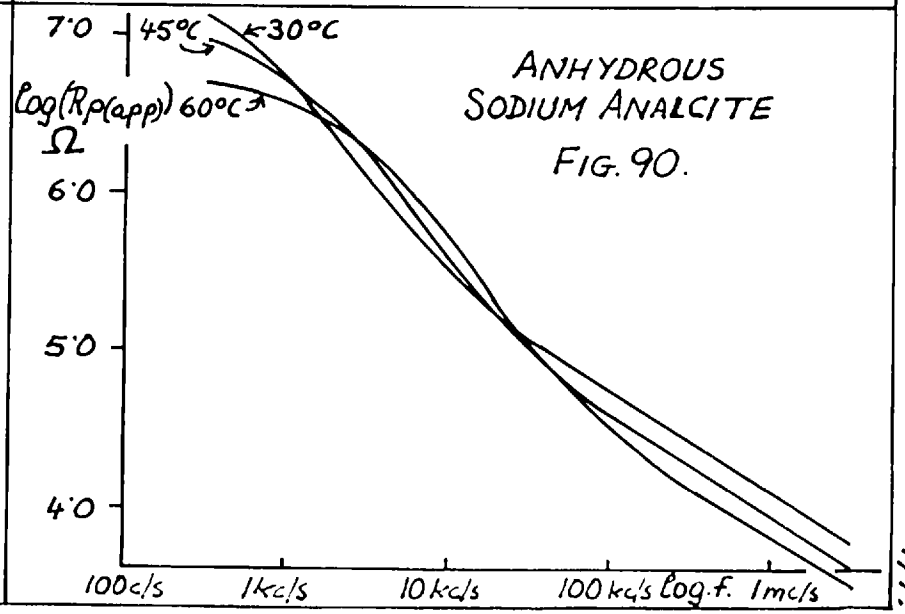
ANHYDROUS
SODIUM ANALCITE
FIG. 91.



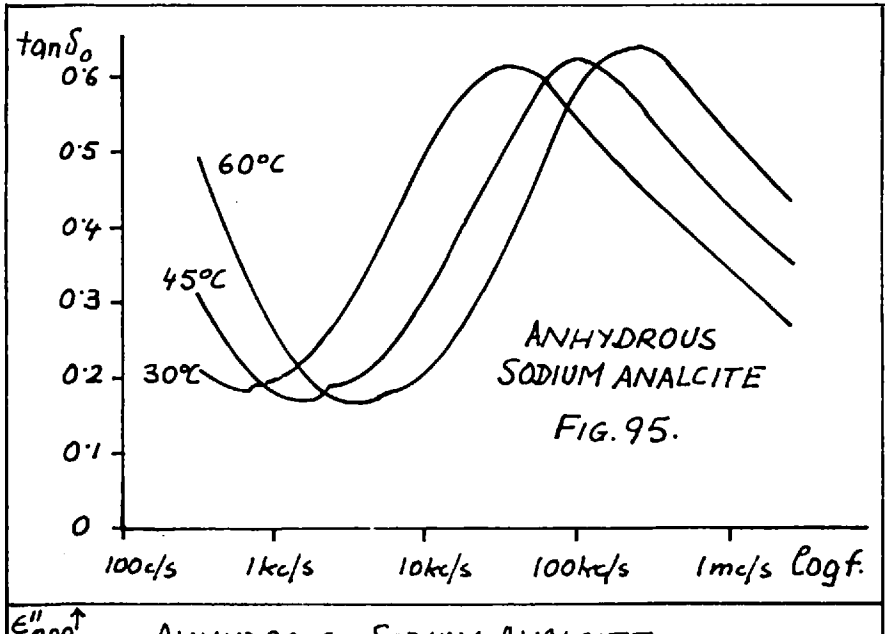
ANHYDROUS
SODIUM ANALCITE
FIG. 89.



ANHYDROUS
SODIUM ANALCITE
FIG. 92.

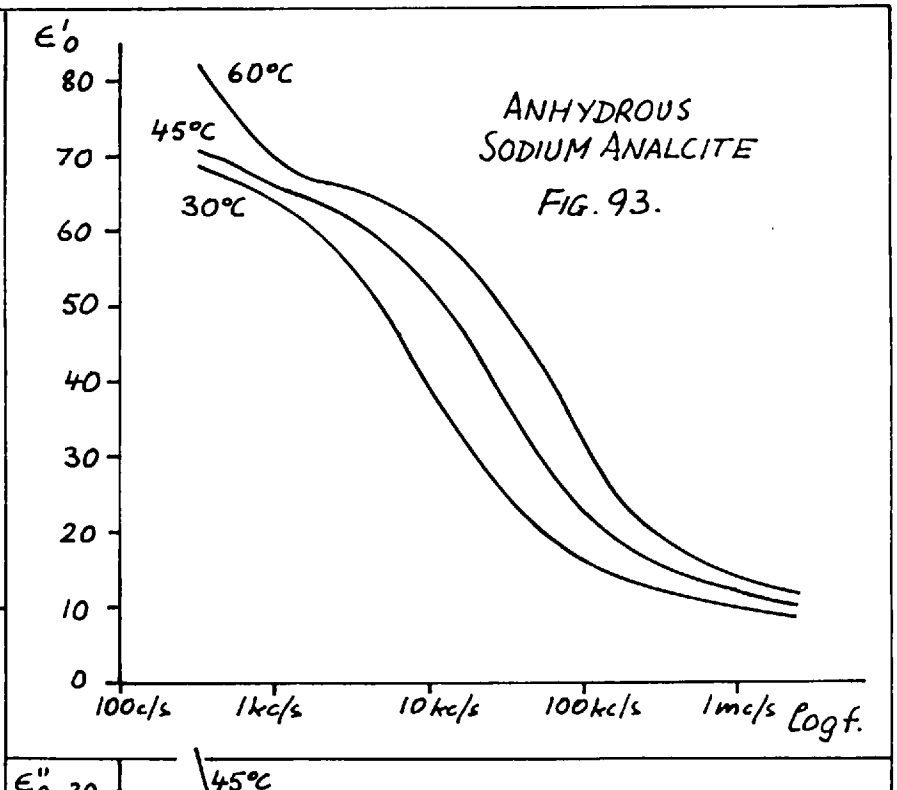


ANHYDROUS
SODIUM ANALCITE
FIG. 90.



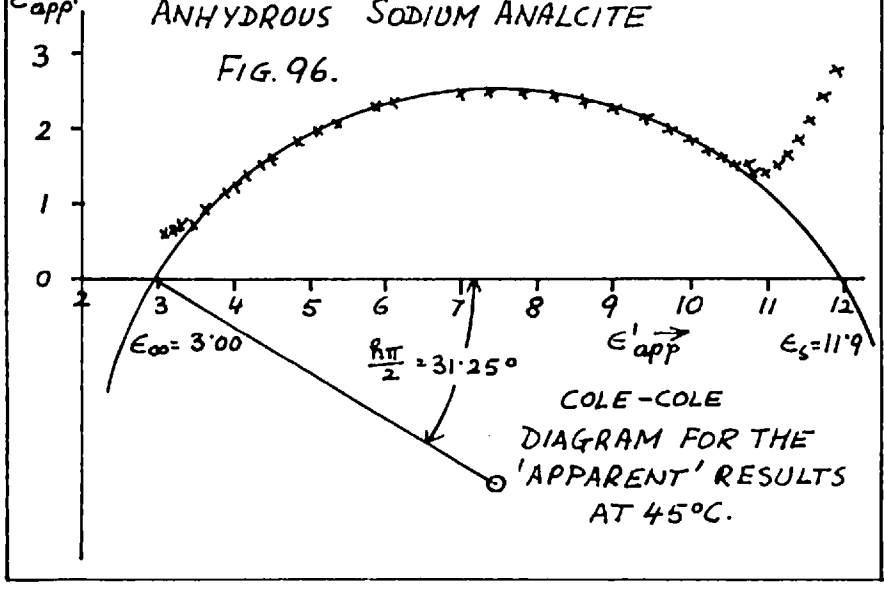
ANHYDROUS SODIUM ANALCITE

FIG. 95.



ANHYDROUS SODIUM ANALCITE

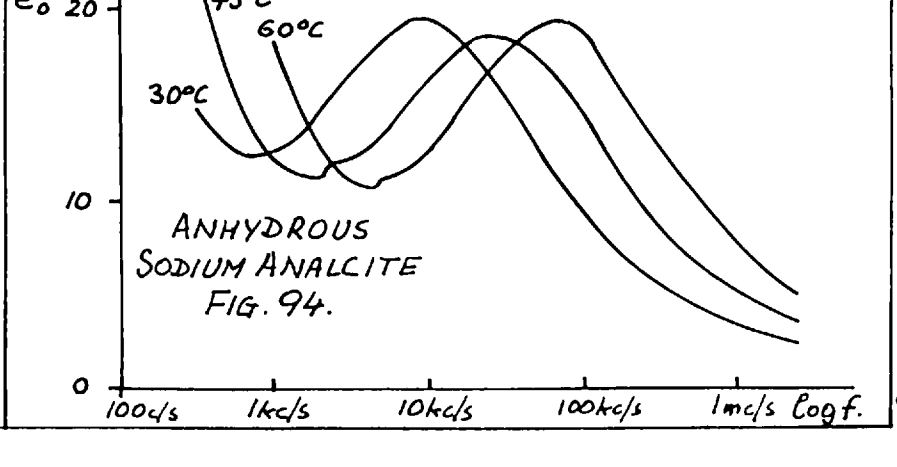
FIG. 93.



ANHYDROUS SODIUM ANALCITE

FIG. 96.

COLE-COLE DIAGRAM FOR THE 'APPARENT' RESULTS AT 45°C.



ANHYDROUS SODIUM ANALCITE

FIG. 94.

The real ϵ'_o, $\tan\delta_o$ and ϵ''_o values calculated by use of the Böttcher equation are given in tables 23 to 25 and plotted against log f in Figs. 93 to 95. Figures 89 to 95 are the typical curves associated with a relaxation phenomenon, which will be discussed later. At the lowest frequencies the onset of barrier layer behaviour is indicated. By plotting ϵ'' against ϵ', Cole-Cole circular arc plots similar to those of Fig. 21 are obtained from both the apparent and real results. All the curves are very similar and indicate a distribution of relaxation times. Figure 96 which is for the apparent results at 45°C is typical of them. They deviate slightly at the highest frequencies and to a great extent at the lowest. At the high frequency end the deviating points are very close and the deviations small. These are probably due to the type of effect described by Garton, i.e. the formation of additional equilibrium positions with small potential energy differences of the relaxing particles, caused by varying cation environment (page 72). The very rapid increase of ϵ'' with ϵ' on lowering the frequency at the lowest frequencies is the effect found both with hydrated basic sodalite and $AgA(AgNO_3)$ and is associated with the onset of interfacial polarisation at the lowest frequencies. This has already been observed in the hydrated sample (page 174) and is also apparent in the ϵ', ϵ'' and $\tan\delta$ against log f curves.

The values of h, ϵ_∞ , ϵ_s and the approximate frequency of $\epsilon''_{\text{maximum}}$ which is the frequency of the centre of the Cole-Cole circle are listed in Table 26. The frequencies at which the peak in the $\tan\delta$ and ϵ'' against log f curves appears are given in Table 27. These peak frequencies were also calculated from the Cole-Cole plots by using equation 93; the results are in Table 28.

Table 23.

Anhydrous Sodium Analcite, real quantities:
Runs 155 and 156, 30°C.

Frequency	ϵ'_o	$\tan\delta_o$	ϵ''_o	Frequency	ϵ'_o	$\tan\delta_o$	ϵ''_o
(320 c/s	69.1	0.214	14.8)	8.0 kc/s	43.0	0.454	19.5
(400	67.9	0.198	13.5)	10	39.1	0.497	19.4
(500	67.2	0.191	12.8)	13	35.1	0.541	19.0
(630	66.5	0.184	12.3)	16	32.3	0.564	18.2
(800	65.4	0.192	12.5)	20	29.5	0.589	17.4
(1.0 kc/s	64.3	0.195	12.5)	25	26.8	0.604	16.2
(1.3	62.6	0.210	13.1)	32	24.1	0.614	14.8
(1.6	61.2	0.227	13.9)	40	22.1	0.614	13.6
(2.0	59.7	0.249	14.9)	63	18.8	0.607	11.4
2.5	57.4	0.268	15.4	74	18.3	0.589	10.8
3.2	54.8	0.307	16.9	256	(12.9	0.459	5.92)
4.0	52.6	0.338	17.8	890	(10.1	0.353	3.56)
5.0	49.7	0.375	18.6	2.54 mc/s	(8.72	0.271	2.36)
6.3	46.5	0.414	19.2				

Table 24.

Anhydrous Sodium Analcite, real quantities:
Runs 159 and 160, 45°C.

Frequency	ϵ'_o	$\tan\delta_o$	ϵ''_o	Frequency	ϵ'_o	$\tan\delta_o$	ϵ''_o
(320 c/s	70.9	0.313	22.2)	25 kc/s	40.6	0.458	18.6
(500	69.7	0.239	16.6)	32	37.2	0.493	18.3
(800	67.5	0.196	13.2)	40	34.2	0.525	18.0
(1.0 kc/s	66.4	0.180	12.0)	50	31.6	0.544	17.2
(1.3	65.3	0.173	11.3)	63	27.6	0.608	16.7
(1.6	64.8	0.172	11.1)	74	26.2	0.613	16.0
(2.0	63.9	0.174	11.1)	101	22.7	0.625	14.2
(2.5	63.2	0.190	12.0)	122	21.0	0.622	13.1
(3.2	61.9	0.193	12.0)	151	19.5	0.612	11.9
4.0	60.6	0.207	12.5	216	17.6	0.582	10.2
5.0	59.0	0.225	13.3	313	15.6	0.543	8.45
13	49.5	0.353	17.5	890	12.2	0.439	5.37
16	46.8	0.385	18.0	2.54 mc/s	(9.94	0.353	3.51)
20	43.8	0.420	18.4				

Table 25.

Anhydrous Sodium Analcite, real quantities:
Runs 157 and 158, 60°C.

Frequency	ϵ'_o	$\tan\delta_o$	ϵ''_o	Frequency	ϵ'_o	$\tan\delta_o$	ϵ''_o
(320 c/s	82.6	0.491	40.6)	50 kc/s	43.7	0.431	18.8
(800	72.1	0.297	21.4)	63	38.1	0.510	19.4
(1.3 kc/s	68.5	0.226	15.5)	74	36.1	0.531	19.2
(2.0	67.1	0.187	12.5)	101	31.4	0.584	18.4
(2.5	66.3	0.177	11.7)	122	29.7	0.595	17.7
(3.2	65.5	0.168	11.0)	216	22.8	0.641	14.6
(4.0	64.7	0.165	10.7)	256	21.6	0.638	13.8
(5.0	63.8	0.178	11.3)	313	19.6	0.639	12.5
(6.3	62.9	0.183	11.5)	417	18.4	0.610	11.2
(8.0	61.8	0.193	11.9)	509	17.1	0.594	10.1
(10	60.4	0.207	12.5)	770	15.3	0.550	8.43
20	54.6	0.287	15.7	1.77 mc/s	(12.3	0.468	5.74)
32	49.4	0.357	17.6	2.54	(11.4	0.437	4.98)
40	46.5	0.396	18.4				

Note to tables 23 to 25: The Cole-Cole plots show that the results are influenced by interfacial polarisation at the lowest frequencies and by other deviations at the highest frequencies. The Böttcher calculation exaggerates these deviations and results so affected are bracketed. Thus only the results between the broken lines give the correct grain values.

Table 26.

Sodium Analcite. Values obtained from Cole-Cole Diagram.

Type of Cole-Cole plot.	ϵ_∞	ϵ_s	h	Frequency of centre of Cole-Cole circle = f_m kc/s.	Fuoss Kirkwood β at w/w_m = -1	+1
Apparent Values.						
30°C	3.3	12.0	0.31	10	$\simeq$ 0.48	$>$ 0.50
45°C	3.0	11.9	0.34	30	$\approx$ 0.48	$>$ 0.50
60°C	3.1	11.6	0.29	69	$>$ 0.50	$>$ 0.50
Real Values.						
30°C	9.9	72.8	0.30	9	$\approx$ 0.46	$>$ 0.50
45°C	9.0	71.8	0.32	25	$\approx$ 0.48	$>$ 0.50
60°C	10.1	68.9	0.26	60	$\approx$ 0.50	$>$ 0.50

Table 27.

Sodium Analcite. Peak Frequencies in kc/s.

1. Hydrated Sodium Analcite.

Type of Curve	30°C	58°C	90°C
$\tan\delta_{app}$/log f using runs 148 and 149	-	2.5	14
$\tan\delta_{app}$/log f using runs 144 and 145	1.0	4.5	14
ϵ''_{app}/log f	Peaks only roughly indicated on Figure 87.		

2. Anhydrous Sodium Analcite.

Type of Curve	30°C	45°C	60°C
$\tan\delta_o$/log f	36	95	230
ϵ''_o/log f	9	24	60
$\tan\delta_{app}$/log f	28	74	180
ϵ''_{app}/log f	10	28	70

Table 28.

Sodium Analcite. Peak Frequencies and Relaxation Times from Cole-Cole Plots and Equation 93.

Temperature °C	Apparent Results		Real Results	
	$f_{max.}$ kc/s	τ	$f_{max.}$ kc/s	τ
30	10.1	$1.58\ 10^{-5}$	8.63	$1.84\ 10^{-5}$
45	29.8	$5.34\ 10^{-6}$	24.7	$6.44\ 10^{-6}$
60	73.2	$2.17\ 10^{-6}$	62.9	$2.53\ 10^{-6}$

The distribution of relaxation times is in the intermediate range, but tends to the narrow. At $w/w_m = 1$ the Fuoss-Kirkwood β is always bigger than 0.5 and at $w/w_m = -1$, β equals or is just smaller than 0.5 in both the real and apparent results (see Table 26). At the low frequencies the slightly lower β may be due to the influence of the barrier layer effect which was shown to give rather large variations in the Cole-Cole diagram. However the Fuoss-Kirkwood curves in Fig. 26 are too close in the region concerned to allow theoretical calculations. The Cole-Cole circular arc plots fit the experimental points fairly well and can be used.

Activation energies were calculated by using equation (155) which is derived from equation (122)

$$E = k \frac{T_1 . T_2}{\triangle T} \log_e \frac{f_{m_1}}{f_{m_2}} = 4.545 \frac{T_1 . T_2}{T_1 - T_2} \log_{10} \frac{f_{m_1}}{f_{m_2}} \qquad (155)$$

This was developed and used by a number of authors (e.g. references 126, 181, 182; see also pages 75 to76). The maximum frequencies f_m were calculated by a number of different methods, and these methods and the results of the

activation free energy calculations are listed in Table 29. Of these (a) to (f) suffer from the disadvantage that the f_m values have to be obtained by interpolations from graphs. f_m in (g) and (h) is also found graphically, but since it depends on all the points of the Cole-Cole plot it is more accurate than f_m in (i) and (j) which is calculated from measurements on a limited number of points. Authors usually use methods (f) and (h) to calculate activation energies; in fact the values obtained by these methods are equal to the average obtained from all other methods when the less accurate values in (i) and (j) are neglected and are less than 1% different from the general average. Thus the activation energy found for anhydrous sodium analcite is 12.6 ± 0.3 kcals/mole. The values obtained from the apparent results in (c) and (d) appear to be lower than those obtained from real results (e) and (f). This is not borne out by results from the Cole-Cole plots and the comparatively small deviation is obviously within experimental error. Thus the apparent values for the powder material will directly give the correct activation energy for the solid material, which shows the power of the powder method of measurement. Also activation energies obtained from $\tan\delta$ peaks are the same, within experimental error, as those obtained from ϵ'' peaks.

The results in (b) of Table 29 in respect of hydrated sodium analcite must be neglected, since in this case the water loss between the temperatures of measurement has caused an apparent decrease in the activation energy values. 12.8 ± 0.3 kcals/mole is thus the activation free energy for hydrated sodium analcite and since the results for the hydrated and anhydrous samples are within experimental error, this shows that water has no influence on the activation energy of sodium analcite.

Table 29.

Activation Energies 'E' from Sodium Analcite Measurements.

Details of the method used to derive the maximum frequencies, f_m	Temperatures used in the calculation °C	E kcal/ mole	Average E, kcal/ mole
(a) From the $\tan\delta_{app}$ peaks of hydrated sodium analcite using runs 149 and 150 which have the same moisture level	58 to 90	12.8	
	30 to 58	-	12.8
	30 to 90	-	
(b) From the $\tan\delta_{app}$ peaks of hydrated sodium analcite using runs 144 and 145, i.e. complicated by water loss effects.	58 to 90	8.4	
	30 to 58	10.6	9.5
	30 to 90	9.5	
(c) From the $\tan\delta_{app}$ peaks of anhydrous sodium analcite	45 to 60	12.4	
	30 to 45	12.3	12.4
	30 to 60	12.4	
(d) From the $\tan\delta_o$ peaks of anhydrous sodium analcite	45 to 60	12.3	
	30 to 45	12.3	12.3
	30 to 60	12.3	
(e) From the ϵ''_{app} peaks of anhydrous sodium analcite	45 to 60	12.8	
	30 to 45	13.1	12.9
	30 to 60	12.9	
(f) From the ϵ''_o peaks of anhydrous sodium analcite	45 to 60	12.8	
	30 to 45	12.4	12.6
	30 to 60	12.6	
(g) f_m are the frequencies at which the centres of the Cole-Cole circles appear, derived from the apparent results of anhydrous sodium analcite	45 to 60	11.6	
	30 to 45	13.9	12.8
	30 to 60	12.8	
(h) f_m are the frequencies at which the centres of the Cole-Cole circles appear, derived from the real results of anhydrous sodium analcite.	45 to 60	12.2	
	30 to 45	13.0	12.6
	45 to 60	12.6	
(i) By averaging the peak frequencies obtained by eq. 93 from 3 points of the Cole-Cole plots of the apparent results.	45 to 60	12.5	
	30 to 45	13.7	13.1
	30 to 60	13.1	
(j) By averaging the peak frequencies obtained by eq. 93 from 3 points of the Cole-Cole plots of the real results.	45 to 60	13.0	
	30 to 45	13.3	13.2
	30 to 60	13.2	

Table 29 (contd.)

Averages of Activation Energy Results for Anhydrous Sodium Analcite:

All results (c) to (j)	12.7	kcal/mole.
All apparent results	12.8	" "
All real results	12.7	" "
tanδ peaks	12.3	" "
ϵ'' peaks	12.8	" "
All Cole-Cole peaks	12.9	" "
Apparent Cole-Cole peaks	12.9	" "
Real Cole-Cole peaks	12.9	" "
Average results not using (i) and (j)	12.6	" "

The explanation of the significance of these activation energies is based on the structure of sodium analcite as determined by Taylor (p. 16 to 20) in which the cations occupy 16 of 24 energetically equivalent positions on a time average basis. Consequently these cations are found mobile and the activation energies in the anhydrous sample must be a measure of the barrier the ions have to overcome in jumps into the vacant equivalent cation positions. In the absence of impurities, which is assumed, the structure as set out on pages 16 to 20 does not allow any other relaxation effect. This is in agreement with Beattie's assumption that conductivity in anhydrous sodium analcite is purely ionic (ref. 21 and page 92) and the activation energy of 12.6 kcal/mole found, agrees well with Beattie's value of 12.5 to 13.0 kcal/mole. The above explanation is correct both if Taylor's 24 equivalent cation positions or the alternative suggestion by Beattie (page 22), of 8 ions of lower energy per unit cell with the other 8 averaging over 16 positions of equivalent higher energy, represent the truth. The following considerations show that the hydrated sample used in these measurements contained much more than 25% of its total water content even though the surface water was removed under vacuum and measurements were made at 90°C water content. The percentage water losses, at various temperatures, of the

sample under atmospheric conditions are: 0.15% at 90°C, 0.82% at 140°, 2.80% at 201°, 4.03% at 246°, 5.69% at 282°, 6.96% at 322° and 8.49% at 497°C. Hence under atmospheric conditions the sample was reduced to 25% water content at about 300°C. Little water will have been lost on out-gassing at room temperature and any water subsequently given off at 90°C still remained in contact with the sample, which must thus have contained more than 25% of its water content. Thus the activation energy of 12.8 kcal/mole found for the hydrated sample is in respect of material containing more than 25% of its water content and is the same as for anhydrous sodium analcite. This disagrees with Beattie's conclusions[23] put forward to explain the activation energy of 16 kcal/mole found by him in the samples of water contents above 25% of the maximum. Beattie suggested that in this case the rate controlling process in the cation migration involves the energy barrier for the migration of the uncharged water molecules which hinder the cation movement (p.92). Beattie's own diffusion experiments agree with his higher result. However more recent values obtained by Rees[163] by a radio-active tracer method are in good agreement with the value found in this work. It must be pointed out however that Figs. 86 and 91 indicate a peak frequency shift on dehydration, which on reference to table 2 should be equivalent to an activation energy difference of 3 kcal/mole. The reason for this has not been resolved, but probably lies in the greater interference of the interfacial polarisation effect on the results for hydrated crystals, as can be evidenced by the broadening of the ϵ''_{app} results (compare Figs. 87 and 92) in the hydrated sample.

Since the activation energies are the same in the anhydrous and hydrated samples it can be concluded that the water molecules have no part in the migration process. This can only be so if the water molecules in hydrated sodium analcite are not in a position to hinder the movement of

the cations. The high value obtained by Beattie may be connected with a barrier layer effect obtained by him at the low frequencies of his measurements with the hydrated sample. Such an effect is actually indicated in the results presented here. It would involve particle-particle energy barriers which must be higher than the intra-particle barriers of the sodium ions, hence a value of 16 kcal/mole. In fact the low frequency results of hydrated sodium analcite, which show the interfacial polarisation effect, indicate that a peak due to this effect may be obtained at a frequency, which on consideration of Table 2 is found to be of the correct order to give an activation energy of 16 kcal/mole.

The activation energy - peak frequency relation listed in Table 2 (from Dryden and Meakins) is well reproduced by the results for the anhydrous crystals and is thus a good guide for finding the frequency at which relaxation peaks of aluminosilicates occur, when the activation energy for the relaxation process is approximately known.

It is interesting to compare the sodium analcite results with those of basic sodalite. In sodium analcite water has little influence on the order of the results and the peak frequencies. On dehydration the $\tan\delta$ peaks become steeper and move to slightly higher frequencies and both hydrated and anhydrous samples show the beginnings of interfacial polarisation effects at the lower frequencies. In basic sodalite water is seen to have a profound effect on the electrical properties. Since the conductivity or relaxation which determines the electrical properties, is due to the cations in both samples, it appears that in basic sodalite only are the water molecules associated with the cations so as to influence their properties. The difference between the two aluminosilicates may lie in the

fact that some of the cations in basic sodalite are in the form of interstitial sodium hydroxide and are not as strongly bound as the framework cations. When the material is in the hydrated state it then behaves almost as an aluminosilicate framework, the cages of which are permeated by sodium hydroxide solution.

The lowest values of ϵ'_o obtained at the highest frequencies do not reach a constant value (Fig. 93), approximating to ϵ'_∞. In fact at 30°C the lowest ϵ'_o value is even lower than ϵ'_∞ obtained from Cole-Cole plots. The difference is due to the deviation of the high frequency results from the Cole-Cole circles, which was discussed earlier (page 181). The Cole-Cole ϵ'_∞ results were thus used to calculate the atomic and dipole contributions to the dielectric constant; the results are given in Table 30.

Table 30.

Temperature °C	ϵ_s	ϵ_∞	ϵ electronic	ϵ atomic	ϵ ionic
30	72.8	9.9	2.1	7.8	62.9
45	71.8	9.0	2.1	6.9	62.8
60	68.9	10.1	2.1	8.0	58.8
Average	-	9.7	2.1	7.6	-

Using $\epsilon_\infty = 9.7$ throughout, the ionic contributions become 63.1 at 30°C, 62.1 at 45° and 59.2 at 60° respectively. In all these results the fact that a graphical method had to be used to determine ϵ'_s and ϵ'_∞ accounts for inaccuracies; however the experimental results could not be used directly because of the low and high frequency deviations discussed earlier. Agfeement between the dielectric constants and those quoted in Table 3 (page 89) is not good. It is obvious that all the workers quoted in

Table 3 measured ϵ'_{∞} , but both their samples and conditions of measurement are not sufficiently defined to add to the comments on page 90 . A liquid immersion method of measurement at very high frequencies might be useful to determine the exact ϵ'_{∞} values; the difficulty in such a method is to keep the sample in an anhydrous state.

8. LEUCITE.

8.1. Description of Sample.

Leucite was prepared by ion exchange from sodium analcite, preparation 23[10,11,12]. Three sealed glass tubes, each containing 5 gms sodium analcite, 10 gms potassium chloride and 10 ml water were rotated for 2 days in an oven thermostatically controlled at 140°C. The product was filtered and washed free from chloride and the whole exchange procedure including washing free of chloride was twice repeated. The sample was dried successively by alcohol, acetone and air. 7 gms of the dry exchange product were sintered for 3 days at 1350°C and then quenched giving the second sample. There was little contraction on sintering and X-ray evidence shows the two samples to be identical. The 'd' spacings of the materials obtained by powder X-ray measurements are compared with the spacings given by Barrer and Baynham[8] for a natural leucite and a sample prepared hydrothermally in Table 31. The X-ray powder photograph of the samples was identical with that of a sample prepared by Dr. L. V. C. Rees[163].

The dimensions of the unit cells of the samples used in this work are compared with those of other samples in Table 32. The crystallites of the ion exchange sample are irregular spheres of varying size from very small to a maximum diameter of 4.10^{-4} cm. The sintered sample consists of spheres of up to 10.10^{-4} cm diameter. Considering van Vessem's experiments and the sodium chloride results on page 123, the particle sizes of the samples are thus small enough to give reliable results on applying the Böttcher equation. The electron microscope, optical microscope and the powder X-rays show that the samples do not contain gel, other aluminosilicate species or impurities.

Table 31.

Powder X-rays of Leucite Samples.

Leucite Exchange			Sintered Leucite			Naray-Szabo(71)	Barrer and Baynham(8)	
'd' spacing	'I' intensity	hkl	'd' spacing	'I' intensity	hkl	Natural Leucite 'd'	Hydrothermally prepared Leucite. 'd'	'I'
9.40	v.v.w.	-	9.52	v.v.w.	101			
5.54	v.w.	112	5.55	w.	112			
5.37	m.	211	5.39	s.	211			
4.76	v.v.w.	202	4.76	w.	202			
3.60	v.v.w	213	3.62	v.v.w	213			
3.51	v.v.w.	321	3.53	v.v.w.	321			
3.44	s.	004	3.45	s.	004	3.45	3.42	v.s.
3.27	v.s.	400	3.28	v.s.	400	3.26	3.23	v.s.
3.15	v.v.w.	410	3.17	v.v.w.	410			
3.09	v.v.w.	411	3.10	v.v.w.	411			
3.04	vvv.w.	204	3.05	v.v.w.	204			
2.92	w.	420	2.93	m.	420	2.91	2.89	s.
2.84	m.	323	2.85	m.	323		283	s.
2.81	w.	332	2.82	w.	332	2.81		
2,64	v.v.w.	314	2.65	w.	314	2.64	2.64	m.
2.37	w.	225	2.37	w.-m.	225	2.38	2.37	s.
		404			404			
2.32	v.v.w.	440	2.32	v.v.w.	440	2.30	2.30	w.
2.13	v.w.	532	2.13	w.	532	2.14	2.14	m.s.
						2.06	2.06	m.w.
1.73	v.v.w.	327	1.73	v.w.	327	1.72	1.72	m.
1.67	w.	-	1.67	w.	-	1.66	1.66	s.

Table 32.

Tetragonal Unit Cell Sizes of Leucite Samples.

Origin and Type of Sample	Angstrom Units 'a'	'c'
Exchange sample used in this work	13.09	13.81
Sintered sample used in this work	13.09	13.76
Exchange sample ex Barrer and Baynham(8)	12.92	13.70
Naray-Szabo's natural leucite(71)	13.01	13.82
Wyart's synthetic leucite(69)	12.95	13.74
Wyart's natural leucite(67,68)	12.95	13.65

The large 'd' spacings found with the experimental samples and Dr. Rees' exchange sample have no counterparts in the comparison samples. This must be due to the use of the Guinier camera in taking the powder X-rays of the former. Undoubtedly this camera gives better resolution at the low diffraction angles than the X-ray cameras which were used to find the 'd' spacings of the comparison species. The exchange material contains 0.30% surface water and loses a further 0.48% at 500°C, while the sintered sample shows 0.14% loss at 500°C. Theoretically surface dried leucite produced from sodium analcite by 100% exchange should show a loss, due to strongly held water, of 0.55% at 500°C. Thus the sample of leucite used in this work, was 100% exchanged.

The densities of the samples calculated from X-ray data, the refractive indices determined by sodium light and the electronic contributions to the dielectric constant are given in Table 33.

Table 33.

Sample	Density gms/cm^3	Mean Refractive Index	ϵ' electronic	Packing Fraction
Exchange sample of Leucite	2.460	1.494	2.23	0.523
Sintered Leucite	2.450	1.500	2.25	0.519

Prior to dielectric measurements the samples were dehydrated, by heating for two days in vacuum at 170°C.

8.2. Leucite (Exchange Sample).

The results of a.c. measurements in the large stainless stell cell made at 30, 60 and 90°C over the whole

available frequency range, are given in Tables LVII to LXII. Tables LXIII to LXVIII are the results of repeat measurements at a number of selected frequencies and of measurements at 105, 74.8 and 45.2°C to determine the temperature dependence of the electrical properties. The results are plotted as a function of frequency in Figs. 97 to 100 and as a function of temperature in Figs. 101 to 104. The 'real' results calculated by Böttcher's equation are shown in Tables 34 to 42 and are plotted in Figs. 105 and 112 both as a function of frequency and temperature.

Table 34.

Leucite, ex Run 130 at 30°C.

Frequency	ϵ'_o	$\tan\delta_o$	ϵ''_o	R_{po} meg-Ohm
400 c/s	6.45	0.054	0.346	58.7
800	6.36	0.039	0.245	41.4
1.3 kc/s	6.33	0.033	0.207	30.2
2.5	6.24	0.026	0.165	19.7
5.0	6.18	0.022	0.138	11.8
10.0	6.15	0.019	0.114	7.12
20.0	6.13	0.016	0.095	4.27
40.0	6.10	0.014	0.085	2.39

Table 35.

Leucite, ex Run 131 at 30°C. 4 points on best straight line.

Frequency	ϵ'_{app}	$\tan\delta_{app}$	ϵ''_{app}	ϵ'_o	$\tan\delta_o$	ϵ''_o	R_{po} meg-Ohm
87 kc/s	2.97	0.0079	0.0235	6.08	0.0115	0.070	1.33
226	2.96	0.0064	0.0189	6.05	0.0093	0.056	0.642
617	2.955	0.0052	0.0154	6.04	0.0076	0.046	0.286
2.01 mc/s	2.855	0.0042	0.0124	6.04	0.0061	0.037	0.109

Table 36.

Leucite, ex Run 132 at 60°C.

Frequency	ϵ'_o	$\tan\delta_o$	ϵ''_o	R_{po} meg-Ohm
400 c/s	7.17	0.126	0.902	22.5
800	6.86	0.091	0.622	16.3
1.3 kc/s	6.71	0.075	0.503	12.4
2.5	6.57	0.057	0.376	8.64
5.0	6.45	0.045	0.292	5.56
10.0	6.36	0.036	0.227	3.58
20.0	6.28	0.029	0.180	2.26
40.0	6.24	0.024	0.150	1.35

Table 37.

Leucite, ex Run 133 at 60°C. 4 points on best straight line.

Frequency	ϵ'_{app}	$\tan\delta_{app}$	ϵ''_{app}	ϵ'_o	$\tan\delta_o$	ϵ''_o	R_{po} meg-Ohm
87 kc/s	3.00	0.0134	0.0402	6.17	0.0194	0.120	0.778
226	2.97	0.0105	0.0312	6.08	0.0152	0.092	0.391
617	2.97	0.0082	0.0244	6.0	0.0119	0.072	0.183
2.01 mc/s	2.97	0.0064	0.0190	6.08	0.0093	0.056	0.0721

Table 38.

Leucite, ex Run 135 at 90°C.

Frequency	ϵ'_o	$\tan\delta_o$	ϵ''_o	R_{po} meg-Ohm
400 c/s	8.72	0.271	2.36	8.60
800	7.98	0.208	1.66	6.11
1.3 kc/s	7.57	0.174	1.32	4.73
2.5	7.16	0.131	0.941	3.45
5.0	6.92	0.100	0.689	2.36
10.0	6.70	0.075	0.502	1.62
20.0	6.58	0.057	0.375	1.08
40.0	6.45	0.046	0.294	0.690

Table 39.

Leucite, ex Run 136 at 90°C. 4 points on best straight line.

Frequency	ϵ'_{app}	$\tan\delta_{app}$	ϵ''_{app}	ϵ'_o	$\tan\delta_o$	ϵ''_o	R_{po} meg-Ohm
87 kc/s	3.06	0.0238	0.0728	6.35	0.034	0.217	0.430
226	3.03	0.0182	0.0551	6.26	0.026	0.165	0.218
617	3.01	0.0133	0.0400	6.20	0.019	0.119	0.111
2.01 mc/s	3.02	0.0102	0.0308	6.23	0.015	0.092	0.0439

Table 40.

Leucite, ex Run 137 at 105°C.

Frequency	ϵ'_o	$\tan\delta_o$	ϵ''_o	R_{po} meg-Ohm
1.3 kc/s	8.40	0.246	2.065	3.02
2.5	7.70	0.191	1.471	2.21
5.0	7.32	0.146	1.065	1.52
10.0	7.01	0.108	0.760	1.07
20.0	6.78	0.081	0.551	0.737
40.0	6.66.	0.064	0.425	0.478

Table 41.

Leucite, ex Run 139 at 74.8°C.

Frequency	ϵ'_o	$\tan\delta_o$	ϵ''_o	R_{po} meg-Ohm
1.3 kc/s	7.04	0.117	0.822	7.60
2.5	6.81	0.087	0.592	5.49
5.0	6.66	0.067	0.446	3.64
10.0	6.50	0.051	0.334	2.43
20.0	6.42	0.040	0.257	1.58
40.0	6.29	0.033	0.206	0.985

Table 42.

Leucite, ex Run 141 at 45.2°C.

Frequency	ϵ'_o	$\tan\delta_o$	ϵ''_o	R_{po} meg-Ohm
1.3 kc/s	6.51	0.050	0.322	19.4
2.5	6.36	0.038	0.240	13.5
5.0	6.30	0.031	0.196	8.29
10.0	6.24	0.025	0.158	5.14
20.0	6.22	0.021	0.128	3.17
40.0	6.18	0.018	0.114	1.78

The results indicate a peak due to either cation relaxation or a barrier layer effect at frequencies lower than were obtained in the measurements. The qualitative evidence, obtained from the frequency dependence of the results, does not provide a firm distinction between these two alternatives, although in general evidence is in favour of the cation relaxation mechanism.

The similarity of Figs. 99 to 106 to the corresponding figures of anhydrous basic sodalite and the

high frequency results of sodium analcite would indicate that leucite undergoes a relaxation effect at lower frequencies. However there also exists a similarity to the very high frequency curves obtained for samples showing interfacial polarisation effects, i.e. hydrated basic sodalite and the AgA($AgNO_3$) samples. This is not surprising since relaxation and interfacial polarisation peaks are indistinguishable except in the order of the ϵ' and tanδ values. Thus the low ϵ' values obtained for leucite again indicate that these values rise to a relaxation rather than an interfacial polarisation peak on lowering the frequency. The same evidence is provided by Figs. 100 and 108 which show that conductance is predominantly by an a.c. mechanism. Consideration of Beattie's results on activation energy[21] is instructive. He finds 17 kcal/mole for the potassium ions in leucite and using Table 2 this would indicate a cation relaxation peak in the region of 1 c/s at 20°C. Approximately the same peak frequency seems indicated by the results obtained in this work. Further evidence for relaxation rather than interfacial polarisation in leucite is that so far only macroscopically heterogeneous aluminosilicates, i.e. those containing guest molecules such as water or silver nitrate, have given interfacial polarisation phenomena. However, although all the evidence seems to point to cation relaxation occurring at lower frequencies, the two mechanisms are so closely related and give such similar results, that a definite decision cannot be reached in absence of the actual loss peak.

The curves of log R_p against temperature are approximately linear and activation energies were calculated by using equation (150). Values were obtained by averaging all possible temperature combinations at a constant frequency and also by averaging results for a particular temperature interval over frequencies between 1.3 and 40 kc/s. The

results from both $R_{p(app)}$ and R_{po} are given in Table 43, and show very good agreement. The activation energies vary considerably, increasing both with increase in measuring temperatures and decrease in frequency. If, as happens with anhydrous basic sodalite, and as suggested earlier, it is assumed that the leucite results tend towards a relaxation peak at lower frequencies, then the variation of the activation energies can be explained in exactly the same way as for anhydrous basic sodalite on pages 154 to 155. The relaxation effect is due to the framework cations, which have a wide distribution of relaxation times caused by the existence of additional equilibrium positions of the cations due to their varying environment within the aluminosilicate framework, i.e. it can be imagined that a number of energy barriers of different heights occur. As the frequency is raised and moves away from the absorption region, the barriers involved are increasingly those of smaller and smaller heights and therefore in this region the activation energies vary with frequency and temperature.

The dielectric measurements are in the region between peaks due to ionic relaxation and atomic resonance absorption. The constant permittivity values at the higher frequencies of measurement are therefore independent of these absorptions and equal the dielectric constant contribution due to the total polarisability. By use of the refractive index values, this can be split into contributions due to atomic and electronic polarisation, with the results given in Table 44. These vary only slightly with temperature.

Table 43.

Leucite, Activation Energies, kcals/mole.

A. Results from all temperature combinations averaged.

Frequency		ex $R_{p(app)}$	ex R_{po}	Frequency		ex $R_{p(app)}$	ex R_{po}
400 c/s	(1)	6.9	7.0	20 kc/s	(2)	5.4	5.5
800	(1)	6.9	7.0	40.0	(2)	4.9	5.0
1.3kc/s	(2)	7.0	7.1	87.0	(1)	4.1	4.1
2.5	(2)	6.7	6.8	226	(1)	3.9	4.0
5.0	(2)	6.3	6.4	617	(1)	3.3	3.5
10.0	(2)	5.8	5.9	2.01mc/s	(1)	3.3	3.3

(1) Only results at 3 temperatures were available and used;
(2) Results at 6 temperatures were used.

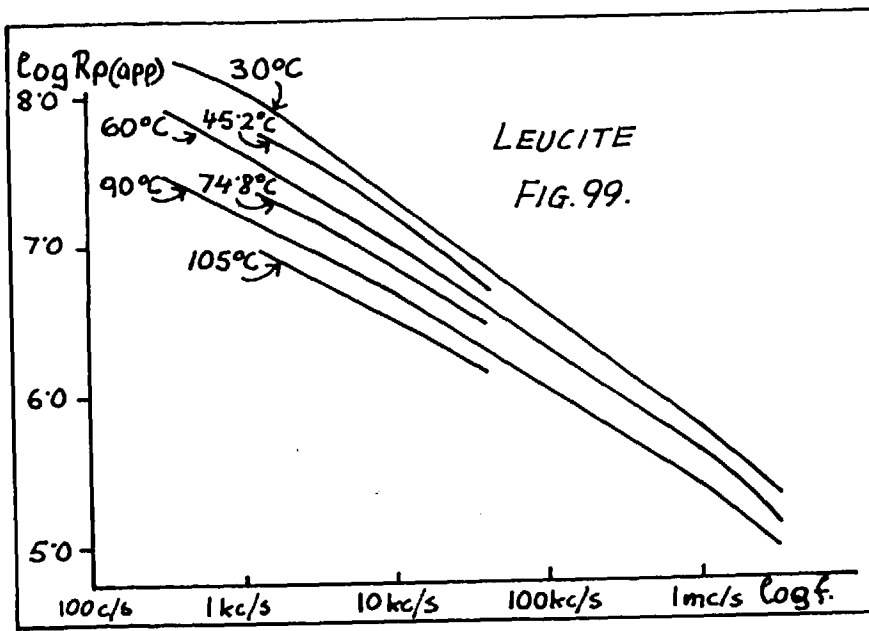
B. Results at 6 frequencies between 1.3 and 40 kc/s averaged.

Temperature Interval, °C	ex $R_{p(app)}$	ex R_{po}
30 - 45.2	4.4	4.4
45.2 - 60	5.3	5.4
60 - 74.8	6.2	6.3
74.8 - 90	6.8	6.9
90 - 105	7.4	7.6

Table 44.

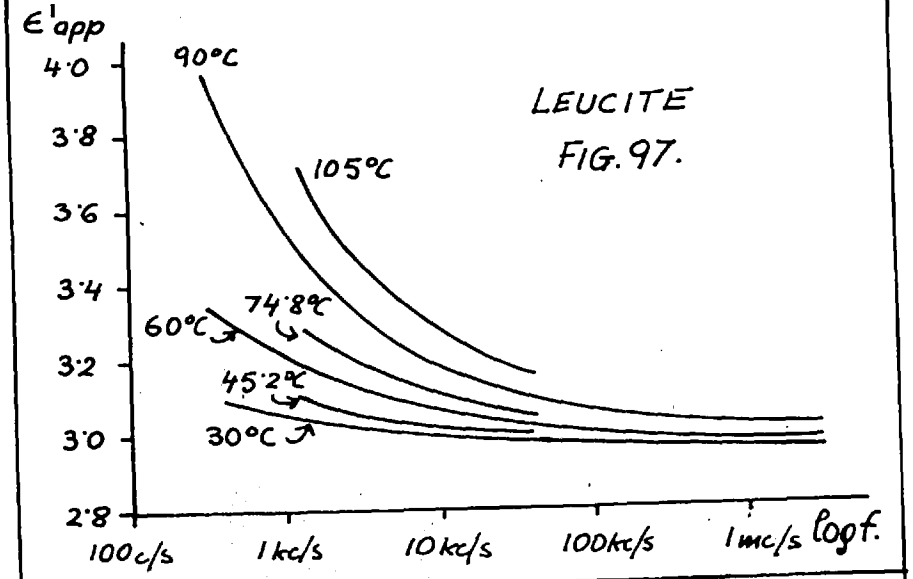
Permittivity of Leucite.

Temperature °C	Constant ϵ'_o due to total polarisability	ϵ' due to electron polarisation	ϵ' due to atomic polarisation
30	6.04	2.23	3.81
60	6.08	2.23	3.85
90	6.22	2.23	3.99
Average	6.11	2.23	3.88



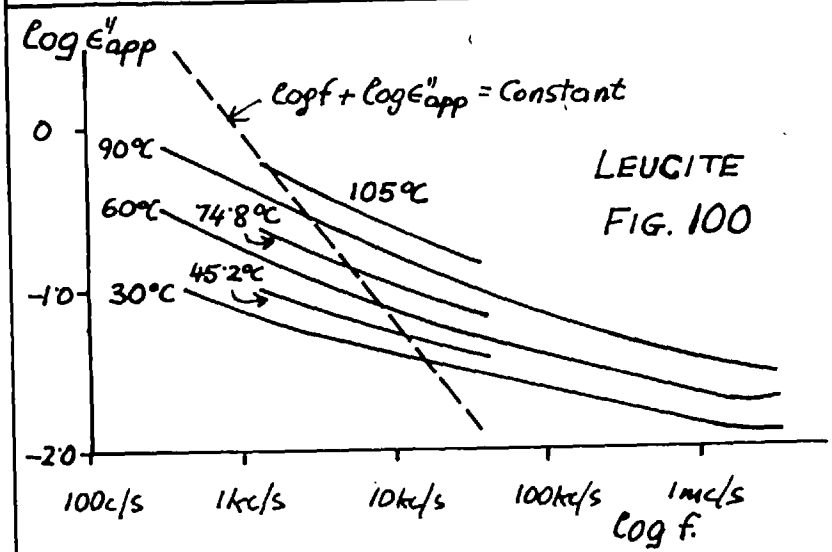
LEUCITE

FIG. 99.



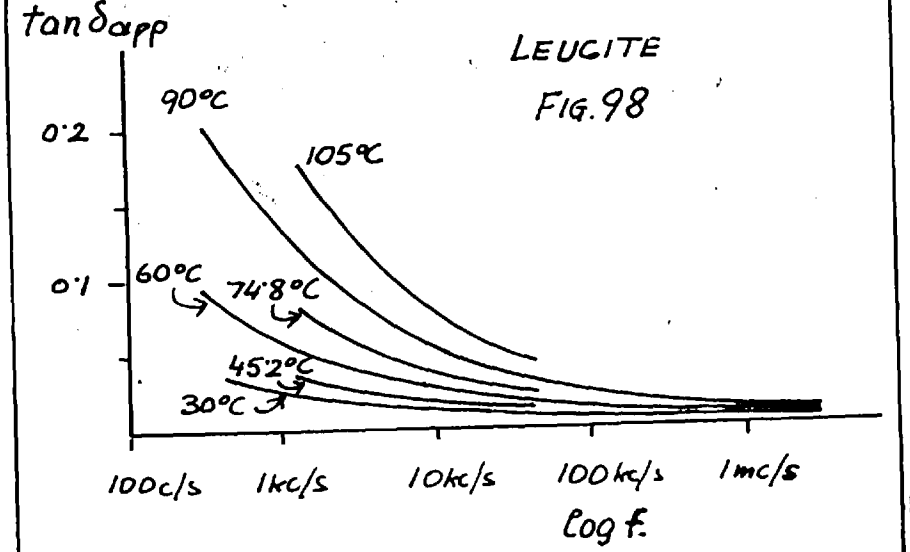
LEUCITE

FIG. 97.



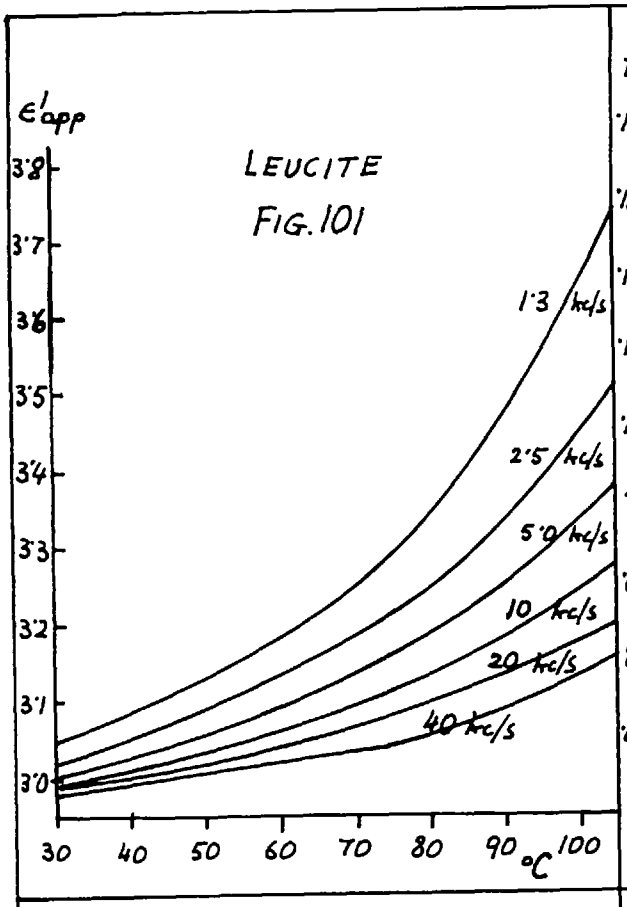
LEUCITE

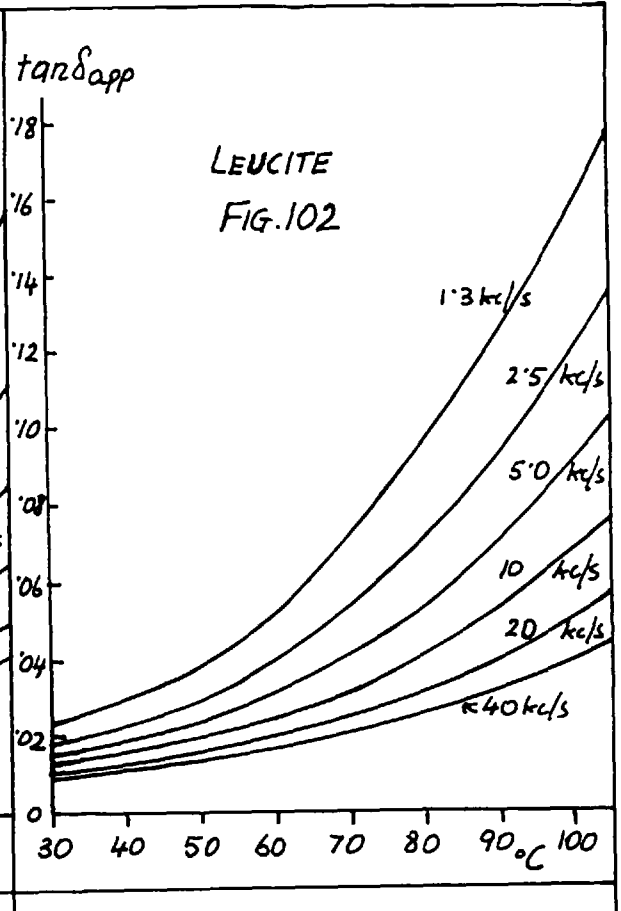
FIG. 100

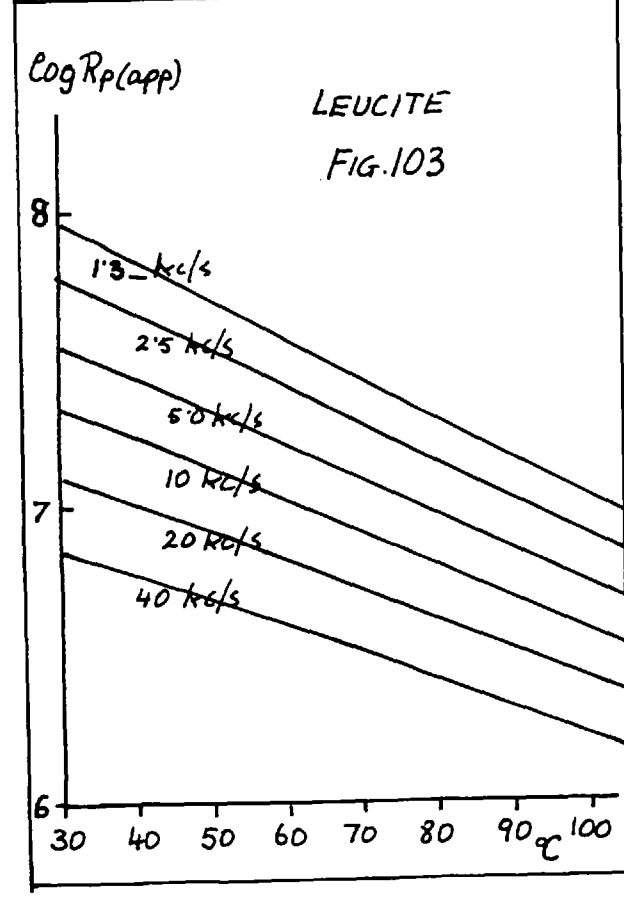


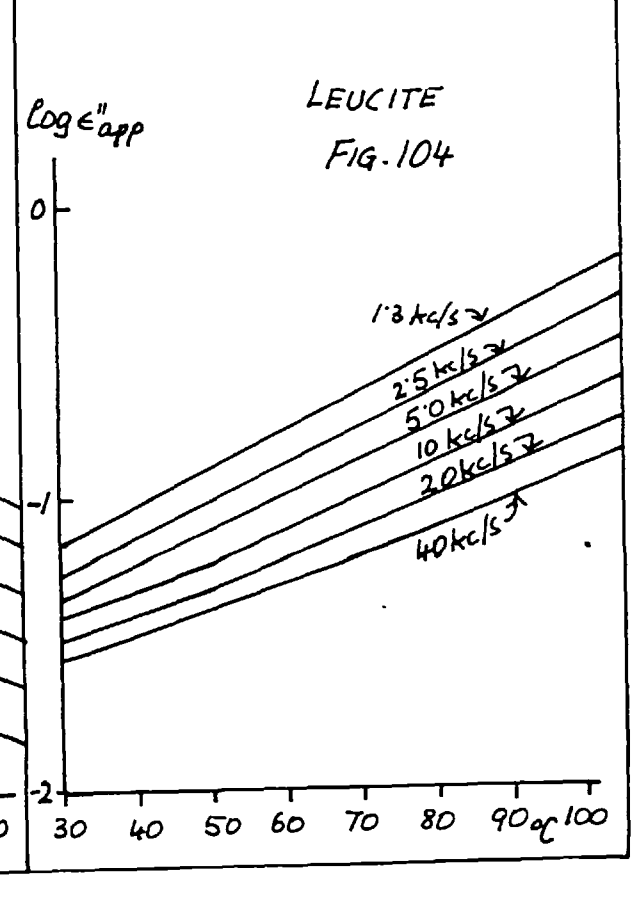
LEUCITE

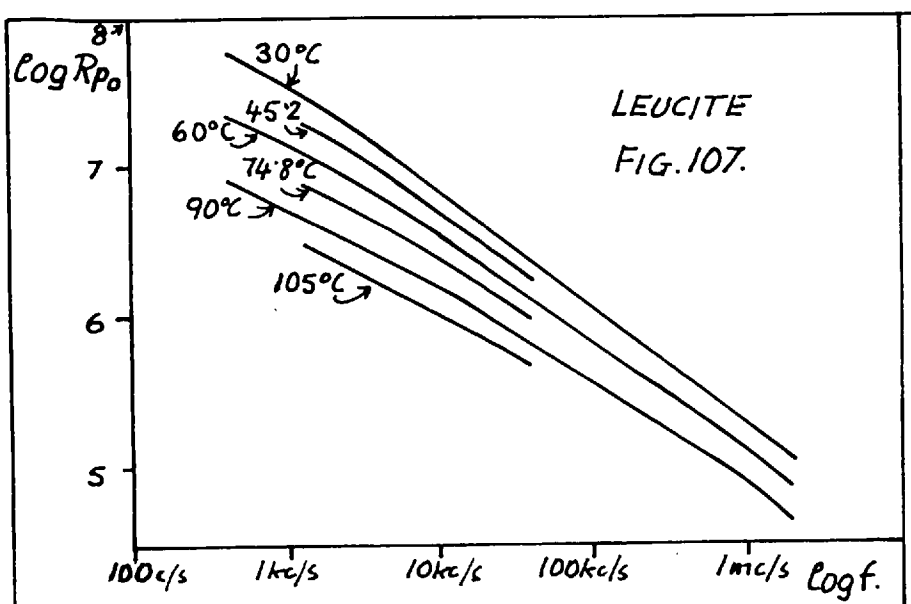
FIG. 98


ϵ'_{app}
LEUCITE
FIG. 101
3·8
3·7
3·6
3·5
3·4
3·3
3·2
3·1
3·0
1·3 kc/s
2·5 kc/s
5·0 kc/s
10 kc/s
20 kc/s
40 kc/s
30 40 50 60 70 80 90 °C 100

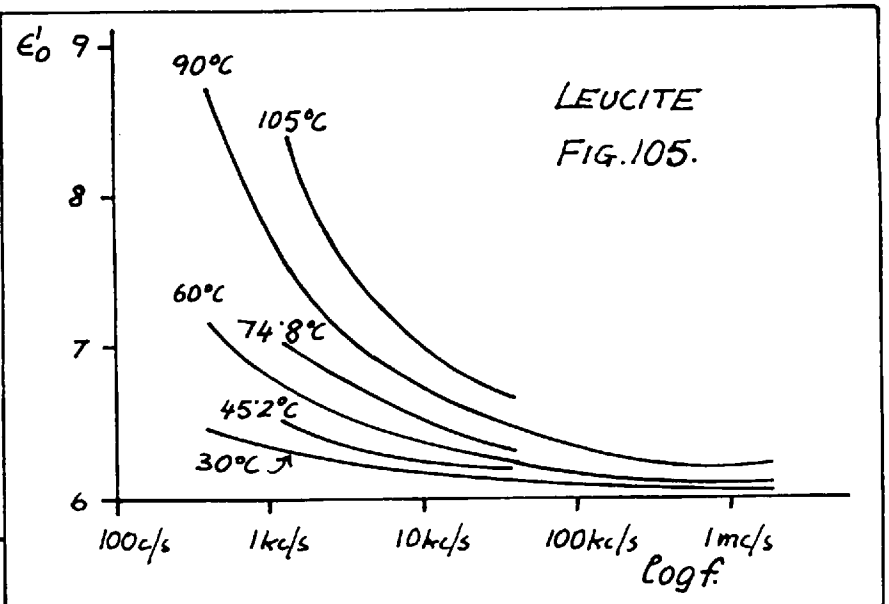

$\tan\delta_{app}$
LEUCITE
FIG. 102
·18
·16
·14
·12
·10
·08
·06
·04
·02
0
1·3 kc/s
2·5 kc/s
5·0 kc/s
10 kc/s
20 kc/s
≈40 kc/s
30 40 50 60 70 80 90 °C 100


$\log R_{p(app)}$
LEUCITE
FIG. 103
8
7
6
1·3 kc/s
2·5 kc/s
5·0 kc/s
10 kc/s
20 kc/s
40 kc/s
30 40 50 60 70 80 90 °C 100

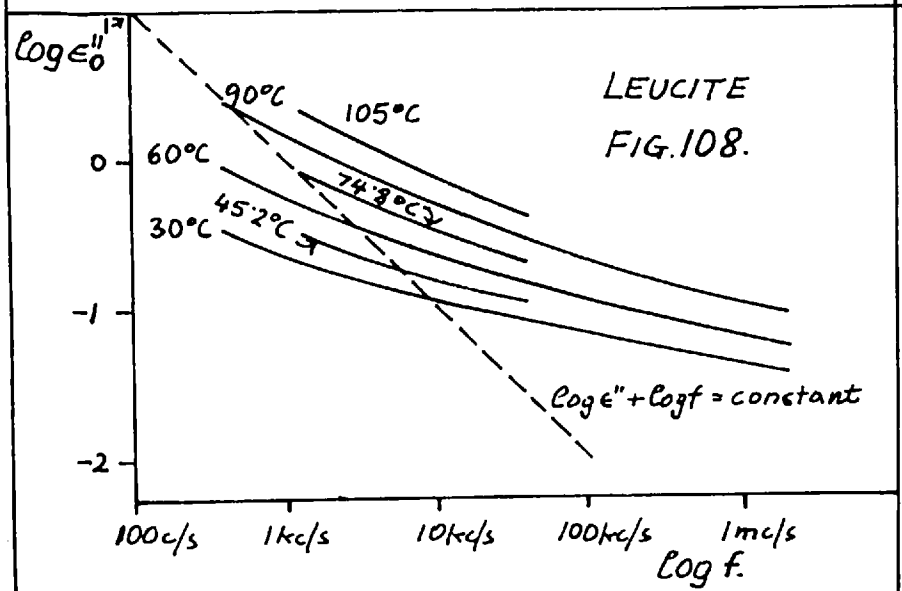

$\log \epsilon''_{app}$
LEUCITE
FIG. 104
0
-1
-2
1·3 kc/s
2·5 kc/s
5·0 kc/s
10 kc/s
20 kc/s
40 kc/s
30 40 50 60 70 80 90 °C 100



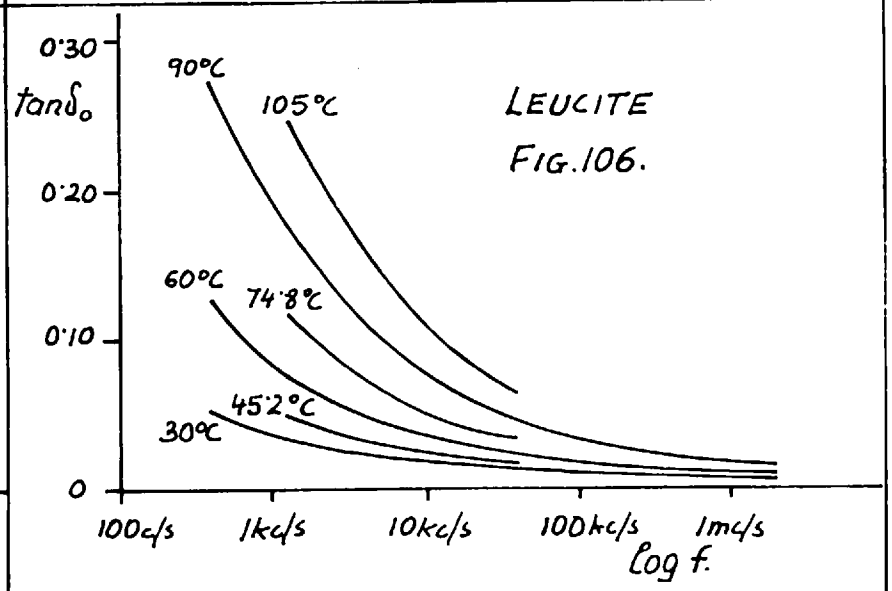
LEUCITE
FIG. 107.



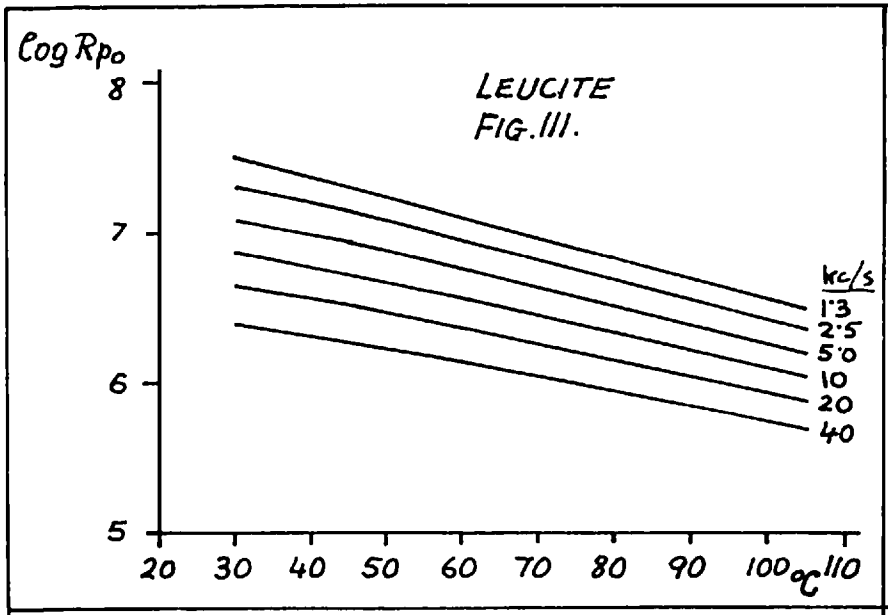
LEUCITE
FIG. 105.

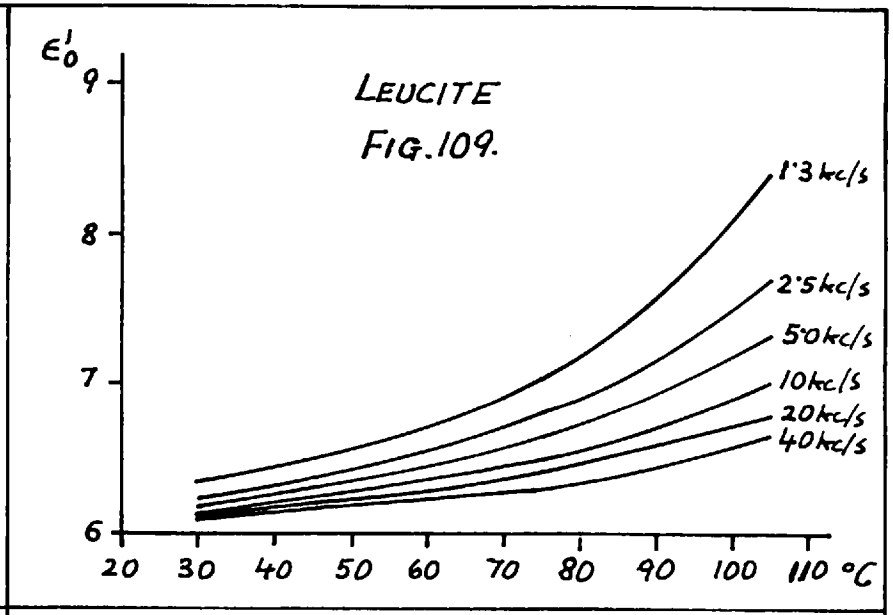


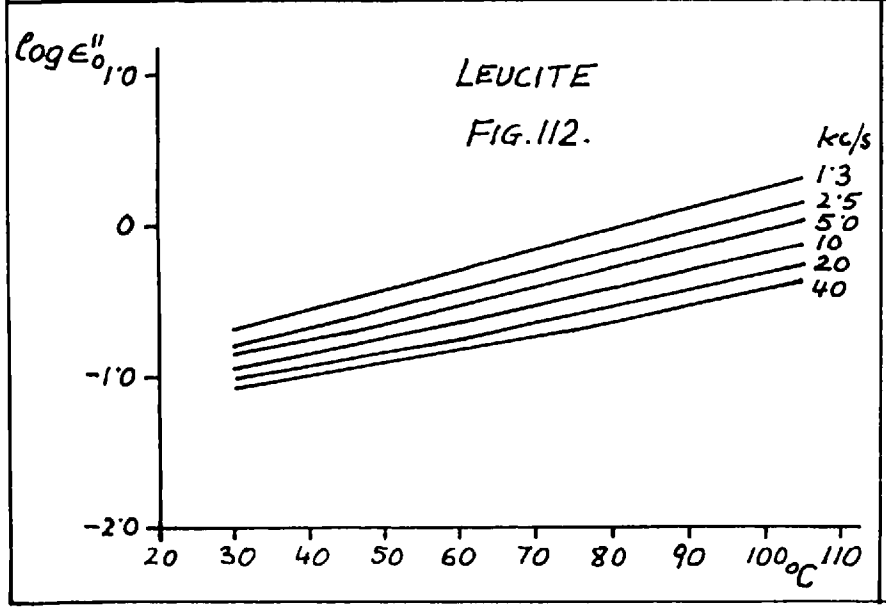
LEUCITE
FIG. 108.

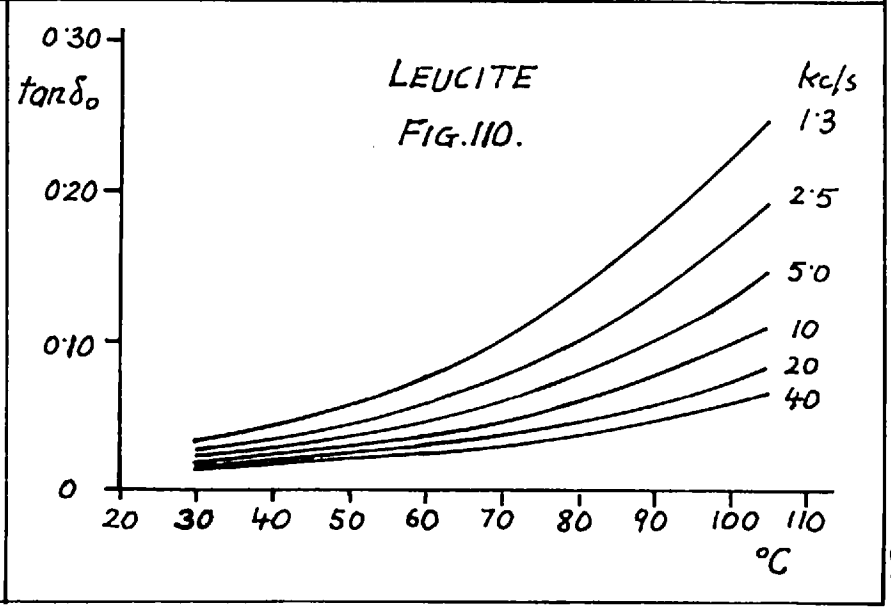


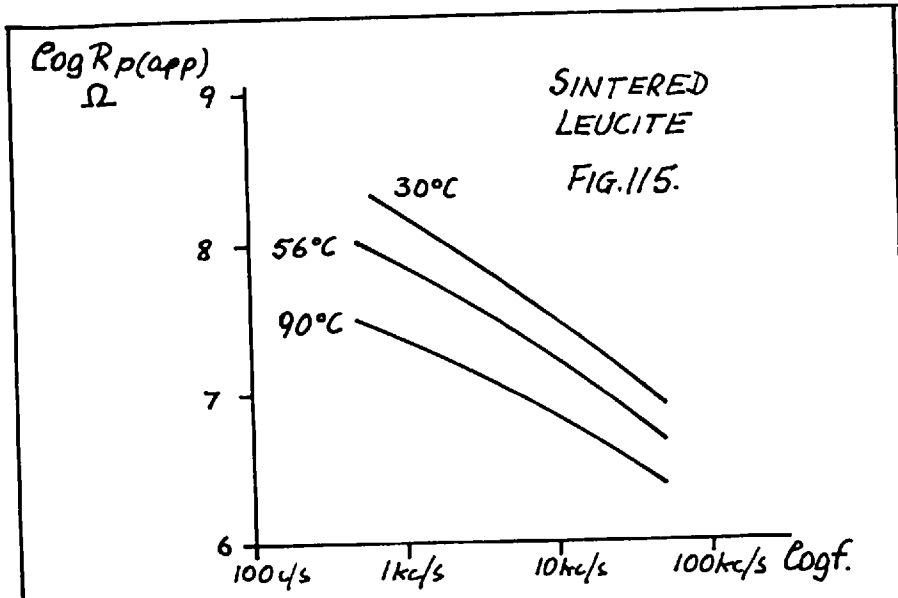
LEUCITE
FIG. 106.


Log Rpo
LEUCITE
FIG. III.
8
7
6
5
20 30 40 50 60 70 80 90 100 °C 110
kc/s
1·3
2·5
5·0
10
20
40


ε'o
LEUCITE
FIG. 109.
9
8
7
6
20 30 40 50 60 70 80 90 100 110 °C
1·3 kc/s
2·5 kc/s
5·0 kc/s
10 kc/s
20 kc/s
40 kc/s

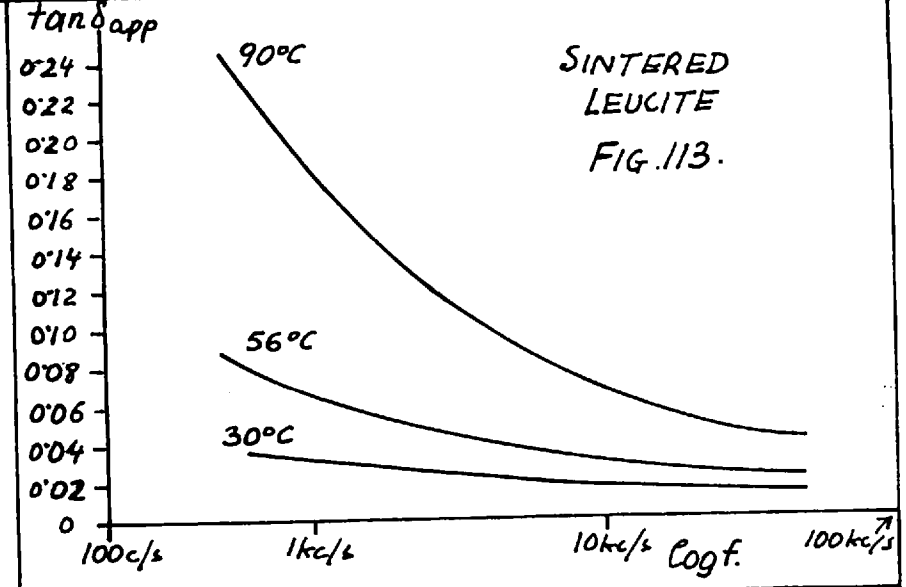

Log ε''o
LEUCITE
FIG. 112.
1·0
0
-1·0
-2·0
20 30 40 50 60 70 80 90 100 °C 110
kc/s
1·3
2·5
5·0
10
20
40


0·30
tan δo
LEUCITE
FIG. 110.
0·20
0·10
0
20 30 40 50 60 70 80 90 100 110
°C
kc/s
1·3
2·5
5·0
10
20
40



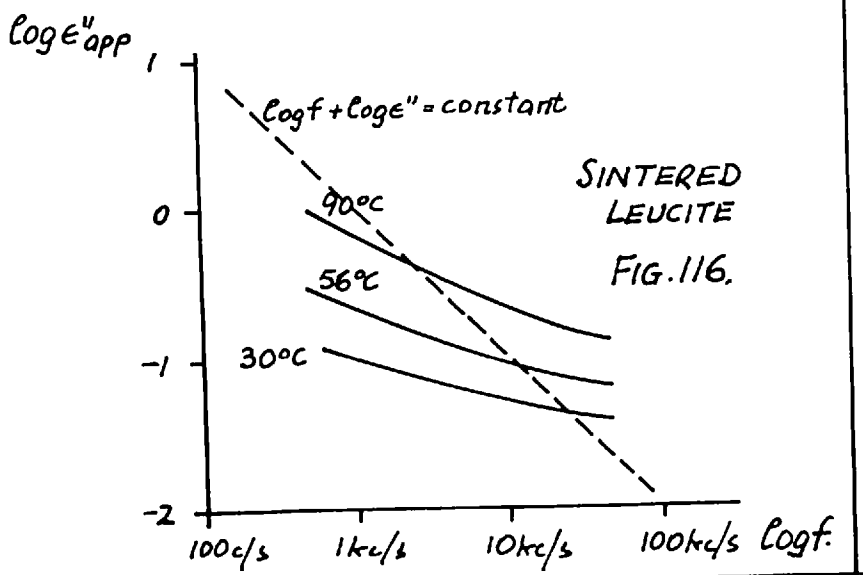
SINTERED LEUCITE

FIG. 115.



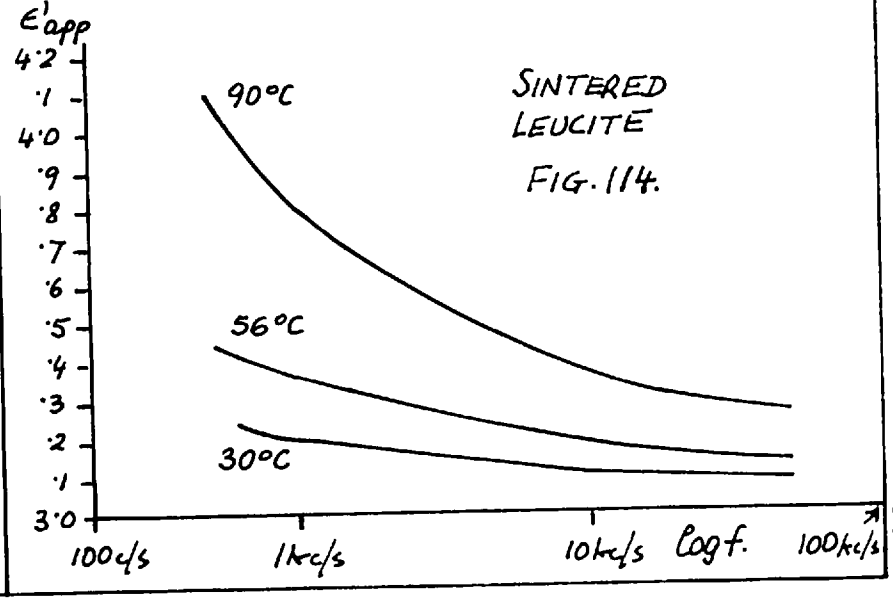
SINTERED LEUCITE

FIG. 113.



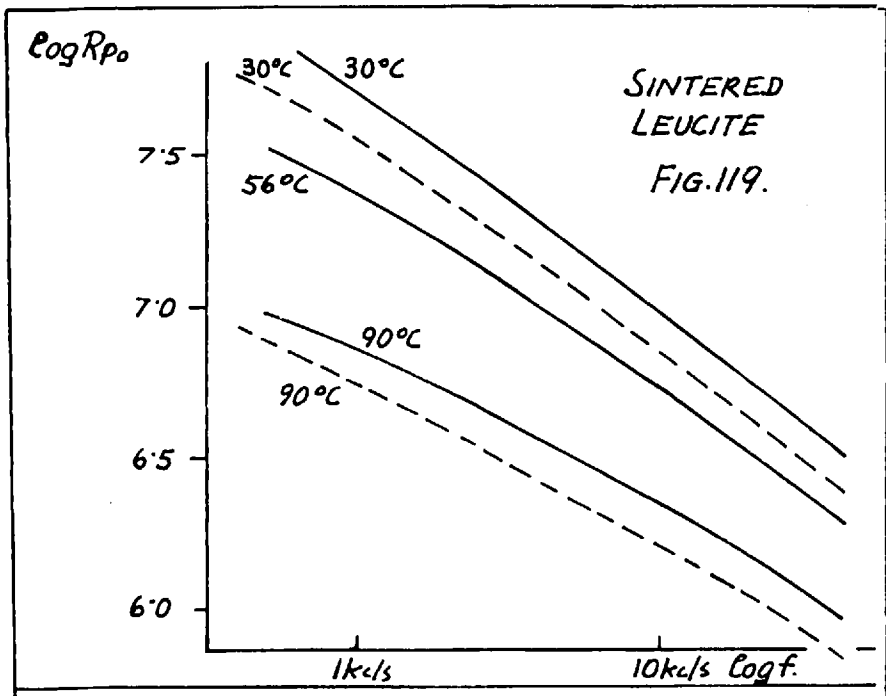
SINTERED LEUCITE

FIG. 116.

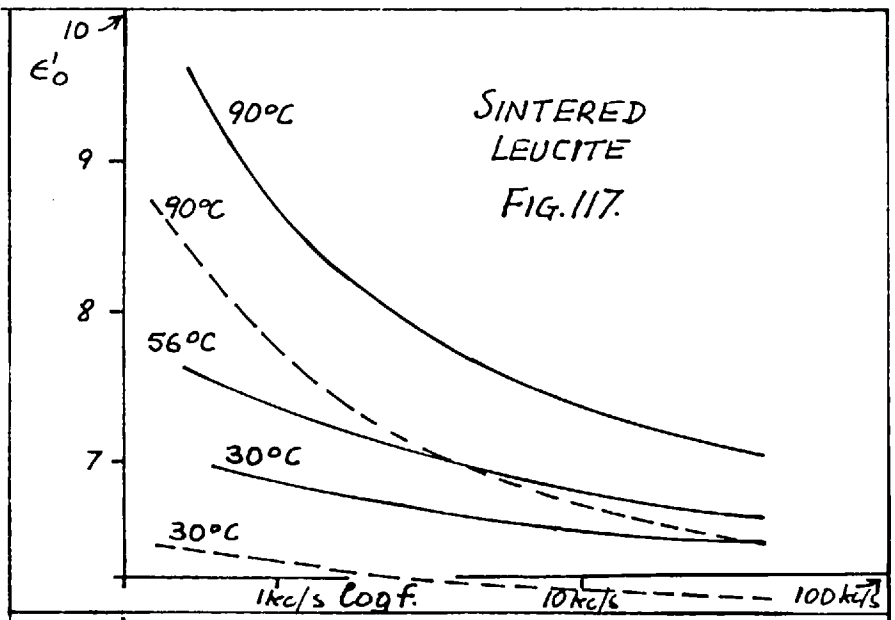


SINTERED LEUCITE

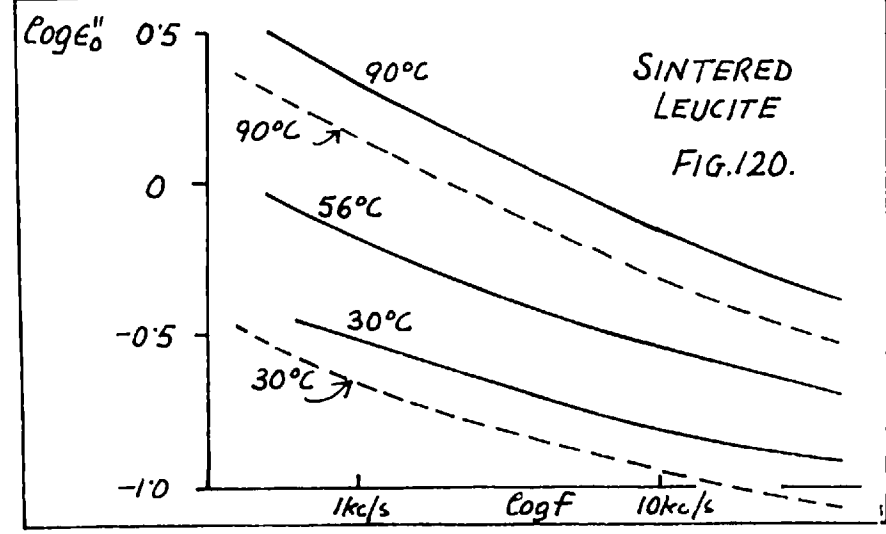
FIG. 114.



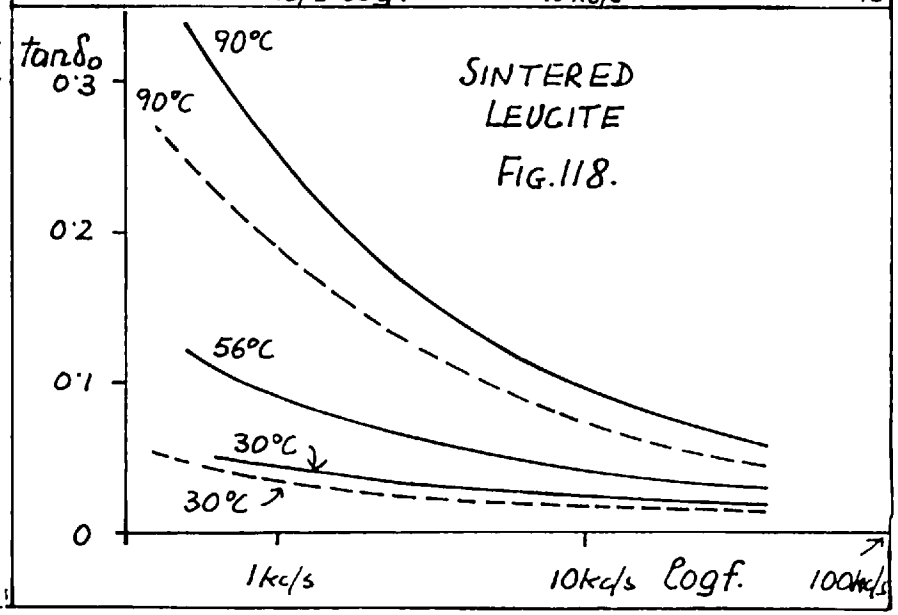
SINTERED LEUCITE
FIG. 119.



SINTERED LEUCITE
FIG. 117.



SINTERED LEUCITE
FIG. 120.



SINTERED LEUCITE
FIG. 118.

8.3. Sintered Leucite.

Measurements cover the frequency range up to 50 kc/s and were made at 30, 56 and 90°C. They are listed in Tables LXIX to LXXIV and are plotted in Figs. 113 to 116. Results of the Böttcher calculations are in Tables 45 to 47 and are plotted in Figs. 117 to 120. Comparison of Figs. 113 to 116 with Figs. 97 to 100 reveals a close similarity to ordinary leucite and thus qualitatively all the remarks made about leucite on pages 198 to 199 also apply to the sintered sample. Since the measurements on the sintered sample were made in the small stainless steel cell, only the real results can be used for quantitative comparison, and these are again qualitatively the same for the two species. Quantitatively ϵ'_o, $\tan\delta_o$ and ϵ''_o of the sintered material at a given frequency and temperature are respectively 10, 30 and 40% higher than those of the ordinary leucite. Figs. 117 to 120 include the results at 30 and 90°C for the latter sample. The comparison clearly shows that the curves are identical, with those of the sintered material moved up the frequency range, indicating a loss peak at a higher frequency than in the ordinary sample. By reference to Table 2 it can be seen that a smaller activation energy must be expected with the sintered sample if there is really such a shift in peak frequency. It seems however possible that the shift of results is due to the peak of sintered leucite being broader than that of the ordinary sample, with the maximum appearing at the same frequency at the same temperature. This would mean that there is a larger distribution of relaxation times in the sintered sample, which is reasonable, since sintering probably results in a material which has a greater disorder in the framework structure. Again this cannot be decided in the absence of the actual relaxation peaks. The activation energies were calculated as for ordinary leucite

Table 45.

Sintered Leucite, ex Run 164 at 30°C.

Frequency	ϵ'_o	$\tan\delta_o$	ϵ''_o	R_{po} meg-Ohm
630 c/s	6.97	0.052	0.362	68.7
2.5 kc/s	6.73	0.035	0.232	27.0
10.0	6.55	0.025	0.164	9.54
40.0	6.48	0.019	0.122	3.22

Table 46.

Sintered Leucite, ex Run 165 at 56°C.

Frequency	ϵ'_o	$\tan\delta_o$	ϵ''_o	R_{po} meg-Ohm
500 c/s	7.62	0.124	0.944	33.2
2.5 kc/s	7.10	0.066	0.467	13.4
10.0	6.82	0.043	0.295	5.31
40.0	6.64	0.030	0.202	1.94

Table 47.

Sintered Leucite, ex Run 166 at 90°C.

Frequency	ϵ'_o	$\tan\delta_o$	ϵ''_o	R_{po} meg-Ohm
500 c/s	9.66	0.337	3.253	9.64
1 kc/s	8.69	0.252	2.188	7.17
2.5	7.99	0.169	1.347	4.66
10.0	7.37	0.096	0.707	2.22
40.0	7.06	0.059	0.419	0.935

and are given in Table 48 and are there compared with the equivalent calculation for the ordinary sample. The same variation with frequency and temperature applies, but as in the ordinary sample results from apparent and real R_p values are very close, as are those of ordinary and sintered leucite.

Table 48.

Sintered Leucite, Activation Energies, kcals/mole.

The sintered leucite results are calculated from the three temperatures of measurement and the ordinary leucite results are taken from Table 43.

A. Results from all temperature combinations averaged.

Frequency	Sintered Leucite ex $R_{p(app)}$	Sintered Leucite ex R_{po}	Ordinary Leucite ex $R_{p(app)}$	Ordinary Leucite ex R_{po}
800 c/s	7.1		6.9	7.0
1.0 kc/s	6.9			
1.3	6.7		7.0	7.1
2.5	6.3	6.4	6.7	6.8
5.0	5.7		6.3	6.4
10.0	5.2	5.3	5.8	5.9
20.0	4.8		5.4	5.5
40.0	4.4	4.5	4.9	5.0

B. Results at a number of frequencies averaged.

Temperature	Interval °C	ex $R_{p(app)}$ at 8 frequencies between 800 c/s and 40 kc/s.	ex R_{po} at 3 frequencies. (2.5, 10 and 40 kc/s).
30 to 90		5.9	5.4
30 to 56		5.0	4.5
56 to 90		6.8	6.2

9. RUBIDIUM ANALCITE.

9.1. Description of Samples.

The original sample was prepared by hydrothermal synthesis in the large autoclave. The 1:1:4 gel of Rb_2O, Al_2O_3,$4SiO_2$ was heated for $2\frac{1}{2}$ days at 278°C in the presence of 30% molar excess rubidium hydroxide[9]. The X-ray powder photograph of the resultant material (Sample 20) shows diffuse lines characteristic of rubidium analcite B, and this together with its refractive index indicates a domain mixture of rubidium analcites B and H with B predominating[17]. The lines were too diffuse for measurement, but appear in exactly the same place as the sharp lines obtained from rubidium analcite B, a sample of which was prepared from the domain mixture by sintering. Thus the 'd' spacings must in general be identical.

Rubidium analcite H could not be obtained from the domain mixture; heating at 870 to 1000°C for 14 days gave no change in X-ray pattern or refractive index. Sintering in an alumina crucible for $2\frac{1}{2}$ days at 1350°C produced a very hard block of material by considerable volume contraction of the powder. The sintered material (sample 20/1350) gave the characteristic X-ray powder pattern of rubidium analcite B, which is compared with the patterns given by Barrer and McCallum[9] in Table 49. The tetragonal unit cell sizes of these samples are compared in Table 50. The differences between the powder X-rays of the rubidium analcite B samples is due to the higher resolution obtainable with the Guinier camera, since X-rays by 9 cm camera are identical. Furthermore 'd' spacings appearing in sample 20/1350 with no counterparts in the other sample, still give the correct unit cell dimensions given in Table 50. This and the electron microscope pictures of the two materials show that the samples contain no gel or other species.

Table 49.

Rubidium Analcite B, Sample 20/1350			Barrer and McCallum (9) Rubidium Analcite B.		Rubidium Analcite H	
d	hkl	I	d	I	d	I
4.79	202	v.v.w.	-	-	5.53	v.w.
-	-	-	-	-	4.03	v.v.w.
3.64	213	m.	3.61	s.	3.63	m.
3.58	321	m.	-	-	-	-
3.44	004	s.	3.40	s.	3.39	v.s.
3.33	104	v.s.	3.31	v.s.	-	-
3.25	410)	v.v.w.	-	-	-	-
3.18	)	and	-	-	-	-
3.17	330)	diffuse	3.16	s.		
2.98	214	m.	2.97	m.	-	-
2.88	323	s.	2.86	v.s.	2.89	s.
2.86	332	m.	-	-	-	-
2.67	314	w.	2.65	s.	2.65	v.w.
2.43	521	v.w.	-	-	2.51	m.w.
2.39	404	m.s.	2.38	s.	2.39	m.
2.36	414	w.	-	-	-	-
-	-	-	2.29	v.v.w.	-	-
2.21	325	v.w.	2.25	v.w.	-	-
2.168	206	m.	2.168	s.	2.197	w.
-	-	-	2.108	v.v.w.	-	-
2.016	622	v.v.w.	-	-	1.999	v.w.
1.975	613	v.v.w.	1.968	m.	-	-
1.964	007	v.v.w.	-	-	1.962	v.v.w.
1.942	326	w.	-	-	-	-
1.892	406	v.v.w.	-	-	-	-
1.869	207	v.v.w.	-	-	-	-
1.850	-	v.v.w.	1.855	w.	-	-
1.818	227	w.	1.815	m.	1.828	w.
1.736	327	w.	1.733	w.	-	-
1.723	-	v.v.w.	-	-	1.702	m.w.
1.696	-	m.	1.695	m.	1.695	v.v.w.
1.664	-	v.v.w.	1.658	v.w.	-	-
1.617	-	w.	1.616	m.w.	-	-

Note: (1) X-rays of sample 20/1350 were taken by Guinier camera and those of other samples by 9 cm camera.

(2) The X-ray of sample 20/1350 by 9 cm camera is identical to that of samples ex Barrer and McCallum.

(3) The 'd' spacings not appearing on the comparison samples (f.i. 4.79, 3.58, 2.86, 2.43, 2.36, 2.016, 1.964) give identical results to the 'd' spacings appearing in all samples when used to calculate the tetragonal unit cell sizes. Most of these 'd' spacings belong to "twinned" lines which appear in tetragonal samples with similar a and c dimensions (leucite and rubidium analcite). These twins are resolved by the Guinier camera but not by the 9 cm camera.

Table 50.

Sample	a, Å(Angstrom)	c, Å
Rubidium analcite B, sample 20/1350	13.34	13.77
Barrer and McCallum, sample B	13.2	13.6
Barrer and McCallum, sample H	13.64	13.32

The densities, refractive indices determined by sodium light, the electronic contributions to the dielectric constant, the packing fractions and the maximum particle sizes of the samples are given in Table 51. The refractive index value of the domain mixture again emphasises the predominance of species B[17]. The density of the domain mixture taken by gravity bottle was so close to the value obtained for species B by calculation from X-rays, that in view of the greater accuracy of the latter method and the large predominance of species B in the domain mixture the X-ray density value could be used for both samples.

Table 51.

Physical Properties of Rubidium Analcite Samples.

Rubidium Analcite Sample	Density gm/cm^3	Refractive Index	ϵ' electronic	Packing Fraction	Maximum Particle size, cm.
Domain Mixture	2.866	1.506	2.27	0.278	2.25×10^{-4}
Species 'B'	2.866	1.522	2.32	0.372	2.4×10^{-4}

The particles of the domainmixture are spherical, while those of species 'B' are of irregular outline still approximating to spheres. All measurements were made in the large stainless steel cell. Even with the largest crystallites the crystal diameter-cell volume proportion is thus only

slightly larger than the proportion used by van Vessem for the sodium chloride measurements, while for the bulk of the crystallites this proportion is less than that used by van Vessem. Thus calculations by Böttcher's equation can be relied upon.

The domain mixture contains 1.51% water and species (B' 0.15%. For dielectric measurements the samples were dehydrated by heating for 2½ days at 170°C in the high vacuum apparatus.

9.2. Rubidium Analcite, Domain Mixture.

The results of dielectric measurements at 30, 60 and 90°C are given in Tables LXXV to LXXX. Tables LXXXI to LXXXVI represent the repeat runs at these temperatures and the results at 105, 75 and 45°C at a number of selected frequencies. Tanδ values in the 74 to 122 kc/s region were non-reproducible and high. A similar effect was obtained at these frequencies with caesium analcite. This was due to outside interference, which is always critical when measuring very small tanδ values on a loosely coupled resonance circuit. The cause of the interference could not be determined. Figures 121 to 123 are the plots of $\tan\delta_{app}$, $\log(R_{p(app)})$ and $\log\epsilon''_{app}$ against frequency and Figures 124 and 125 of $\tan\delta_{app}$ and $\log(R_{p(app)})$ against temperature.

The ϵ'_{app} results show so little change with frequency or temperature that plotting is fruitless. The ϵ'_{app} values from the bridge measurements are more accurate and are taken as representative. Their averages are 1.88 at 30°C, 1.89 at 60°C and 1.90 at 90°C. Since this apparent temperature variation is within the repeatability of the measurements (page 107), 1.89 is taken as the correct temperature and frequency independent value of the apparent dielectric constant. The increase of the tanδ values which occurs at the very high frequency end has also been noticed

with anhydrous basic sodalite (page 148) and is due to the influence of induction effects above 2.07 mc/s, when using an outside circuit with the conventional resonance apparatus. For the same reason the $\log(R_{p(app)})$ and $\log\epsilon''_{app}$ results show deviations above 2.07 mc/s. In the 30 and 60°C curves of Fig. 121 ($\tan\delta_{app}$) the best straight line has been used for results between 63 kc/s and 3.22 and 2.54 mc/s respectively. The 50 kc/s results are often out of line. This was noticed with all measurements of low $\tan\delta$ samples and is due to oscillator inaccuracy at its maximum working frequency.

The results of the Böttcher calculations are given in Tables 52 to 60.

Table 52.

Rubidium Analcite, Domain Mixture, ex Run 105 at 30°C.

Frequency	ϵ'_o	$\tan\delta_o$	R_{po} meg-Ω	ϵ''_o
1.3 kc/s	7.12	0.0055	159	0.0392
2.5	7.12	0.0052	87.8	0.0370
3.2	7.12	0.0049	72.7	0.0349
5.0	7.12	0.0045	50.3	0.0323
6.3	7.12	0.0045	40.5	0.0318
10.0	7.12	0.0042	27.2	0.0299
20.0	7.12	0.0038	15.0	0.0271
32.0	7.12	0.0037	9.65	0.0263
40.0	7.12	0.0037	7.72	0.0263

Table 53.

Rubidium Analcite, Domain Mixture, ex Run 106 at 30°C.

The best straight line between 63 kc/s and 3.22 mc/s.

Frequency	ϵ'_o	$\tan\delta_o$	R_{po} meg-Ω	ϵ''_o
179 kc/s	7.19	0.0032	1.97	0.0230
1.43 mc/s	7.33	0.0016	0.494	0.0115

Table 54.

Rubidium Analcite, Domain Mixture, ex Run 107 at 60°C.

Frequency	ϵ'_o	$\tan\delta_o$	R_{po} meg-Ω	ϵ''_o
1.3 kc/s	7.25	0.0100	86.2	0.0725
2.5	7.25	0.0085	52.7	0.0616
5.0	7.20	0.0075	30.1	0.0540
6.3	7.20	0.0071	25.2	0.0511
10.0	7.20	0.0065	17.4	0.0468
20.0	7.20	0.0057	9.90	0.0410
32.0	7.20	0.0054	6.53	0.0389
40.0	7.20	0.0053	5.31	0.0382

Table 55.

Rubidium Analcite, Domain Mixture, ex Run 108 at 60°C.

The best straight line between 63 kc/s and 2.54 mc/s.

Frequency	ϵ'_o	$\tan\delta_o$	R_{po} meg-Ω	ϵ''_o
217 kc/s	7.25	0.0044	1.17	0.0319
1.22 mc/s	7.35	0.0036	0.251	0.0265

Table 56.

Rubidium Analcite, Domain Mixture, ex Run 109 at 90°C.

Frequency	ϵ'_o	$\tan\delta_o$	R_{po} meg-Ω	ϵ''_o
1.3 kc/s	7.34	0.0184	46.2	0.1351
2.5	7.31	0.0154	28.9	0.1126
5.0	7.25	0.0129	17.4	0.0935
10.0	7.25	0.0107	10.5	0.0776
20.0	7.25	0.0090	6.22	0.0653
40.0	7.20	0.0081	3.48	0.0583

Table 57.

Rubidium Analcite, Domain Mixture, ex Run 110 at 90°C.

The best straight line between 63 kc/s and 2.07 mc/s.

Frequency	ϵ'_o	$\tan\delta_o$	R_{po} meg-Ω	ϵ''_o
164 kc/s	7.48	0.0060	1.10	0.0449
1.02 mc/s	7.61	0.0044	0.238	0.0335

Table 58.

Rubidium Analcite, Domain Mixture, ex Run 111 at 105°C.

Frequency	ϵ'_o	$\tan\delta_o$	R_{po} meg-Ω	ϵ''_o
1.3 kc/s	7.57	0.0270	30.6	0.2044
2.5	7.51	0.0216	20.0	0.1622
5.0	7.46	0.0171	12.7	0.1276
10.0	7.40	0.0139	7.89	0.1029
20.0	7.29	0.0116	4.80	0.0846
40.0	7.25	0.0102	2.74	0.0740

Table 59.

Rubidium Analcite, Domain Mixture, ex Run 113 at 75°C.

Frequency	ϵ'_o	$\tan\delta_o$	R_{po} meg-Ω	ϵ''_o
1.3 kc/s	7.29	0.0138	62.1	0.1006
2.5	7.25	0.0111	40.3	0.0805
5.0	7.29	0.0094	23.7	0.0685
10.0	7.18	0.0081	14.0	0.0582
20.0	7.18	0.0070	8.07	0.0503
40.0	7.23	0.0064	4.38	0.0463

Table 60.

Rubidium Analcite, Domain Mixture, ex Run 115 at 45°C.

Frequency	ϵ'_o	$\tan\delta_o$	R_{po} meg-Ω	ϵ''_o
1.3 kc/s	7.25	0.0075	115	0.0544
2.5	7.25	0.0067	66.8	0.0486
5.0	7.20	0.0058	39.0	0.0418
10.0	7.18	0.0051	22.2	0.0366
20.0	7.09	0.0046	12.5	0.0326
40.0	7.09	0.0044	6.51	0.0312

The value of the real dielectric constant is 7.20, calculated from the temperature and frequency independent value of 1.89 (see pages 213 to 214). Figures 126 to 128 are the plots of $\tan\delta_o$, $\log(R_{po})$ and $\log(\epsilon''_o)$ against frequency.

The results reveal that the sample is a much better insulator than anhydrous basic sodalite, although not being outstanding in this respect. The $\log\epsilon''$ curves show that d.c. conductivity is quite negligible. The change of the $\tan\delta$ values at the low frequencies of the

higher temperature curves suggests the onset of interfacial polarisation of relaxation effects, but the actual tanδ values are smaller by a factor of 10 (compare Fig. 106 with 126) than in the case of leucite where the latter explanation is probably correct. However the relative frequency variations of the tanδ values of leucite and of the domain mixture of rubidium analcite are the same. According to Table 2 and Beattie's cation activation energy result of 18 kcal/mole (page 89), the cation relaxation peak of the domain mixture of rubidium analcite would be expected at 0.1 c/s. Comparison with leucite, where this peak is expected at 1 c/s, would explain both the frequency dependance and smaller value of the tanδ results of the domain mixture of rubidium analcite, if the explanation of the frequency dependance of the domain mixture results is really a low frequency relaxation peak due to the cations. However the ϵ' results indicate no effect with frequency, such as noticeable with the leucite samples and consideration of the rubidium analcite B results (see later) suggests that a different phenomenon is the cause of the indicated relaxation peak.

Activation energies calculated from the R_p values are given in Table 61. These were calculated in the same manner as for leucite (page 199). The activation energies are smaller than those of leucite, but decrease in the same manner both with temperature decrease and frequency increase. Results from $R_{p(app)}$ and R_{po} are in good agreement. The results fit in well with the relaxation effect explanation given earlier and thus the activation energies can be explained in the same way as for leucite (pages 198 and 199). Since measurements are farther away from the relaxation peak in case of the domain mixture of rubidium analcite, activation energies would be expected to be smaller than with leucite and this is found. However,

Table 61.

Rubidium Analcite, Domain Mixture.
Activation Energies, kcal/mole.

A. Results from all temperature combinations averaged.

Frequency		ex $R_{p(app)}$	ex R_{po}	Frequency		ex $R_{p(app)}$	ex R_{po}
1.0 kc/s	(1)	5.0	-	32.0 kc/s	(1)	3.0	-
1.3	(2)	4.9	5.0	40.0	(2)	3.1	3.2
1.6	(1)	4.5	-	50.0	(1)	2.6	-
2.0	(1)	4.2	-	63.0	(1)	3.0	-
2.5	(2)	4.4	4.5	151.0	(1)	2.1	-
3.2	(1)	4.0	-	216.0	(1)	2.0	-
4.0	(1)	3.8	-	256.0	(1)	2.1	-
5.0	(2)	4.1	4.2	313.0	(1)	1.6	-
6.3	(1)	3.7	-	417.0	(1)	1.5	
8.0	(1)	3.5	-	509.0	(1)	1.9	-
10.0	(2)	3.8	3.8	770.0	(1)	1.7	-
13.0	(1)	3.4	-	890	(1)	1.8	-
16.0	(1)	3.4	-	1.1 mc/s	(1)	1.5	-
20.0	(2)	3.5	3.5	1.32	(1)	1.6	-
25.0	(1)	2.9	-				

(1) Only results at 3 temperatures were available and used.
(2) Results at 6 temperatures were used.

B. Results at 6 frequencies (1.3,2.5,5.0,10, 20 and 40 kc/s) averaged.

Temperature Interval, °C	ex $R_{p(app)}$	ex R_{po}
30 - 45	3.0	3.0
45 - 60	3.3	3.4
60 - 75	3.6	3.7
75 - 90	4.8	4.8
90 - 105	5.4	5.7

as already mentioned, another explanation for both the cause of the relaxation peak and the activation energies is given in the discussion of the rubidium analcite B results.

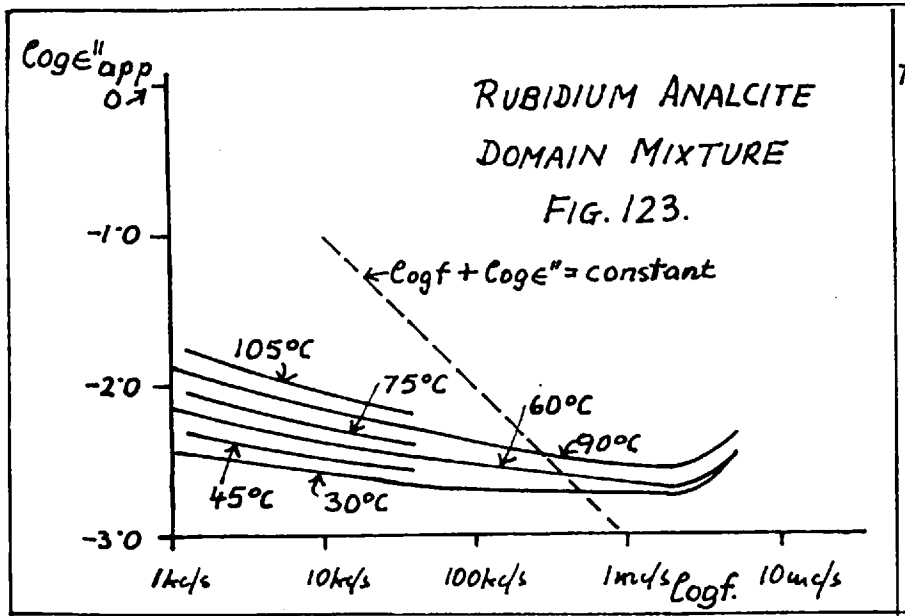
Since permittivity is constant, the region of measurement is independent of ionic relaxation which must occur at much lower frequencies and of the region of atomic resonance absorption at higher frequencies. The contributions to the permittivity of the various polarisations are therefore as follows:

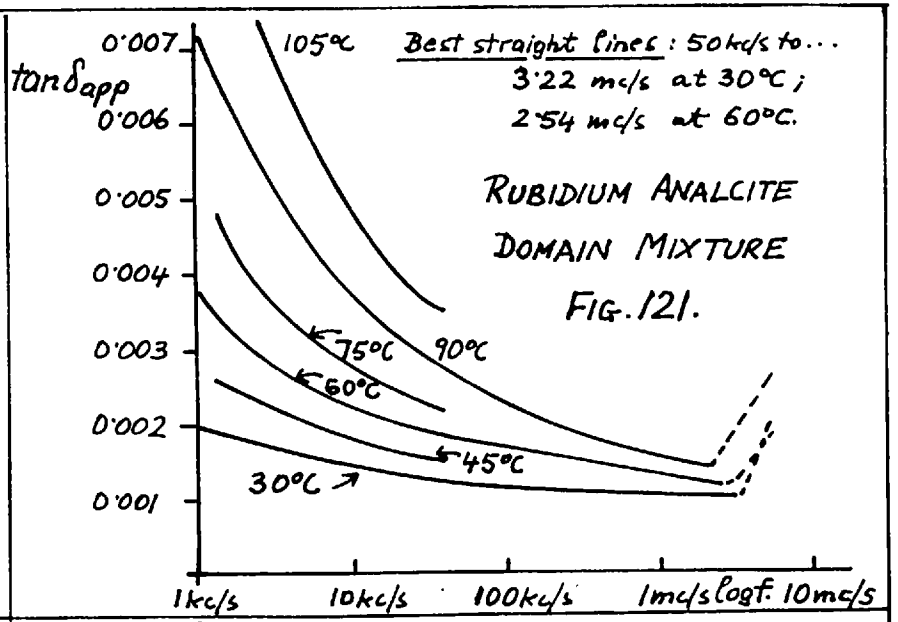
ϵ'_o due to the total polarisability	7.20
ϵ'_o due to electron polarisation	2.27
ϵ'_o due to atomic polarisation	4.93.

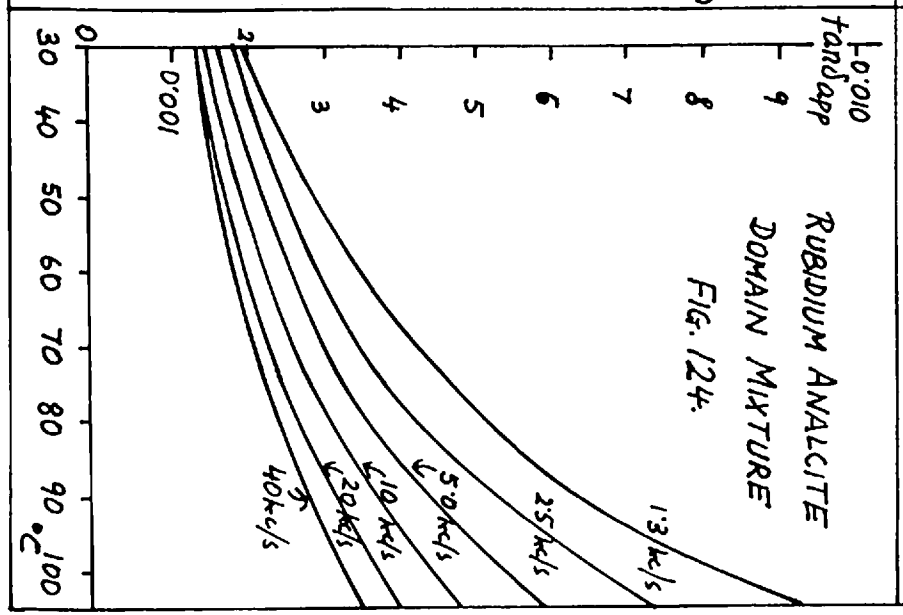
9.3. Rubidium Analcite B.

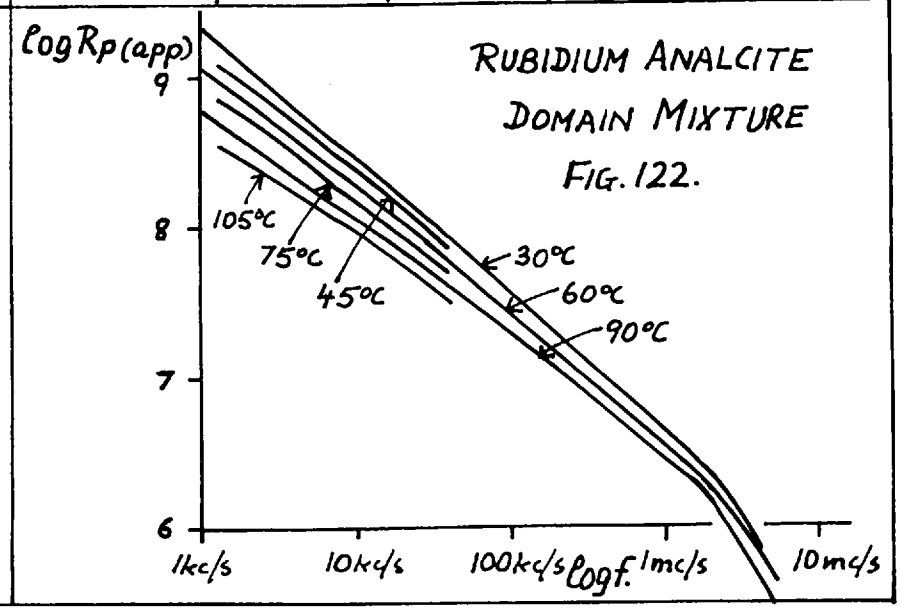
Results of measurements at 30, 60 and 90°C are given in Appendix Tables LXXXVII to XCIV. The variation with frequency and temperature of the apparent and real results is too small to allow comparative plotting. The $\tan\delta_{app}$ values obtained are of the order of repeatability and sensitivity of the apparatus (0.0001 for the bridge and 0.0002 for the Hartshorn-Ward apparatus) and therefore the resistance results are in themselves quite inaccurate without however causing an equivalent inaccuracy of $\tan\delta$ values. Thus activation energies cannot be calculated. However the minuteness of the $\tan\delta$ values indicates that no process causing dielectric loss occurs.

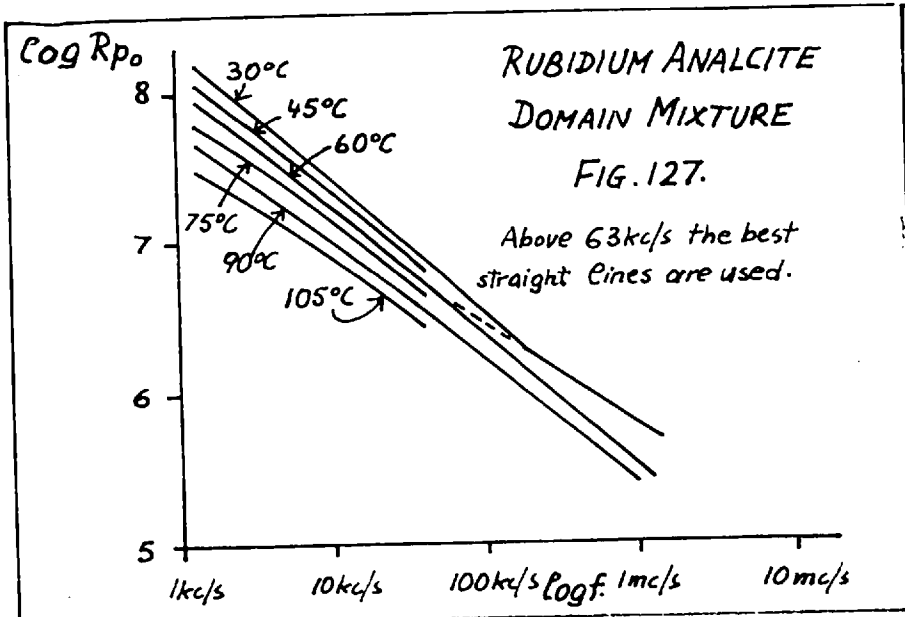
The remarks made about the $\tan\delta_{app}$ values are of importance when considering the real results, calculated by Böttcher's equation and given in Tables 62 to 67. Since the sensitivity of the apparatus and repeatability of $\tan\delta_{app}$ results are the same as the value of the results in most instances, there may be large percentage errors, which will be multiplied by the Böttcher equation. In all cases the correct


Log ε'' app
0
-1·0
-2·0
-3·0
RUBIDIUM ANALCITE
DOMAIN MIXTURE
FIG. 123.
← Log f + Log ε'' = constant
105°C
75°C
60°C
90°C
45°C
30°C
1kc/s
10kc/s
100kc/s
1mc/s
Log f.
10mc/s


tan δ app
0·007
0·006
0·005
0·004
0·003
0·002
0·001
105°C
Best straight lines: 50kc/s to...
3·22 mc/s at 30°C;
2·54 mc/s at 60°C.
RUBIDIUM ANALCITE
DOMAIN MIXTURE
FIG. 121.
75°C
90°C
60°C
45°C
30°C
1kc/s
10kc/s
100kc/s
1mc/s
Log f.
10mc/s

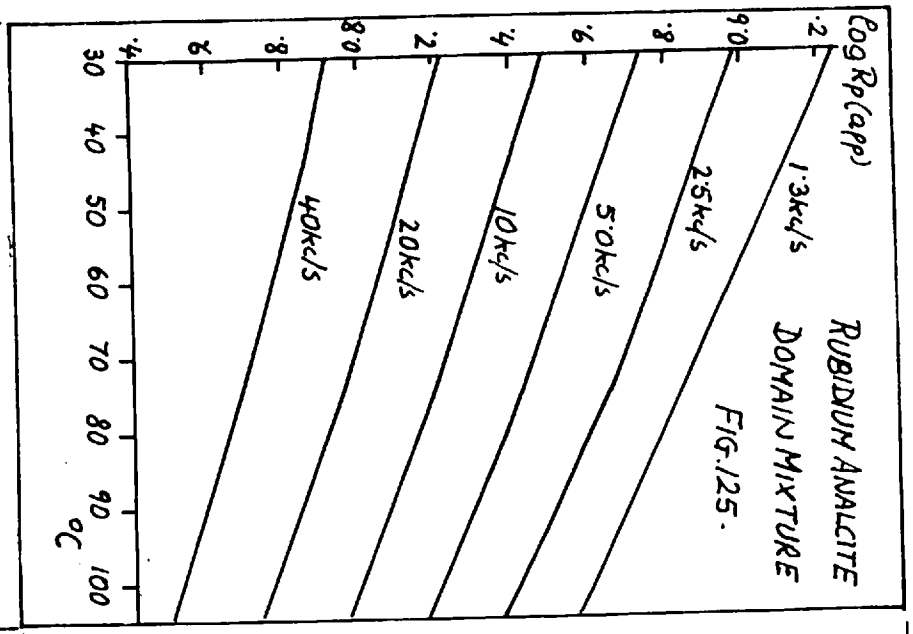

0
2
tan δ app
0·001
0·010
3
4
5
6
7
8
9
30
40
50
60
70
80
90
°C
100
RUBIDIUM ANALCITE
DOMAIN MIXTURE
FIG. 124.
40kc/s
20kc/s
10 kc/s
5·0kc/s
2·5kc/s
1·3kc/s


Log Rp (app)
9
8
7
6
RUBIDIUM ANALCITE
DOMAIN MIXTURE
FIG. 122.
105°C
75°C
45°C
30°C
60°C
90°C
1kc/s
10kc/s
100kc/s
Log f.
1mc/s
10mc/s

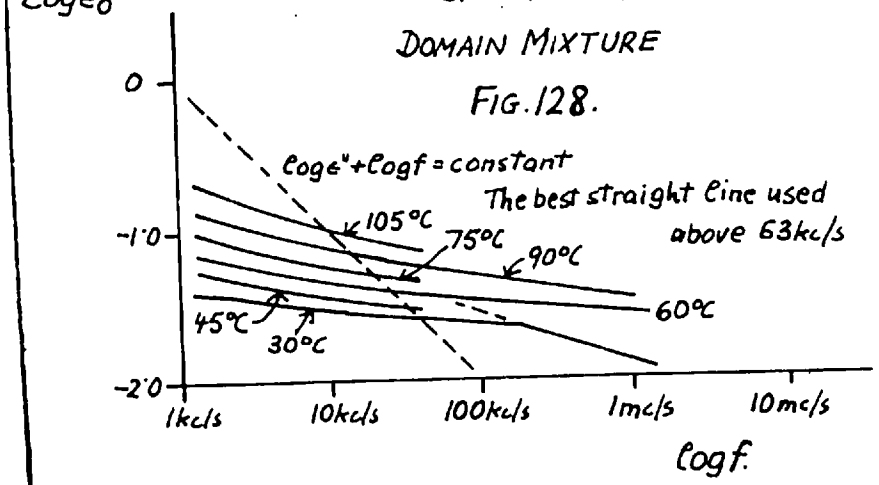


RUBIDIUM ANALCITE
DOMAIN MIXTURE
FIG. 127.

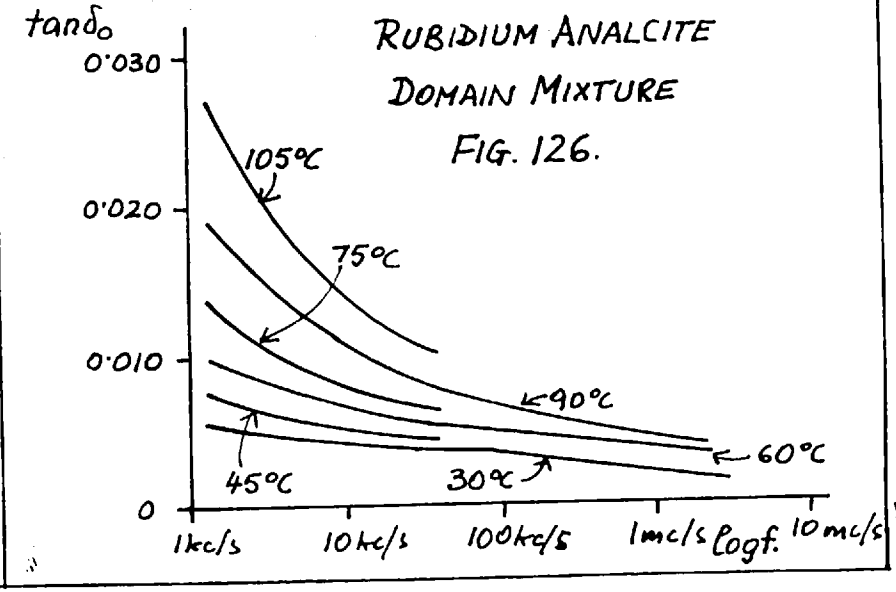
Above 63kc/s the best straight lines are used.



RUBIDIUM ANALCITE
DOMAIN MIXTURE
FIG. 125.



RUBIDIUM ANALCITE
DOMAIN MIXTURE
FIG. 128.



RUBIDIUM ANALCITE
DOMAIN MIXTURE
FIG. 126.

Table 62.

Rubidium Analcite B, ex Run 121 at 30°C.

Frequency	ϵ'_{app}	$\tan\delta_{app}$	ϵ''_{app}	ϵ'_o	$\tan\delta_o$	ϵ''_o
ϵ' between 1 and 50 kc/s, $\tan\delta$ 5 to 50 kc/s.	2.207	0.00010	0.00022	6.20	0.0002	0.0012

Table 63.

Rubidium Analcite B, ex Run 122 at 30°C.

Best straight line between 63 kc/s and 3.22 mc/s, using only the points at which $\tan\delta$ results were obtained.

Frequency	ϵ'_{app}	$\tan\delta_{app}$	ϵ''_{app}	ϵ'_o	$\tan\delta_o$	ϵ''_o
288 kc/s	2.219	0.00028	0.00062	6.27	0.0006	0.0036
1.56 mc/s	2.234	0.00036	0.00080	6.36	0.0007	0.0046

Table 64.

Rubidium Analcite B, ex Run 123 at 60°C.

Frequency	ϵ'_{app}	$\tan\delta_{app}$	ϵ''_{app}	ϵ'_o	$\tan\delta_o$	ϵ''_o
$\tan\delta$ between 6.3 and 50 kc/s, ϵ' between 1 and 50 kc/s	2.217	0.00008	0.00018	6.26	0.0002	0.0011

Table 65.

Rubidium Analcite B, ex Run 124 at 60°C.

Best straight line between 151 kc/s and 3.22 mc/s, using only the points at which $\tan\delta$ results were obtained.

Frequency	ϵ'_{app}	$\tan\delta_{app}$	ϵ''_{app}	ϵ'_o	$\tan\delta_o$	ϵ''_o
287 kc/s	2.233	0.00031	0.00069	6.35	0.0006	0.0040
1.71 mc/s	2.250	0.00042	0.00095	6.45	0.0009	0.0055

Table 66.

Rubidium Analcite B, ex Run 125 at 90°C.

Frequency	ϵ'_{app}	$\tan\delta_{app}$	ϵ''_{app}	ϵ'_o	$\tan\delta_o$	ϵ''_o
1-2 kc/s	2.222	-	-	6.29	-	-
2.5	2.222	0.00043	0.00096	6.29	0.00088	0.0055
3.2	2.222	0.00039	0.00087	6.29	0.00080	0.0050
4.0	2.222	0.00037	0.00082	6.29	0.00075	0.0047
5.0	2.222	0.00035	0.00078	6.29	0.00072	0.0045
6.3	2.222	0.00034	0.00076	6.29	0.00070	0.0044
8.0	2.222	0.00031	0.00069	6.29	0.00063	0.0040
10.0	2.222	0.00027	0.00060	6.29	0.00055	0.0036
13.0	2.222	0.00026	0.00058	6.29	0.00053	0.0033
16.0	2.222	0.00023	0.00051	6.29	0.00047	0.0030
20.0	2.222	0.00024	0.00053	6.29	0.00049	0.0031
25.0	2.222	0.00022	0.00049	6.29	0.00045	0.0028
32.0	2.222	0.00023	0.00051	6.29	0.00047	0.0030
40.0	2.222	0.00019	0.00042	6.29	0.00039	0.0025
50.0	2.222	0.00020	0.00044	6.29	0.00040	0.0025

Table 67.

Rubidium Analcite B, ex Run 126 at 90°C.

Best straight line using 63 kc/s and between 151 kc/s and 3.22 mc/s.

Frequency	ϵ'_{app}	$\tan\delta_{app}$	ϵ''_{app}	ϵ'_o	$\tan\delta_o$	ϵ''_o
231 kc/s	2.242	0.00029	0.00065	6.41	0.00059	0.0038
1.56 mc/s	2.258	0.00052	0.00117	6.50	0.00105	0.0068

apparent tanδ and ϵ'' results are probably much smaller than shown (see bracket values in Tables LXXVII to XCIV) and thus the Böttcher equation gives the possible maximum tanδ_o and ϵ''_o values. To obtain the exact values, measurements on a compressed sample with specially designed apparatus are required.

This sample is an excellent insulator. The constant ϵ'_o value is 6.25 (average at the three temperatures below 50 kc/s), which is due to the total polarisability. Therefore splitting the permittivity gives:

ϵ'_o due to the total polarisability	6.25
ϵ'_o due to the electronic polarisation	2.32
ϵ'_o due to the atomic polarisation	3.93.

The difference between the results obtained with the domain mixture and species B is curious. Since the former consists mainly of domains of type B, little difference can be expected unless domain changes take place under a.c. stress. This cannot happen since the domain change involves a change of the framework structure. The framework is rigid (see Tables 49 and 50) and would not be expected to change under the electrical conditions involved. If the domain mixture results indicate cation relaxation at much lower frequencies with accompanying dielectric loss at the higher frequencies due to varying equilibrium positions of the cations as in leucite, then the same effect would occur in rubidium analcite B. That this is not so indicates that a different process is responsible for the results obtained with the domain mixture. It is therefore suggested than on sintering terminal OH bonds are driven off. This OH loss gives the sample better insulating properties. In the domain mixture the dielectric loss is due to the OH substituents which show a relaxation peak at a lower frequency than that of measurements. The activation energy too can then be explained as a function of the OH substituents, which are also responsible

for a permittivity contribution of $\epsilon'_o = 1.00$ to the permittivity contribution of the atomic polarisation. No such loss occurs in species B. The OH substituent effect is of a much lesser order of magnitude than cation relaxation effects. The same mechanism probably also takes place in ordinary leucite, but cannot be detected due to the larger and screening effect of cation relaxation at the lower frequencies. In rubidium analcite the relaxation peak occurs at a much lower frequency than in leucite and can therefore not be detected, nor cause, at the frequencies of measurement, the screening of the dielectric loss due to the OH-substituents in the domain mixture. The explanation of the dielectric properties of the rubidium analcite samples by the OH substitution effect cannot be proved, but it is the only explanation which fits all the experimental and known facts.

10. POLLUCITE.

10.1. Description of Sample.

The caesium analcite, pollucite was prepared by hydrothermal synthesis in the large autoclave. The resultant material will be called ordinary pollucite to distinguish it from the sintered material. The 1:1:4 gel of $Cs_2O, Al_2O_3, 4SiO_2$ was heated for $1\frac{1}{2}$ days at 280°C in the presence of 20% molar excess caesium hydroxide[9]. The sintered sample was produced by sintering ordinary pollucite at 1350°C for 2 days. This was accompanied by considerable volume contraction. The d-spacings of the powder X-rays and the cubic unit cell sizes of the two samples are compared with those of pollucite prepared hydrothermally by Barrer and McCallum[9] in Table 68, which reveals that no crystalline change occurred on sintering. The X-rays and electron microscope pictures also show that there is no gel or other impurity. The densities, refractive indices determined by sodium light, electronic contributions to the dielectric constant, packing fractions, particle sizes and water contents of the samples are given in Table 69.

The particles of ordinary pollucite are spherical, those of the sintered material are irregular spheres. The particle dimensions are such that the Böttcher equation will give reliable results. Before measurements, the samples were dehydrated by heating in the high vacuum apparatus for $2\frac{1}{2}$ days at 170°C. Measurements on ordinary pollucite were made in the large and those on the sintered material in the small stainless steel cell.

Table 68.

Ordinary pollucite			Sintered pollucite			Pollucite of Barrer and McCallum (9)		
d	I	hkl	d	I	hkl	d	I	hkl
5.61	v.w.	112	5.59	w.	211	5.64	w.	
3.67	s.	312	3.66	s.	312	3.65	s.	
3.43	v.s.	400	3.43	v.s.	400	3.43	v.s.	
3.05	v.v.w.	402	3.06	v.w.	402	3.05	v.w.	
2.93	s.	332	2.92	s.	332	2.91	s.	
2.68	v.v.w.	510	2.69	v.w.	431	2.68	v.w.	
2.50	w.	521	2.50	m.	521	2.49	m.	
2.42	m.	440	2.42	s.	440	2.41	s.	
2.225	m.	532	2.221	m.-s.	532	2.219	s.	
2.019	v.w.	631	2.018	w.	631	2.013	m.w.	
1.970	v.v.w.	444	1.995	v.w.	-	1.976	w.	
1.865	m.	721	1.861	m.-s.	721	1.862	s.	
1.742	m.	732	1.738	m.-s.	732	1.737	s.	
1.705	v.v.w.	-	1.710	w.	-	1.710	v.w.	
-	-	-	1.684	v.v.w.	-	1.681	v.v.w.	
-	-	-	-	-	-	1.659	v.v.w.	
1.634	v.v.w.	-	1.634	w.	-	1.634	v.w.	
-	-	-	1.590	v.v.w.	-	1.591	v.w.	
1.545	v.v.w.	-	1.547	w.	-	1.550	w.	
1.525	v.w.	-	-	-	-	1.529	m.w.	
1.473	v.v.w.	-	-	-	-	1.475	w.	
1.410	v.w.	-	-	-	-	1.411	w.	
-	-	-	-	-	-	1.396	v.w.	
1.355	v.w.	-	-	-	-	1.354	m.w.	
1.302	w.	-	-	-	-	1.305	m.	

The cubic unit cell sizes are:-

a = 13.71 Å, a = 13.69 Å, a = 13.7 Å.

Table 69.

Sample	Density gms/cm^3	Refractive Index	Water Content %	ϵ' electronic	Packing Fraction	Max. Particle Size cm.
Ordinary Pollucite	3.216	1.525	1.09	2.33	0.234	2.6×10^{-5}
Sintered Pollucite	3.230	1.525	0.13	2.33	0.454	1.3×10^{-4}

10.2. Ordinary Pollucite.

Dielectric measurements were made at 30, 60 and 90°C and are given in Tables XCV to C, and the check runs and measurements at a number of selected frequencies at 45, 75 and 105°C in Tables CI to CVI. The $\tan\delta$ and R_p values in the 101 to 216 kc/s region show the same interference effect as in the domain mixture of rubidium analcite (see p. 213). These values are neglected in all calculations, although shown in the tables. The neglected values are: 122 kc/s at 30°C, 101 and 122 kc/s at 60°C and 151 and 216 kc/s at 90°C.

The ϵ'_{app} values show little variation with frequency and temperature and therefore cannot conveniently be plotted. As with rubidium analcite the temperature and frequency independent value can be taken from the more accurate bridge results; it is 1.705. $\tan\delta_{app}$, $\log(R_{p(app)})$ and $\log \epsilon''_{app}$ are plotted against frequency in Figures 129 to 131; in the $\tan\delta$ curves the best straight line is used between 63 kc/s and 3.22 mc/s at 30°C, between 63 kc/s and 2.54 mc/s at 60°C and between 256 kc/s and 2.54 mc/s at 90°C. Above that, the usual deviation due to induction effects occurs and this is also reflected in the $\log(R_{p(app)})$ and $\log\epsilon''_{app}$ curves. The real results calculated by

Böttcher's equation are given in Tables 70 to 78 and plotted in Figures 132 to 134. Figures 135 to 138 are the temperature plots of the R_p and tanδ results.

Table 70.

Ordinary Pollucite, ex Run 93 at 30°C.

Frequency	ϵ'_{app}	tanδ_{app}	ϵ''_{app}	ϵ'_o	tanδ_o	ϵ''_o	R_{po}, meg-Ω
1.3 kc/s	1.707	0.0020	0.0034	7.35	0.0073	0.054	116
2.5	1.704	0.0018	0.0031	7.30	0.0066	0.048	67.7
5.0	1.702	0.0017	0.0029	7.28	0.0062	0.045	36.1
10.0	1.702	0.0015	0.0026	7.28	0.0056	0.041	19.8
16.0	1.702	0.0014	0.0024	7.28	0.0051	0.037	13.7
20.0	1.702	0.0014	0.0024	7.28	0.0051	0.037	11.0
40.0	1.702	0.0013	0.0022	7.28	0.0047	0.034	5.97

Table 71.

Ordinary Pollucite, ex Run 94 at 30°C.

Best straight line between 63 kc/s and 3.22 mc/s.

Frequency	ϵ'_{app}	tanδ_{app}	ϵ''_{app}	ϵ'_o	tanδ_o	ϵ''_o	R_{po}, meg-Ω
163 kc/s	1.690	0.00115	0.00194	7.09	0.0042	0.030	1.66
1.45 mc/s	1.687	0.00109	0.00184	7.04	0.0040	0.028	0.200

Table 72.

Ordinary Pollucite ex Run 95 at 60°C.

Frequency	ϵ'_{app}	$\tan\delta_{app}$	ϵ''_{app}	ϵ'_o	$\tan\delta_o$	ϵ''_o	R_{po} meg-Ω
1.3 kc/s	1.712	0.0034	0.0058	7.43	0.0124	0.092	67.9
2.5	1.709	0.0029	0.0050	7.38	0.0107	0.079	41.1
5.0	1.707	0.0025	0.0043	7.35	0.0092	0.068	23.9
10.0	1.705	0.0022	0.0038	7.32	0.0081	0.059	13.8
20.0	1.704	0.0019	0.0032	7.30	0.0068	0.050	8.12
40.0	1.704	0.0018	0.0031	7.30	0.0066	0.048	4.23

Table 73.

Ordinary Pollucite, ex Run 96 at 60°C.

Best straight line between 63 kc/s and 2.54 mc/s.

Frequency	ϵ'_{app}	$\tan\delta_{app}$	ϵ''_{app}	ϵ'_o	$\tan\delta_o$	ϵ''_o	R_{po} meg-Ω
151 kc/s	1.696	0.00156	0.00265	7.18	0.0057	0.041	1.31
1.20 mc/s	1.701	0.00133	0.00226	7.26	0.0049	0.036	0.188

Table 74.

Ordinary Pollucite, ex Run 97 at 90°C.

Frequency	ϵ'_{app}	$\tan\delta_{app}$	ϵ''_{app}	ϵ'_o	$\tan\delta_o$	ϵ''_o	R_{po} meg-Ω
1.3 kc/s	1.714	0.0062	0.0106	7.46	0.0226	0.169	37.0
2.5	1.709	0.0050	0.0085	7.38	0.0182	0.134	24.2
5.0	1.707	0.0042	0.0072	7.35	0.0154	0.113	14.3
10.0	1.704	0.0035	0.0060	7.30	0.0128	0.0934	8.70
20.0	1.704	0.0030	0.0051	7.30	0.0109	0.0796	5.10
32.0	1.702	0.0028	0.0048	7.28	0.0103	0.0750	
40.0	1.702	0.0027	0.0046	7.28	0.0099	0.0721	2.82

Table 75.

Ordinary Pollucite, ex Run 98 at 90°C.

The best straight line between 256 kc/s and 2.54 mc/s.

Frequency	ϵ'_{app}	$\tan\delta_{app}$	ϵ''_{app}	ϵ'_o	$\tan\delta_o$	ϵ''_o	R_{po} meg-Ω
63 kc/s	1.702	0.0024	0.0041	7.28	0.0088	0.0641	2.01
74	1.694	0.0023	0.0039	7.15	0.0084	0.0601	1.83
101	1.704	0.0021	0.0036	7.30	0.0077	0.0562	1.43
122	1.704	0.0020	0.0034	7.30	0.0073	0.0533	1.25
Best straight line is:							
421 kc/s	1.700	0.00178	0.00303	7.24	0.0065	0.0471	0.410
1.70 mc/s	1.707	0.00165	0.00282	7.35	0.0060	0.0441	0.108

Table 76.

Ordinary Pollucite, ex Run 99 at 105°C.

Frequency	ϵ'_{app}	$\tan\delta_{app}$	ϵ''_{app}	ϵ'_o	$\tan\delta_o$	ϵ''_o	R_{po} meg-Ω
1.3 kc/s	1.724	0.0090	0.0155	7.62	0.0329	0.251	24.9
2.5	1.719	0.0069	0.0119	7.54	0.0253	0.191	17.0
5.0	1.712	0.0057	0.0098	7.43	0.0209	0.155	10.5
10.0	1.709	0.0046	0.0079	7.38	0.0169	0.125	6.51
20.0	1.707	0.0039	0.0067	7.35	0.0143	0.105	3.86
40.0	1.704	0.0033	0.0056	7.30	0.0120	0.088	2.32

Table 77.

Ordinary Pollucite, ex Run 101 at 75°C.

Frequency	ϵ'_{app}	$\tan\delta_{app}$	ϵ''_{app}	ϵ'_o	$\tan\delta_o$	ϵ''_o	R_{po} meg-Ω
1.3 kc/s	1.709	0.0047	0.0080	7.38	0.0171	0.126	49.5
2.5	1.709	0.0038	0.0065	7.38	0.0139	0.103	31.7
5.0	1.707	0.0033	0.0056	7.35	0.0120	0.082	19.8
10.0	1.704	0.0028	0.0048	7.30	0.0103	0.075	10.8
20.0	1.704	0.0024	0.0041	7.30	0.0088	0.064	6.32
40.0	1.704	0.0023	0.0039	7.30	0.0083	0.061	3.34

Table 78.

Ordinary Pollucite, ex Run 103 at 45°C.

Frequency	ϵ'_{app}	$\tan\delta_{app}$	ϵ''_{app}	ϵ'_o	$\tan\delta_o$	ϵ''_o	R_{po} meg-Ω
1.3 kc/s	1.707	0.0026	0.0044	7.35	0.0094	0.0691	90.4
2.5	1.707	0.0023	0.0039	7.35	0.0083	0.0610	53.3
5.0	1.704	0.0020	0.0034	7.30	0.0073	0.0533	30.5
10.0	1.702	0.0018	0.0031	7.28	0.0066	0.0480	16.9
20.0	1.702	0.0016	0.0027	7.28	0.0058	0.0422	9.62
40.0	1.702	0.0015	0.0026	7.28	0.0056	0.0408	4.98

Table 79.

Ordinary Pollucite, Activation Energies, kcal/mole.

A. Results from all temperature combinations averaged.

Frequency		ex $R_{p(app)}$	ex R_{po}	Frequency		ex $R_{p(app)}$	ex R_{po}
1.0 kc/s	(1)	4.5	-	20.0 kc/s	(2)	3.2	3.3
1.3	(2)	4.6	4.7	25.0	(1)	2.8	-
1.6	(1)	4.0	-	32.0	(1)	2.7	-
2.0	(1)	4.2	-	40.0	(2)	2.9	2.9
2.5	(2)	4.2	4.2	63.0	(1)	2.5	-
3.2	(1)	3.8	-	74.0	(1)	2.6	-
4.0	(1)	3.6	-	313.0	(1)	1.6	-
5.0	(2)	3.8	3.8	509.0	(1)	1.4	-
6.3	(1)	3.3	-	890.0	(1)	1.7	-
8.0	(1)	3.3	-	1.77 mc/s	(1)	1.7	-
10.0	(2)	3.5	3.5	2.07	(1)	2.2	-
13.0	(1)	3.0	-	2.54	(1)	0.90	-
16.0	(1)	2.9	-				

B. Results at 6 frequencies (1.3,2.5,5.0,10.0,20.0 and 40.0 kc/s) averaged.

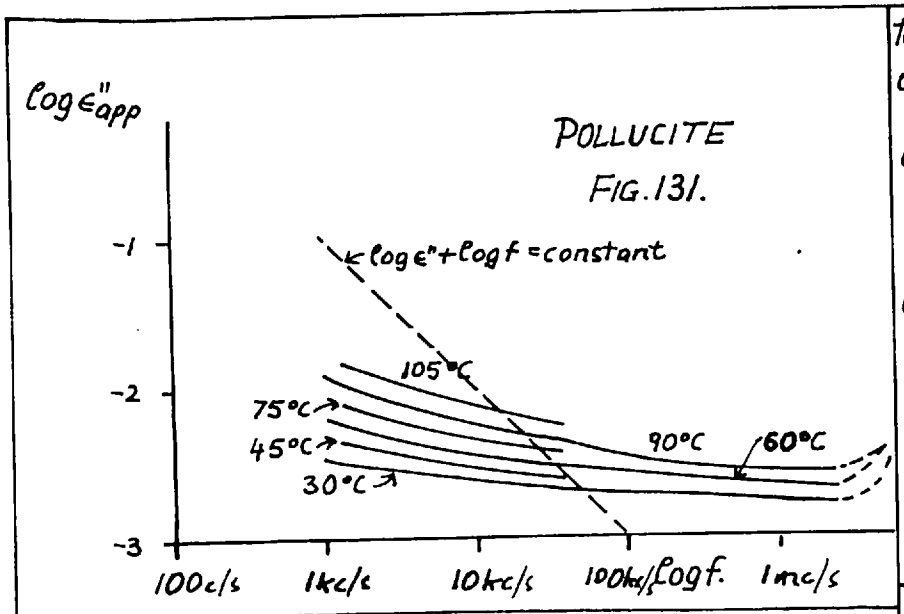
Temperature Interval, °C	ex $R_{p(app)}$	ex R_{po}
30 - 45	2.6	2.4
45 - 60	2.9	3.1
60 - 75	4.0	3.8
75 - 90	3.9	4.1
90 - 105	5.3	5.5

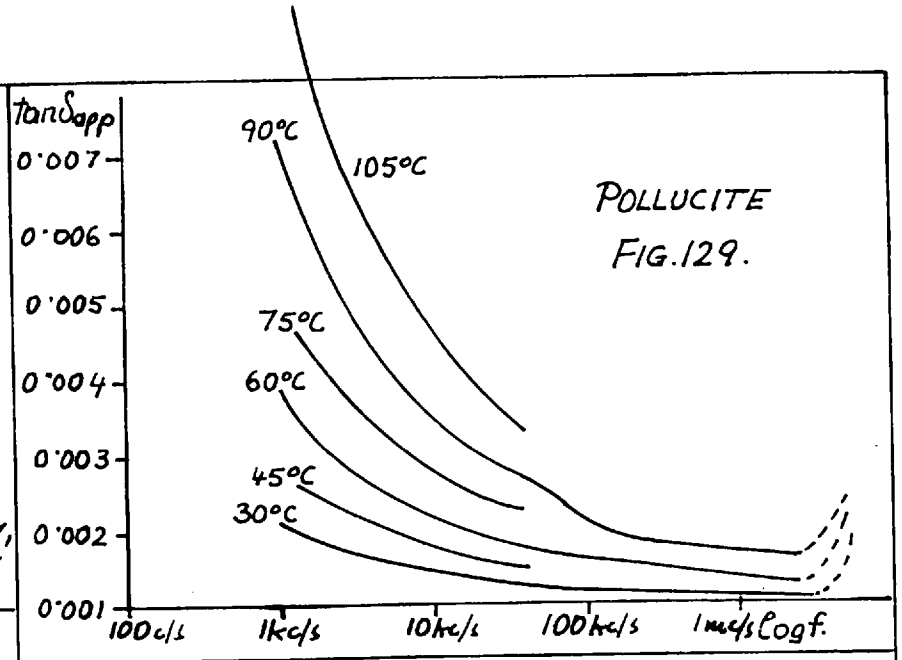
(1) Only results at 3 temperatures were available.

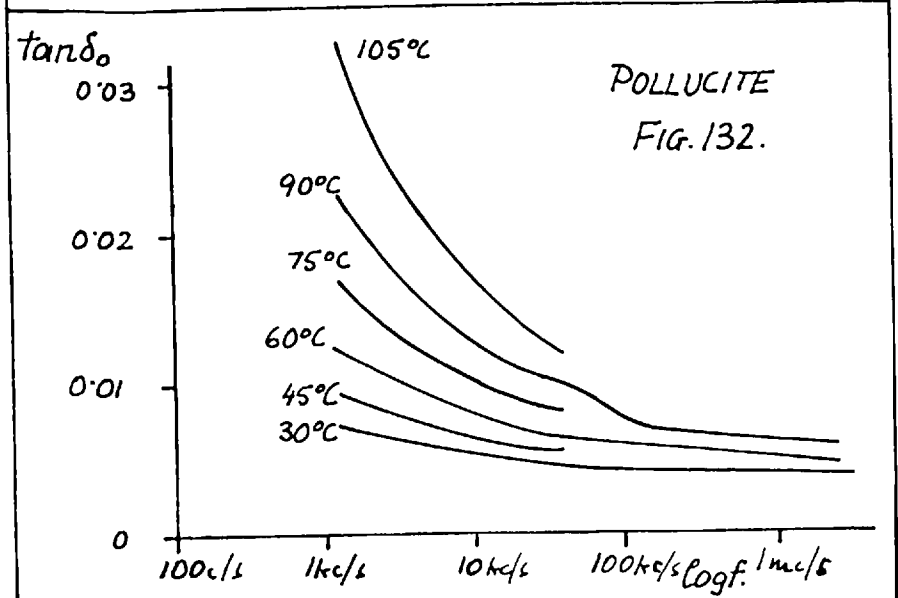
(2) Results at 6 temperatures were used.

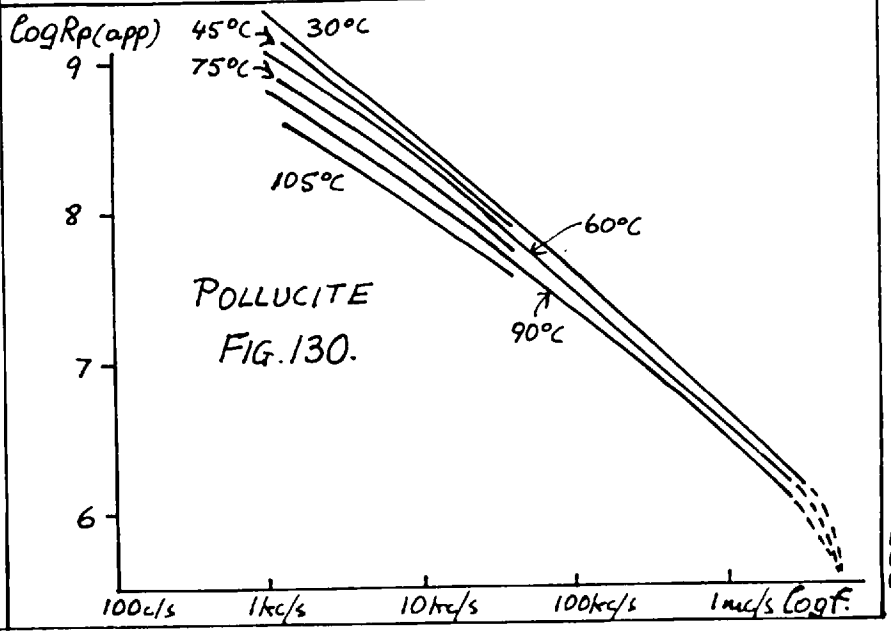
The value of the real dielectric constant independent of temperature and frequency, calculated from the corresponding apparent value of 1.705 is 7.32. In general, the ϵ'_o values are slightly higher than those of the domain mixture of rubidium analcite, but the two are equal within experimental error. Ordinary pollucite has higher $\tan\delta$ values than the domain mixture of rubidium analcite, showing it to be not quite as good an insulator, but the shapes of the plots of the dielectric properties are exactly the same as those of the corresponding plots of the domain mixture of rubidium analcite. Again the $\log \epsilon''$ curves show that d.c. conductivity is quite negligible. Relaxation effects are again indicated, as with the domain mixture of rubidium analcite (pages 217 to 218), with the $\tan\delta$ values much smaller than in the case of leucite. According to Beattie[21] the activation energy for cation jumps in synthetic pollucite is 24 kcal/mole which according to Table 2 means a relaxation peak, at 20°C, at a much lower frequency than in the case of leucite or even rubidium analcite. It is thus obvious that the relaxation indicated is not due to the cations. Also as with the domain mixture of rubidium analcite, the constancy of ϵ' indicates that interfacial polarisation plays no part. The phenomenon responsible for the dielectric loss in ordinary pollucite has already been suggested for the domain mixture of rubidium analcite. For convenience this phenomenon will be discussed in connection with the sintered sample. The activation energies, calculated from the R_p values as with earlier samples are given in Table 79. Splitting the permittivity value into the contributions due to the various polarisations gives:

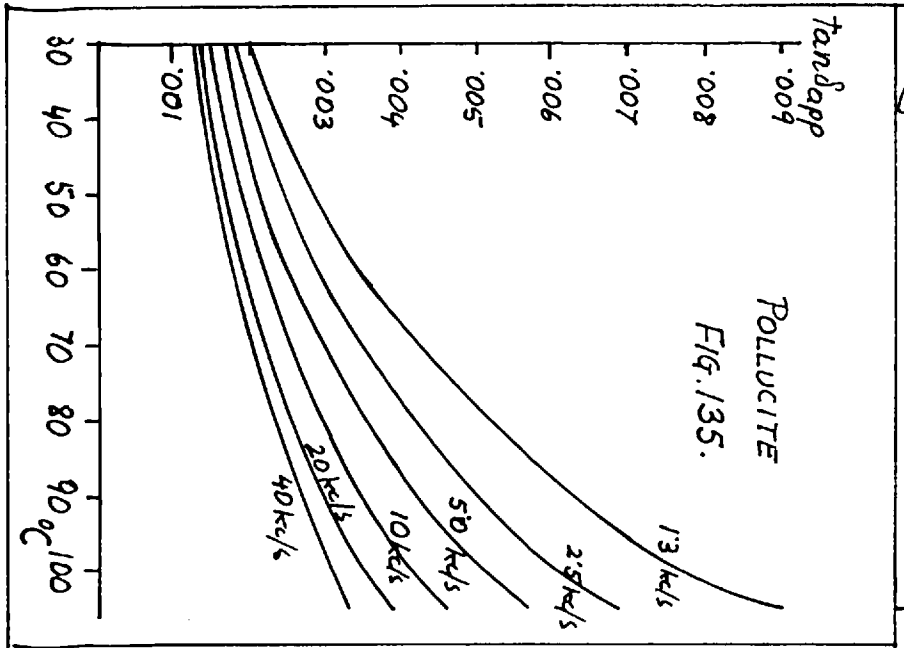
ϵ'_o due to the total polarisability	7.32
ϵ'_o due to the electronic polarisation	2.33
ϵ'_o due to the atomic polarisation	4.99.


log ε"app
POLLUCITE
FIG. 131.
log ε" + log f = constant
105°C
75°C
45°C
30°C
90°C
60°C
-1
-2
-3
100c/s
1kc/s
10kc/s
100kc/s
log f.
1mc/s

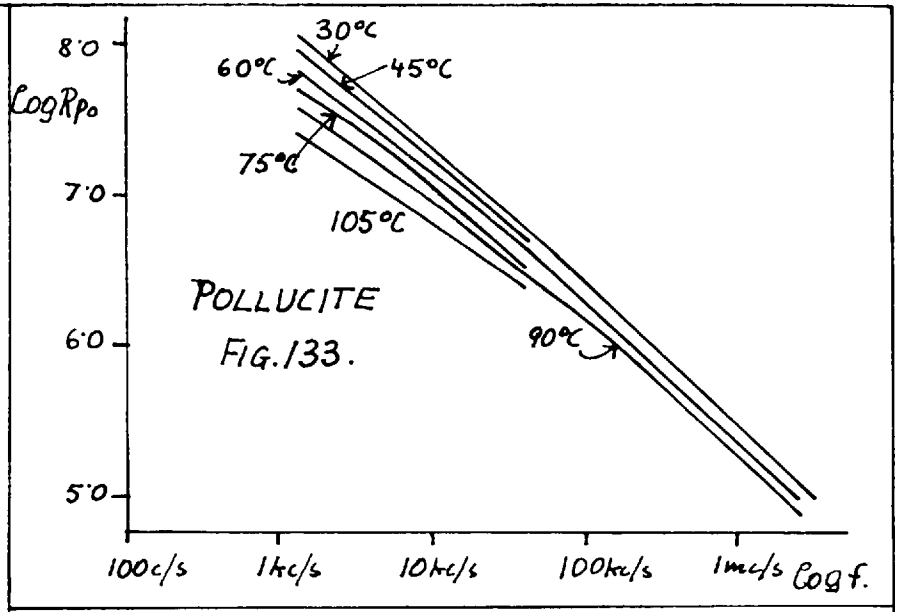

tanδapp
POLLUCITE
FIG. 129.
90°C
105°C
75°C
60°C
45°C
30°C
0·007
0·006
0·005
0·004
0·003
0·002
0·001
100c/s
1kc/s
10kc/s
100kc/s
1mc/s log f.


tanδo
POLLUCITE
FIG. 132.
105°C
90°C
75°C
60°C
45°C
30°C
0·03
0·02
0·01
0
100c/s
1kc/s
10kc/s
100kc/s
log f.
1mc/s

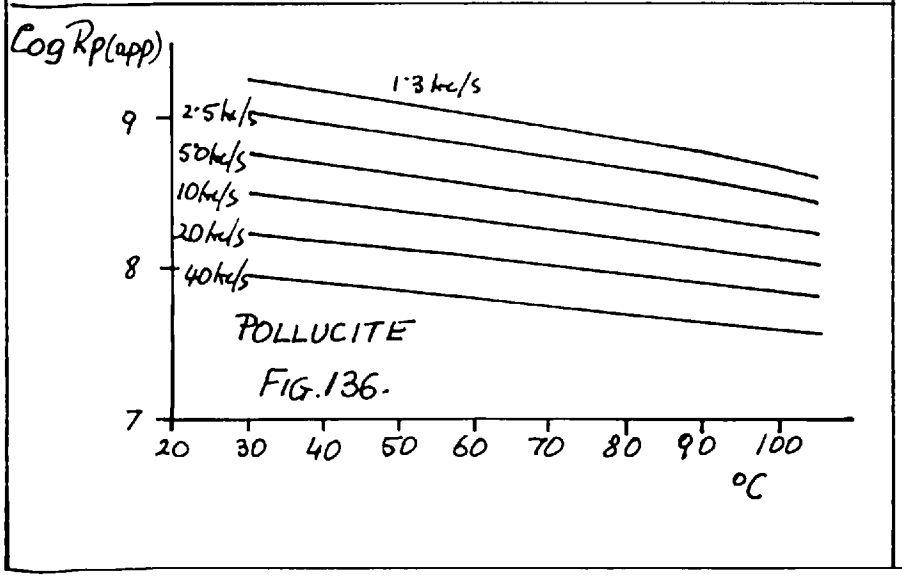

log Rp(app)
45°C
30°C
75°C
105°C
60°C
90°C
POLLUCITE
FIG. 130.
9
8
7
6
100c/s
1kc/s
10kc/s
100kc/s
1mc/s log f.



POLLUCITE
FIG. 135.

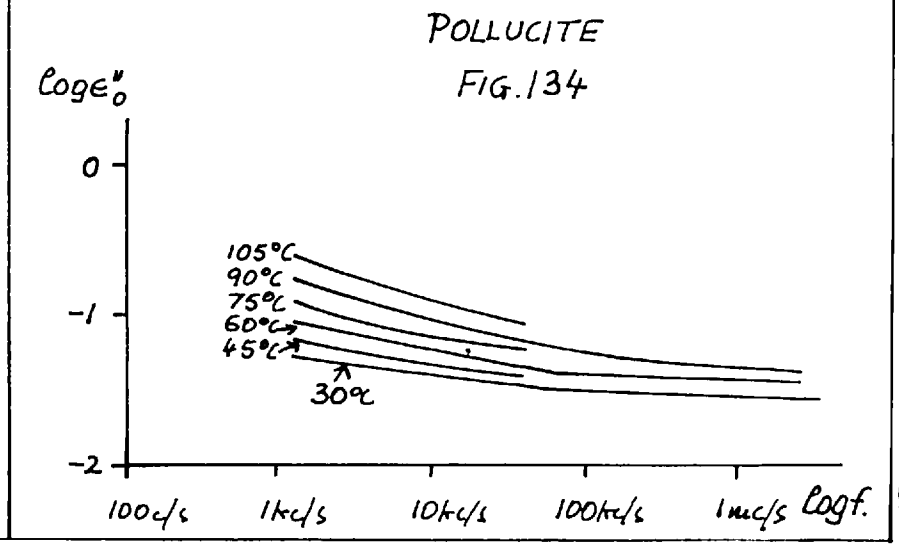


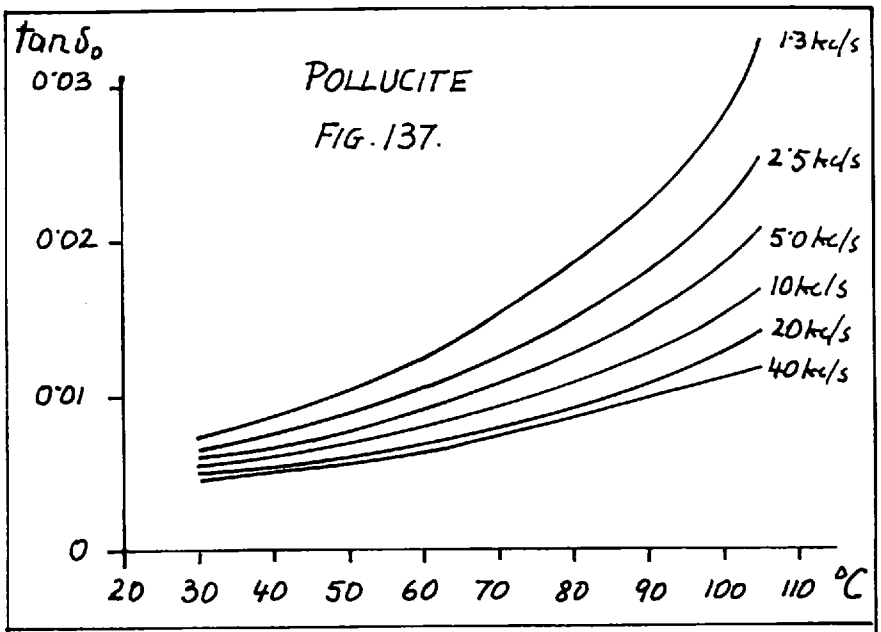
POLLUCITE
FIG. 133.



POLLUCITE
FIG. 136.

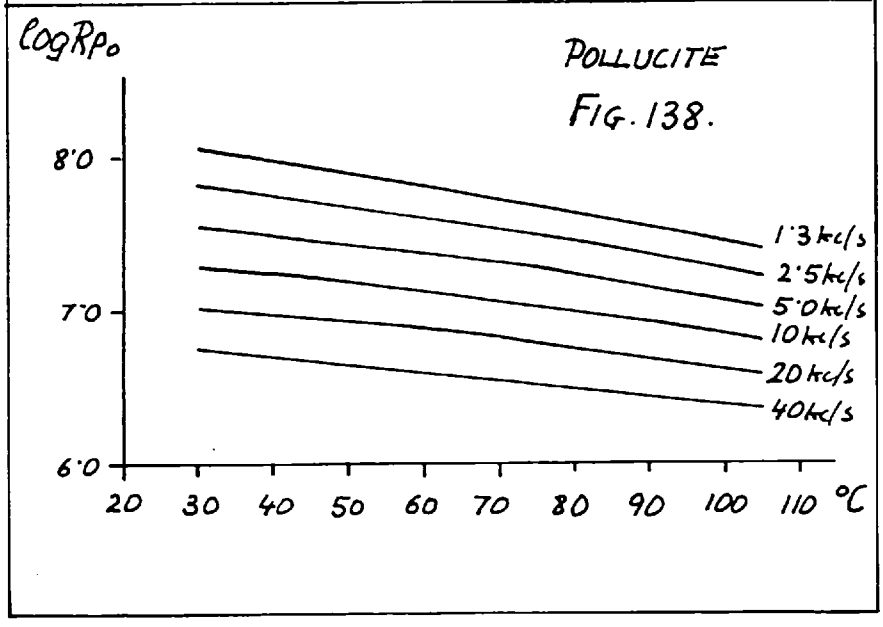
POLLUCITE
FIG. 134





POLLUCITE

FIG. 137.



POLLUCITE

FIG. 138.

10.3. Sintered Pollucite.

Results of the dielectric measurements at 30 and 90°C are given in Appendix tables CVIII to CXI. The temperature coefficient of the dielectric properties is so small, that measurements at only two temperatures were sufficient. All the remarks made about rubidium analcite on page 220 apply. Plotting of results is again unfruitful, and again the $\tan\delta$ values are of the order of repeatability and reproducibility of the results, making it impossible to calculate activation energies sensibly. No process causing dielectric loss is indicated. The results of the Böttcher calculations are given in Tables 80 and 81.

Table 80.

Sintered Pollucite, ex Runs 143 and 152 at 30°C.

Results are constant between 1 and 50 kc/s and are as follows: $\epsilon'_{app} = 2.635$, $\tan\delta_{app} = 0.00009$, $\epsilon''_{app} = 0.00024$, $\epsilon'_{o} = 6.25$, $\tan\delta_{o} = 0.0002$ and $\epsilon''_{o} = 0.0009$.

Table 81.

Sintered Pollucite, ex Run 153 at 90°C.

Frequency	ϵ'_{app}	$\tan\delta_{app}$	ϵ''_{app}	ϵ'_{o}	$\tan\delta_{o}$	ϵ''_{o}
1.0-3.2 kc/s	2.631	-	-	6.23	-	-
4.0	2.631	0.00043	0.00113	6.23	0.0007	0.0044
5.0	2.631	0.00036	0.00095	6.23	0.0006	0.0037
6.3	2.631	0.00031	0.00082	6.23	0.0005	0.0032
8.0	2.631	0.00026	0.00068	6.23	0.0004	0.0027
10.0	2.631	0.00023	0.00061	6.23	0.0004	0.0024
13.0	2.631	0.00019	0.00050	6.23	0.0003	0.0019
16.0	2.631	0.00017	0.00045	6.23	0.0003	0.0017
20.0	2.631	0.00014	0.00037	6.23	0.0002	0.0014
25.0	2.631	0.00012	0.00032	6.23	0.0002	0.0013
32.0	2.631	0.00011	0.00029	6.23	0.0002	0.0011
40.0	2.631	0.00009	0.00024	6.23	0.0002	0.0009
50.0	2.631	0.00009	0.00024	6.23	0.0002	0.0009

In view of the remarks on the accuracy of the results (page 220), the dielectric losses of the samples of rubidium analcite B and sintered caesium analcite are the same, those of the latter sample, if anything, being the lower. Both materials are excellent insulators, but work on compressed samples with an apparatus more sensitive to very low losses, would be interesting. Splitting the permittivity into its various components gives:-

ϵ'_o due to total polarisability	6.24
ϵ'_o due to electron polarisation	2.33
ϵ'_o due to atomic polarisation	3.91.

It is beyond doubt that the dielectric loss in the ordinary sample is due to a cause other than cation relaxation, since sintering does not change the crystal structure of pollucite[17] but removes the cause of the dielectric loss. The slight crystalline difference between the rubidium analcite samples does not allow the same certainty in their case, without using the pollucite analogy. The dielectric loss in ordinary pollucite is simply explained as due to terminal OH substituents which are lost on sintering. The relaxation peak of these OH substituents occurs at a frequency lower than those of measurement, but not as low as the frequency at which the cations relaxation peak would be expected. The tailing off of the dielectric loss with increasing frequency and decreasing temperature and the parallel decrease of the activation energies shows that the OH substituents have a wide distribution of relaxation times, caused by the formation of additional equilibrium positions due to their varying environment (see page 154 where a similar effect is explained in basic sodalite). As the frequency is raised and moves away from the main absorption region, the heights and numbers of the energy barriers against OH relaxation gradually decrease and the activation energy which is a measure of these barriers, decreases with frequency increase. The

relaxation of the OH substituents is numerically a much smaller effect than cation relaxation, the peak of which occurs at a much lower frequency in pollucite and thus does not screen the dielectric loss due to the OH substituents. The type of relaxation is probably similar to that described by Dryden and Meakins[126] for aliphatic secondary alcohols which show a wide distribution of relaxation times due to the rotation of the OH groups around the C-O bonds. In this case the absorption frequency is independent of the molecular weight of the alcohol, just as in rubidium analcite (domain mixture) and pollucite where it seems to appear at the same frequency.

Comparison of the two pollucite samples reveals that the OH groups contribute 1.00 units to the permittivity caused by atomic polarisation.

The results obtained with the rubidium analcites, in particular the dielectric loss and the change which occurs on sintering, are almost the same as in the pollucite samples. It has already been pointed out that the crystalline change which accompanies the sintering of the domain mixture of rubidium analcite, does not allow a definite statement to be made about the cause of the dielectric loss in the domain mixture; however comparison with pollucite shows beyond reasonable doubt that it must also be due to the OH groups. The similarities of the two materials which allow this deduction are summarised here:-

1. The shapes of the dielectric curves and their change on sintering are very similar.

2. The numerical values of the dielectric properties and their changes on sintering are almost identical.

3. The contributions to the permittivities are as follows:

Permittivity Contribution due to:	Rubidium Analcite Domain Mixt.	B	Pollucite Ordinary	Sintered
Total polarisability	7.20	6.25	7.32	6.24
Electron polarisation	2.27	2.32	2.33	2.33
Atomic polarisation	4.93	3.93	4.99	3.91
Change of atomic polarisation on sintering	1.00		1.08	

4. The average activation energies of the non sintered samples are equal within experimental and calculation error.

It is thus clear that the dielectric loss in the domain mixture of rubidium analcite is also due to terminal OH groups which are lost on sintering.

11. Comparative Discussion of Results.

A wide variety of interesting dielectric properties have been revealed in synthetic powdered aluminosilicates. In order to obtain full details of all the aspects of this electrical information, the frequency and temperature range of the measurements will have to be increased. At the beginning of this research the choice lay between building all the apparatus for this wide temperature and frequency range and leaving only time for the detailed examination of one system, or to assemble the apparatus covering only the main practical temperature and frequency range and to examine a larger variety of materials. Both the money and time available dictated the latter course, but it is hoped that future workers in this team will be able to extend the range of the apparatus. After proving the apparatus, the aim of this work has been to determine the range of dielectric properties which can be expected of three-dimensional aluminosilicates, in the hope of being able to forecast species with good insulating or interesting dielectric properties. To the latter end occlusion compounds were investigated and in order to help in systematic forecasting of dielectric properties, the influence of the cation on the dielectric properties of the analcite series were determined.

The materials examined can be divided into three classes:

(a) those showing interfacial polarisation;

(b) those showing dielectric loss due to a relaxation phenomenon, and

(c) samples showing no dielectric loss.

The phenomenon of interfacial polarisation has its cause in either a special structural feature of the aluminosilicate or is due to ion conduction combined with the powder method of measurement. The latter, which must be classed as

unwanted interference with the method used to determine dielectric properties, is indicated only at the lower frequencies for sodium analcite, and is discussed first.

In three-dimensional aluminosilicates interfacial polarisation, due to the cations neutralising the framework charge, will occur when the barriers preventing movement of cations from one crystallite to the next are much larger than the barriers against cation jumps between cation positions in the framework. Consideration of Table 2 reveals that at a given temperature the relaxation peak due to interfacial polarisation should therefore occur at a lower frequency than the corresponding cation relaxation peak. Since in the series of ion exchanged analcites a frequency lower than that of the cation relaxation peak is obtained only with the sodium form, the other samples cannot show effects due to interfacial polarisation. Consideration of Beattie's activation energies in conjunction with Table 2 shows that at ordinary temperatures the interfacial polarisation peak of these samples occurs at extremely low frequencies and therefore this polarisation for these particular powdered aluminosilicates is of little practical significance.

When interfacial polarisation is due to a special structural feature, the material may well be of practical interest. Barrier layer dielectrics are now being investigated as a means of obtaining large capacitances with very small condensers. This type of dielectric usually shows a comparatively large dielectric loss and investigations are aimed at improving this property. The aluminosilicates with interfacial polarisation peaks in the frequency and temperature range of our measurements are all materials with occluded molecules, e.g. hydrated basic sodalite, hydrated and anhydrous AgA($AgNO_3$). They are all very lossy.

In basic sodalite the interfacial polarisation disappears on dehydration, showing that in the hydrated sample the effect is caused by the water molecules which, possibly in conjunction with the interstitial sodium hydroxide molecules, behave as occluded rather than sorbed molecules. In sodium analcite the chemisorbed water molecules are held by a stronger binding force than in basic sodalite and the comparatively small change of dielectric properties on dehydration shows that these water molecules are much less conducting and their only effect is to modify slightly the dielectric behaviour of the sample including the interfacial polarisation, caused principally by the cations. In the $AgA(AgNO_3)$ compounds the interfacial polarisation is caused by the Ag^+ ions of the framework and the $AgNO_3$ molecules, in conjunction with the unavoidable defects in the structure of the occluded molecules.

In anhydrous basic sodalite the dielectric loss encountered is due to a cation relaxation phenomenon with a very wide distribution of relaxation times, characteristic of which is an activation energy which decreases with frequency increase.

The properties of the analcite series are governed by the frequency at which the cation relaxation peak appears at the temperatures of measurement. The mobility of the cation decreases with increasing cation size and therefore the barrier between equivalent cation positions and the activation energy required to surmount this barrier also increases with cation size. In agreement with Table 2 the frequency at which the relaxation peak due to the cations neutralising the framework appears at any temperature, therefore decreases with increasing cation size. In sodium analcite this peak appears in the range of the measurements and interfacial polarisation is shown at even lower frequencies. The material shows a wide distribution of relaxation times. In leucite the

cation relaxation moves to a lower frequency and due to the very wide distribution of relaxation times is just indicated at the lowest frequencies. This relaxation phenomenon is characterised by an activation energy which decreases with increase in frequency and decrease in temperature. The domain mixture of rubidium analcite and ordinary pollucite do not show any relaxation due to the cations but a lesser relaxation phenomenon due to terminal OH bonds is indicated at the lowest frequencies. This relaxation phenomenon shows a similar variation of activation energies with frequency and temperature as do basic sodalite and the leucite samples. The sintered rubidium analcite B and sintered pollucite do not show any dielectric loss at all since the OH substituents have been driven off. A summary of the activation energies is found in Table 81.

The phenomenon of activation energies which vary linearly with frequency and temperature occurs with anhydrous basic sodalite, probably with sodium analcite, with the leucite samples, the domain mixture of rubidium analcite and with ordinary pollucite. It suggests a range of environments for one relaxing species or else less probably a range of relaxing species. A continuous variation in the heights of the potential barriers measured by the activation energies is unlikely. Instead one expects a limited number of energy barriers of varying height (see Fig. 139) which the relaxing species must overcome in transitions between positions. The linear relation between apparent activation energies and frequency may then be caused by interaction of two factors:
(a) the lower the barrier the higher is the frequency at which the relaxation peak due to this energy barrier occurs;
(b) the distribution function for the relaxation times may be of the type shown in Fig. 140, where the number of barriers of a particular kind decreases with decrease in the energy of the barrier. Figure 140 shows a maximum activation energy

Table 81.

Summary of Activation Energies of Aluminosilicates.

Sample	Activation Energy kcal/mole	Remarks
Hydrated Basic Sodalite	2.8	Constant over a large frequency range. Due to d.c. conductivity within the grains, caused by the process: $H_2\underline{O} + OH^- = \underline{O}H^- + H_2O$.
Anhydrous Basic Sodalite	4.5 at 1.3 kc/s decreasing to 0.26 at 2.07 mc/s.	Due to cation relaxation with a peak below the frequencies of measurement. Gradual decrease with frequency increase due to a wide distribution of relaxation times caused by the varying environment of the cations.
Hydrated $AgA(AgNO_3)$	14.1 at 1.3 kc/s, 13.6 at 13 kc/s.	Slight variation with frequency. Due to a d.c. conduction effect within the grains by the Ag^+ ions.
Anhydrous $AgA(AgNO_3)$	11.2	Due to a d.c. conduction effect within the grains caused by the Ag^+ ions.
Hydrated Sodium Analcite	12.8 ± 0.3	a.c. effect due to cation jumps within the crystallites. The change on dehydration suggests that water has little influence. Large distribution of relaxation times.
Anhydrous Sodium Analcite	12.6 ± 0.3	
Leucite, Exchange Sample	7.1(1.3 kc/s), 5.8(10 kc/s), 3.3(2.01 mc/s).	Cation relaxation peak at about 1 c/s (30°C). Variation with frequency and temperature because of wide distribution of relaxation times, caused by the varying environment of the cations in the framework.
Sintered Leucite	6.7(1.3 kc/s), 5.3(10 kc/s).	As for ordinary leucite. Distribution of relaxation times may be larger, because of greater disorder in the framework structure; or a loss peak at slightly higher frequency.

Table 81 (contd.)

Sample	Activation Energy kcal/mole	Remarks
Domain Mixture of Rubidium Analcite	5.0(1.3 kc/s) 3.8(10 kc/s)	Due to relaxation peak at very low frequencies, caused by terminal OH bonds which are driven off on sintering. The consequent activation energies vary for the same reason as those in leucite.
Rubidium Analcite B		No process causing dielectric loss takes place.
Pollucite	4.7(1.3 kc/s) 3.5(10 kc/s)	Due to relaxation peak at very low frequencies, caused by terminal OH bonds which are driven off on sintering. The consequent activation energies vary for the same reason as those in leucite.
Sintered Pollucite		No process causing dielectric loss takes place.

above which the distribution function $G_n(\tau)$ is zero. This maximum corresponds with the activation energy calculated from the dielectric loss peak. Comparison of the results for sodium analcite in this work with the activation energies obtained by Beattie and by Rees shows that this activation energy remains constant at frequencies below the maximum loss frequency and equals the activation energy obtained from d.c. measurements and by ionic self-diffusion. In the case of sodium analcite this corresponds to sodium ion transitions between minimum potential energy positions via the maximum barrier of zero potential energy.

Equation 75 shows that the smaller the number of relaxing particles the lower is the value of their loss peak. Thus as the frequency increases, loss peaks of decreasing

height overlap giving the smooth, decreasing tanδ and ϵ'' curves found experimentally. This is really a restatement of the concept of the distribution of relaxation times. Activation energies calculated from the resistance values by equation 150 will therefore also vary linearly with frequency and temperature. Figure 141 is the plot of the activation energies, averaged over the temperatures of measurement, against frequency; the broken lines indicate theoretical values not actually obtained in measurements. Since the frequency at which the maximum activation energy appears depends on temperature, Fig. 141 is only qualitative.

A variation of energy barriers as visualised above may arise in two ways:

(a) The relaxing species jump across barriers between positions of equal minimum potential energy. Due to the varying environment of these positions the heights of the barriers between equivalent positions vary up to a maximum barrier of maximum probability. This situation is shown in Figure 142 and is representative of the cation relaxation in aluminosilicates, where the cations are all in equivalent minimum potential energy positions.

(b) The relaxing species can occupy a number of different energy levels down to the one of minimum potential energy as shown in Fig. 143. This type of behaviour can be expected from dipole orientation and may occur in the domain mixture of rubidium analcite and in ordinary pollucite with the terminal OH substituents acting as the orientating dipoles.

Decrease in temperature which moves the relaxation peaks to a lower frequency has obviously the same effect on the activation energies as increase in frequency.

The permittivities of the samples are compared in Table 82. It is seen that the atomic polarisation contributions to the permittivity of the leucite exchange sample, of rubidium analcite B and sintered pollucite are equal and that the contributions due to electronic polarisation to the permittivity of these materials are also almost equal. This bears out that the three materials have the same structure. It is difficult to see why sodium analcite does not give the same result. It is possible that in this case the calculation of the total polarisation contribution to the dielectric constant is in error, which may be due to the deviations of the Cole-Cole plot at the lowest and highest frequencies.

Table 82.

Sample	Permittivities (Averages between all the temperatures of measurement)		
	ϵ'_o (atomic)	ϵ'_o (electronic)	ϵ'_o (Total polarisation)
Anhydrous Basic Sodalite, 30 to 80°C.	2.00	2.04	4.04
Sodium Analcite, anhydrous	7.6	2.10	9.7
Leucite, exchange sample	3.88	2.23	6.11
Rubidium Analcite, domain mixture	4.93	2.27	7.20
Rubidium Analcite B	3.93	2.32	6.25
Pollucite=	4.99	2.33	7.32
Sintered Pollucite	3.91	2.33	6.24

The domain mixture of rubidium analcite and ordinary pollucite show an atomic polarisation contribution of 1.0, which is due to the OH substituents, to the permittivity. This is not found in the leucite exchange sample although it would be expected by analogy, which shows that, contrary to an earlier suggestion, relaxation due to OH substituents does not exist in this compound.

Since $AgA(AgNO_3)$, anhydrous basic sodalite and anhydrous sodium analcite show unusual electrical properties in the range of the measurements, no conclusions can be drawn about the systematic change in dielectric properties with decreasing size of intra-crystalline cavities.

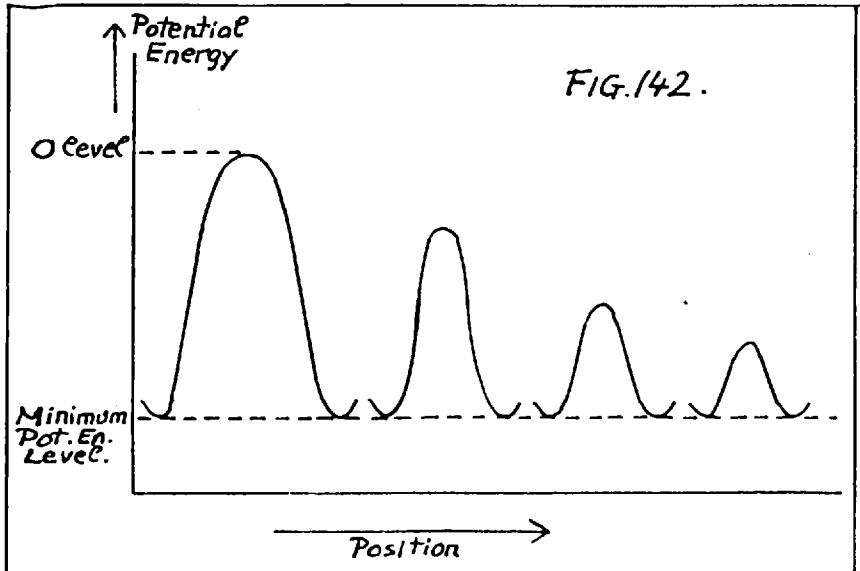


FIG. 142.

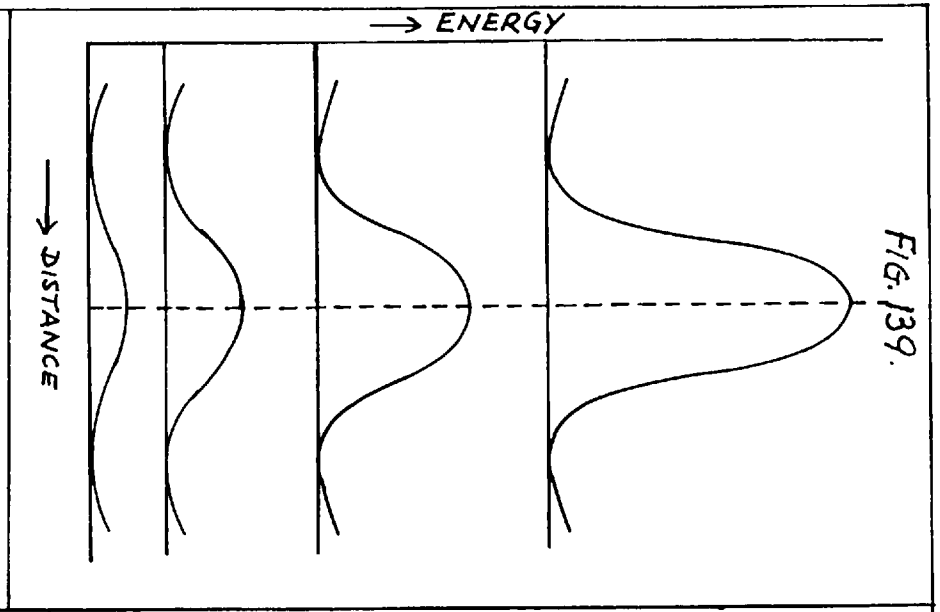


FIG. 139.

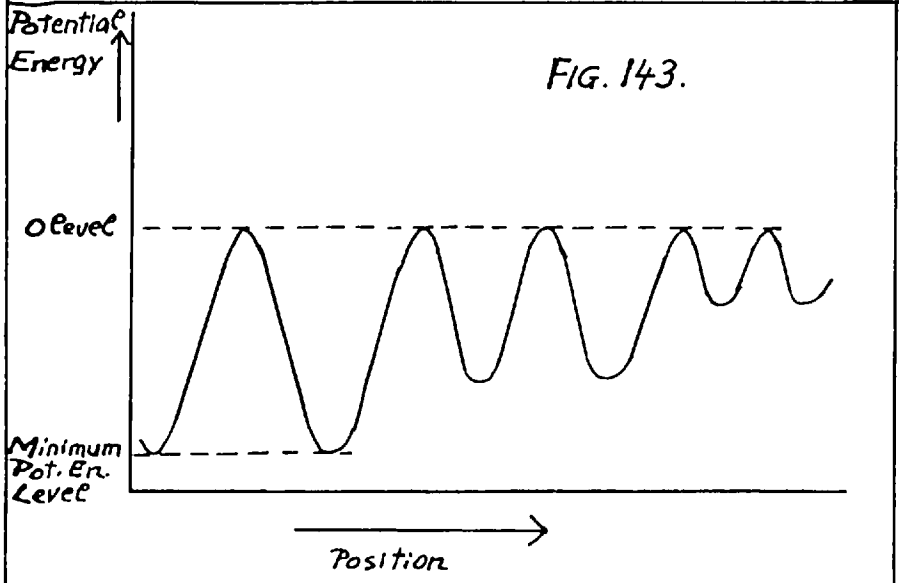


FIG. 143.

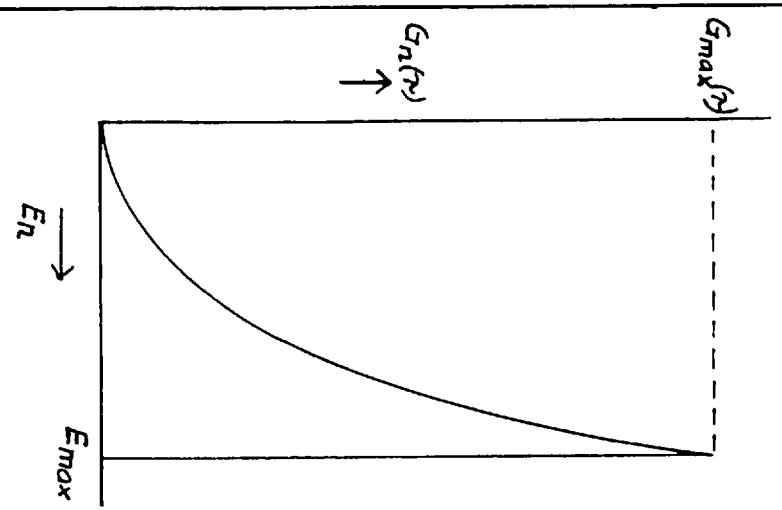
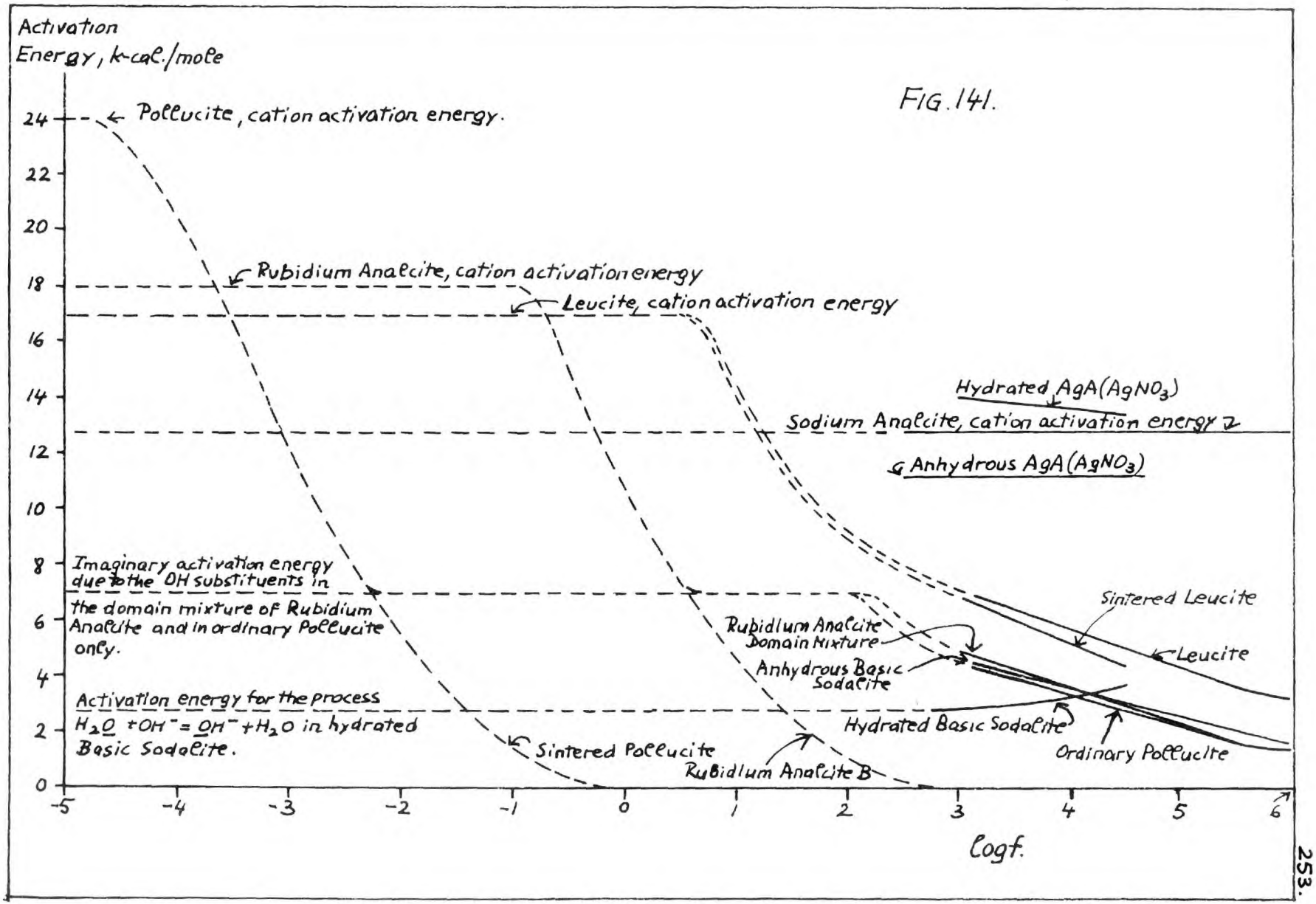


FIG. 140.


Activation
Energy, k-cal./mole
FIG. 141.
Pollucite, cation activation energy.
Rubidium Analcite, cation activation energy
Leucite, cation activation energy
Hydrated AgA($AgNO_3$)
Sodium Analcite, cation activation energy
Anhydrous AgA($AgNO_3$)
Imaginary activation energy due to the OH substituents in the domain mixture of Rubidium Analcite and in ordinary Pollucite only.
Activation energy for the process $H_2O + OH^- = OH^- + H_2O$ in hydrated Basic Sodalite.
Sintered Leucite
Leucite
Rubidium Analcite Domain Mixture
Anhydrous Basic Sodalite
Hydrated Basic Sodalite
Ordinary Pollucite
Sintered Pollucite
Rubidium Analcite B
24
22
20
18
16
14
12
10
8
6
4
2
0
-5
-4
-3
-2
-1
0
1
2
3
4
5
6
Logf.

References.

1. L. Massey, Trans. Inst. Rubber Ind., 16, 325, (1941).
2. M. Gevers, Phil. Res. Rep., 1, 279, (1946).
3. M. Gevers, Phil. Res. Rep., 1, 447, (1946).
4. R. M. Barrer, Trans. Cer. Soc., 56, 155, (1957).
5. R. M. Barrer and E. A. D. White, J.C.S., 1167, (1949).
6. R. M. Barrer and E. A. D. White, J.C.S., 1561, (1952).
7. R. M. Barrer and F. W. Bultitude, In press.
8. R. M. Barrer and J. W. Baynham, J.C.S., 2882, (1956).
9. R. M. Barrer and N. McCallum, J.C.S., 4029, (1953).
10. R. M. Barrer, J.C.S., 2342, (1950).
11. R. M. Barrer and L. Hinds, J.C.S., 1879, (1953).
12. R. M. Barrer, L. Hinds and E. A. D. White, J.C.S., 1466, (1953).
13. R. M. Barrer and J. D. Falconer, Proc. Roy. Soc., A.236, 227, (1956).
14. R. M. Barrer and W. M. Meier, Trans. Faraday Soc., 54, 1074, (1958).
15. R. M. Barrer and D. W. Riley, Trans. Faraday Soc., 46, 853, (1950).
16. R. M. Barrer and W. M. Meier, J.C.S., 299, (1958).
17. R. M. Barrer, J. W. Baynham And N. McCallum, J.C.S., 4035, (1953).
18. R. M. Barrer and W. M. Meier, Helv. Phys. Acta, 29, 230, (1956).
19. O. Weigel, Z. Kryst., 58, 183, (1923).
20. Rabinowitch and Wood, Z . Electrochem., 39, 562, (1933).
21. I. R. Beattie, Trans. Faraday Soc., 50, 561, (1954).

22. I. R. Beattie, Trans. Faraday Soc., 51, 712, (1955).

23. I. R. Beattie, Trans. Faraday Soc., 53, 61, (1957).

24. Liebisch and Rubens, Int. Crit. Tables, Vol. VI, p. 99; Sitzungsberichte der Preussischen Akademie der Wissenschaften, 876, (1919).

25. E. E. Fairbanks, Amer. Mineralogist, 11, 249, (1926).

26. R. L. Rosenholtz and D. T. Smith, Amer. Mineralogist, 21, 115, (1936).

27. J. Takubo, Mem. Coll. Sci. Kyoto Imp. Univ., Ser. B., 16, 95, (1941).

28. J. Takubo, Y. Ukai and Katitani, Min. Journal, Min. Soc., Japan, 1, 3, (1953).

29. K. Wetzlar, Zeit. für angew. Mineralogie, 1, 125, (1938).

30. O. Glemser, Z. anorg. Chemie., 252, 305, (1944).

31. J. v. Keymeulen and W. Dekeyser, J. Chem. Phys., 27, 173, (1957).

32. Bragg, Atomic Structure of Minerals, Cornell Univ. Press.

33. L. Pauling, The Structure of the Chemical Bond.

34. W. Lowenstein, Amer. Mineralogist, 39, 92, (1954).

35. L. Pauling, J. Amer. Chem. Soc., 51, 1010, (1929).

36. Hey, Min. Mag., 22, 422, (1929).

37. Taylor, Proc. Roy. Soc., A.145, 80, (1934).

38. Hendricks, Ind. Eng. Chem., 37, 625, (1945).

39. Winchell, Amer. Mineralogist, 10, 88, (1925).

40. Naray-Szabo, Z. Krist., 99, 277, (1938).

41. I. R. Beattie, Acta.Cryst., 7, 357, (1954).

42. I. R. Beattie, Nature, 172, 999, (1953).

43. Taylor, Z. Krist., 74, 1, (1930).

44. Taylor and Jackson, Z. Krist., 86, 53, (1933).

45. Barrer and Raitt, J.C.S., 4641, (1954).

46. Barrer and Sammon, J.C.S., 2838, (1955).

47. Weiser and Milligan, J. Phys. Chem., 41, 1029, (1937).

48. Beutell and Blaschke, Central Min., 14, 4, (1915).

49. Stoklossa, Neues Jab. Min., 1 (1917).

50. Beutell, Central Min., 694, 721, (1921).

51. Wyart, Compt. Rend., 191, 1342, (1930).

52. Weigel, Naturwiss., (Marburg), Oct. 5, 1919.

53. Tamman, Z. Phys. Chem., 252, 305, (1944).

54. Hartwig, Z. Krist., 78, 173, (1931).

55. Lengyel, Z. Physik., 77, 133, (1932).

56. Koizumi, Min. J. (Min. Soc, Japan), 1, 36, (1953).

57. R. M. Barrer and D. Langley, private communication.

58. Weigel, Central Miner. Geol. Palaantologie, Abt. A, 164, 201, (1922).

59. Jaeger, Trans. Faraday Soc., 25, 334, (1929).

60. W. Hartwig, Fortschritte. Krist Petrog., 13, 38, (1929). Naturwiss., 18, 600, (1930).

61. E. Schiebold, Naturwiss., 18, 705, (1930).

62. L. Pauling, Proc. Nat. Acad. Sci., 16, 4053, (1930).

63. T. W. Gruner, Z. Krist., 68, 363, (1928).

64. Bernal and Fowler, J. Chem. Phys., 1, 315, (1933).

65. R. M. Barrer and D. A. Ibbitson, Trans. Faraday Soc., 40, 195, 1944.

66. R. M. Barrer, Proc. Roy. Soc., A.167, 392, (1938).

67. J. Wyart, Compt. rend., 203, 938, (1936).

68. J. Wyart, Compt. rend., 205, 1077, (1937).

69. J. Wyart, Bull. Soc. franc. minéral, 63, 5, (1940).
Compt. rend., 212, 356, (1941).
Chem. Zentr., I, 3063, (1941).

70. Eitel, Bowen and Scherrer, Amer. J. Sci., 5, 18, 305, (1929).

71. Naray Szabo, Z. Krist., 104, 39, (1942).

72. H. Strunz, Z. Krist., 95, 1, (1936).

73. R. M. Barrer and N. McCallum, Nature, 167, 1071, (1951).

74. Barrer and Sammon, J. C. S., 675, (1956).

75. W. H. Taylor, Z. Krist., 99, 283, (1938).

76. T. Barth, Z. Krist., 83, 405, (1932).

77. F. W. Bultitude, Thesis (London), pp. 100 and 176, (1957).

78. R. M. Barrer and W. M. Meier, Helv. Phys. Acta., 29, 229, (1956).

79. Gossner and Reindl, Centr. Mineral Geol., A., 330, (1932).

80. W. M. Meier, Thesis (London), (1957).

81. D. W. Breck, W. G. Eversole, R. M. Milton, T. B. Reed and T. L. Thomas, J. Amer. Chem. Soc., 78, 5963, (1956).

82. T. B. Reed and D. W. Breck., J. Amer. Chem. Soc., 78, 5972, (1956).

83. C. J. F. Böttcher, Theory of Electric Polarisation, Elsevier Publishing Company, (1952).

84. H. Fröhlich, Theory of Dielectrics, Clarendon Press, Oxford, (1958).

85. L. Onsager, J. Amer. Chem. Soc., 58, 1486, (1936).

86. H. A. Lorentz, Theory of Electrons, Leipzig, 138, 306, (1909).

87. P. Debye, Phys. Z., 13, 97, (1912).

88. A. D. Buckingham, Proc. Roy. Soc., A.238, 235, (1956).

89. R. Clausius, Die mechanische Wärmetheorie, Braunschweig, 62, (1879).

90. O. F. Mosotti, Mem. dimathem. e fisico Modena, 24, II, 49, (1850).

91. Bell, Trans. Faraday Soc., 27, 797, (1931).

92. J. G. Kirkwood, J. Chem. Phys., 4, 592, (1936); 7, 911, (1939).

93. H. Fröhlich, Trans. Faraday Soc., 44, 238, (1948).

94. J. G. Powles, Trans. Faraday Soc., 51, 377, (1955).

95. Mansel Davies, Quart Rev., 8, 250, (1954).

96. J. G. Powles and C. P. Smyth, Weissberger, Technique of Organic Chemistry, 1. Phys. Methods and Organic Chemistry. 2nd ed.; Part 3, 2279, (1954).

97. H. A. Lorentz, Wied. Ann. Phys., 9, 641, (1880).

98. L. V. Lorenz, Wied. Ann. Phys., 11, 70, (1880).

99. C. J. F. Böttcher, Thesis, Leiden, 1940.

100. E. A. Guggenheim, Trans. Faraday Soc., 45, 714, (1949).

101. R. H. Cole, J. Chem. Phys., 23, 493, (1955).

102. R. H. Cole and K. S. Cole, J. Chem. Phys., 9, 341, (1941).

103. D. Debye, Polar Molecules, New York, Chapter V, (1929).

104. H. Eyring, J. Chem. Phys., 14, 283, (1936).

105. A. E. Stearn and H. Eyring, J. Chem. Phys., 113, 5, (1937).

106. S. Glasstone, K. J. Laidler and H. Eyring, The Theory of Rate Processes, New York and London, 544, (1941).

107. W. Kauzmann, Rev. Mod. Phys., 14, 12, (1942).

108. J. G. Powles, J. Chem. Phys., 21, 633, (1953).

109. E. von Schweidler, Ann. Physik. (4), 24, 711, (1907).

110. K. W. Wagner, Anh. Physik (4), 40, 817, (1913).

111. W. A. Yager, Physics, 7, 434, (1936).

112. J. G. Kirkwood and R. M. Fuoss, J. Chem. Phys., 9, 329, (1941).

113. R. M. Fuoss and J. G. Kirkwood, J. Amer. Chem. Soc., 63, 385, (1941).

114. J. Ross MacDonald, J. Chem. Phys., 20, 1107, (1952).

115. D. W. Davidson and R. H. Cole, J. Chem. Phys., 18, 1417, (1950).

116. K. H. Stark, Nature, 166, 436, (1950).

117. C. G. Garton, Trans. Faraday Soc., 42A, 56, (1946).

118. Y. J. Errera and H. Brasseur, Physik. Z., 34, 368, (1933).

119. C. P. Smyth, Chem. Revs., 19, 329, (1936).
Trans. Faraday Soc., 42A, 175, (1946).

120. C. P. Smyth and W. S. Wallis, J. Chem. Phys., 3, 557, (1935

121. C. P. Smyth and C. S. Hitchcock, J. Amer. Chem. Soc., 54, 4631, (1932).

122. C. P. Smyth and C. S. Hitchcock, J. Amer. Chem. Soc., 55, 1830, (1933).

123. C. P. Smyth and C. S. Hitchcock, J. Amer. Chem. Soc., 55, 296, (1933).

124. C. P. Smyth and S. A. McNeight, J. Amer. Chem. Soc., 58, 723, (1936).

125. A. H. White and S. O. Morgan, J. Amer. Chem. Soc., 57, 2078, (1935).

126. J. S. Dryden and R. J. Meakins, Revs. Pure Appl Chem., Australia, 7, 15, (1957).

127. J. D. Hoffmann and H. G. Pfeiffer, J. Chem. Phys., 22, 132, 1144, (1954).

128. M. Gevers, Philips Research Reports, 1, 298, (1946).

129. M. Gevers and F. K. Du Pré, Trans. Faraday Soc., 42A, 47, (1946).

130. A. Gemant, J. Appl. Physics, 10, 508, (1939).

131. L. Suchow and G. R. Pond, J. Amer. Chem. Soc., 75, 5242, (1953).

132. K. W. Wagner, Archiv. Elektrotech., 2, 371; 3, 100, (1914).

133. R. W. Sillars, J. Inst. Elec. Eng., 80, 378, (1937).

134. K. W. Wagner, Elektrotechn. Z., 36, 111, 121, 135, 163, (1915).

135. J. Hirsch, The electrical properties of WO_3, The British Electrical and Allied Industries Research Association Report, Section L, Ref. L/T, 326 and L/T, 351.

136. R. P. Chasmar, Nature, 161, 281, (1948).

137. E. Billig and K. W. Plenner, Proc. Phys. Soc., B64, 361, (1951).

138. K. W. Plenner, Proc. Phys. Soc., B64, 671, 681, (1951).

139. R. T. Lewis and L. R. Bickford jr., J. Amer. Cer. Soc., Cer. Abstr., 3, 9, 6, 222, (1956).

140. R. M. Fuoss, J. Amer. Chem. Soc., 59, 1703, (1937).

141. L. Sosnowski, J. Starkrevicz and O. Simpson, Nature, 159, 818, (1947).

142. O. Simpson, Nature, 160, 791, (1947).

143. A. C. Jason and J. L. Wood, Proc. Phys.Soc., B., Vol. LXVIII, 1105, (1955).

144. B. V. Hamon, Aust. J. Phys., 16, 304, (1953).

145. S. O. Morgan, Trans. Electrochem. Soc., 65, (1934).

146. J. Ross MacDonald, Phys. Rev., 91, 412, (1953).

147. C. T. O'Konski, J. Chem. Phys., 23, 1559, (1955).

148. S. Badzioch and G. B. Cornford, Bull. Brit. Coal Utilisation Res. Assoc., 16, 77, (1952).

149. J. A. Reynolds and J. M. Hough, Proc. Phys. Soc., 70B, 769, (1957).

150. J. W. Rayleigh, Phil. Mag., (5) 34,481, (1892).

151. G. Breit, Proc. Acad. Sci. Amsterdam, 25, 293, (1922).

152. F. Ollendorf, Arch. Elektrochem., 25, 436, (1931).

153. W. Niesel, Ann. Phys. Lpz., 10, 336, (1952).

154. D. Polder and J. H. van Santen, Physica, 12, 257, (1946).

155. O. Wiener, Abh. math. phys. Kl. Sächs. Akad. Wiss. Lpz., 32, 509, (1912).

156. D. A. G. Brüggeman, Ann. Physik, (5), 24,636, (1935).

157. W. I. Higuchi, J. Phys. Chem., 62, 649, (1958).

158. C. J. F. Böttcher, Rec. trav. chim., 64, 47, (1945); Physica, 9, 937, (1942).

159. Lichtenecker and Rother, Phys. Z., 32, 255, (1931).

160. J. P. Poley, Physica, 19, 298, (1953).

161. J. C. Van Vessem and J. M. Bijvoet, Rec. trav. chim., 67, 191, (1948).

162. A. Hélaine, S. Le Montagner and J. Le Bot, C.R. Acad. Sci. Paris, 232, 403, (1951).

163. L. V. C. Rees, Private communication.

164. K. A. Vodop'yanov, Doklady Akad. Nauk. S.S.S.R., 84, 919, 1952; Abs. 9359d, (1952).

165. J. Muir, Trans. Faraday Soc., 50, 249, (1954).

166. Alphabetical Index of X-ray Diffraction Data (American Society for Testing Materials).

167. Bunn, Chemical Crystallography, Clarendon Press, Oxford.

168. B. Hague, Alternating Current Bridge Methods, Pitman and Sons, (1945).

169. L. Hartshorn, Radiofrequency Measurements, Chapman and Hall, (1940).

170. C. T. O'Konski, J. Amer. Chem. Soc., 73, 5093, (1951).

171. Harris, Haycock and Alder, J. Chem. Phys., 21, (1943).

172. R. H. Cole and R. M. Gross jr., Rev. Sci. Instr., 20, 252, (1949).

173. Mullard Material Research Laboratories Report MR762.

174. R. J. Meakins, Austr. J. Sci. Res., A2, 405, (1949); Trans. Faraday Soc., 51, 371, (1955).

R. J. Meakins and R. A. Sack, Austr. J. Sci. Res., A4, 213, (1951).

175. S. Kurosaki, J. Phys. Chem., 58, 320, (1954).

176. L. Hartshorn and Ward, J. Inst. Elec. Eng., 79, 597, (1936).

177. L. H. Hartshorn, Radiofrequency Measurements, Chapman and Hall, (1940).

178. Hartshorn and Oliver, J.C.S., 123A, 664, (1929).

179. J. Nesbitt and R. C. Pink, Electrical Phenomena and Solid/Liquid Interface, Proc. second Int. Congress of Surface Activity, Butterworth, p16, (1957).

180. H. E. Taylor, Trans. Faraday Soc., 52, 873, (1956).

181. Breckenridge, J. Chem. Phys., 16, 959, (1948).

182. Volger, Disc. Faraday Soc., 125, (1957).

TABLE I.

Natural Sodalite (ex A.S.T.M.)		Compound I (ex Bultitude) Cubic a=8.94 Å			Sample II Hydrated Cubic a=8.96 Å			Sample II Anhydrous Cubic a=9.02 Å			Sample II sealed into tube after thermogravimetric determination Cubic a=8.98Å		
d	I	hkl	I	d	hkl	I	d	hkl	I	d	hkl	I	d
6.3	17	110	v.s.	6.36	110	v.s.	6.34	110	v.s.	6.31	110	s.	6.25
4.42	3	200	w.	4.43	200	v.w.	4.48						
		210	w.	4.04									
3.63	100	211	v.s.	3.67	211	v.s.	3.66	211	v.s.	3.67	211	s.	3.63
		220	w.	3.15	220	w.	3.17						
2.81	5	301	s.	2.83	310	s.	2.84	310	m.	2.86	310	m.	2.85
2.56	13	222	v.s.	2.58	222	s.	2.58	222	s.	2.61	222	s.	2.59
2.37	17	312	w.	2.39	321	w.	2.40	321	w.	2.41			
2.08	33	303	s.	2.11	411	s.	2.11	400	m.	2.25			
1.98	2	402	v.w.	2.01				411	s.	2.12	411	s.	2.12
1.88	2	332	v.w.	1.90	332	v.v.w.	1.88	332	v.v.w.	1.93			
1.80	2	224	w.	1.83	422	w.	1.83						
1.73	2	314	m.s.	1.75	431	m.	1.76	510	m.	1.77	510	m.	1.76
1.61	1	215	w.	1.63	521	v.v.w.	1.64	521	w.	1.65			
1.56	10	404	m.s.	1.59	440	m.	1.59	440	m.	1.60	440	m.	1.59
1.52	5	334	m.	1.54	530	w.m.	1.54	433	w.	1.55	433	w.m.	1.54
1.48	7	600	m.	1.49	442	w.	1.50	442	v.w.	1.51	442	w.m.	1.50
1.43	8	611	m.	1.45	611	w.	1.45	611	w.	1.47	611	w.m.	1.46
1.40	1	620	v.v.w.	1.42									
1.37	2	541	w.	1.38	541	w.	1.38						
1.33	2	622	m.	1.35	622	m.	1.35	622	m.	1.37	622	w.	1.35
1.31	2	631	w.	1.32	631	v.w.	1.31	631	v.v.w.	1.33			
1.28	1	444	w.	1.29	444	v.v.w.	1.28	444	v.w.	1.31			
					453	v.v.w.	1.26	453	v.v.w.	1.28			
1.20	7				721	w.	1.22	721	w.	1.23	721	w.	1.22
1.12	3												

TABLE II.

Hydrated Basic Sodalite, Run 2A, 30°C, Bridge.

Frequency	$C_{p(app)}$ pF	ϵ^1_{app}	$R_{p(app)}$ Ω	$\tan\delta_{app}$
500 c/s	2539	153	3863	32.5
560	2201	133	3854	33.5
620	1963	118	3848	34.0
700	1722	104	3843	34.4
800	1496	90.1	3834	34.7
890	1378	83.0	3828	33.9
1.0kc/s	1210	72.9	3824	34.4
1.15	1064	64.1	3816	34.1
1.3	966.8	58.2	3810	33.2
1.6	794.2	47.8	3793	33.0
2.0	659.7	39.7	3778	31.9
2.5	545.0	32.8	3765	31.0
3.2	450.0	27.1	3747	29.5
4.0	385.0	23.2	3734	27.7
5.0	332.1	20.0	3719	25.8
6.3	286.7	17.3	3707	23.8
8.0	249.3	15.0	3689	21.6
10	221.4	13.3	3678	19.5
13	197.1	11.9	3663	17.0
16	181.5	10.9	3650	15.0
20	168.3	10.1	3645	13.0
25	161.3	9.72	3623	10.9
32	152.6	9.19	3599	9.06
40	143.5	8.64	3581	7.74
50	137.7	8.30	3567	6.48

TABLE III.

Hydrated Basic Sodalite, Run 2B, 30°C, H.-W. apparatus.

Frequency	$C_{p(app)}$ pF	ϵ'_{app}	$R_{p(app)}$ Ω	$\tan\delta_{app}$
216 kc/s	115.3	6.95	2859	2.24
256	112.3	6.77	2754	2.01
313	110.8	6.67	2795	1.64
417	103.2	6.22	2512	1.47
509	99.9	6.02	2470	1.27
621	93.4	5.63	2296	1.20
770	91.9	5.54	2144	1.05
890	88.3	5.32	1991	1.02
1.1 mc/s	83.8	5.05	1861	0.928
1.317	79.5	4.79	1803	0.843
1.77	73.8	4.45	1584	0.769
2.07	71.0	4.28	1461	0.741
2.54	67.3	4.05	1336	0.697
3.22	62.9	3.79	1243	0.632
4.3	59.0	3.55	1071	0.586
5.3	57.8	3.48	988	0.526
6.52	56.5	3.40	882	0.490
7.6	55.9	3.37	811	0.462
8.8	55.2	3.33	726	0.451
10.9	55.3	3.33	626	0.422
12.97	58.6	3.53	518	0.404
16.0	65.3	3.93	409	0.372

TABLE IV.

Hydrated Basic Sodalite, Run 3A, 50°C, Bridge.

Frequency	$Cp_{(app)}$ pF	ϵ^1_{app}	$Rp_{(app)}$ Ω	$\tan\delta_{app}$
560 c/s	4112	248	2882	24.0
620	3726	225	2874	24.0
700	3339	201	2868	23.7
800	2979	179	2855	23.4
890	2755	166	2853	22.8
1.0 kc/s	2509	151	2843	22.3
1.15	2271	137	2832	21.5
1.3	2069	125	2825	21.0
1.6	1802	109	2809	19.7
2.0	1571	94.6	2790	18.2
2.5	1374	82.8	2769	16.7
3.2	1202	72.4	2743	15.1
4.0	1060	63.8	2718	13.8
5.0	916.0	55.2	2690	12.9
6.3	793.2	47.8	2657	12.0
8.0	648.2	39.1	2622	11.7
10.0	541.6	32.6	2588	11.4
13.0	438.6	26.4	2546	11.0
16.0	373.3	22.5	2520	10.6
20.0	315.8	19.0	2487	10.1
25.0	269.3	16.2	2463	9.60
32.0	226.7	13.7	2436	9.01
40.0	199.0	12.0	2416	8.28
50.0	182.0	11.0	2404	7.28

TABLE V.

Hydrated Basic Sodalite, Run 3B, 50°C, H.-W. apparatus.

Frequency	$C_{p(app)}$ pF	ϵ^1_{app}	$R_{p(app)}$ Ω	$\tan\delta_{app}$
216 kc/s	120.6	7.27	2446	2.50
256	123.1	7.42	2377	2.13
313	113.6	6.84	2351	1.90
417	109.6	6.60	2197	1.59
509	107.3	6.46	2076	1.40
621	100.4	6.05	1968	1.30
770	96.8	5.83	1870	1.14
890	93.4	5.63	1788	1.07
1.1 mc/s	88.3	5.32	1639	1.000
1.317	83.8	5.05	1592	0.906
1.77	77.4	4.66	1422	0.817
2.07	74.8	4.51	1325	0.776
2.54	71.4	4.30	1224	0.717
3.22	67.2	4.05	1096	0.671
4.3	63.1	3.80	927	0.633
5.3	61.3	3.69	843	0.581
6.52	59.6	3.59	758	0.540
7.6	58.4	3.52	687	0.522
8.8	58.1	3.50	629	0.495
10.9	58.1	3.50	561	0.448
12.97	60.9	3.67	426	0.473

TABLE VI.

Hydrated Basic Sodalite, Run 4A, 80°C, Bridge.

Frequency	$C_{p(app)}$ pF	ϵ'_{app}	$R_{p(app)}$ Ω	$\tan\delta_{app}$
320 c/s	8386	505	7348	8.07
400	6686	403	7272	8.18
500	5439	328	7162	8.17
560	4955	299	7091	8.09
620	4588	276	7000	7.99
700	4161	251	6971	7.84
800	3762	227	6963	7.60
890	3497	211	6905	7.41
1.0 kc/s	3223	194	6845	7.21
1.15	2936	177	6762	6.97
1.3	2726	164	6681	6.72
1.6	2395	144	6533	6.36
2.0	2085	126	6369	5.99
2.5	1825	110	6204	5.62
3.2	1581	95.2	6018	5.23
4.0	1373	82.7	5819	4.98
5.0	1191	71.7	5622	4.75
6.3	1015	61.1	5430	4.59
8.0	833.0	50.2	5185	4.61
10.0	670.7	40.4	4993	4.75
13	532.9	32.1	4787	4.80
16	435.6	26.2	4633	4.93
20	355.3	21.4	4501	4.98
25	285.3	17.2	4414	5.06
32	243.7	14.7	4340	4.70
40	209.3	12.6	4288	4.43
50	182.3	11.0	4243	4.12

TABLE VII.

Hydrated Basic Sodalite, Run 4B, 80°C, H.-W. apparatus.

Frequency	$Cp_{(app)}$ pF	ϵ^1_{app}	$Rp_{(app)}$ Ω	$\tan\delta_{app}$
63 kc/s	163.9	9.87	-	-
74	164.2	8.89	4036	3.25
101.2	151.5	9.13	3979	2.61
122	142.4	8.58	3988	2.30
151	135.7	8.17	3826	2.03
216	115.3	6.95	4161	1.54
256	114.8	6.92	3874	1.40
313	104.3	6.28	3824	1.28
417	103.2	6.22	3473	1.07
509	95.2	5.73	3298	0.996
621	91.8	5.53	3021	0.924
770	87.3	5.26	2832	0.836
890	83.0	5.00	2667	0.808
1.1 mc/s	78.3	4.72	2477	0.746
1.317	75.7	4.56	2324	0.687
1.77	70.8	4.27	2079	0.611
2.07	68.1	4.10	1907	0.592
2.54	64.8	3.90	1771	0.546
3.22	62.5	3.77	1554	0.509
4.3	58.2	3.51	1309	0.486
5.3	56.4	3.40	1218	0.437
6.52	56.4	3.40	1085	0.399
7.6	55.6	3.35	999	0.377
8.8	55.9	3.37	896	0.361
10.9	56.0	3.37	751	0.347
12.97	59.5	3.58	616	0.335
16.0	66.4	4.00	504	0.297
19.85	74.2	4.47	307	
23.0	94.8	5.71	178	

TABLE VIII.

Hydrated Basic Sodalite, Run 5A, 114.7°C, Bridge.

Frequency	$Cp_{(app)}$ pF	ϵ^1_{app}	$Rp_{(app)}$ Ω	$\tan\delta_{app}$
320 c/s	2637	159	97880	1.93
400	2334	141	90380	1.89
500	2095	126	83790	1.81
560	1974	119	80540	1.79
620	1860	112	77390	1.78
700	1739	105	73570	1.78
800	1587	95.6	69820	1.80
890	1468	88.5	66880	1.82
1.0 kc/s	1261	76.0	63800	1.98
1.15	1105	66.6	60670	2.06
1.8	740.4	44.6	53220	2.24
2.0	618.3	37.3	50810	2.53
2.2	589.7	35.5	49740	2.47
2.5	567.0	34.2	48950	2.29
2.8	505.4	30.5	47790	2.35
3.2	440.6	26.5	46060	2.45
4.0	364.3	22.0	44330	2.46
5.0	306.0	18.4	42980	2.42
6.3	266.7	16.1	41800	2.27
8.0	237.6	14.3	40610	2.06
10	217.2	13.1	39430	1.86
13	198.9	12.0	37950	1.62
16	187.7	11.3	36600	1.45
20	176.8	10.7	35020	1.29
25	166.7	10.0	33130	1.15
32	157.9	9.51	31060	1.01
40	150.3	9.05	28890	0.92
50	145.5	8.77	26660	0.82

TABLE IX.

Hydrated Basic Sodalite, Run 5B, 114.7°C, H.-W. apparatus.

Frequency	$C_{p(app)}$ pF	ϵ^1_{app}	$R_{p(app)}$ Ω	$\tan\delta_{app}$
63 kc/s	128.4	7.73	24380	0.807
74	126.4	7.61	22630	0.752
101.2	116.0	6.99	19910	0.681
122	107.9	6.50	17960	0.673
151	103.6	6.24	17330	0.587
216	93.6	5.64	14240	0.553
256	89.1	5.37	12870	0.542
313	84.9	5.11	11580	0.517
417	79.3	4.78	9883	0.487
509	76.6	4.61	8874	0.460
621	73.9	4.45	7829	0.443
770	70.2	4.23	7078	0.416
890	68.2	4.11	6458	0.406
1.1 mc/s	64.7	3.90	5719	0.391
1.317	62.9	3.79	5165	0.372
1.77	59.2	3.57	4377	0.347
2.07	57.6	3.47	3949	0.338
2.54	56.0	3.37	3508	0.319
3,22	54.7	3.30	2982	0.303
4.3	51.8	3.12	2358	0.303
5.3	49.1	2.96	2200	0.278
6.52	50.8	3.06	1907	0.252
7.6	50.0	3.01	1724	0.243
8.8	49.8	3.00	1539	0.236
10.9	51.1	3.08	1264	0.226
12.92	54.3	3.27	986	0.230
16.0	61.1	3.68	664	0.245
19.85	68.8	4.14	447	0.261
23.0	87.1	5.25	266	0.299

TABLE X.

Anhydrous Basic Sodalite, Run 16A, -183°C, Bridge.

Frequency	$Cp_{(app)}$ pF	ϵ'_{app}
500 c/s	21.25	1.77
800	21.30	1.78
1.3 kc/s	21.25	1.77
2.0	21.25	1.77
3.2	21.25	1.77
5.0	21.15	1.76
7.0	21.25	1.77
13	21.15	1.76
20	21.10	1.76
32	21.05	1.75
50	21.05	1.75

TABLE XI.

Anhydrous Basic Sodalite, Run 18, -183°C, Bridge.

Frequency	$Cp_{(app)}$ pF	ϵ'_{app}	$Rp_{(app)}$ meg.Ω	$\tan\delta_{app}$
1.6 kc/s	21.35	1.78	473	0.0099
2.5	21.30	1.78	354	0.0085
4.0	21.30	1.78	232	0.0081
6.3	21.25	1.77	144	0.0082
10	21.15	1.76	116	0.0065
16	21.15	1.76	81.9	0.0057
25	21.15	1.76	56.4	0.0053
40	21.10	1.76	37.2	0.0051

TABLE XII.

Anhydrous Basic Sodalite, Run 29, -183°C, Bridge.

Frequency	$C_{p(app)}$ pF	ϵ'_{app}	$R_{p(app)}$ meg. Ω	$\tan\delta_{app}$
2.0 kc/s	21.40	1.78	402	0.0093
2.5	21.40	1.78	344	0.0087
3.2	21.35	1.78	279	0.0084
4.0	21.35	1.78	236	0.0079
5.0	21.35	1.78	190	0.0078
8.0	21.30	1.78	137	0.0068
10	21.35	1.78	120	0.0062
13	21.30	1.78	88.5	0.0065
16	21.25	1.77	82.7	0.0057
20	21.25	1.77	65.1	0.0058
25	21.25	1.77	51.7	0.0058
32	21.25	1.77	-	-
40	21.25	1.77	-	-
50	21.25	1.77	-	-

TABLE XIII.

Anhydrous Basic Sodalite, Run 16B, -183°C, H.-W. apparatus.

Frequency	$Cp_{(app)}$ pF	ϵ'_{app}	$Rp_{(app)}$ meg. Ω	$\tan\delta_{app}$
74 kc/s	21.15	1.76	21.8	0.0047
122	21.00	1.75	14.4	0.0043
216	21.00	1.75	9.15	0.0038
313	21.00	1.75	6.74	0.0036
509	21.00	1.75	4.17	0.0036
770	21.05	1.75	2.68	0.0037
1.10 mc/s	21.00	1.75	2.00	0.0035
1.77	21.05	1.75	1.17	0.0036
2.54	21.20	1.77	0.841	0.0035
3.70	21.25	1.77	0.584	0.0035
5.30	21.15	1.76	0.313	-

TABLE XIV.

Anhydrous Basic Sodalite, Run 17, -183°C, H.-W. apparatus

Frequency	$Cp_{(app)}$ pF	ϵ'_{app}	$Rp_{(app)}$ meg. Ω	$\tan\delta_{app}$
63 kc/s	20.95	1.75	25.6	0.0047
101	21.00	1.75	19.1	0.0039
151	21.00	1.75	13.4	0.0037
256	20.95	1.75	-	-
2.07 mc/s	21.15	1.76	1.09	0.0033

TABLE XV.

Anhydrous Basic Sodalite, Run 12A, 30°C, Bridge.

Frequency	$Cp_{(app)}$ pF	ϵ'_{app}	$Rp_{(app)}$ meg.Ω	$\tan\delta_{app}$
320 c/s	22.15	1.85	-	-
500	22.15	1.85	-	-
800	22.05	1.84	-	-
1.3 kc/s	21.95	1.83	591	0.0094
2.0	22.00	1.83	397	0.0091
3.2	21.90	1.83	274	0.0083
5.0	21.95	1.83	186	0.0078
7.0	21.95	1.83	131	0.0079
13	21.90	1.83	83.8	0.0067
20	21.80	1.82	56.6	0.0064
32	21.90	1.83	38.6	0.0059
50	21.85	1.82	23.8	0.0061

TABLE XVI.

Anhydrous Basic Sodalite, Run 20, 30°C, Bridge.

Frequency	$C_{p(app)}$ pF	ϵ'_{app}	$R_{p(app)}$ meg.Ω	$\tan\delta_{app}$
620 c/s	21.75	1.81	-	-
1.0 kc/s	21.85	1.82	-	-
1.6	21.85	1.82	-	-
2.5	21.75	1.81	-	-
4.0	21.70	1.81	227	0.0081
6.3	21.75	1.81	151	0.0077
10	21.70	1.81	104	0.0070
16	21.70	1.81	68.9	0.0067
25	21.70	1.81	47.2	0.0062
40	21.65	1.80	29.1	0.0063

TABLE XVII.

Anhydrous Basic Sodalite, Run 28, 30°C, Bridge.

Frequency	$C_{p(app)}$ pF	ϵ'_{app}	$R_{p(app)}$ meg.Ω	$\tan\delta_{app}$
1.3 kc/s	21.80	1.82	-	-
1.6	21.85	1.82	479	0.0095
2.0	21.90	1.83	431	0.0085
2.5	21.90	1.83	361	0.0080
3.2	21.80	1.82	282	0.0081

TABLE XVIII.

Anhydrous Basic Sodalite, Run 12B, 30°C, H.-W. apparatus

Frequency	$Cp_{(app)}$ pF	ϵ'_{app}	$Rp_{(app)}$ meg.Ω	$\tan\delta_{app}$
74 kc/s	21.60	1.80	18.2	0.0055
122	21.75	1.81	11.0	0.0054
216	21.75	1.81	6.92	0.0049
313	21.65	1.80	4.73	0.0050
509	21.75	1.81	3.02	0.0048
770	21.75	1.81	1.45	0.0066
1.32 mc/s	21.95	1.83	0.798	0.0069
2.07	21.90	1.82	0.388	0.0090
3.22	22.05	1.84	-	-
5.30	22.45	1.87	0.0726	-
8.80	22.80	1.90	-	-

TABLE XIX.

Anhydrous Basic Sodalite, Run 21, 30°C, H.-W. apparatus.

Frequency	$Cp_{(app)}$ pF	ϵ'_{app}	$Rp_{(app)}$ meg.Ω	$\tan\delta_{app}$
151 kc/s	21.55	1.80	9.58	0.0051
1.10 mc/s	21.55	1.80	1.07	0.0063
1.77	21.70	1.81	0.482	0.0086

TABLE XX.

Anhydrous Basic Sodalite, Run 27, 30°C, Q-meter.

Frequency	$Cp_{(app)}$ pF	ϵ'_{app}	$Rp_{(app)}$ meg.Ω	$\tan\delta_{app}$
10 mc/s	22.80	1.90	-	-
13	23.20	1.93	-	-
16	24.45	2.04	-	-
20	26.15	2.18	-	-
25	34.55	2.88	-	-

TABLE XXI.

Anhydrous Basic Sodalite, Run 14A, 80°C, Bridge.

Frequency	$Cp_{(app)}$ pF	ϵ'_{app}	$Rp_{(app)}$ meg.Ω	$\tan\delta_{app}$
320 c/s	22.80	1.90	-	-
400	22.95	1.91	-	-
620	22.70	1.89	326	0.0347
1.0 kc/s	22.60	1.88	246	0.0286
1.6	22.45	1.87	180	0.0246
2.5	22.35	1.86	134	0.0213
4.0	22.25	1.85	95.7	0.0187
6.3	22.25	1.85	66.2	0.0172
10	22.20	1.85	45.0	0.0159
16	22.10	1.84	31.7	0.0142
25	22.15	1.85	21.9	0.0131
40	22.15	1.85	14.6	0.0123

TABLE XXII.

Anhydrous Basic Sodalite, Run 23, 80°C, Bridge.

Frequency	$Cp_{(app)}$ pF	ϵ'_{app}	$Rp_{(app)}$ meg. Ω	$\tan\delta_{app}$
1.3 kc/s	22.30	1.86	207	0.0265
2.0	22.25	1.85	156	0.0230
3.2	22.15	1.85	111	0.0203
5.0	22.05	1.84	78.2	0.0185
7.0	22.05	1.84	60.0	0.0172
13	22.00	1.83	36.7	0.0152
20	21.95	1.83	26.3	0.0138
32	21.95	1.83	18.0	0.0126
50	21.90	1.83	11.6	0.0126

TABLE XXIII.

Anhydrous Basic Sodalite, Run 14B, 80°C, H.-W. apparatus.

Frequency	$Cp_{(app)}$ pF	ϵ'_{app}	$Rp_{(app)}$ meg. Ω	$\tan\delta_{app}$
63 kc/s	21.80	1.82	10.5	0.0110
101	21.90	1.82	7.44	0.0096
151	21.80	1.82	5.44	0.0089
256	21.85	1.82	3.77	0.0076
417	21.80	1.82	2.24	0.0078
739	21.90	1.82	1.38	0.0071
1.10 mc/s	22.00	1.83	0.785	0.0084
1.77	22.05	1.84	0.422	0.0097
2.54	22.20	1.85	0.275	0.0103
4.30	21.80	1.82	-	-
7.60	22.60	1.88	0.0668	0.0137

TABLE XXIV.

Anhydrous Basic Sodalite, Run 22, 80°C, H.-W. apparatus.

Frequency	$Cp_{(app)}$ pF	ϵ'_{app}	$Rp_{(app)}$ meg.Ω	$\tan\delta_{app}$
216 kc/s	21.70	1.81	4.03	0.0084
313	21.65	1.80	2.90	0.0081
890	21.80	1.82	1.15	0.0072
1.58 mc/s	22.00	1.83	0.506	0.0091
2.07	21.80	1.82	0.365	0.0097

TABLE XXV.

Anhydrous Basic Sodalite, Run 25, 80°C, Q-meter.

Frequency	$Cp_{(app)}$ pF	ϵ'_{app}	$Rp_{(app)}$ meg.Ω	$\tan\delta_{app}$
4.25 mc/s	-	-	0.177	-
5.0	22.10	1.84	0.114	0.0127
6.30	-	-	0.0873	-
8.00	22.70	1.89	0.0674	-
10.0	22.85	1.90	-	-
10.5	23.10	1.93	-	-
16.0	24.80	2.07	0.0340	-
20.0	26.45	2.20	0.0215	-
25.0	31.20	2.60	0.0116	-
32.0	59.00	4.92	-	-

TABLE XXVI.

Anhydrous Basic Sodalite, Run 31, Bridge.

Constant Frequency: 5 kc/s.

Temperature °C	1/T (T=°absolute)	$Cp_{(app)}$ pF	ϵ'_{app}	$Rp_{(app)}$ meg.Ω	$\tan\delta_{app}$
-183.0	11.09	21.35	1.78	190	0.0078
-147.2	7.94	21.90	1.82	470	0.0031
-121.9	6.61	21.90	1.82	515	0.0028
-100.3	5.79	21.85	1.82	402	0.0036
-66.1	4.83	21.75	1.81	369	0.0040
30.0	3.30	21.95	1.83	186	0.0078
80.0	2.83	22.05	1.84	78.2	0.0185
130.2	2.48	23.40	1.95	24.9	0.0546
171.0	2.25	25.85	2.15	8.23	0.150
205.8	2.09	28.90	2.41	3.33	0.331
250.0	1.91	41.85	3.49	1.24	0.616

TABLE XXVII.

Anhydrous Basic Sodalite, Run 19, Bridge.
Constant Frequency: 32 kc/s.

Temperature °C	1/T (T=°absolute)	$Cp_{(app)}$ pF	ϵ'_{app}	$Rp_{(app)}$ meg	$\tan\delta_{app}$
-183.0	11.09	21.25	1.77	35.7	0.0066
-147.7	7.97	21.85	1.82	54.3	0.0042
-122.1	6.62	21.85	1.82	86.8	0.0026
-100.3	5.79	21.85	1.82	83.6	0.0027
-66.1	4.83	21.80	1.82	74.8	0.0031
0.0	3.66	21.80	1.82	-	-
30.0	3.30	21.90	1.82	38.6	0.0059
39.4	3.20	21.70	1.81	33.5	0.0068
49.9	3.10	21.80	1.82	28.5	0.0080
59.0	3.01	21.85	1.82	25.0	0.0091
69.5	2.92	21.90	1.82	21.1	0.0107
80.0	2.83	21.95	1.83	18.0	0.0126
130.2	2.48	22.75	1.90	7.34	0.0298
171.0	2.25	23.70	1.98	3.15	0.0666
205.8	2.09	25.45	2.12	1.43	0.137
250.0	1.91	30.65	2.55	0.518	0.314

TABLE XXVIII.

Hydrated AgA($AgNO_3$), Run 8A, 30°C, Bridge.

Frequency	$Cp_{(app)}$ pF	ϵ'_{app}	$Rp_{(app)}$ Ω	$\tan\delta_{app}$
400 c/s	3663	231	74440	1.46
530	2710	171	65700	1.69
620	2274	143	61990	1.82
800	1683	106	57250	2.06
1.0 kc/s	1318	83.1	54440	2.22
1.3	1033	65.2	51720	2.29
1.6	847.6	53.5	49930	2.35
2.0	697.8	44.0	48310	2.36
2.5	598.0	37.7	46760	2.28
3.2	507.4	32.0	45080	2.17
4.0	451.4	28.5	43610	2.02
5.0	409.1	25.8	42150	1.85
6.3	373.9	23.6	40550	1.67
8.0	344.0	21.7	38860	1.48
10	320.8	20.2	37150	1.34
13	292.8	18.5	35220	1.19
16	277.9	17.5	33580	1.07
20	262.8	16.6	31760	0.953
25	249.7	15.8	29920	0.852
32	236.7	14.9	27860	0.754
40	226.9	14.3	25900	0.677
50	218.2	13.8	24020	0.608

TABLE XXIX.

Hydrated AgA($AgNO_3$), Run 8B, 30°C, H.-W. apparatus.

Frequency	$Cp_{(app)}$ pF	ϵ'_{app}	$Rp_{(app)}$ Ω	$\tan\delta_{app}$
74 kc/s	203.3	12.8	21700	0.487
101	194.4	12.3	18630	0.434
151	182.7	11.5	15410	0.374
216	175.7	11.1	-	-
256	172.5	10.9	11050	0.326
313	168.2	10.6	9595	0.315
417	161.0	10.2	7825	0.303
509	156.9	9.90	6830	0.292
621	152.7	9.64	5597	0.300
770	149.3	9.42	4649	0.298
1.10 mc/s	139.4	8.80	3336	0.311
1.32	136.1	8.59	2861	0.310
1.77	127.5	8.04	2136	0.331
2.07	124.1	7.83	1814	0.341
2.54	119.6	7.55	1547	0.339
3.22	114.2	7.20	1218	0.356
4.30	107.8	6.80	934	0.368
5.30	104.3	6.58	785	0.367
6.52	98.90	6.24	601	0.410
7.60	97.65	6.16	507	0.423
8.80	98.95	6.24	452	0.405
10.9	101.9	6.43	357	0.402

TABLE XXX.

Hydrated AgA($AgNO_3$), Run 10A, 80°C, Bridge.

Frequency	$Cp_{(app)}$ pF	ϵ'_{app}	$Rp_{(app)}$ Ω	$\tan\delta_{app}$
1.3 kc/s	10680	674	1856	6.24
1.6	9387	592	1824	5.81
2.0	8070	509	1789	5.51
2.5	6992	441	1754	5.19
3.2	5976	377	1710	4.87
4.0	5120	323	1664	4.67
5.0	4505	284	1626	4.35
6.3	3945	249	1584	4.04
8.0	3435	217	1527	3.79
10	3033	191	1478	3.55
13	2596	164	1419	3.32
16	2299	145	1367	3.17
20	2000	126	1310	3.04
25	1728	109	1252	2.94
32	1466	92.5	1187	2.86
40	1246	78.6	1128	2.83
50	995	62.8	1076	2.97

TABLE XXXI.

Hydrated AgA($AgNO_3$), Run 10B, 80°C, H.W.-apparatus.

Frequency	$Cp_{(app)}$ pF	ϵ'_{app}	$Rp_{(app)}$ Ω	$\tan\delta_{app}$
1.77 mc/s	192.9	12.2	-	-
2.07	186.4	11.8	-	-
2.54	182.4	11.5	462	0.743
3.22	174.8	11.0	398	0.711
4.30	167.4	10.6	323	0.686

TABLE XXXII.

Anhydrous AgA($AgNO_3$), Run 41, 0°C, Bridge.

Frequency	$Cp_{(app)}$ pF	ϵ'_{app}	$Rp_{(app)}$ Ω	$\tan\delta_{app}$
320 c/s	296.2	18.7	1550000	1.083
500	251.8	15.9	1377000	0.918
800	223.4	14.1	1185000	0.751
1.3 kc/s	200.7	12.7	1015000	0.601
2.0	184.3	11.6	863600	0.500
3.2	170.3	10.7	714600	0.409
5.0	160.0	10.1	581800	0.342
8.0	151.1	9.53	452200	0.291
13	143.5	9.05	329500	0.259
20	134.7	8.50	239600	0.247
32	127.2	8.03	153100	0.255
50	119.2	7.52	97970	0.273

TABLE XXXIII.

Anhydrous AgA($AgNO_3$), Run 43, 0°C, Bridge.

Frequency	$Cp_{(app)}$ pF	ϵ'_{app}	$Rp_{(app)}$ Ω	$\tan\delta_{app}$
400 c/s	267.6	16.9	1482000	1.003
620	236.1	14.9	1322000	0.822
1.0 kc/s	210.7	13.3	1131000	0.668
1.6	191.2	12.1	957100	0.544
2.5	176.3	11.1	831800	0.434
4.0	164.1	10.4	673000	0.360
6.3	155.0	9.78	524500	0.311
10	147.1	9.28	398100	0.272
16	137.1	8.65	289800	0.250
25	131.2	8.28	193800	0.250
40	122.9	7.75	122900	0.263

TABLE XXXIV.

Anhydrous AgA($AgNO_3$), Run 42, 0°C, H.W.-apparatus.

Frequency	$Cp_{(app)}$ pF	ϵ'_{app}	$Rp_{(app)}$ Ω	$\tan\delta_{app}$
74 kc/s	110.8	6.99	63830	0.304
122	98.6	6.22	39490	0.335
216	86.4	5.45	23710	0.360
313	78.5	4.95	17830	0.363
509	69.7	4.40	12940	0.347
770	64.2	4.05	10110	0.319
1.10 mc/s	60.2	3.80	8417	0.286
2.07	55.7	3.51	6090	0.277
3.22	53.9	3.40	5393	0.170
5.30	53.6	3.38	-	-
7.60	54.1	3.41	2746	0.141

TABLE XXXV.

Anhydrous AgA($AgNO_3$), Run 33, 30°C, Bridge.

Frequency	$Cp_{(app)}$ pF	ϵ'_{app}	$Rp_{(app)}$ Ω	$\tan\delta_{app}$
320 c/s	-	-	219500	-
500	-	-	187900	-
800	750.0	47.3	161800	1.64
1.3 kc/s	512.7	32.4	144700	1.65
2.0	400.7	25.3	131500	1.51
3.2	325.2	20.5	117800	1.30
5.0	279.3	17.6	105500	1.08
8.0	242.6	15.3	92500	0.887
13	214.8	13.6	79540	0.717
20	195.9	12.4	68720	0.591
32	179.2	11.3	57370	0.484
50	166.8	10.5	47250	0.404

TABLE XXXVI.

Anhydrous AgA($AgNO_3$), Run 35, 30°C, Bridge.

Frequency	$Cp_{(app)}$ pF	ϵ'_{app}	$Rp_{(app)}$ Ω	$\tan\delta_{app}$
400 c/s	1288	81.2	205000	1.51
620	925.1	58.4	175100	1.58
1.0 kc/s	634.1	40.0	151800	1.65
1.6	462.9	29.2	135100	1.59
2.5	370.2	23.4	122200	1.41
4.0	305.3	19.3	108900	1.20
6.3	263.3	16.6	96690	0.992
10	231.1	14.6	84400	0.816
16	206.9	13.1	72590	0.662
25	188.8	11.9	61840	0.545
40	173.6	11.0	51090	0.449

TABLE XXXVII.

Anhydrous AgA($AgNO_3$), Run 34, 30°C, H.W.-apparatus.

Frequency	$Cp_{(app)}$ pF	ϵ'_{app}	$Rp_{(app)}$ Ω	$\tan\delta_{app}$
74 kc/s	156.3	9.86	37370	0.368
122	143.4	9.05	28570	0.318
216	134.3	8.47	18190	0.302
313	127.5	8.04	13930	0.286
509	119.2	7.52	8812	0.298
770	110.9	7.00	5939	0.314
1.32 mc/s	98.5	6.21	3549	0.346
2.07	89.3	5.63	2343	0.367
3.22	82.1	5.18	1603	0.376
5.30	72.7	4.59	1048	0.394
7.60	72.2	4.56	806	0.360

TABLE XXXVIII.

Anhydrous AgA($AgNO_3$), Run 37, 50°C, Bridge.

Frequency	$Cp_{(app)}$ pF	ϵ'_{app}	$Rp_{(app)}$ Ω	$\tan\delta_{app}$
320 c/s	3090	195	71170	2.26
500	2654	167	63700	1.88
800	2244	142	53580	1.65
1.3 kc/s	1727	109	44410	1.60
2.0	1302	82.1	38290	1.60
3.2	912.2	57.6	32570	1.67
5.0	652.2	41.2	28690	1.70
8.0	475.8	30.0	25610	1.63
13	362.3	22.9	22970	1.47
20	303.8	19.2	20830	1.26
32	260.5	16.4	18500	1.03
50	227.6	14.4	16370	0.854

TABLE XXXIX.

Anhydrous AgA($AgNO_3$), Run 39, 50°C, Bridge.

Frequency	$Cp_{(app)}$ pF	ϵ'_{app}	$Rp_{(app)}$ Ω	$\tan\delta_{app}$
400 c/s	2817	178	66210	2.13
620	2400	151	58430	1.83
1.0 kc/s	1983	125	49040	1.64
1.6	1497	94.5	41160	1.61
2.5	1088	68.7	35280	1.66
4.0	751.5	47.4	30430	1.74
6.3	553.3	34.9	27080	1.69
10	418.2	26.4	24370	1.56
16	330.5	20.9	21960	1.37
25	280.8	17.7	19720	1.15
40	240.8	15.2	17450	0.947

TABLE XL.

Anhydrous AgA($AgNO_3$), Run 38, 50°C, H.-W. apparatus.

Frequency	$C_{p(app)}$ pF	ϵ'_{app}	$R_{p(app)}$ Ω	$\tan\delta_{app}$
74 kc/s	199.8	12.6	-	-
122	182.2	11.5	12010	0.596
216	161.6	10.2	9659	0.472
313	153.7	9.70	8046	0.411
509	142.4	8.98	6010	0.365
770	134.5	8.49	4517	0.340
1.32 mc/s	125.8	7.94	2986	0.322
2.07	114.7	7.24	1975	0.339
3.22	110.5	6.97	1284	0.348
6.52	99.7	6.29	600	0.408
7.60	94.3	5.95	475	0.467

TABLE XLI.

Anhydrous AgA($AgNO_3$), Run 47, Bridge.
Constant Frequency: 5 kc/s.

Temperature °C	1/T (T=°absolute)	$Cp_{(app)}$ pF	ϵ'_{app}	$Rp_{(app)}$ Ω	$\tan\delta_{app}$
0	3.66	164.4	10.4	523500	0.370
10	3.53	193.4	12.2	303800	0.542
30	3.30	295.1	18.6	106400	1.01
40	3.19	408.5	25.8	62220	1.25
50	3.09	633.8	40.0	37740	1.33
60	3.00	1061	66.9	25290	1.19
70	2.91	1598	101	18420	1.08
80	2.83	2310	146	14840	0.929
90	2.75	3020	191	12110	0.870
100	2.68	3593	227	9677	0.915
109.9	2.61	4076	257	7372	1.06
120.2	2.54	4419	279	4904	1.47
130.2	2.48	4720	298	3115	2.17
140.4	2.42	5086	321	2246	2.79

TABLE XLII.

Anhydrous AgA($AgNO_3$), Run 46, Bridge.
Constant Frequency: 32 kc/s.

Temperature °C	1/T (T=°absolute)	$Cp_{(app)}$ pF	ε'_{app}	$Rp_{(app)}$ Ω	$\tan\delta_{app}$
0	3.66	131.3	8.28	161100	0.235
10	3.53	144.8	9.14	128000	0.268
30	3.30	182.7	11.5	56840	0.480
40	3.19	215.8	13.6	35290	0.653
50	3.09	258.9	16.3	21750	0.883
60	3.00	329.7	20.8	13660	1.10
70	2.91	432.0	27.3	8676	1.33
80	2.83	611.6	38.6	5837	1.39
90	2.75	891.1	56.2	4180	1.34
100	2.68	1265	79.8	3159	1.25
109.9	2.61	1734	109	2528	1.14
120.2	2.54	2287	144	2075	1.05
130.2	2.48	2753	174	1713	1.06
140.4	2.42	3199	202	1458	1.07

TABLE XLIII.

Hydrated Sodium Analcite, Run 144, 30°C, Bridge.

Frequency	$C_{p(app)}$ pF	ϵ'_{app}	$R_{p(app)}$ meg.-Ω	$\tan\delta_{app}$
250 c/s	161.4	8.23	9.89	0.399
320	151.5	7.73	7.96	0.412
400	142.5	7.27	6.57	0.425
500	133.9	6.83	5.48	0.434
630	124.7	6.36	-	-
800	116.5	5.94	3.77	0.453
1.0 kc/s	108.6	5.54	-	-
1.3	100.0	5.10	2.72	0.450
1.6	94.0	4.80	2.36	0.449
2.0	88.8	4.53	2.06	0.434
2.5	83.3	4.25	1.85	0.414
3.2	78.5	4.01	1.57	0.403
4.0	74.8	3.82	1.39	0.382
5.0	71.3	3.64	1.24	0.359
6.3	68.4	3.49	1.11	0.333
8.0	65.9	3.36	0.989	0.305
10	63.4	3.23	0.903	0.278
13	61.3	3.13	0.803	0.249
16	60.0	3.06	0.734	0.226
20	58.8	3.00	0.665	0.203
25	57.9	2.95	0.602	0.183
32	57.0	2.91	0.538	0.162
40	56.0	2.86	0.484	0.147
50	55.4	2.83	0.433	0.133
Check after 1 day without temperature change between				
13 kc/s	61.3	3.13	0.792	0.252
32	57.0	2.91	0.531	0.164

TABLE XLIV.

Hydrated Sodium Analcite, Run 145, 58°C, Bridge.

Frequency	$C_{p(app)}$ pF	ϵ'_{app}	$R_{p(app)}$ meg.-Ω	$\tan\delta_{app}$
250 c/s	217.3	11.09	7.45	0.393
320	209.8	10.70	6.27	0.378
400	202.8	10.35	5.32	0.369
500	195.4	9.97	4.43	0.368
630	185.1	9.44	3.52	0.388
800	177.7	9.07	2.90	0.386
1.0 kc/s	168.3	8.59	2.45	0.387
1.3	157.5	8.04	1.91	0.406
1.6	148.8	7.59	1.58	0.423
2.0	140.4	7.16	1.32	0.428
2.5	130.4	6.65	-	-
3.2	121.2	6.18	0.909	0.451
4.0	113.7	5.80	0.769	0.455
5.0	106.2	5.42	0.656	0.457
6.3	99.6	5.08	0.561	0.452
8.0	93.3	4.76	0.481	0.443
10	88.2	4.50	0.419	0.431
13	82.5	4.21	0.360	0.413
16	78.9	4.03	0.320	0.394
20	72.8	3.71	0.291	0.376
25	69.6	3.55	0.258	0.354
32	66.7	3.40	0.227	0.329
40	63.8	3.26	0.206	0.303
50	62.5	3.19	0.188	0.271
Check after 2 days without temperature change in between.				
2.5 kc/s	126.7	6.46	-	-
25	68.2	3.48	0.272	0.343

TABLE XLV.

Hydrated Sodium Analcite, Run 148, 90°C, Bridge.

Frequency	$Cp_{(app)}$ pF	ϵ'_{app}	$Rp_{(app)}$ meg.-Ω	$\tan\delta_{app}$
250 c/s	250.7	12.79	-	-
320	241.5	12.32	3.61	0.571
400	233.6	11.92	3.31	0.515
500	226.9	11.58	3.00	0.467
630	220.6	11.26	2.69	0.427
800	213.4	10.89	2.30	0.406
1.0 kc/s	204.7	10.44	2.01	0.386
1.3	195.0	9.95	1.64	0.383
1.6	188.6	9.62	1.37	0.385
2.0	180.4	9.20	1.14	0.387
2.5	171.1	8.73	0.967	0.385
3.2	161.8	8.26	0.753	0.408
4.0	153.7	7.84	0.622	0.416
5.0	144.5	7.37	0.513	0.429
6.3	135.6	6.92	0.424	0.439
8.0	126.5	6.45	0.351	0.448
10	116.7	5.95	0.296	0.461
13	107.4	5.48	0.246	0.464
16	100.6	5.13	0.214	0.463
20	94.2	4.81	0.185	0.456
25	88.6	4.52	0.161	0.446
32	82.9	4.23	0.140	0.429
40	78.5	4.01	0.123	0.411
50	74.7	3.81	0.110	0.388
Check on day before without altering the temperature in between.				
13 kc/s	107.0	5.46	0.247	0.463
25	89.2	4.55	0.160	0.447

TABLE XLVI.

Hydrated Sodium Analcite, Run 149, 58°C, Bridge.

Frequency	$C_{p(app)}$ pF	ϵ'_{app}	$R_{p(app)}$ meg.-Ω	$\tan\delta_{app}$
320 c/s	191.5	9.77	5.78	0.450
400	183.6	9.37	4.97	0.436
500	175.8	8.97	4.20	0.431
630	168.8	8.61	3.56	0.421
800	158.3	8.08	2.86	0.440
1.0 kc/s	149.0	7.60	2.46	0.435
1.3	137.7	7.03	1.98	0.450
1.6	129.6	6.61	1.66	0.461
2.0	120.8	6.16	1.42	0.464
2.5	112.9	5.76	-	-
4.0	99.0	5.05	0.883	0.455
10	73.9	4.03	0.514	0.392
25	67.1	3.42	0.322	0.295
40	60.8	3.10	0.262	0.250

TABLE XLVII.

Hydrated Sodium Analcite, Run 150, 30°C, Bridge.

Frequency	$Cp_{(app)}$ pF	ϵ'_{app}	$Rp_{(app)}$ meg.-Ω	$\tan\delta_{app}$
250 c/s	144.6	7.38	-	-
320	135.2	6.90	7.69	0.478
400	126.9	6.47	6.58	0.476
500	119.2	6.08	5.61	0.476
630	110.4	5.63	4.83	0.474
800	104.1	5.31	4.07	0.470
1.0 kc/s	97.5	4.97	3.60	0.454
1.3	90.3	4.61	3.04	0.447
1.6	85.7	4.37	2.68	0.433
2.0	81.4	4.15	2.38	0.412
2.5	77.0	3.93	2.15	0.384
6.3	65.4	3.34	1.33	0.292
16	58.7	2.99	0.856	0.198
40	55.6	2.84	0.547	0.131

TABLE XLVIII.

Anhydrous Sodium Analcite, Run 155, 30°C, Bridge.

Frequency	$Cp_{(app)}$ pF	ϵ'_{app}	$Rp_{(app)}$ meg.-Ω	$\tan\delta_{app}$
250 c/s	227.6	11.61	-	-
320	224.8	11.47	13.6	0.163
400	221.9	11.32	11.9	0.151
500	220.0	11.22	9.95	0.145
630	218.4	11.14	8.26	0.140
800	215.5	10.99	6.38	0.145
1.0 kc/s	212.7	10.85	5.11	0.147
1.3	208.6	10.64	3.72	0.158
1.6	205.3	10.47	2.85	0.170
2.0	201.2	10.27	2.13	0.186
2.5	195.8	9.99	1.64	0.199
3.2	189.4	9.66	1.16	0.226
4.0	183.6	9.37	0.877	0.247
5.0	176.4	9.00	0.667	0.271
6.3	168.3	8.59	0.509	0.295
8.0	159.5	8.14	0.391	0.319
10	149.4	7.62	0.310	0.343
13	139.0	7.09	0.241	0.366
16	131.6	6.71	0.201	0.376
20	123.6	6.31	0.167	0.386
25	116.2	5.93	0.141	0.389_4
32	108.6	5.54	0.118	0.389
40	102.6	5.23	0.101	0.383
50	97.7	4.98	-	-

TABLE XLIX.

Anhydrous Sodium Analcite, Run 156, 30°C, H.W.-apparatus.

Frequency	$Cp_{(app)}$ pF	ϵ'_{app}	$Rp_{(app)}$ Ω	$\tan\delta_{app}$
63 kc/s	92.5	4.72	73800	0.370
74	90.7	4.63	66200	0.358
101	84.45	4.31	55600	0.335
122	81.0	4.13	50400	0.320
151	79,45	4.05	44100	0.301
216	74.0	3.78	35500	0.280
256	72.8	3.71	31800	0.269
313	70.75	3.61	28300	0.254
417	67.8	3.46	23400	0.241
509	66.45	3.39	20700	0.228
770	63.95	3.26	15400	0.209
890	62.5	3.19	14200	0.202
1.10 mc/s	61.05	3.11	12900	0.184
1.77	58.05	2.96	9100	0.170
2.07	57.4	2.93	8140	0.165
2.54	57.15	2.92	7180	0.153
3.22	55.5	2.83	6300	0.141

TABLE L.

Anhydrous Sodium Analcite, Run 160, 45°C, Bridge.

Frequency	$Cp_{(app)}$ pF	ϵ'_{app}	$Rp_{(app)}$ meg.-Ω	$\tan\delta_{app}$
320 c/s	233.1	11.89	9.09	0.235
400	229.6	11.71	8.38	0.207
500	226.3	11.55	7.73	0.182
630	223.6	11.41	6.99	0.162
800	220.7	11.26	6.06	0.149
1.0 kc/s	218.0	11.12	5.33	0.137
1.3	215.3	10.98	4.34	0.131
1.6	214.0	10.92	3.59	0.130
2.0	211.7	10.80	2.88	0.131
2.5	210.2	10.72	2.12	0.143
3.2	206.8	10.55	1.66	0.145
4.0	203.4	10.38	1.26	0.155
5.0	199.6	10.18	0.947	0.168
6.3	195.4	9.97	0.698	0.185
8.0	190.7	9.73	0.509	0.205
10	183.7	9.37	0.381	0.227
13	175.8	8.97	0.274	0.255
16	169.0	8.62	0.214	0.275
20	161.4	8.23	0.166	0.297
25	153.1	7.81	0.131	0.319
32	144.2	7.36	0.102	0.338
40	136.4	6.96	0.0825	0.354
50	129.4	6.60	-	-

TABLE LI.

Anhydrous Sodium Analcite, Run 159, 45°C, H.W.-apparatus.

Frequency	$C_{p(app)}$ pF	ϵ'_{app}	$R_{p(app)}$ Ω	$\tan\delta_{app}$
63 kc/s	118.45	6.04	54200	0.393
74	114.45	5.84	47800	0.393
101	104.25	5.32	38600	0.391
122	99.4	5.07	34100	0.385
151	94.6	4.83	29700	0.375
216	88.55	4.52	23700	0.352
256	85.45	4.36	21400	0.341
313	82.0	4.18	19100	0.324
417	78.3	3.99	16000	0.305
509	76.8	3.92	14300	0.286
770	70.75	3.61	10900	0.269
890	70.3	3.59	9920	0.256
1.10 mc/s	67.85	3.46	8640	0.247
1.77	64.4	3.29	6350	0.220
2.07	63.05	3.22	5690	0.214
2.54	61.9	3.16	5010	0.202
3.22	59.85	3.05	4280	0.193

TABLE LII.

Anhydrous Sodium Analcite, Run 157, 60°C, Bridge.

Frequency	$Cp_{(app)}$ pF	ϵ'_{app}	$Rp_{(app)}$ meg.-Ω	$\tan\delta_{app}$
320 c/s	259.5	13.24	5.05	0.380
400	251.1	12.81	4.69	0.338
500	244.2	12.46	4.39	0.297
630	237.7	12.13	4.09	0.260
800	232.4	11.86	3.77	0.227
1.0 kc/s	227.6	11.61	3.52	0.199
1.3	223.2	11.39	3.19	0.172
1.6	221.4	11.30	2.80	0.160
2.0	219.8	11.21	2.55	0.142
2.5	217.8	11.11	2.18	0.134
3.2	215.8	11.01	1.81	0.127
4.0	213.6	10.90	1.49	0.125
5.0	211.4	10.79	1.12	0.134
6.3	209.2	10.67	0.879	0.138
8.0	206.5	10.54	0.663	0.145
10	203.0	10.36	0.507	0.155
13	198.3	10.12	0.355	0.174
16	194.0	9.90	0.269	0.190
20	188.8	9.63	0.200	0.211
25	182.8	9.33	0.150	0.233
32	175.6	8.96	0.110	0.258
40	168.4	8.59	0.0836	0.283
50	161.4	8.23	0.0650	0.304
Check points 2 days later without temperature change in between.				
16 kc/s	194.0	9.90	0.271	0.189
32	175.3	8.94	0.110	0.258

TABLE LIII.

Anhydrous Sodium Analcite, Run 158, 60°C, H.W.-apparatus.

Frequency	$C_{p(app)}$ pF	ϵ'_{app}	$R_{p(app)}$ Ω	$\tan\delta_{app}$
63 kc/s	146.75	7.49	49100	0.350
74	141.85	7.22	42100	0.361
101	129.2	6.59	31400	0.387
122	124.5	6.35	26900	0.390
151	114.85	5.86	-	-
216	104.85	5.35	17500	0.401
256	101.3	5.17	15500	0.396
313	95.1	4.85	13700	0.390
417	91.1	4.65	11300	0.370
509	87.05	4.44	10100	0.357
770	81.1	4.14	7790	0.327
890	79.0	4.03	7090	0.320
1.10 mc/s	75.9	3.87	6260	0.305
1.77	70.5	3.60	4690	0.272
2.07	68.7	3.51	4190	0.267
2.54	67.45	3.44	3690	0.252
3.22	65.2	3.33	3150	0.241

TABLE LIV.

Anhydrous Sodium Analcite, Run 161, 30°C, Bridge.

Frequency	$Cp_{(app)}$ pF	ϵ'_{app}	$Rp_{(app)}$ meg.-Ω	$\tan\delta_{app}$
4 kc/s	183.2	9.35	0.944	0.230
13	141.6	7.22	0.253	0.342
20	126.7	6.46	0.173	0.362
25	119.5	6.10	0.145	0.368
32	112.1	5.72	0.121	0.368
40	106.4	5.43	0.103	0.364
50	101.6	5.18	0.0885	0.354

TABLE LV.

Anhydrous Sodium Analcite, Run 162, 45°C, Bridge.

Frequency	$Cp_{(app)}$ pF	ϵ'_{app}	$Rp_{(app)}$ meg.-Ω	$\tan\delta_{app}$
400 c/s	228.8	11.67	8.49	0.205
1.3 kc/s	214.8	10.96	4.41	0.129
4.0	202.8	10.35	1.27	0.154
13	175.6	8.96	0.277	0.252
40	136.6	6.97	0.0833	0.350

TABLE LVI.

Anhydrous Sodium Analcite, Run 163, 60°C, Bridge.

Frequency	$C_{p(app)}$ pF	ϵ'_{app}	$R_{p(app)}$ meg.-Ω	$\tan\delta_{app}$
400 c/s	249.3	12.72	4.82	0.331
1.3 kc/s	220.5	11.25	3.30	0.169
4.0	211.9	10.81	1.40	0.134
13	197.3	10.07	0.367	0.169
40	168.5	8.60	0.0857	0.276

TABLE LVII.

Leucite, Run 130, 30°C, Bridge.

Frequency	$Cp_{(app)}$ pF	ϵ'_{app}	$Rp_{(app)}$ meg.	$\tan\delta_{app}$
400 c/s	60.65	3.09	176	0.0373
500	60.45	3.08	154	0.0341
630	60.25	3.07	140	0.0299
800	60.05	3.06	124	0.0268
1.0 kc/s	59.95	3.06	110	0.0242
1.3	59.85	3.05	90.0	0.0227
1.6	59.65	3.04	76.9	0.0217
2.0	59.45	3.03	66.8	0.0200
2.5	59.25	3.02	58.9	0.0183
3.2	59.05	3.01	48.1	0.0175
4.0	58.95	3.01	41.2	0.0164
5.0	58.85	3.00	35.1	0.0154
6.3	58.85	"	29.7	0.0144
8.0	58.75	3.00	25.0	0.0136
10	58.65	2.99	21.2	0.0128
13	58.55	2.99	17.4	0.0120
16	58.55	"	14.9	0.0114
20	58.55	"	12.7	0.0107
25	58.35	2.98	10.6	0.0102
32	"	"	8.66	0.0098
40	"	"	7.11	0.0096
50	"	"	5.67	0.0096

TABLE LVIII.

Leucite, Run 131, 30°C, H.W.-apparatus.

Frequency	$Cp_{(app)}$ pF	ϵ'_{app}	$Rp_{(app)}$ meg.-Ω	$\tan\delta_{app}$
63 kc/s	58.05	2.96	5.03	0.0087
74	58.35	2.98	4.65	0.0079
101	58.20	2.97	3.54	0.0076
122	58.30	2.97	3.05	0.0073
151	58.15	2.97	2.65	0.0068
216	58.15	2.97	1.97	0.0064
256	57.80	2.95	1.75	0.0062
313	58.10	2.96	1.42	0.0062
417	58.30	2.97	1.15	0.0057
509	57.85	2.95	0.979	0.0055
770	57.60	2.94	0.715	0.0050
890	58.10	2.96	0.652	0.0047
1.10 mc/s	57.85	2.95	0.514	0.0049
1.77	57.90	2.95	0.378	0.0041
2.07	58.05	2.96	0.326	0.0041
2.54	58.15	2.97	0.268	0.0040
3.22	57.60	2.94	0.210	0.0041

TABLE LIX.

Leucite, Run 132, 60°C, Bridge.

Frequency	$C_{p(app)}$ pF	ϵ'_{app}	$R_{p(app)}$ meg.-Ω	$\tan\delta_{app}$
320 c/s	65.45	3.34	82.2	0.0924
400	65.35	3.33	68.6	0.0888
500	64.75	3.30	61.8	0.0796
630	63.85	3.26	55.7	0.0710
800	63.35	3.23	49.4	0.0636
1.0 kc/s	62.85	3.21	43.4	0.0583
1.3	62.35	3.18	37.5	0.0524
1.6	62.15	3.17	32.6	0.0491
2.0	61.85	3.16	28.8	0.0447
2.5	61.45	3.14	26.0	0.0399
3.2	61.15	3.12	22.0	0.0370
4.0	60.85	3.10	19.2	0.0340
5.0	60.65	3.09	16.7	0.0315
6.3	60.45	3.08	14.4	0.0290
10	60.05	3.06	10.7	0.0248
13	59.85	3.05	8.99	0.0228
16	59.75	3.05	7.82	0.0213
20	59.55	3.04	6.73	0.0199
25	59.45	3.03	5.74	0.0186
32	59.35	3.03	4.76	0.0176
40	59.25	3.02	4.06	0.0166
50	59.15	3.02	3.45	0.0156

TABLE LX.

Leucite, Run 133, 60°C, H.W.-apparatus.

Frequency	$C_{p(app)}$ pF	ϵ'_{app}	$R_{p(app)}$ meg.-Ω	$\tan\delta_{app}$
63 kc/s	53.85	3.00	2.96	0.0145
74	59.05	3.01	2.68	0.0136
101	58.75	3.00	2.05	0.0130
122	58.70	2.99	1.80	0.0124
151	58.25	2.97	1.60	0.0112
216	58.20	2.97	1.20	0.0106
256	58.30	2.97	1.01	0.0105
313	57.95	2.96	0.909	0.0097
417	58.35	2.98	0.750	0.0087
509	57.90	2.95	0.624	0.0087
770	58.15	2.97	0.452	0.0079
890	58.05	2.96	0.420	0.0073
1.10 mc/s	58.15	2.97	0.399	0.0062
1.77	58.05	2.96	0.248	0.0063
2.07	58.20	2.97	0.206	0.0064
2.54	58.75	3.00	0.169	0.0063
3.22	58.15	2.97	0.128	0.0066

TABLE LXI.

Leucite, Run 135, 90°C, Bridge.

Frequency	$Cp_{(app)}$ pF	ϵ'_{app}	$Rp_{(app)}$ meg.-Ω	$\tan\delta_{app}$
320 c/s	77,9	3.97	31.7	0.202
400	75.4	3.85	26.9	0.196
500	73.4	3.74	24.3	0.179
630	72.1	3.68	21.6	0.162
800	70.6	3.60	18.9	0.149
1.0 kc/s	69.4	3.54	16.8	0.136
1.3	68.0	3.47	14.5	0.124
1.6	67.2	3.43	12.9	0.114
2.0	66.3	3.38	11.5	0.104
2.5	65.3	3.33	10.5	0.0928
3.2	64.7	3.30	9.07	0.0848
4.0	64.2	3.28	8.10	0.0765
5.0	63.7	3.25	7.15	0.0699
6.3	63.1	3.22	6.31	0.0635
8.0	62.6	3.19	5.53	0.0575
10	62.3	3.18	4.88	0.0524
13	62.0	3.16	4.19	0.0471
16	61.6	3.14	3.70	0.0436
20	61.5	3.14	3.25	0.0398
25	61.4	3.13	2.84	0.0366
32	61.0	3.11	2.39	0.0341
40	60.6	3.09	2.07	0.0317
50	60.4	3.08	1.76	0.0300

TABLE LXII.

Leucite, Run 136, 90°C, H.W.-apparatus.

Frequency	$C_{p(app)}$ pF	ϵ'_{app}	$R_{p(app)}$ meg.-Ω	$\tan\delta_{app}$
63.kc/s	60.25	3.07	1.61	0.0260
74	60.10	3.07	1.40	0.0255
101	60.15	3.07	1.20	0.0218
122	59.60	3.04	0.995	0.0220
151	59.90	3.06	0.868	0.0203
216	59.55	3.04	0.676	0.0183
256	59.05	3.01	0.603	0.0175
313	59.40	3.03	0.517	0.0165
417	59.10	3.02	0.407	0.0159
509	59.45	3.03	0.383	0.0137
770	58.85	3.00	0.297	0.0118
890	58.75	3.00	0.259	0.0118
1.10 mc/s	59.10	3.02	0.214	0.0114
1.77	58.85	3.00	0.144	0.0106
2.07	59.05	3.01	0.129	0.0101
2.54	59.60	3.04	0.110	0.0096
3.22	58.90	3.01	0.0892	0.0094

TABLE LXIII.

Leucite, Run 137, 105°C, Bridge.

Frequency	$Cp_{(app)}$ pF	ϵ'_{app}	$Rp_{(app)}$ meg.-Ω	$\tan\delta_{app}$
1.3 kc/s	73.3	3.74	9.43	0.177
2.5	68.8	3.51	6.80	0.136
5.0	66.3	3.38	4.66	0.103
10	64.3	3.28	3.24	0.0763
20	62.8	3.20	2.22	0.0570
40	62.0	3.16	1.44	0.0446

TABLE LXIV.

Leucite, Run 138, 90°C, Bridge.

Frequency	$Cp_{(app)}$ pF	ϵ'_{app}	$Rp_{(app)}$ meg.-Ω	$\tan\delta_{app}$
1.3 kc/s	68.0	3.47	14.4	0.125
2.5	65.3	3.33	10.6	0.0921
5.0	63.7	3.25	7.19	0.0695
10	62.3	3.18	4.90	0.0522
20	61.4	3.13	3.27	0.0396
40	60.6	3.09	2.08	0.0315

TABLE LXV.

Leucite, Run 139, 74.8°C, Bridge.

Frequency	$Cp_{(app)}$ pF	ϵ'_{app}	Rp(app) meg.-Ω	$\tan\delta_{app}$
1.3 kc/s	64.5	3.29	23.1	0.0822
2.5	63.0	3.21	16.6	0.0610
5.0	62.0	3.16	11.0	0.0468
10	61.0	3.11	7.28	0.0358
20	60.4	3.08	4.72	0.0279
40	59.6	3.04	2.94	0.0227

TABLE LXVI.

Leucite, Run 140, 60°C, Bridge.

Frequency	$Cp_{(app)}$ pF	ϵ'_{app}	Rp(app) meg.-Ω	$\tan\delta_{app}$
1.3 kc/s	62.35	3.18	37.0	0.0531
2.5	61.45	3.14	26.2	0.0396
5.0	60.65	3.09	16.7	0.0314
10	60.05	3.06	10.7	0.0248
20	59.55	3.04	6.72	0.0199
40	59.25	3.02	4.07	0.0165

TABLE LXVII.

Leucite, Run 141, 45.2°C, Bridge.

Frequency	$C_{p(app)}$ pF	ϵ'_{app}	$R_{p(app)}$ meg.-Ω	$\tan\delta_{app}$
1.3 kc/s	61.05	3.11	58.2	0.0345
2.5	60.05	3.06	40.3	0.0263
5.0	59.65	3.04	24.8	0.0216
10	59.25	3.02	15.3	0.0175
20	59.05	3.01	9.40	0.0143
40	58.85	3.00	5.32	0.0127

TABLE LXVIII.

Leucite, Run 142, 30°C, Bridge.

Frequency	$C_{p(app)}$ pF	ϵ'_{app}	$R_{p(app)}$ meg.-Ω	$\tan\delta_{app}$
1.3 kc/s	59.85	3.05	90.2	0.0227
2.5	59.25	3.02	60.1	0.0179
5.0	58.85	3.00	35.8	0.0151
10	58.65	2.99	21.6	0.0126
20	58.55	2.99	12.8	0.0106
40	58.25	2.97	7.14	0.0096

TABLE LXIX.

Sintered Leucite, Run 164, 30°C, Bridge.

Frequency	$C_{p(app)}$ pF	ϵ'_{app}	$R_{p(app)}$ meg.-Ω	$\tan\delta_{app}$
630 c/s	32.9	3.24	211	0.0364
800	32.6	3.21	178	0.0342
1.0 kc/s	32.5	3.20	154	0.0317
1.3	32.4	3.19	128	0.0295
1.6	32.3	3.18	110	0.0279
2.0	32.2	3.17	94.9	0.0260
2.5	32.1	3.16	82.8	0.0240
3.2	32.1	"	67.5	0.0230
4.0	32.0	3.15	57.4	0.0217
5.0	31.8	3.13	48.6	0.0206
6.3	31.7	3.12	41.1	0.0194
8.0	31.5	3.10	34.2	0.0185
10	"	"	29.0	0.0174
13	"	"	23.7	0.0164
16	31.4	3.09	20.4	0.0155
20	"	"	17.2	0.0147
25	"	"	14.4	0.0141
32	31.3	3.08	11.7	0.0136
40	"	"	9.79	0.0130
50	"	"	8.03	0.0127

TABLE LXX.

Sintered Leucite, Run 165, 56°C, Bridge.

Frequency	$C_{p(app)}$ pF	ϵ'_{app}	$R_{p(app)}$ meg.-Ω	$\tan\delta_{app}$
500 c/s	35.0	3.45	104	0.0877
630	34.7	3.42	93.7	0.0777
800	34.4	3.39	80.0	0.0723
1.0 kc/s	34.1	3.36	71.1	0.0657
1.3	33.9	3.34	60.9	0.0593
1.6	33.7	3.32	53.1	0.0556
2.0	33.5	3.30	46.6	0.0510
2.5	33.3	3.28	41.4	0.0461
3.2	33.2	3.27	34.7	0.0432
4.0	33.0	3.25	30.1	0.0401
5.0	32.8	3.23	25.9	0.0374
6.3	32.7	3.22	22.2	0.0348
8.0	32.6	3.21	19.0	0.0322
10	32.4	3.19	16.3	0.0302
13	32.2	3.17	13.6	0.0281
16	32.1	3.16	11.8	0.0263
20	32.1	"	10.1	0.0247
25	32.0	3.15	8.50	0.0234
32	32.0	"	6.94	0.0224
40	31.8	3.13	5.92	0.0211
50	31.8	"	4.86	0.0206

TABLE LXXI.

Sintered Leucite, Run 166, 90°C, Bridge.

Frequency	$C_{p(app)}$ pF	ϵ'_{app}	$R_{p(app)}$ meg.-Ω	$\tan\delta_{app}$
500 c/s	41.7	4.11	31.1	0.245
630	40.4	3.98	28.1	0.223
800	39.5	3.89	25.0	0.202
1.0 kc/s	38.6	3.80	22.7	0.181
1.3	37.8	3.72	20.0	0.162
1.6	37.4	3.68	18.0	0.148
2.0	36.8	3.63	16.2	0.134
2.5	36.2	3.57	14.7	0.120
3.2	35.8	3.53	12.8	0.109
4.0	35.5	3.50	11.3	0.0988
5.0	35.1	3.46	10.1	0.0901
6.3	34.8	3.43	8.89	0.0840
8.0	34.4	3.39	7.80	0.0742
10	34.2	3.37	6.89	0.0676
13	34.1	3.36	5.90	0.0609
16	33.7	3.32	5.23	0.0564
20	33.5	3.30	4.56	0.0521
25	33.5	"	3.93	0.0483
32	33.4	3.29	3.35	0.0444
40	33.2	3.27	2.88	0.0416
50	33.0	3.25	2.38	0.0405

TABLE LXXII.

Sintered Leucite, Run 167, 56°C, Bridge.

Frequency	$C_{p(app)}$ pF	ϵ'_{app}	$R_{p(app)}$ meg.-Ω	$\tan\delta_{app}$
1.3 kc/s	33.9	3.34	60.6	0.0596
4.0	33.0	3.25	29.9	0.0404
13	32.2	3.17	13.5	0.0281
40	31.7	3.12	5.91	0.0212

TABLE LXXIII.

Sintered Leucite, Run 168, 90°C, Bridge.

Frequency	$C_{p(app)}$ pF	ϵ'_{app}	$R_{p(app)}$ meg.-Ω	$\tan\delta_{app}$
1.3 kc/s	37.8	3.72	20.0	0.162
4.0	35.3	3.48	11.4	0.098c
13	33.9	3.34	5.91	0.0611
40	33.2	3.27	2.87	0.0418

TABLE LXXIV.

Sintered Leucite, Run 169, 30°C, Bridge.

Frequency	$C_{p(app)}$ pF	ϵ'_{app}	$R_{p(app)}$ meg.-Ω	$\tan\delta_{app}$
1.3 kc/s	32.4	3.19	127	0.0298
4.0	31.8	3.13	56.6	0.0221
13	31.5	3.10	23.6	0.0164
40	31.1	3.06	10.2	0.0126

TABLE LXXV.

Rubidium Analcite (Domain Mixture), Run 105, 30°C, Bridge.

Frequency	$Cp_{(app)}$ pF	ϵ'_{app}	$Rp_{(app)}$ meg. Ω	$\tan \delta_{app}$
1.0 kc/s	36.90	1.88	2300	0.0019
1.3	"	"	1770	0.0019
1.6	"	"	1460	0.0019
2.0	"	"	1160	0.0019
2.5	"	"	965	0.0018
3.2	"	"	792	0.0017
4.0	"	"	642	0.0017
5.0	"	"	552	0.0016
6.3	"	"	445	0.0015
8.0	"	"	361	0.0015
10	"	"	299	0.0014
13	"	"	238	0.0014
16	"	"	202	0.0013
20	"	"	166	0.0013
25	"	"	127	0.0014
32	"	"	106	0.0013
40	"	"	83.8	0.0013
50	"	"	63.4	0.0014

TABLE LXXVI.

Rubidium Analcite (Domain Mixture), Run 106, 30°C, H.W.-apparatus.

Frequency	$Cp_{(app)}$ pF	ϵ'_{app}	$Rp_{(app)}$ meg. Ω	$\tan\delta_{app}$
63 kc/s	36.80	1.88	60.2	0.0011
74	36.90	1.88	59.7	0.0010
101	37.15	1.90	-	-
122	37.00	1.89	34.3	0.0010
151	37.05	1.89	24.5	0.0012
216	36.65	1.87	18.2	0.0011
256	37.15	1.90	16.3	0.0010
313	36.95	1.89	11.3	0.0012
417	37.65	1.92	8.97	0.0011
509	37.15	1.90	7.32	0.0011
770	37.15	1.90	5.51	0.0010
890	37.50	1.91	5.11	0.0009
1.10 mc/s	37.30	1.90	3.91	0.0010
1.32	37.35	1.91	3.36	0.0010
1.77	37.35	1.91	2.69	0.0009
2.07	37.40	1.91	2.03	0.0010
2.54	37.25	1.90	1.38	0.0012
3.22	36.95	1.89	1.13	0.0012
4.30	37.60	1.92	0.655	0.0015
5.30	37.15	1.90	0.404	0.0020

TABLE LXXVII.

Rubidium Analcite (Domain Mixture), Run 107, 60°C, Bridge.

Frequency	$Cp_{(app)}$ pF	ϵ'_{app}	$Rp_{(app)}$ meg. Ω	$\tan\delta_{app}$
1.0 kc/s	37.15	1.90	1140	0.0038
1.3	"	"	957	0.0034
1.6	"	"	819	0.0033
2.0	"	"	703	0.0031
2.5	"	"	585	0.0029
3.2	37.05	1.89	478	0.0028
4.0	"	"	398	0.0027
5.0	"	"	333	0.0026
6.3	"	"	279	0.0024
8.0	"	"	231	0.0023
10	"	"	194	0.0022
13	"	"	155	0.0021
16	"	"	131	0.0021
20	"	"	109	0.0020
25	"	"	90.9	0.0019
32	"	"	72.0	0.0019
40	"	"	58.3	0.0018
50	"	"	43.8	0.0020

TABLE LXXVIII.

Rubidium Analcite (Domain Mixture), Run 108, 60°C, H.W.-apparatus.

Frequency	$Cp_{(app)}$ pF	ϵ'_{app}	$Rp_{(app)}$ meg. Ω	$\tan\delta_{app}$
63 kc/s	37.20	1.90	40.8	0.0017
74	37.10	1.89	-	-
101	37.20	1.90	-	-
122	37.30	1.90	-	-
151	37.35	1.91	18.0	0.0016
216	37.00	1.89	13.3	0.0015
256	37.05	1.89	11.5	0.0015
313	37.30	1.90	9.78	0.0014
417	36.80	1.88	6.58	0.0016
509	37.45	1.91	5.85	0.0014
770	37.05	1.89	4.18	0.0013
890	37.30	1.90	3.65	0.0013
1.10 mc/s	37.35	1.91	3.15	0.0012
1.32	37.35	1.91	3.00	0.0011
1.77	37.25	1.90	-	-
2.07	37.35	1.91	1.86	0.0011
2.54	37.45	1.91	1.34	0.0013
3.22	36.90	1.89	1.01	0.0013
4.30	37.55	1.92	0.607	0.0016
5.30	37.85	1.93	0.424	0.0019

TABLE LXXIX.

Rubidium Analcite (Domain Mixture), Run 109, 90°C, Bridge.

Frequency	$C_{p(app)}$ pF	ϵ'_{app}	$R_{p(app)}$ meg.Ω	$\tan\delta_{app}$
1.0 kc/s	37.30	1.90	590	0.0072
1.3	"	"	517	0.0063
1.6	"	"	429	0.0062
2.0	37.25	"	367	0.0058
2.5	"	"	321	0.0053
3.2	"	"	268	0.0050
4.0	37.20	"	228	0.0047
5.0	37.15	"	193	0.0044
6.3	"	"	163	0.0042
8.0	"	"	138	0.0039
10	"	"	117	0.0037
13	"	"	95.3	0.0035
16	"	"	81.1	0.0033
20	"	"	69.2	0.0031
25	37.05	1.89	57.7	0.0030
32	"	"	46.7	0.0029
40	"	"	38.4	0.0028
50	"	"	31.1	0.0028

TABLE LXXX.

Rubidium Analcite (Domain Mixture), Run 110, 90°C, H.W.-apparatus.

Frequency	$Cp_{(app)}$ pF	ϵ'_{app}	$Rp_{(app)}$ meg.Ω	$\tan\delta_{app}$
63 kc/s	37.55	1.92	26.5	0.0025
74	37.70	1.92	-	-
101	37.30	1.90	18.4	0.0023
122	37.85	1.93	15.8	0.0022
151	37.55	1.92	13.9	0.0020
216	37.30	1.90	10.5	0.0019
256	37.65	1.92	9.20	0.0018
313	37.35	1.91	7.32	0.0019
417	37.75	1.93	5.83	0.0017
509	37.40	1.91	4.70	0.0018
770	37.65	1.92	3.45	0.0016
890	37.85	1.93	3.11	0.0015
1.10 mc/s	37.55	1.92	2.57	0.0015
1.32	37.80	1.93	2.17	0.0015
1.77	38.05	1.94	1.73	0.0014
2.07	38.10	1.94	1.44	0.0014
2.54	37.60	1.92	1.01	0.0017
3.22	37.35	1.91	0.696	0.0019
4.30	38.20	1.95	0.518	0.0019
5.30	38.20	1.95	0.305	0.0026

TABLE LXXXI.

Rubidium Analcite (Domain Mixture), Run 111, 105°C, Bridge.

Frequency	$Cp_{(app)}$ pF	ϵ'_{app}	$Rp_{(app)}$ meg.Ω	$\tan \delta_{app}$
1.3 kc/s	37.70	1.92	350	0.0093
2.5	37.60	1.92	228	0.0074
5.0	37.50	1.91	144	0.0059
10	37.40	1.91	88.4	0.0048
20	37.20	1.90	53.5	0.0040
40	37.15	1.90	30.6	0.0035

TABLE LXXXII.

Rubidium Analcite (Domain Mixture), Run 112, 90°C, Bridge.

Frequency	$Cp_{(app)}$ pF	ϵ'_{app}	$Rp_{(app)}$ meg.Ω	$\tan \delta_{app}$
1.3 kc/s	37.35	1.91	507	0.0065
2.5	37.30	1.90	330	0.0052
5.0	37.20	1.90	197	0.0043
10	37.15	1.90	119	0.0036
20	37.15	1.90	70.3	0.0031
40	37.15	1.90	39.2	0.0027

TABLE LXXXIII.

Rubidium Analcite (Domain Mixture), Run 113, 75°C, Bridge.

Frequency	$Cp_{(app)}$ pF	ϵ'_{app}	$Rp_{(app)}$ meg.Ω	$\tan\delta_{app}$
1.3 kc/s	37.20	1.90	691	0.0048
2.5	37.15	1.90	449	0.0038
5.0	37.20	1.90	265	0.0032
10	37.00	1.89	155	0.0028
20	37.00	1.89	89.4	0.0024
40	37.10	1.89	48.7	0.0022

TABLE LXXXIV.

Rubidium Analcite (Domain Mixture), Run 114, 60°C, Bridge.

Frequency	$Cp_{(app)}$ pF	ϵ'_{app}	$Rp_{(app)}$ meg.Ω	$\tan\delta_{app}$
1.3 kc/s	37.15	1.90	951	0.0035
2.5	"	"	586	0.0029
5.0	"	"	348	0.0025
10	"	"	201	0.0021
20	"	"	113	0.0019
40	"	"	60.1	0.0018

TABLE LXXXV.

Rubidium Analcite (Domain Mixture), Run 115, 45°C, Bridge.

Frequency	$Cp_{(app)}$ pF	ϵ'_{app}	$Rp_{(app)}$ meg. Ω	$\tan\delta_{app}$
1.3 kc/s	37.15	1.90	1270	0.0026
2.5	37.15	1.90	742	0.0023
5.0	37.05	1.89	429	0.0020
10	37.00	1.89	246	0.0018
20	36.85	1.88	136	0.0016
40	36.85	1.88	71.2	0.0015

TABLE LXXXVI.

Rubidium Analcite (Domain Mixture), Run 116, 30°C, Bridge.

Frequency	$Cp_{(app)}$ pF	ϵ'_{app}	$Rp_{(app)}$ meg. Ω	$\tan\delta_{app}$
1.3 kc/s	37.10	1.89	1750	0.0019
2.5	37.00	1.89	942	0.0018
5.0	36.85	1.88	549	0.0016
10	36.95	1.89	297	0.0015
20	36.85	1.88	163	0.0013
40	37.00	1.89	81.7	0.0013

TABLE LXXXVII.

Rubidium Analcite B, Run 121, 30°C, Bridge.

Frequency	$Cp_{(app)}$ pF	ϵ'_{app}	$Rp_{(app)}$ meg.-Ω	$\tan\delta_{app}$
1.0 kc/s	43.25	2.21	-	-
1.3	"	"	-	-
2.0	"	"	-	-
3.2	"	"	-	-
4.0	"	"	-	-
5.0	"	"	19300	0.00004
6.3	"	"	8540	0.0001 (0.00007)
8.0	"	"	-	-
10	"	"	3480	0.0001 (0.00011)
13	"	"	2500	0.0001 (0.00011)
16	"	"	1870	0.0001 (0.00012)
20	"	"	1940	0.0001 (0.00010)
25	"	"	1560	0.0001 (0.00009)
32	"	"	1260	0.0001 (0.00009)
40	"	"	903	0.0001 (0.00010)
50	"	"	496	0.0001 (0.00015)

TABLE LXXXVIII.

Rubidium Analcite B, Run 122, 30°C, H.W.-apparatus.

Frequency	$Cp_{(app)}$ pF	ϵ'_{app}	$Rp_{(app)}$ meg.-Ω	$\tan\delta_{app}$
63 kc/s	43.55	2.22	-	-
74	43.70	2.23	-	-
122	43.90	2.24	119	0.0002 (0.00024)
151	43.50	2.22	123	0.0002 (0.00020)
216	43.60	2.22	98.2	0.0002 (0.00017)
256	43.65	2.23	-	-
313	43.55	2.22	53.5	0.0002 (0.00022)
417	43.55	2.22	28.2	0.0003 (0.00031)
509	43.65	2.23	18.4	0.0004 (0.00039)
621	42.75	2.18	14.5	0.0004 (0.00041)
770	43.85	2.24	15.9	0.0003 (0.00030)
890	43.90	2.24	12.3	0.0003 (0.00033)
1.10 mc/s	43.65	2.23	15.2	0.0002 (0.00022)
1.77	43.80	2.23	8.18	0.0003 (0.00025)
2.07	43.90	2.24	6.19	0.0003 (0.00028)
2.54	43.95	2.24	2.33	0.0006 (0.00061)
3.22	43.50	2.22	2.15	0.0005 (0.00053)

TABLE LXXXIX.

Rubidium Analcite B, Run 123, 60°C, Bridge.

Frequency	$Cp_{(app)}$ pF	ϵ'_{app}	$Rp_{(app)}$ meg.-Ω	$\tan\delta_{app}$
1.0 kc/s	43.45	2.22	-	-
1.3	"	"	-	-
1.6	"	"	-	-
2.0	"	"	-	-
2.5	"	"	-	-
3.2	"	"	-	-
4.0	"	"	-	-
5.0	"	"	-	-
6.3	"	"	11400	0.0001 (0.00005)
8.0	"	"	9410	0.0001 (0.00005)
10	"	"	4830	0.0001 (0.00008)
13	"	"	5100	0.0001 (0.00006)
16	"	"	1980	0.0001 (0.00012)
20	"	"	1540	0.0001 (0.00012)
25	"	"	2740	0.0001 (0.00005)
32	"	"	1560	0.0001 (0.00007)
40	"	"	1210	0.0001 (0.00008)
50	"	"	783	0.0001 (0.00009)

TABLE XC.

Rubidium Analcite B, Run 124, 60°C, H.W.-apparatus.

Frequency	$Cp_{(app)}$ pF	ϵ'_{app}	$Rp_{(app)}$ meg.-Ω	$\tan\delta_{app}$	
63 kc/s	43.90	2.24	-	-	
74	44.00	2.24	-	-	
122	44.10	2.25	-	-	
151	43.80	2.23	83.8	0.0003	(0.00029)
216	43.80	2.23	56.7	0.0003	(0.00030)
256	43.80	2.23	68.6	0.0002	(0.00021)
313	43.65	2.23	26.1	0.0004	(0.00044)
417	43.70	2.23	17.7	0.0005	(0.00049)
509	43.80	2.23	62.5	0.0001	(0.00011)
770	44.00	2.24	10.3	0.0005	(0.00045)
1.10 mc/s	43.85	2.24	15.2	0.0002	(0.00022)
1.77	44.00	2.24	12.0	0.0002	(0.00017)
2.07	44.55	2.27	4.41	0.0004	(0.00039)
2.54	44.25	2.26	2.29	0.0006	(0.00062)
3.22	43.90	2.24	1.73	0.0007	(0.00065)

TABLE XCI.

Rubidium Analcite B, Run 125, 90°C, Bridge.

Frequency	$C_{p(app)}$ pF	ϵ'_{app}	$R_{p(app)}$ meg.-Ω	$\tan\delta_{app}$
1.0 kc	43.55	2.22	-	-
1.3	"	"	-	-
1.6	"	"	- -	-
2.0	"	"	-	-
2.5	"	"	3360	0.0004 (0.00043)
3.2	"	"	2950	0.0004 (0.00039)
4.0	"	"	2470	0.0004 (0.00037)
5.0	"	"	2100	0.0004 (0.00035)
6.3	"	"	1730	0.0003 (0.00034)
8.0	"	"	1500	0.0003 (0.00031)
10	"	"	1330	0.0003 (0.00027)
13	"	"	1090	0.0003 (0.00026)
16	"	"	997	0.0002 (0.00023)
20	"	"	747	0.0002 (0.00024)
25	"	"	666	0.0002 (0.00022)
32	"	"	499	0.0002 (0.00023)
40	"	"	476	0.0002 (0.00019)
50	"	"	365	0.0002 (0.00020)

Rubidium Analcite B, Run 127, 90°C, Bridge.

Check points at 10, 20 and 40 kc/s give the same result as in Run 125.

TABLE XCII.

Rubidium Analcite,B, Run 126, 90°C, H.W.-apparatus.

Frequency	$Cp_{(app)}$ pF	ϵ'_{app}	$Rp_{(app)}$ meg.-Ω	$\tan\delta_{app}$
63 kc/s	43.75	2.23	459	0.0001 (0.00013)
74	44.45	2.27	252	0.0002 (0.00019)
122	43.95	2.24	-	-
151	43.85	2.24	95.2	0.0003 (0.00025)
216	43.95	2.24	38.8	0.0004 (0.00043)
256	44.00	2.24	49.5	0.0003 (0.00029)
313	44.05	2.25	40.7	0.0003 (0.00028)
417	44.10	2.25	27.3	0.0003 (0.00032)
509	43.90	2.24	23.2	0.0003 (0.00031)
770	43.90	2.24	10.6	0.0004 (0.00044)
890	44.15	2.25	8.32	0.0005 (0.00049)
1.10 mc/s	43.90	2.24	6.89	0.0005 (0.00049)
1.77	44.45	2.27	4.09	0.0005 (0.00050)
2.07	44.35	2.26	4.06	0.0004 (0.00043)
2.54	44.35	2.26	2.63	0.0005 (0.00054)
3.22	44.70	2.28	1.54	0.0007 (0.00072)

TABLE XCIII.

Rubidium Analcite B, Run 128, 60°C, Bridge.

Frequency	$Cp_{(app)}$ pF	ϵ'_{app}	$Rp_{(app)}$ meg.-Ω	$\tan\delta_{app}$
10 kc/s	43.45	2.22	3780	0.0001 (0.00010)
20	"	"	1380	0.0001 (0.00013)
40	"	"	737	0.0001 (0.00012)

TABLE XCIV.

Rubidium Analcite B, Run 129, 30°C, Bridge.

Frequency	$Cp_{(app)}$ pF	ϵ'_{app}	$Rp_{(app)}$ meg.-Ω	$\tan\delta_{app}$
10 kc/s	43.25	2.21	3780	0.0001 (0.00010)
20	"	"	1380	0.0001 (0.00013)
40	"	"	886	0.0001 (0.00010)

TABLE XCV.

Caesium Analcite, Run 93, 30°C, Bridge.

Frequency	$Cp_{(app)}$ pF	ϵ'_{app}	$Rp_{(app)}$ meg.-Ω	$\tan\delta_{app}$
500 c/s	33.45	1.71	-	-
630	"	"	-	-
800	"	"	-	-
1.0 kc/s	"	"	2240	0.0021
1.3	"	"	1840	0.0020
1.6	"	"	1570	0.0019
2.0	33.40	1.70	1320	0.0018
2.5	"	"	1060	0.0018
3.2	"	"	851	0.0017
4.0	33.35	"	711	0.0017
5.0	"	"	572	0.0017
6.3	"	"	473	0.0016
8.0	"	"	389	0.0015
10.0	"	"	319	0.0015
13	"	"	252	0.0015
16	"	"	210	0.0014
20	"	"	172	0.0014
25	"	"	143	0.0013
32	"	"	111	0.0013
40	"	"	90.7	0.0013

TABLE XCVI.

Caesium Analcite, Run 94, 30°C, H.-W. apparatus.

Frequency	$Cp_{(app)}$ pF	ϵ'_{app}	$Rp_{(app)}$ meg.-Ω	$\tan\delta_{app}$
63 kc/s	33.15	1.69	63.2	0.0012
74	33.15	1.69	57.3	0.0011
101	33.25	1.70	40.5	0.0012
122	33.15	1.69	28.1	0.0014
151	33.05	1.69	28.5	0.0011
216	33.00	1.68	20.5	0.0011
256	33.30	1.70	15.9	0.0012
313	33.15	1.69	13.4	0.0011
417	33.00	1.68	9.79	0.0012
509	33.05	1.69	8.23	0.0011
890	32.95	1.68	4.90	0.0011
1.10 mc/s	33.00	1.68	3.86	0.0011
1.32	32.90	1.68	3.32	0.0011
1.77	33.25	1.70	2.75	0.0010
2.07	33.10	1.69	2.43	0.0010
2.54	33.25	1.70	1.55	0.0012
3.22	33.10	1.69	1.37	0.0011
4.30	33.40	1.70	0.881	0.0013
5.30	33.65	1.72	0.476	0.0019

TABLE XCVII.

Caesium Analcite, Run 95, 60°C, Bridge.

Frequency	$Cp_{(app)}$ pF	ϵ'_{app}	$Rp_{(app)}$ meg.-Ω	$\tan\delta_{app}$
1.0 kc/s	33.60	1.71	1230	0.0039
1.3	33.55	"	1070	0.0034
1.6	"	"	889	0.0033
2.0	33.50	"	770	0.0031
2.5	"	"	654	0.0029
3.2	"	"	551	0.0027
4.0	"	"	455	0.0026
5.0	33.45	"	378	0.0026
6.3	"	"	319	0.0024
8.0	"	"	262	0.0023
10	"	"	217	0.0022
13	33.40	1.70	178	0.0021
16	"	"	150	0.0020
20	"	"	125	0.0019
25	"	"	101	0.0019
32	"	"	82.0	0.0018
40	"	"	65.2	0.0018

TABLE XCVIII.

Caesium Analcite, Run 96, 60°C, H.W.-apparatus.

Frequency	$Cp_{(app)}$ pF	ϵ'_{app}	$Rp_{(app)}$ meg.Ω	$\tan\delta_{app}$
63 kc/s	33.30	1.70	50.5	0.0015
74	33.30	"	39.1	0.0017
101	33.30	"	20.0	0.0024
122	33.05	1.69	16.8	0.0023
151	33.20	"	20.2	0.0016
216	33.20	"	14.3	0.0016
313	33.20	"	10.4	0.0015
417	33.20	"	8.39	0.0014
509	33.05	"	6.58	0.0014
621	33.15	"	-	-
770	33.20	"	-	-
890	33.35	1.70	3.89	0.0014
1.10 mc/s	33.20	1.69	-	-
1.77	33.55	1.71	1.99	0.0013
2.07	33.45	1.71	1.99	0.0012
2.54	33.35	1.70	1.48	0.0013
4.30	33.95	1.73	0.507	0.0021
5.30	33.75	1.72	0.413	0.0022

TABLE XCIX.

Caesium Analcite, Run 97, 90°C, Bridge.

Frequency	$Cp_{(app)}$ pF	ϵ'_{app}	$Rp_{(app)}$ meg.-Ω	$\tan\delta_{app}$
1.0 kc/s	33.65	1.72	652	0.0073
1.3	33.60	1.71	592	0.0062
1.6	"	"	519	0.0057
2.0	33.55	"	424	0.0056
2.5	33.50	"	380	0.0050
3.2	"	"	308	0.0048
4.0	33.45	"	265	0.0045
5.0	"	"	227	0.0042
6.3	"	"	191	0.0040
8.0	33.40	1.70	160	0.0037
10	"	"	136	0.0035
13	"	"	111	0.0033
16	"	"	95.1	0.0031
20	"	"	79.2	0.0030
25	"	"	66.4	0.0029
32	33.35	"	54.1	0.0028
40	"	"	44.2	0.0027

TABLE C.

Caesium Analcite, Run 98, 90°C, H.W.-apparatus.

Frequency	$C_{p(app)}$ pF	ϵ'_{app}	$R_{p(app)}$ meg.-Ω	$\tan\delta_{app}$
63 kc/s	33.55	1.70	32.2	0.0024
74	33.20	1.69	28.1	0.0023
101	33.40	1.70	22.8	0.0021
122	33.40	1.70	19.2	0.0020
151	33.15	1.69	14.9	0.0021
216	33.20	1.69	9.82	0.0023
256	33.50	1.71	10.4	0.0018
313	33.30	1.70	8.69	0.0018
509	33.10	1.69	5.58	0.0017
770	33.40	1.70	3.53	0.0018
890	33.75	1.72	3.07	0.0017
1.77 mc/s	33.30	1.70	1.71	0.0016
2.07	33.45	1.71	1.34	0.0017
2.54	33.30	1.70	1.21	0.0016
3.22	33.30	1.70	0.696	0.0021
4.30	33.95	1.73	0.525	0.0021
5.30	33.65	1.72	0.372	0.0024

TABLE CI.

Caesium Analcite, Run 99, 105°C, Bridge.

Frequency	$Cp_{(app)}$ pF	ϵ'_{app}	$Rp_{(app)}$ meg.Ω	$\tan\delta_{app}$
1.3 kc/s	33.80	1.72	401	0.0090
2.5	33.70	1.72	272	0.0069
5.0	33.55	1.71	167	0.0057
10	33.50	1.71	103	0.0046
20	33.45	1.71	61.5	0.0039
40	33.40	1.70	36.0	0.0033

TABLE CII.

Caesium Analcite, Run 100, 90°C, Bridge.

Frequency	$Cp_{(app)}$ pF	ϵ'_{app}	$Rp_{(app)}$ meg.Ω	$\tan\delta_{app}$
1.3 kc/s	33.60	1.71	578	0.0063
2.5	33.50	1.71	369	0.0052
5.0	33.50	1.71	222	0.0043
10	33.45	1.71	134	0.0036
20	33.40	1.70	78.6	0.0030
40	33.35	1.70	42.5	0.0028

TABLE CIII.

Caesium Analcite, Run 101, 75°C, Bridge.

Frequency	$Cp_{(app)}$ pF	ϵ'_{app}	$Rp_{(app)}$ meg.Ω	$\tan\delta_{app}$
1.3 kc/s	33.50	1.71	777	0.0047
2.5	33.50	1.71	502	0.0038
5.0	33.45	1.71	288	0.0033
10	33.40	1.70	170	0.0028
20	33.40	1.70	98.4	0.0024
40	33.40	1.70	52.2	0.0023

TABLE CIV.

Caesium Analcite, Run 102, 60°C, Bridge.

Frequency	$Cp_{(app)}$ pF	ϵ'_{app}	$Rp_{(app)}$ meg.Ω	$\tan\delta_{app}$
1.3 kc/s	33.55	1.71	1070	0.0034
2.5	33.45	1.71	650	0.0029
5.0	33.45	1.71	378	0.0025
10	33.40	1.70	215	0.0022
20	33.40	1.70	122	0.0020
40	33.40	1.70	65.2	0.0018

TABLE CV.

Caesium Analcite, Run 103, 45°C, Bridge.

Frequency	$C_{p(app)}$ pF	ϵ'_{app}	$R_{p(app)}$ meg.Ω	$\tan\delta_{app}$
1.3 kc/s	33.45	1.71	1390	0.0026
2.5	33.45	1.71	840	0.0023
5.0	33.40	1.70	469	0.0020
10	33.35	1.70	264	0.0018
20	33.35	1.70	146	0.0016
40	33.35	1.70	77.7	0.0015

TABLE CVI.

Caesium Analcite, Run 104, 30°C, Bridge.

Frequency	$C_{p(app)}$ pF	ϵ'_{app}	$R_{p(app)}$ meg.Ω	$\tan\delta_{app}$
1.3 kc/s	33.40	1.70	1860	0.0020
2.5	33.40	1.70	1090	0.0018
5.0	33.35	1.70	609	0.0016
10	33.35	1.70	338	0.0014
20	33.30	1.70	187	0.0013
40	33.30	1.70	92.1	0.0013

TABLE CVII.

Caesium Analcite, Run 129A, 30°C, Bridge.

Sample in small stainless steel cell to compare with Runs 93 and 104 in large stainless steel cell.

Frequency	$Cp_{(app)}$ pF	ϵ'_{app}	$Rp_{(app)}$ meg.-Ω	$\tan\delta_{app}$
2.0 kc/s	17.80	1.75	2480	0.0018
2.5	"	"	2080	0.0017
3.2	"	"	1590	0.0018
4.0	"	"	1300	0.0017
5.0	17.75	"	1070	0.0017
6.3	"	"	911	0.0016
10	"	"	613	0.0015
13	"	"	473	0.0015
16	17.70	1.74	402	0.0014
20	"	"	332	0.0014
25	"	"	277	0.0013
32	"	"	205	0.0014
40	"	"	163	0.0014

TABLE CVIII.

Sintered Caesium Analcite, Run 143, 30°C, Bridge.

Frequency	$Cp_{(app)}$ pF	ϵ'_{app}	$Rp_{(app)}$ meg.-Ω	$\tan\delta_{app}$
1.0-3.2 kc/s	26.75	2.64	-	-
4.0 kc/s	"	"	19800	0.0001 (0.00008)
5.0	"	"	12000	0.0001 (0.00010)
6.3	"	"	9530	0.0001 (0.00010)
8.0	"	"	5930	0.0001 (0.00013)
10	"	"	4840	0.0001 (0.00012)
13	"	"	7070	0.0001 (0.00007)
16	"	"	4650	0.0001 (0.00008)
20	"	"	3840	0.0001 (0.00008)
25	"	"	2930	0.0001 (0.00008)
32	"	"	2290	0.0001 (0.00008)
40	"	"	1980	0.0001 (0.00008)
50	"	"	1110	0.0001 (0.00011)

TABLE CIX.

Sintered Caesium Analcite, Run 152, 30°C, Bridge.

Frequency	$Cp_{(app)}$ pF	ϵ'_{app}	$Rp_{(app)}$ meg.-Ω	$\tan\delta_{app}$
13 kc/s	26.70	2.63	3550	0.0001 (0.00013)
16	"	"	3590	0.0001 (0.00010)
20	"	"	4020	0.0001 (0.00007)
25	"	"	5230	0.0001 (0.00005)
32	26.75	2.64	4750	0.00004
40	"	"	3180	0.0001 (0.00005)
50	26.70	2.63	2100	0.0001 (0.00007)

TABLE CX.

Sintered Caesium Analcite, Run 154, 31°C, Bridge.

Check shows between 20 and 50 kc/s:-

ϵ'_{app} = 2.63

$\tan\delta_{app}$ = 0.00001 to 0.00004.

ϵ''_{app} = 0.00003 to 0.00011.

TABLE CXI.

Sintered Caesium Analcite, Run 153, 90°C, Bridge.

Frequency	$Cp_{(app)}$ pF	ϵ'_{app}	$Rp_{(app)}$ meg.-Ω	$\tan\delta_{app}$
1.0-3.2 kc/s	26.70	2.63	-	-
4.0 kc/s	"	"	3500	0.0004 (0.00043)
5.0	"	"	3290	0.0004 (0.00036)
6.3	"	"	3010	0.0003 (0.00031)
8.0	"	"	2820	0.0003 (0.00026)
10	"	"	2600	0.0002 (0.00023)
13	"	"	2370	0.0002 (0.00019)
16	"	"	2230	0.0002 (0.00017)
20	"	"	2090	0.0001 (0.00014)
25	"	"	1980	0.0001 (0.00012)
32	"	"	1760	0.0001 (0.00011)
40	"	"	1670	0.0001 (0.00009)
50	"	"	1340	0.0001 (0.00009)